JESSICA PANMAN

NEUROIMAGING TRAJECTORIES IN PRESYMPTOMATIC FRONTOTEMPORAL DEMENTIA

NEUROIMAGING TRAJECTORIES IN PRESYMPTOMATIC FRONTOTEMPORAL DEMENTIA

JESSICA L. PANMAN

The research projects described in this thesis have been supported by The Netherlands Organization for Scientific Research (NWO), ZonMW Memorabel, the Association for Frontotemporal Dementia Research, the Dioraphte Foundation, Alzheimer Nederland, and the Bluefield Project.

Printing of this thesis was supported by:

Cover art	Bas Boon
Lay out	Bas Boon
Printing	Proefschriftmaken.nl
ISBN	978-94-6380-880-4

Neuroimaging Trajectories in Presymptomatic Frontotemporal Dementia

Longitudinale beeldvorming in de presymptomatische fase van frontotemporale dementie

Proefschrift

ter verkrijging van de graad van doctor aan de
Erasmus Universiteit Rotterdam
op gezag van de rector magnificus

Prof.dr. R.C.M.E. Engels

en volgens het besluit van het College voor Promoties.
De openbare verdediging zal plaatsvinden op

vrijdag 11 september 2020 om 09.30 uur

Jessica Larissa Panman

geboren te Delfzijl

Erasmus University Rotterdam

Promotoren

Prof. dr. J.C. van Swieten

Prof. dr. S.A.R.B. Rombouts

Overige leden

Prof. dr. M.W. Vernooij

Prof. dr. M. Masellis

Dr. J. van der Grond

Copromotor

Dr. J.M. Papma

Thesis contents

1. General introduction 7

2. Genotypic neuroimaging patterns in presymptomatic frontotemporal dementia 17

2.1. Modelling the cascade of biomarker changes in *GRN* related frontotemporal dementia 19

2.2. Cognition and gray and white matter characteristics of presymptomatic *C9orf72* repeat expansion 49

3. Longitudinal neuroimaging trajectories in the FTD-RisC study 67

3.1. Gray and white matter changes in presymptomatic frontotemporal dementia: a longitudinal MRI study 69

3.2. Longitudinal multimodal imaging as prognostic and diagnostic biomarker in presymptomatic frontotemporal dementia 97

3.3. Regional blood flow changes in genetic frontotemporal dementia – a pilot study 137

4. Recommendations for neuroimaging analyses in frontotemporal dementia research 163

4.1. Review and comparison of software packages for grey matter biomarkers in presymptomatic frontotemporal dementia 165

4.2. Bias introduced by multiple head coils in MRI research: an 8 channel and 32 channel coil comparison 199

5. General discussion 221

6. Summary 245

6.1. English summary 246

6.2. Nederlandse samenvatting 250

Dankwoord 254

Curriculum Vitae 256

List of Publications 257

PhD portfolio 263

List of Abbreviations 265

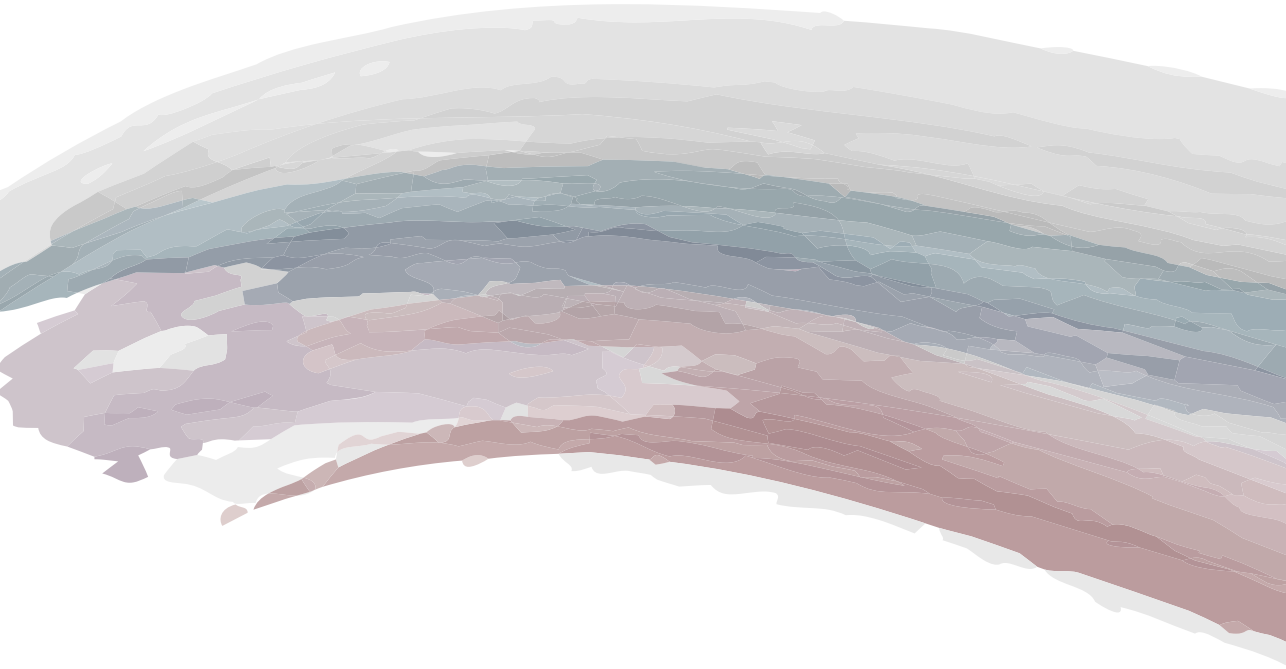

CHAPTER 1

GENERAL INTRODUCTION

Frontotemporal lobar degeneration (FTLD) describes a wide spectrum of neurodegenerative disorders, with heterogeneous pathology, clinical phenotypes, and underlying genetic causes. Symptom onset is usually before the age of 65, and FTLD is diagnosed in approximately 10% of all dementia cases under 65 [1] making it the second most common form of early onset dementia after Alzheimer's disease (AD). Within the FTLD spectrum, the two most typical clinical manifestations are behavioral variant frontotemporal dementia (bvFTD) [2] and primary progressive aphasia (PPA), together commonly referred to as frontotemporal dementia (FTD). BvFTD is characterized by behavioral disturbances such as disinhibition, perseverative behavior, apathy, loss of empathy, and abnormal eating habits [2]. PPA consists of language disorders and can be subdivided in non-fluent variant PPA (nfvPPA) and semantic variant PPA (svPPA) [3]. FTLD variants can present with (concomitant) movement disorders such as motor neuron disease (MND), amyotrophic lateral sclerosis (ALS), cortico-basal syndromes (CBS), and progressive supranuclear palsy (PSP) [4-6].

Further to the typical clinical features, FTD variants are characterized by their distinct spatial patterns of brain atrophy. In bvFTD, atrophy is usually visible as a symmetrical pattern of grey matter loss in the frontal or temporal lobes [7, 8], focal atrophy of the anterior temporal lobes (mostly left sided) is a hallmark of svPPA [9], and nfvPPA patients typically have left-sided asymmetrical atrophy starting in the temporal lobe [8] (Figure 1).

Figure 1. Phenotypic and genotypic atrophy

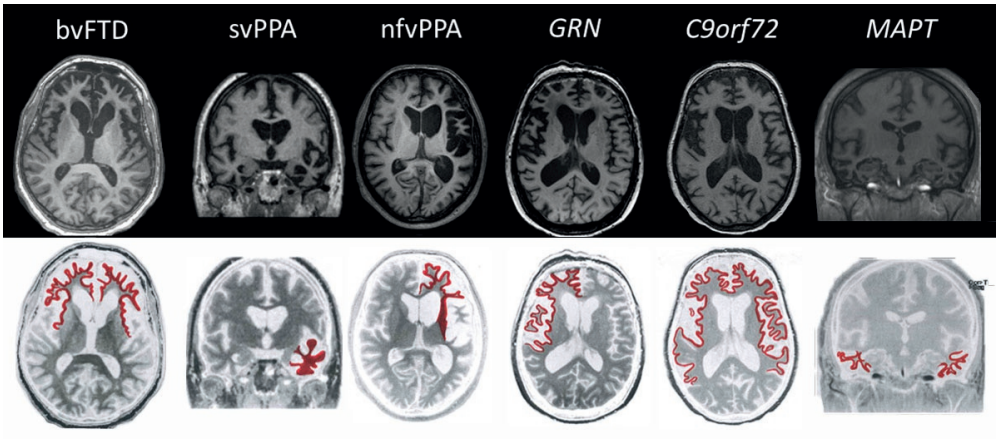

Abbreviations: bvFTD = behavioral variant frontotemporal dementia; svPPA = semantic variant primary progressive aphasia; nfvPPA = non-fluent variant primary progressive aphasia; GRN = progranulin; C9orf72 = chromosome 9 open reading frame 72; MAPT = microtubule-associated protein tau. Modified with permission from Meeter, L et al. Nature Reviews Neurology, 2017; 13(7):406-419.

GENETICS OF FTD

FTD is highly heritable: approximately 10-30% of cases have an autosomal dominant pattern of inheritance [4, 5, 10]. The three most common genetic causes are mutations in microtubule associated protein tau *(MAPT),* progranulin *(GRN)*, or a repeat expansion in chromosome 9 open reading frame 72 *(C9orf72)*. Other rare forms of genetic FTD include *TARDP*, *CHMP2B*, *TBK1*, and *VCP* mutations [10].

GRN

FTD-*GRN* is associated with a large clinical heterogeneity, even within families carrying the same mutation. Symptom onset is highly variable and ranges between the ages 35 to 90 [11, 12]. Common phenotypes in *GRN* patients are bvFTD and nfvPPA, but some patients present with (concomitant) cortico-basal syndrome symptoms [13, 14]. Atrophy can be asymmetrical, widespread over the frontal, temporal, and parietal lobes, including the insula, in (most often) the left hemisphere [8, 15] (Figure 1).

C9orf72

The *C9orf72* repeat expansion is the major genetic cause of familial FTD and ALS [16, 17], and is manifest as bvFTD, ALS, or as a combination of both; patients can also present with severe neuropsychiatric symptoms [18, 19]. Age at symptom onset is variable, ranging from 27 to 83 years [12]. Widespread bilateral atrophy is seen in *C9orf72* repeat expansion patients [15], with a stronger involvement of the precentral gyri in the case of ALS [20] (Figure 1).

MAPT

The age of onset in *MAPT* patients is lower than in *GRN*, *C9orf72*, and sporadic FTD patients; usually ranging between 45 and 65 years [4, 12]. Clinically, patients with *MAPT* mutations often have a bvFTD phenotype, with typical symptoms such as behavioral and semantic deficits [21], but atypical parkinsonism such as PSP can also be present [4, 5]. Atrophy is predominantly located in both temporal and frontal lobes [15, 21] (Figure 1).

BIOMARKER DEVELOPMENT FOR GENETIC FTD

First-degree relatives of genetic FTD patients are 50% at-risk of carrying a gene mutation. Through DNA genotyping, these mutation carriers can be identified before symptom onset ('presymptomatic') while cognitively healthy. Family members without the mutation (non-carriers) form the ideal control group for group-wise and longitudinal comparisons [22] (Figure 2). Research into presymptomatic mutation carriers is an ideal opportunity to study the early disease mechanisms of FTD. As previously demonstrated in genetic AD, the disease

Figure 2. FTD-RisC study flowchart

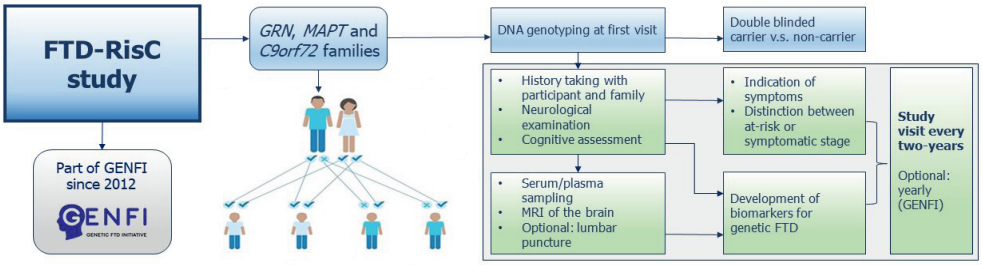

Abbreviations: FTD-RisC = Frontotemporal Dementia Risk Cohort, GENFI = Genetic Frontotemporal Dementia Initiative, *GRN* = progranulin, *MAPT* = microtubule associated protein tau, *C9orf72* = chromosome 9 open reading frame 72, MRI = magnetic resonance imaging, FTD = frontotemporal dementia. √ = healthy allele, × = affected allele (mutation carrier)

processes are long underway before clinical symptom onset [23, 24]. By investigating presymptomatic mutation carriers from a healthy status into the symptomatic stage, and by comparing their characteristics with healthy non-carrying relatives, we can extend our knowledge and understanding of genotypic and phenotypic patterns of neurodegeneration [25]. Moreover, presymptomatic research helps us to identify sensitive fluid, imaging, and cognitive biomarkers that may be valuable as early diagnostic markers, as measurements of disease progression, or as clinical endpoints for clinical trials [22, 26].

In 2010, the Dutch FTD Risk cohort (FTD-RisC) was the first longitudinal cohort study with presymptomatic FTD mutation carriers [27]. Initially, *GRN* and *MAPT* families were included and followed every two years. After discovery of the *C9orf72* repeat expansion, the families involved were also invited to participate in the FTD-RisC study. At every study visit, we interviewed at-risk individuals and patients, including spouses or caregivers, on possible changes in behavior, language, cognition, and daily functioning. We also collected blood samples, cognitive assessments, a brain MRI, and lumbar punctures in some participants (Figure 2). Currently, large multicenter studies into genetic FTD such as the European/Canadian cohort study "Genetic Frontotemporal Dementia Initiative (GENFI)" and the United States study "Longitudinal Evaluation of Familial Frontotemporal Dementia (LEFFTDS)", have been set up to increase sample sizes, to enhance scientific impact, and to facilitate clinical trials [22, 28]. The FTD-RisC study has collaborated with the GENFI cohort since 2012, and has introduced optional yearly follow-up for participants to meet GENFI standardization (Figure 2).

Neuroimaging research in presymptomatic FTD

Within the FTD-RisC study, one of the tools used to investigate the earliest brain changes is MR imaging. MRI enables a detailed study of the brain's multiple tissues and processes. Grey matter atrophy, traditionally depicted with T1-weighted imaging, is currently used as a biomarker of neurodegeneration, and the spatial patterns of atrophy aid differential diagnosis of phenotypes and genotypes (Figure 1) [7]. More advanced MRI techniques include diffusion tensor imaging (DTI), measuring integrity of white matter microstructure [29], resting state functional MRI (rs-fMRI) – showing activation and connectivity of brain regions and networks in rest [30], and arterial spin labeling (ASL) – showing oxygenated blood flow and brain metabolism in the cortex [31].

Results from neuroimaging studies in presymptomatic FTD showed that, in contrast to other types of dementia such as AD, white matter integrity loss is more pronounced than grey matter atrophy [8, 32]. Furthermore, DTI measures in presymptomatic mutation carriers indicate that associative white matter tracts such as the uncinate fasciculus (connecting the frontal and temporal lobe), the forceps major (connecting both frontal lobes) [27], and the inferior fronto-occipital fasciculus (connecting the frontal lobe with posterior regions) [33] may be affected before changes in grey matter volume become apparent. Therefore, DTI may be a potential imaging biomarker for disease onset in genetic FTD [7]. Rs-fMRI measures of functional connectivity in the presymptomatic stage show altered connectivity in the fronto-insula and anterior cingulate regions in several presymptomatic cohorts of *GRN* and/or *MAPT* mutation carriers [27, 34, 35]. Moreover, decreased cerebral blood flow has been demonstrated in two mutation carriers that converted to symptomatic stages during follow-up in a longitudinal ASL study [36]. This may indicate that functional changes precede structural changes in presymptomatic FTD.

Presymptomatic FTD studies have touched on the identification of genotypic imaging hallmarks prior to major brain volume loss. For example, frontal and temporal grey matter atrophy and hypometabolism have been reported in presymptomatic *GRN* mutation carriers [37, 38]. However, grey matter differences in presymptomatic *GRN* and *MAPT* mutation carriers were not present in other studies [27, 33, 39]. Cortical thinning was found in presymptomatic *C9orf72* repeat expansion carriers, resembling patterns in symptomatic FTD and ALS patients with the *C9orf72* repeat expansion [40]. Grey matter changes may occur as early as 25 years before estimated symptom onset in *C9orf72* repeat expansion carriers, starting in the insula, thalamus and posterior cortical areas, as indicated by the GENFI cohort [28]. Furthermore, volumetric changes may start 15 years before estimated symptom onset in the insula for *GRN* mutation carriers, and for *MAPT* mutation carriers in the hippocampus and amygdala [28].

CHALLENGES IN MRI RESEARCH

At the start of this thesis in 2015, neuroimaging research in presymptomatic genetic FTD was expanding quickly, and multi-center cohorts were underway. Therefore, to facilitate these developments, overcoming methodological MRI issues became the next great challenge [41]. First, MRI data acquired with different hardware or acquisition parameters requires harmonization before pooling, as bias can be introduced through endless variability in images acquisition. This can affect data reliability [41] and pose serious issues for longitudinal imaging studies: even the slightest change in parameters changes the metrics of the tissue or connectivity, harming the reliability of longitudinal analyses [42-45]. Moreover, clinical researchers may not always be aware of the variability of MRI data. Second, another important challenge for neuroimaging research is the translation of experimental findings to clinical practice. Quantitative markers of specific regions are interesting as potential markers determining symptom onset [28, 46], or aiding differential diagnoses between phenotypes [7, 47], for example using reference data from population studies [48]. Other clinically useful tools may be the use of continuous disease staging models. By placing individual patients within a disease timeline, we can predict future disease development, and therefore also contribute to patient care, disease anticipation, and treatment optimization [49]. Furthermore, it becomes essential to determine best practice guidelines for acquisition, analyses, and interpretation of specific MRI sequences and biomarkers. If we are able to derive recommendations from empirical and validation studies in the genetic FTD population, we can further optimize the sensitivity of the biomarkers and clinical trial design [50].

OUTLINE OF THIS THESIS

In conclusion, the groundwork for neuroimaging research in presymptomatic genetic FTD mutation carriers has been laid. In this thesis, I have built on these first studies and greatly extended our knowledge of disease mechanisms of genetic FTD using MRI, and on the impact of MRI variability on the reliability of longitudinal imaging biomarkers. Current areas of interest for neuroimaging research with presymptomatic FTD mutation carriers are, amongst others, to: determine genotypic imaging signatures, investigate temporal trajectories of brain change, and address and overcome methodological challenges in neuroimaging research. In this thesis, I address these areas of interest in my projects, ordered per chapter.

Chapter 2 focusses on cross-sectional presymptomatic genotypic patterns in neuroimaging, cognition and other biomarkers. In **Chapter 2.1.** we unravel the genotypic and phenotypic disease timeline of *GRN* mutation carriers through discriminative event-based modelling using fluid, imaging, cognitive, and clinical biomarkers. In **Chapter 2.2.** we characterize the

presymptomatic stage of *C9orf72* repeat expansion carriers based on grey matter volume, white matter integrity, and cognition.

In **Chapter 3**, we investigated longitudinal neuroimaging trajectories of presymptomatic mutation carriers. In **Chapter 3.1.** we describe the three main genotypes of genetic FTD at baseline and after two-year follow up using volumetric data, cortical thickness measurements, and white matter integrity. In **Chapter 3.2**. we study the conversion stage of *MAPT* and *GRN* mutation carriers to symptomatic FTD with grey matter and white matter measurements, and propose potential markers for disease onset. In **Chapter 3.3.** we investigate genotypic and phenotypic trajectories of perfusion by presenting our data and model for longitudinal analyses of regional cerebral blood flow.

Chapter 4 mainly discusses methodological MRI challenges that will aid future neuroimaging research in the genetic FTD population. In **Chapter 4.1.** we review the existing literature on presymptomatic grey matter volume changes, and we determine which software and type of analysis may be used for each genotype in order to obtain maximal sensitivity. In **Chapter 4.2**. we assess what bias can be attributed to the use of multiple head coils in a longitudinal study, to increase awareness for possible problems of multi-hardware studies.

In **Chapter 5** we summarize, interpret and discuss our results. We review our main findings in relation to the field of genetic FTD and neuroimaging research, and suggest new areas of interest for future studies.

REFERENCES

1. Hogan, D.B., et al., The Prevalence and Incidence of Frontotemporal Dementia: a Systematic Review. Can J Neurol Sci, 2016. 43 Suppl 1: p. S96-S109.
2. Rascovsky, K., et al., Sensitivity of revised diagnostic criteria for the behavioural variant of frontotemporal dementia. Brain, 2011. 134(Pt 9): p. 2456-77.
3. Gorno-Tempini, M.L., et al., Classification of primary progressive aphasia and its variants. Neurology, 2011. 76(11): p. 1006-14.
4. Seelaar, H., et al., Clinical, genetic and pathological heterogeneity of frontotemporal dementia: a review. J Neurol Neurosurg Psychiatry, 2011. 82(5): p. 476-86.
5. Lashley, T., et al., Review: an update on clinical, genetic and pathological aspects of frontotemporal lobar degenerations. Neuropathol Appl Neurobiol, 2015. 41(7): p. 858-81.
6. Young, J.J., et al., Frontotemporal dementia: latest evidence and clinical implications. Ther Adv Psychopharmacol, 2018. 8(1): p. 33-48.
7. Meeter, L.H., et al., Imaging and fluid biomarkers in frontotemporal dementia. Nat Rev Neurol, 2017. 13(7): p. 406-419.
8. Gordon, E., J.D. Rohrer, and N.C. Fox, Advances in neuroimaging in frontotemporal dementia. J Neurochem, 2016. 138 Suppl 1: p. 193-210.
9. Landin-Romero, R., et al., An update on semantic dementia: genetics, imaging, and pathology. Alzheimers Res Ther, 2016. 8(1): p. 52.
10. Blauwendraat, C., et al., The wide genetic landscape of clinical frontotemporal dementia: systematic combined sequencing of 121 consecutive subjects. Genet Med, 2018. 20(2): p. 240-249.
11. van Swieten, J.C. and P. Heutink, Mutations in progranulin (GRN) within the spectrum of clinical and pathological phenotypes of frontotemporal dementia. Lancet Neurol, 2008. 7(10): p. 965-74.
12. Olszewska, D.A., et al., Genetics of Frontotemporal Dementia. Curr Neurol Neurosci Rep, 2016. 16(12): p. 107.
13. Hsiung, G.Y.R. and H.H. Feldman, GRN-Related Frontotemporal Dementia. 1993.
14. Alexander, C., D. Pisner, and C. Jacova, Predementia Brain Changes in Progranulin Mutation: A Systematic Review of Neuroimaging Evidence. Dement Geriatr Cogn Disord, 2019. 47(1-2): p. 1-18.
15. Whitwell, J.L., et al., Neuroimaging signatures of frontotemporal dementia genetics: C9ORF72, tau, progranulin and sporadics. Brain, 2012. 135(Pt 3): p. 794-806.
16. Renton, A.E., et al., A hexanucleotide repeat expansion in C9ORF72 is the cause of chromosome 9p21-linked ALS-FTD. Neuron, 2011. 72(2): p. 257-68.
17. Majounie, E., et al., Frequency of the C9orf72 hexanucleotide repeat expansion in patients with amyotrophic lateral sclerosis and frontotemporal dementia: a cross-sectional study. Lancet Neurol, 2012. 11(4): p. 323-30.
18. Burrell, J.R., et al., The frontotemporal dementia-motor neuron disease continuum. Lancet, 2016. 388(10047): p. 919-31.
19. Patel, A.N. and J.B. Sampson, Cognitive Profile of C9orf72 in Frontotemporal Dementia and Amyotrophic Lateral Sclerosis. Curr Neurol Neurosci Rep, 2015. 15(9): p. 59.
20. Omer, T., et al., Neuroimaging patterns along the ALS-FTD spectrum: a multiparametric imaging study. Amyotroph Lateral Scler Frontotemporal Degener, 2017. 18(7-8): p. 611-623.
21. Ghetti, B., et al., Invited review: Frontotemporal dementia caused by microtubule-associated protein tau gene (MAPT) mutations: a chameleon for neuropathology and neuroimaging. Neuropathol Appl Neurobiol, 2015. 41(1): p. 24-46.
22. Rohrer, J.D., et al., Presymptomatic studies in genetic frontotemporal dementia. Rev Neurol (Paris), 2013. 169(10): p. 820-4.
23. Bateman, R.J., et al., Clinical and biomarker changes in dominantly inherited Alzheimer's disease. N Engl J Med, 2012. 367(9): p. 795-804.
24. Moulder, K.L., et al., Dominantly Inherited Alzheimer Network: facilitating research and clinical trials. Alzheimers Res Ther, 2013. 5(5): p. 48.
25. Schuster, C., et al., Presymptomatic and longitudinal neuroimaging in neurodegeneration--from snapshots to motion picture: a systematic review. J Neurol Neurosurg Psychiatry, 2015. 86(10): p. 1089-96.
26. Desmarais, P., et al., Therapeutic trial design for frontotemporal dementia and related disorders. J

Neurol Neurosurg Psychiatry, 2018.
27. Dopper, E.G., et al., Structural and functional brain connectivity in presymptomatic familial frontotemporal dementia. Neurology, 2014. 83(2): p. e19-26.
28. Rohrer, J.D., et al., Presymptomatic cognitive and neuroanatomical changes in genetic frontotemporal dementia in the Genetic Frontotemporal dementia Initiative (GENFI) study: a cross-sectional analysis. Lancet Neurol, 2015. 14(3): p. 253-62.
29. Alexander, A.L., et al., Diffusion tensor imaging of the brain. Neurotherapeutics, 2007. 4(3): p. 316-29.
30. Seeley, W.W., et al., Neurodegenerative diseases target large-scale human brain networks. Neuron, 2009. 62(1): p. 42-52.
31. Alsop, D.C., et al., Recommended implementation of arterial spin-labeled perfusion MRI for clinical applications: A consensus of the ISMRM perfusion study group and the European consortium for ASL in dementia. Magn Reson Med, 2015. 73(1): p. 102-16.
32. Lam, B.Y., et al., Longitudinal white matter changes in frontotemporal dementia subtypes. Hum Brain Mapp, 2014. 35(7): p. 3547-57.
33. Borroni, B., et al., Brain magnetic resonance imaging structural changes in a pedigree of asymptomatic progranulin mutation carriers. Rejuvenation Res, 2008. 11(3): p. 585-95.
34. Borroni, B., et al., Granulin mutation drives brain damage and reorganization from preclinical to symptomatic FTLD. Neurobiol Aging, 2012. 33(10): p. 2506-20.
35. Premi, E., et al., Multimodal FMRI resting-state functional connectivity in granulin mutations: the case of fronto-parietal dementia. PLoS One, 2014. 9(9): p. e106500.
36. Dopper, E.G., et al., Cerebral blood flow in presymptomatic MAPT and GRN mutation carriers: A longitudinal arterial spin labeling study. Neuroimage Clin, 2016. 12: p. 460-5.
37. Caroppo, P., et al., Lateral Temporal Lobe: An Early Imaging Marker of the Presymptomatic GRN Disease? J Alzheimers Dis, 2015. 47(3): p. 751-9.
38. Jacova, C., et al., Anterior brain glucose hypometabolism predates dementia in progranulin mutation carriers. Neurology, 2013. 81(15): p. 1322-31.
39. Whitwell, J.L., et al., Altered functional connectivity in asymptomatic MAPT subjects: a comparison to bvFTD. Neurology, 2011. 77(9): p. 866-74.
40. Walhout, R., et al., Brain morphologic changes in asymptomatic C9orf72 repeat expansion carriers. Neurology, 2015. 85(20): p. 1780-8.
41. Smith, S.M. and T.E. Nichols, Statistical Challenges in "Big Data" Human Neuroimaging. Neuron, 2018. 97(2): p. 263-268.
42. Takao, H., et al., Effect of scanner in longitudinal diffusion tensor imaging studies. Hum Brain Mapp, 2012. 33(2): p. 466-77.
43. Venkatraman, V.K., et al., Region of interest correction factors improve reliability of diffusion imaging measures within and across scanners and field strengths. Neuroimage, 2015. 119: p. 406-16.
44. Mutsaerts, H., et al., Comparison of arterial spin labeling registration strategies in the multi-center GENetic frontotemporal dementia initiative (GENFI). J Magn Reson Imaging, 2018. 47(1): p. 131-140.
45. Mutsaerts, H.J., et al., Multi-vendor reliability of arterial spin labeling perfusion MRI using a near-identical sequence: implications for multi-center studies. Neuroimage, 2015. 113: p. 143-52.
46. Staffaroni, A.M., et al., Longitudinal multimodal imaging and clinical endpoints for frontotemporal dementia clinical trials. Brain, 2019. 142(2): p. 443-459.
47. Steketee, R.M., et al., Early-stage differentiation between presenile Alzheimer's disease and frontotemporal dementia using arterial spin labeling MRI. Eur Radiol, 2016. 26(1): p. 244-53.
48. Vernooij, M.W., et al., Automatic normative quantification of brain tissue volume to support the diagnosis of dementia: A clinical evaluation of diagnostic accuracy. Neuroimage Clin, 2018. 20: p. 374-379.
49. Venkatraghavan, V., et al., Disease progression timeline estimation for Alzheimer's disease using discriminative event based modeling. Neuroimage, 2019. 186: p. 518-532.
50. Kumar, V., et al., Radiomics: the process and the challenges. Magn Reson Imaging, 2012. 30(9): p. 1234-48

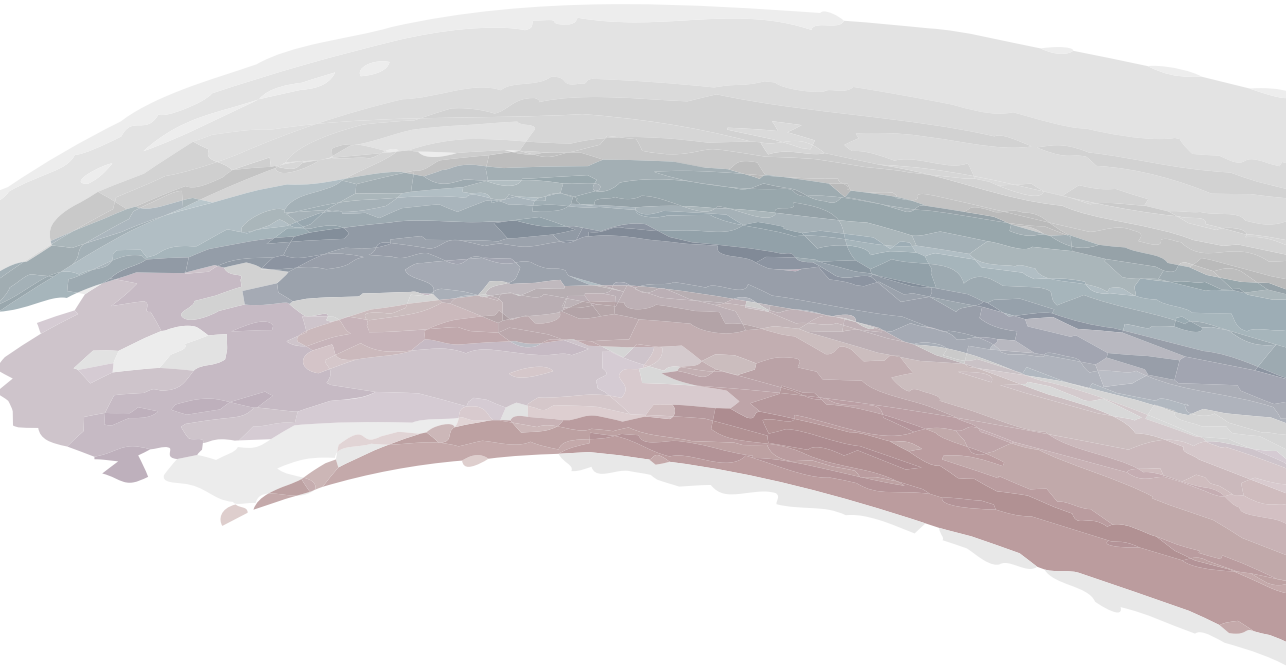

CHAPTER 2

NEUROIMAGING IN MULTIMODAL PRESYMPTOMATIC FTD RESEARCH

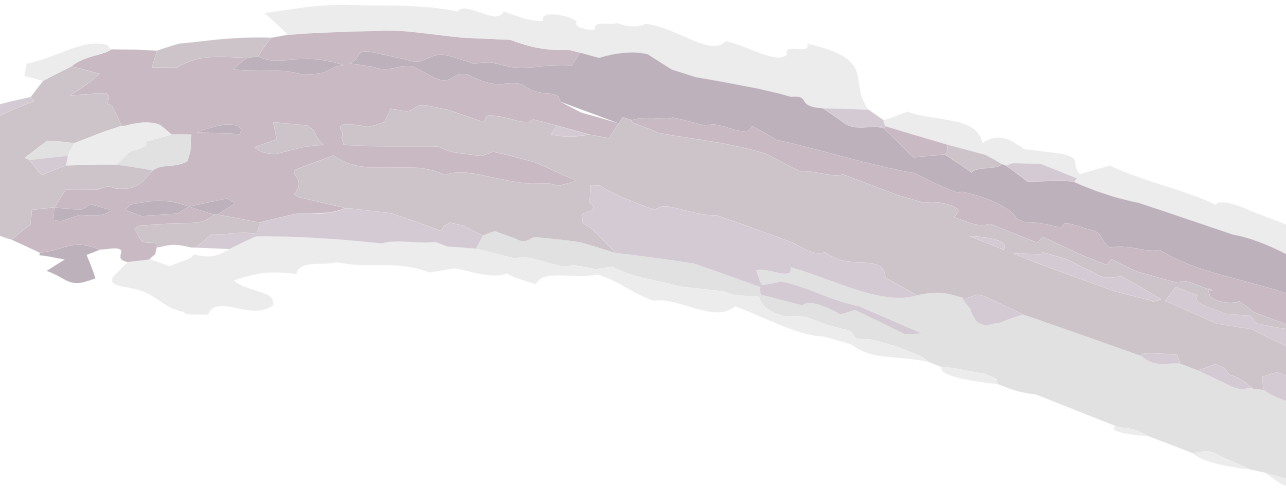

Chapter 2.1

Modelling the cascade of biomarker changes in *GRN* related frontotemporal dementia

Panman, J.L.*
Venkatraghavan, V.*
van der Ende, E.L
Steketee, R.M.E.
Jiskoot, L.C.
Poos, J.M.
Dopper, E.G.P.
Meeter, L.H.H.
Donker Kaat, L.
Rombouts, S.A.R.B.
Vernooij, M.W.
Kievit, A.J.A.
Premi, E.
Cosseddu, M.
Bonomi, E.
Olives, J.
Rohrer, J.D.
Sanchez-Valle, R.
Borroni, B.
Bron, E.E.
van Swieten, J.C.
Papma, J.M.
Klein, S.
GENFI consortium investigators.

* these authors contributed equally to this work

Submitted (Journal of Neurology, Neurosurgery, and Psychiatry)

ABSTRACT

Objective: Progranulin related frontotemporal dementia (FTD-*GRN*) is a fast progressive disease. Modelling the cascade of multimodal biomarker changes aids in understanding the etiology of this disease and enables monitoring of individual mutation carriers. In this cross-sectional study, we estimated the temporal cascade of biomarker changes for FTD-*GRN*, in a data-driven way.

Methods: We included 56 presymptomatic and 35 symptomatic *GRN* mutation carriers, and 35 healthy non-carriers. Selected biomarkers were neurofilament light chain (NfL), grey matter volume, white matter microstructure, and cognitive domains. We used discriminative event-based modelling to infer the cascade of biomarker changes in FTD-*GRN* and estimated individual disease severity through cross-validation. We derived the biomarker cascades in non-fluent variant primary progressive aphasia (nfvPPA) and behavioural variant FTD (bvFTD) to understand the differences between these phenotypes.

Results: Language functioning and NfL were the earliest abnormal biomarkers in FTD-*GRN*. White matter tracts were affected before grey matter volume, and the left hemisphere degenerated before the right. Based on individual disease severities, presymptomatic carriers could be delineated from symptomatic carriers with a sensitivity of 100% and specificity of 96.1%. The estimated disease severity strongly correlated with functional severity in nfvPPA, but not in bvFTD. In addition, the biomarker cascade in bvFTD showed more uncertainty than nfvPPA.

Conclusion: Degeneration of axons and language deficits are indicated to be the earliest biomarkers in FTD-*GRN*, with bvFTD being more heterogeneous in disease progression than nfvPPA. Our data-driven model could help identify presymptomatic *GRN* mutation carriers at risk of conversion to the clinical stage.

INTRODUCTION

Mutations in the progranulin (*GRN*) gene on chromosome 17q21 are a major cause of autosomal dominant inherited frontotemporal dementia (FTD) [1, 2]. The majority of mutation carriers develops a behavioural variant FTD (bvFTD) phenotype [3], and another significant proportion of patients present with non-fluent variant primary progressive aphasia (nfvPPA) [3, 4]. The age of symptom onset varies between 35 and 90 in *GRN* mutation carriers [1, 2], without clear associations with familial age of onset [4]. Brain changes in FTD-*GRN* patients can evolve symmetrically, or predominantly asymmetrically, in either the left or right hemisphere [5, 6].

Recent longitudinal studies have suggested that the time-window between emerging pathophysiological changes and the first clinical symptoms is short in *GRN* mutation carriers, and covers only two to four years [7, 8]. During this period, the serum neurofilament light chain (NfL) level – a marker of axonal degeneration – increases two to three-fold [9, 10], loss of grey and white matter emerges [7, 11], and cognitive functioning declines [8]. However, most of the biomarker studies in FTD-*GRN* have investigated one type of biomarker, i.e. fluid, neuroimaging, or cognition, leaving the temporal relations and ordering of these biomarkers unknown. These temporal relations could potentially provide novel insights into disease progression mechanisms in *GRN* mutation carriers. Moreover, because of the fast progression of pathophysiological changes, determining the earliest abnormal biomarker is crucial, as the optimal window of opportunity for treatment might be small.

Recently, novel data-driven methods for disease progression modelling have emerged, focusing on the cascade of biomarker changes [12, 13]. Event-based models are a class of disease progression models that estimate the cascade of biomarker changes derived from cross-sectional data [6, 13, 14]. This is done without strong *a priori* assumptions regarding the relationship between different biomarkers. A promising novel method that estimates the cascade of biomarker change is Discriminative Event-Based Modelling (DEBM) [13, 15]. This model is robust to disease phenotypic heterogeneity in a cohort and can handle missing data.

In this study, we use DEBM to estimate the temporal cascade of biomarker changes in presymptomatic and symptomatic FTD-*GRN* mutation carriers, distinguishing between early and late biomarkers. Furthermore, we determine phenotypic differences in patterns of biomarker changes in nfvPPA and bvFTD, to gain more insights into their distinct disease progression mechanisms.

METHODS

Sample and study procedures

Subjects were recruited prospectively from three European centres of the Genetic Frontotemporal dementia Initiative (GENFI): Rotterdam (the Netherlands), Brescia (Italy), and Barcelona (Spain). We collected cognitive and clinical data, MRI, and serum samples from 126 participants. We included 35 symptomatic *GRN* mutation carriers (Rotterdam: n=11, Brescia: n=22, Barcelona: n=2), 56 presymptomatic *GRN* mutation carriers (Rotterdam: n=33, Brescia: n=17, Barcelona: n=6), and 35 cognitively healthy non-carriers (Rotterdam: n=34, Brescia: n=0, Barcelona: n=1). Local clinical genetics departments performed DNA genotyping to confirm the presence of a *GRN* mutation. Non-carriers were first-degree family members of *GRN* patients without a mutation. Symptomatic mutation carriers were diagnosed based on the established clinical criteria for bvFTD [16] (n=17), nfvPPA [17] (n=16), or cortico-basal syndrome [18] (n=2). Mutation carriers were defined as presymptomatic when clinical criteria were not fulfilled, i.e., behavioural or cognitive symptoms were absent [19]. Clinical questionnaires were administered to the caregiver, spouse, or a family member, i.e. the Frontotemporal Lobar Degeneration Clinical Dementia Rating scale sum of boxes (FTD-CDR-SB) [20], the Neuropsychiatric Inventory (NPI) [21], and the Frontotemporal Dementia Rating scale (FRS) [22]. The study was carried out according to the declaration of Helsinki, approved by the local medical ethics board at each site, and all participants provided written informed consent.

Biomarker collection and processing

Biomarker selection. For biomarker selection, we performed a literature search using Pubmed. We included studies that (i) performed research in presymptomatic *GRN* mutation carriers, and (ii) biomarker studies that examined biomarkers in blood or CSF, neuroimaging biomarkers and cognition. We selected serum NfL [9], MMSE, cognitive domains of attention and processing speed, executive functioning, language, and social cognition [8, 23]; left and right grey matter volumes of the insula, frontal lobe, parietal lobe and temporal lobe [7, 11]; left and right white matter tracts of the anterior thalamic radiation, superior longitudinal fasciculus, uncinate fasciculus, and the forceps minor [7, 24]. For detailed information about the literature review and subsequent biomarker selection, see Appendix A.

Neurofilament light chain. Serum samples were obtained through venepunctures and analysed with single molecular assay technology, as described previously [10]. Samples were measured in a single laboratory, in duplicate, with an intra-assay coefficient of variation below 5%. Inter-assay variation between batches was below 8%. NfL concentrations were expressed in pg/ml.

MRI. 3D T1-weighted and diffusion tensor imaging were acquired with 3T MRI scanners across the three sites. MRI was missing in 25 participants due to unavailability (n=16) and insufficient quality due to motion artefacts (n=9). Availability of MRI and an overview of the scanning protocols are listed in Appendix A, Table A.1. Image processing was carried out in FMRIB Software Library [25], using default pipelines for grey matter volumes and white matter tracts. For grey matter volumetric regions of interest (ROI), we used the Montreal Neurological Institute (MNI) atlas [26], and for the fractional anisotropy of white matter tracts, we used the Johns Hopkins' University atlas [27]. Left and right regions and tracts were considered separately. Raw regional volumes and fractional anisotropy values were transformed to z-scores, based on the mean and standard deviation from the non-carriers. A detailed description of processing and ROI calculation is reported in Appendix A.

Cognitive assessment. Cognitive data were collected from all participants in four cognitive domains, described in detail in Appendix A. Raw cognitive test scores were transformed to z-scores based on the mean and standard deviation in non-carriers, and then combined into cognitive domain scores similar to previous studies [8].

Confounding factors correction. All selected biomarkers were tested for normality (see Appendix A for details) and log-transformed in case of a skewed distribution. As most non-carriers originated from one centre, we used presymptomatic subjects for regressing out possible confounding effects using multiple linear regression, before continuing with event-based modelling. NfL levels were corrected for age and sex. Grey matter volumes and fractional anisotropy values were corrected for age, sex, total intracranial volume, and MRI scanning protocol. Cognitive domain scores were corrected for confounding effects of age, sex, and total years of education.

Temporal cascade of biomarker changes

The DEBM model introduced in Venkatraghavan et al. [13, 15] estimates the cascade of biomarker changes in a three-step process. For each biomarker, it first estimates the distributions of normal and pathological (or abnormal) values using Gaussian mixture modelling (GMM), and uses these to compute, for each subject, the probability that the biomarker is abnormal (explained in detail in Appendix B). This is followed by the estimation of a cascade of events for each subject, by ordering these probabilities, and estimating the mean cascade for the population. Lastly, the severity of disease as a summary measure for each subject is computed by estimating the subject's progression along the resulting disease progression timeline. In this section, we describe the experiments we performed for estimating the cascade of biomarker changes for non-imaging biomarkers, as well as for neuroimaging and non-imaging biomarkers together.

DEBM model for non-imaging biomarkers. As imaging was missing in a lot of subjects (n=25),

we first estimated the cascade of biomarker changes procedure with solely NfL and cognitive biomarkers. Since the non-carriers are healthy in this cohort, the normal Gaussians were fixed at the mean and standard deviation of the biomarker values of the non-carriers. We used GMM only to estimate the abnormal Gaussian and the mixing parameter for each biomarker. In order to estimate the positional variance in the estimated cascade, the entire dataset was randomly sampled using bootstrap sampling with *100* different random seeds, and the cascade of biomarker change was estimated for each of those randomly sampled datasets [13, 15].

DEBM model for neuroimaging and non-imaging biomarkers together. For the imaging biomarkers, we modified the GMM step in DEBM to make it better suited for the FTD-*GRN* population, known for its asymmetric pattern of atrophy [5]. Abnormal values of biomarkers that typically become abnormal late in the disease are usually under-represented in a specific patient population as compared to the early biomarkers. This could make the GMM of late biomarkers unstable, as previously reported [15]. Due to the asymmetrical atrophy patterns of FTD-*GRN* [5, 6], lateralized neuroimaging biomarkers that become abnormal early in the disease process may have a corresponding biomarker from the other hemisphere that remains stable until much later in the disease process. To exploit this, we assumed that the normal and abnormal Gaussians from the left and right hemispheric biomarkers (expressed as z-scores) are the same, and the biomarkers from both hemispheres only differ in their position along the disease progression timeline. With this assumption, we proposed a novel modification to the GMM optimization called Siamese GMM, in which the biomarkers of the same region from left and right hemispheres are jointly optimized. The abnormal and normal Gaussians are shared between the left and right hemispheres, but the mixing parameters are independently estimated (see Appendix B for details). In this way, the numerical stability of GMM optimization in the late neuroimaging biomarkers improved.

For non-imaging biomarkers, GMM was performed as described in the previous section. After GMM, further steps of DEBM modelling were carried out as usual, to estimate the complete cascade of neuroimaging and non-imaging biomarker changes in presymptomatic and symptomatic *GRN* mutation carriers. The positional variance in the estimated cascade was again estimated using bootstrap sampling with 100 different random seeds. For brevity, in the remainder of the paper we refer to this model, which integrates neuroimaging and non-imaging biomarkers, as the *multimodal DEBM*.

Validation. To validate the DEBM models, we used 10-fold cross-validation. In each fold of the cross-validation, the DEBM model was built in the training set and the disease severity was estimated in the test set. We distinghuished symptomatic mutation carriers from presymptomatic mutation carriers, and reported the corresponding sensitivity and specificity. Furthermore, in bvFTD and nfvPPA subjects, the estimated disease severity was correlated

with years since symptom onset and FTD-CDR-SB scores, using Pearson correlation. Symptomatic carriers without imaging biomarkers were excluded for the validation of the multimodal DEBM but were included in the non-imaging DEBM.

Differential phenotype analysis

In order to examine the differences between bvFTD and nfvPPA variants of FTD-GRN, we built separate DEBM models. Presymptomatic subjects were excluded from this analysis as no phenotype information is available. The numbers of symptomatic subjects in each group (17 with bvFTD, 16 with nfvPPA) are too small to build complete DEBM models reliably. As a solution, we assumed that the biomarkers for the two phenotypes shared the same normal and abnormal biomarker distributions, and that they only differ in their position along the disease progression timeline. We hence optimized the GMM such that the normal and abnormal Gaussians were estimated without considering the phenotypes, whereas the mixing parameters were estimated separately for each phenotype. As before, we estimated the cascade of biomarker changes in the two phenotypes for non-imaging and multimodal (neuroimaging and non-imaging together) biomarkers.

RESULTS

Sample

A total of 126 subjects were included in this study. Availability and characteristics of the data are presented in Table 1. Details on biomarker availability and characteristics can be found in Appendix A, Tables A.2 and A.3. Symptomatic mutation carriers were older, had fewer years of education, and had higher scores on the NPI and FTD-CDR-SB, and lower scores on the FRS than both presymptomatic mutation carriers and non-carriers. There were no differences in demographic or clinical characteristics between presymptomatic mutation carriers and non-carriers.

Cascade of biomarker changes

Non-imaging and multimodal DEBM models. In Figure 1A and 1B, we show the estimated mean cascade of biomarker changes and the uncertainty within the model for non-imaging and multimodal biomarkers. Language was the earliest biomarker to become abnormal, followed by neurofilament light chain. It can be seen in Figure 1B that the left anterior thalamic radiation, left insula, and bilateral uncinate fasciculi were the earliest imaging biomarkers. It can also be observed that imaging biomarkers from the left-hemisphere became abnormal earlier than their right counterpart. GMM estimations with normal and abnormal Gaussian distributions are shown in Appendix B, Figure B.2, where the estimated Gaussians are seen to fit the observed histograms well. Figure 1C shows the positional variance of the cascade

Table 1. Data availability and characteristics

	Symptomatic			Presymptomatic	Non-carriers
	Total	bvFTD	nfvPPA		
N					
Subjects (% female)	35* (60.0%)	17 (47.1%)	16 (75%)	56 (69.6%)	35 (54.4%)
Rotterdam	11	8	3	33	34
Brescia	22*	9	11	17	0
Barcelona	2	0	2	6	1
Data availability					
Serum NfL	91.7%	88.9%	93.8%	69.64%	91.67%
Cognitive assessment	91.7%	88.9%	93.8%	98.21%	91.67%
T1-weighted MRI	44.4%	38.9%	50.0%	96.4%	88.6%
DTI	50.0%	44.4%	56.3%	92.9%	91.4%
Sample characteristics					
Age (years)	62.57 ± 6.72†	62.93 ± 6.11‡	61.78 ± 7.78§	51.52 ± 11.42	55.15 ± 12.55
Education (years)	10.61 ± 4.59†	10.27 ± 4.91‡	11.79 ± 4.02	13.79 ± 3.27	13.21 ± 2.84
TIV (litres)	1.44 ± 0.17	1.50 ± 0.17	1.42 ± 0.14	1.39 ± 0.15	1.40 ± 0.14
NPI	23.77 ± 28.38†	28.90 ± 30.64‡,¶	6.67 ± 6.03¶	1.87 ± 3.37	2.24 ± 4.32
FRS	56.50 ± 30.43†	48.86 ± 29.91‡	67.20 ± 30.96§	97.27 ± 10.11	95.47 ± 7.45
FTD-CDR-SB	7.64 ± 6.52†	9.68 ± 7.47‡,¶	5.25 ± 4.37§,¶	0.04 ± 0.21	0.00 ± 0.00
Disease duration (years)	2.45 ± 2.01	2.37 ± 1.92	2.48 ± 2.29	N/A	N/A

Abbreviations: bvFTD = behavioural variant frontotemporal dementia, nfvPPA = non-fluent variant primary progressive aphasia, NfL = neurofilament light chain, DTI = diffusion tensor imaging, TIV = total intracranial volume, GM = grey matter, NPI = Neuropsychiatric inventory, FRS = Frontotemporal dementia rating scale, FTD-CDR-SB = Frontotemporal dementia Clinical Dementia Rating Scale Sum of Boxes. Data availability variables represent numbers of cases and percentages of availability. Sample characteristic variables are expressed as mean ± standard deviation.

* The two remaining patients presented with cortico-basal syndrome

† Significant difference between symptomatic carriers and presymptomatic as well as non-carriers

‡ Significant difference between bvFTD patients and presymptomatic as well as non-carriers

§ Significant difference between nfvPPA patients and presymptomatic as well as non-carriers

¶ Significant difference between bvFTD patients and nfvPPA patients

Figure 1. Cascade of biomarker changes in FTD-*GRN*

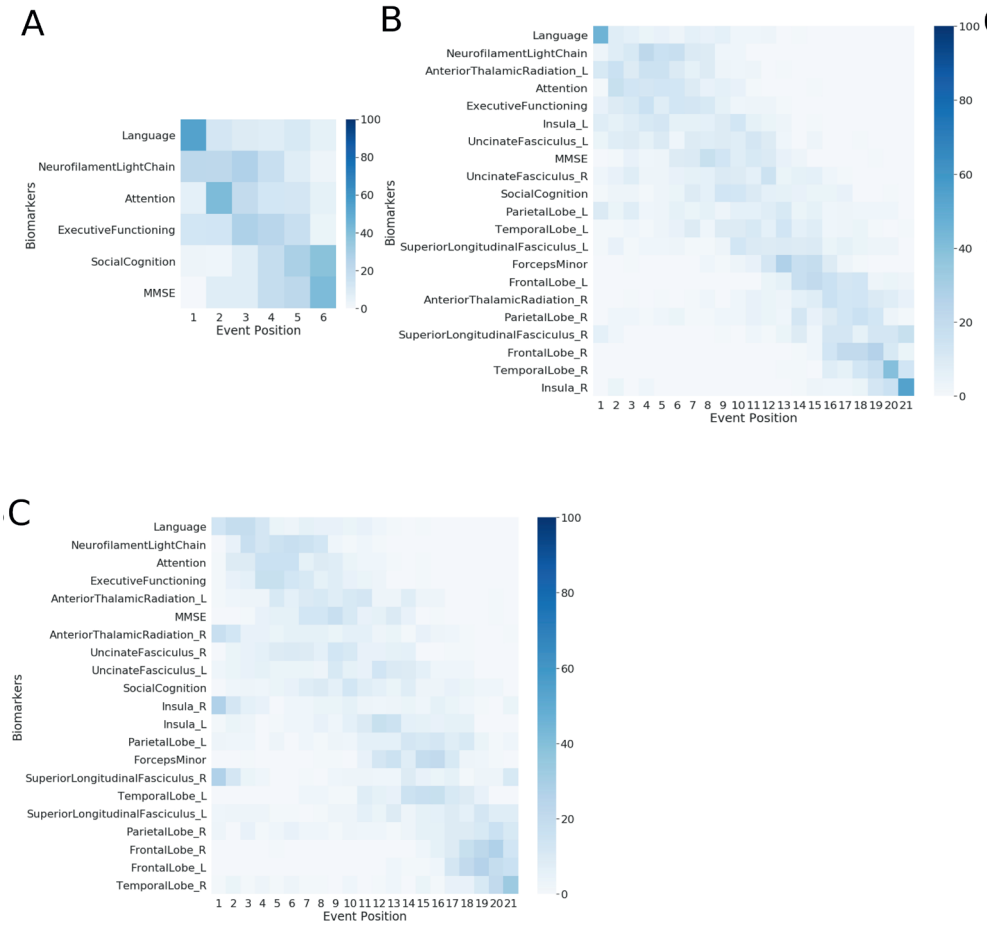

Cascade of biomarkers changes and the uncertainy associated with it. (A) Non-imaging biomarkers, (B) Multimodal biomarkers with Siamese GMM, (C) Multimodal biomarkers without Siamese GMM. The biomarkers are ordered based on the position in the estimated cascade. The color-map is based on the number of times a biomarker is at a position in 100 repetitions of bootstrapping.

of multimodal biomarker changes obtained when GMM of the imaging biomarkers was done without using Siamese GMM. Generally, the positional variance was smaller with Siamese GMM than without.

Validation. Figure 2A and 2B shows the estimated disease severity when using non-imaging and multimodal biomarkers respectively. It can be seen that estimated disease severity delineated the symptomatic subjects from the pre-symptomatic subjects. The sensitivity and specificity of this delineation were 1.0 and 0.982 respectively while using non-imaging

Figure 2. Disease severity estimation

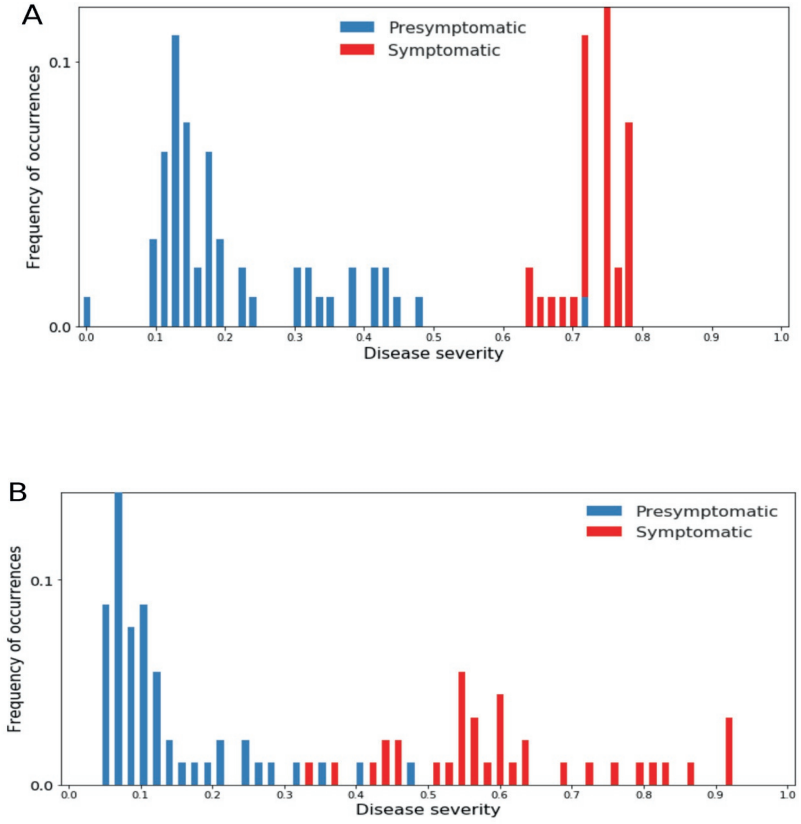

Frequency of occurrence of subjects with different disease severities, estimated using cross-validation. (A) results using non-imaging biomarkers in DEBM, (B) results using multimodal biomarkers in DEBM.

biomarkers, and 1.0 and 0.961 respectively while using multimodal biomarkers.

Figure 3 shows the correlation of the estimated disease severity with years since symptom onset and FTD-CDR-SB for nfvPPA and bvFTD subjects, when using multimodal DEBM. It can be seen from Figure 3 that estimated disease severity strongly correlated with years since symptom onset (R=0.95, p=0.0003), and the FTD-CDR-SB (R=0.84, p=0.0189), in nfvPPA patients. However, estimated disease severity correlated poorly with years since symptom onset (R=0.22, p=0.6331) and the FTD-CDR-SB (R=0.28, p=0.5866) in bvFTD patients. Figure B.3 in Appendix B shows a similar plot when using non-imaging biomarkers, where estimated disease severity did not correlate with years since symptom onset and FTD-CDR-

Figure 3. Correlation of disease severity in nfvPPA and bvFTD

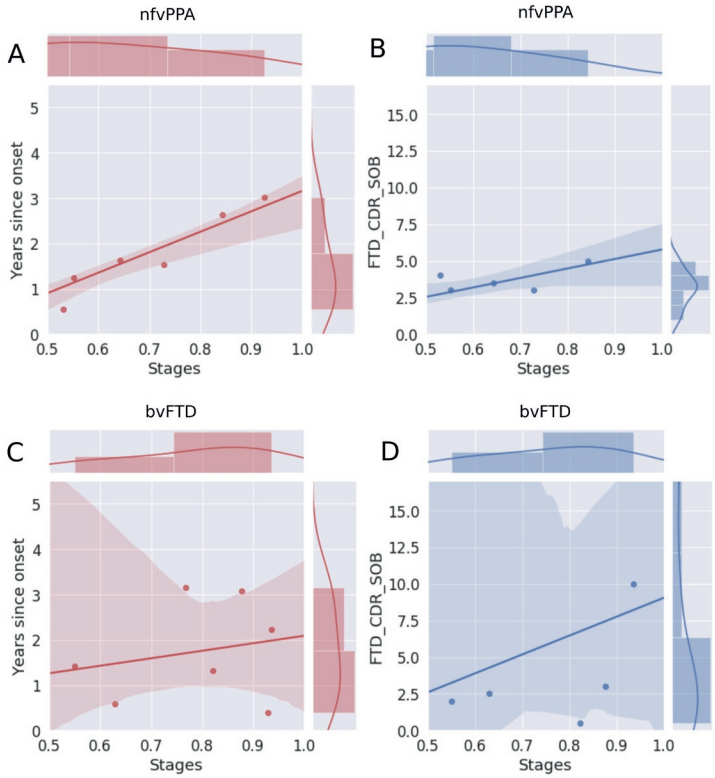

Correlation of disease severity (as estimated by multimodal DEBM using cross-validation) with years since onset and FTD-CDR-SOB. The 2D scatter plots in figures A and C show the correlations of disease severity with years since onset, for symptomatic nfvPPA and bvFTD subjects respectively. The 2D scatter plot in figures B and D show the correlations of disease severity with FTD-CDR-SOB. The plot on top of each subfigure shows the probability density function of the disease stages. The plots on the right of figures A and C show the probability density functions of years since symptom onset. The plots on the right of figures B and D show the probability density function of FTD-CDR-SOB._

SB, neither for nfvPPA nor for bvFTD subjects.

Differential phenotype analysis. Figure 4 shows the multimodal biomarker cascade for nfvPPA and bvFTD phenotypes. NfvPPA patients showed language and NfL as first abnormal biomarkers followed by other cognitive domains. Left-hemispheric imaging biomarkers became abnormal before right-hemispheric imaging biomarkers, starting with the uncinated fasciculus (white matter integrity), insula and temporal lobe (grey matter volume). Only the left superior longitudinal fasciculus was estimated as late biomarker, even later then its right-sided counterpart.

Interestingly, in bvFTD patients, the biomarker ordering also indicated that language and

Figure 4. Cascade of multimodal biomarker changes in nfvPPA and bvFTD.

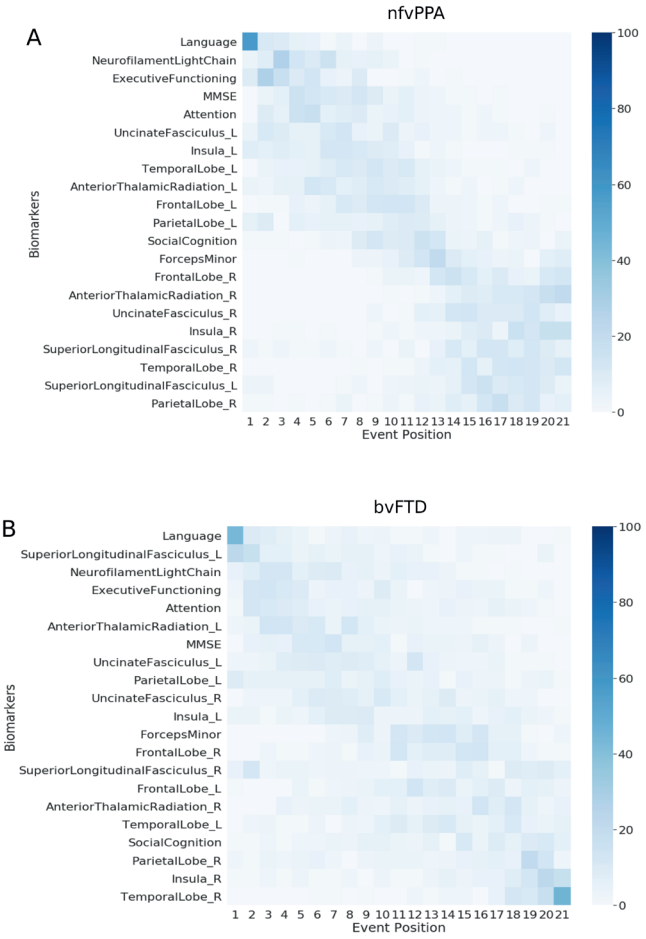

Cascade of biomarker changes in nfvPPA (A) and bvFTD (B) along with the uncertainty associated with it. The biomarkers are ordered based on the position in the estimated cascade. The color-map is based on the number of times a biomarker is at a position in 100 repetitions of bootstrapping.

NfL were the earliest abnormal biomarkers. In contrast to the nfvPPA, the left superior longitudinal fasciculus (white matter integrity) was estimated as the first abnormal imaging biomarker in bvFTD. However, the biomarker orderings in bvFTD were predominantly characterized by large uncertainty in the positioning of biomarkers in the disease timeline, with hardly any observable distinction between early and late biomarkers. Figure B.4 in Appendix B presents the non-imaging biomarker cascade for the two phenotypes, showing that the uncertainty in the mean cascade in bvFTD is more than in nfvPPA.

DISCUSSION

In this study, we estimated the cascade of biomarker changes in FTD-*GRN.* We validated our model by delineating the symptomatic mutation carriers from the presymptomatic mutation carriers using the estimated disease severity. We demonstrated that language and NfL levels are the earliest biomarkers to become abnormal in the FTD-*GRN* spectrum. Other early biomarkers were the white matter microstructure of the thalamic radiation and the cognitive domain of attention and mental processing speed.

Our findings support other studies that proposed NfL as an early biomarker for disease onset in FTD-*GRN* [9, 10]. We demonstrated that the left anterior thalamic radiation also degenerated early. This is also supported by previous studies which suggested that white matter microstructure markers may correlate with changes in NfL [9, 28]. Cognitive changes in attention, mental processing speed, and executive functioning occurred relatively early in the estimated disease progression timeline. This corresponds well with the early white matter changes (i.e. NfL and fractional anisotropy changes), as attention and processing speed are cognitive functions that highly depend upon the integrity of axons and their myelin sheaths [29, 30]. The early involvement of these biomarkers point towards axonal degeneration as one of the first pathological processes in *GRN* mutation carriers.

With the differential phenotypic analysis, we estimated the biomarker cascade for nfvPPA and bvFTD patients. Strikingly, language functions deteriorated early in both nfvPPA and bvFTD. While not currently embedded in the clinical criteria for bvFTD [16], our results demonstrate the importance of decreased language functions in both phenotypes. This is in line with multiple previous studies [31-33]. In addition, multiple determinants of the complex language network were also affected early, for example the left insula, and uncinate fasciculus [34]. For nfvPPA, NfL levels and other cognitive domains became abnormal in early disease stages, consistent with findings from previous studies [9, 10, 35]. In addition, we showed that left hemispheric tracts and regions were affected in nfvPPA patients before right regions, accordant with the previously reported strong involvement of the left hemisphere in primary progressive aphasia [36, 37]. We showed that NfL levels and cognitive domains may be possible biomarkers for disease onset, while neuroimaging markers were highly correlated with clinical indicators of progression (years since onset, FTD-CDR-SB).

For bvFTD, however, the biomarker cascade was characterized by large uncertainty, and the estimated disease severities did not correlate with actual years since onset or FTD-CDR-SB. This uncertainty could indicate large neuroanatomical heterogeneities between bvFTD patients. Differences in neuroanatomical atrophy patterns have been associated with FTD-*GRN* patients before [5, 6]. Here, we demonstrated that this anatomical heterogeneity is predominantly associated with the bvFTD phenotype, while nfvPPA patients showed a

clear pattern of left hemispheric degeneration before the right hemisphere was affected. Furthermore, bvFTD patients present with cognitive symptoms such as impaired social conduct and executive function but can also have severe memory problems. In summary, within the group of bvFTD, spatial and temporal brain degeneration and cognitive changes are more heterogeneous than in the nfvPPA group.

From a methodological point of view the strength of this paper lies in the introduction of the Siamese GMM approach in DEBM. We showed that Siamese GMM reduces the positional variance in neuroimaging biomarkers, most notably in the right insula, the right anterior thalamic radiation and the right superior longitudinal fasciculus. This is because GMM is known to be unstable in the presence of biomarkers with a large overlap between the normal and abnormal Gaussians [13]. This is often the case in biomarkers becoming abnormal late in the disease and having very few samples representative of the typical abnormal values expected in the disease. The joint GMM in the Siamese counterpart exploits the knowledge that FTD-*GRN* is generally an asymmetric brain disease, and uses the neuroimaging biomarkers that become abnormal early in the disease process to aid the GMM of its hemispheric counterpart that becomes abnormal far later in the disease process. Another strong point about the DEBM model is that it infers disease progression from cross-sectional data, which is more readily available than longitudinal data, especially in a rare disease as FTD-*GRN*.

From the clinical point of view, a major strength of our study is the large, well-defined cohort of presymptomatic and symptomatic *GRN* mutation carriers, and availability of multimodal (i.e. fluid, imaging, and cognitive) biomarkers. Although we did not have FLAIR or T2 imaging data available for the current study, it would be interesting to incorporate white matter lesions in a future version of the model, as a number of studies have indicated the presence of white matter lesions in FTD-*GRN* carriers [38]. A minor limitation in our study is the difference in mean age between the non-carrier, presymptomatic, and symptomatic mutation carrier groups. We adjusted for this in the analysis rather than matching the groups. It should be noted that the small sample size may have caused a large part of the uncertainty of our model, especially in the case of missing (neuroimaging) biomarkers. Our bvFTD and nfvPPA samples due to *GRN* mutations were relatively large compared to previous studies [39]. However, the DEBM model would improve substantially if the phenotypic samples were larger, as we could only include symptomatic subjects for the phenotypic analysis. Uncertainties in the estimation of the phenotypic biomarker cascades may be improved with upcoming longitudinal data, when some of the converted mutation carriers can be included in the phenotypic models.

In conclusion, with this DEBM study in the FTD-*GRN* spectrum, we were able to demonstrate that language functions and NfL levels are the earliest abnormal biomarkers, regardless of phenotype. However, bvFTD show more heterogeneity and uncertainty in disease progression,

pointing towards more variability in biomarkers than nfvPPA. Our analyses suggest axonal degeneration and damage to the language network as the earliest biomarkers in *GRN* mutation carriers, which could potentially be used as endpoints in clinical trials for disease modifying treatments. Future efforts should be directed at confirmation and validation of these findings with longitudinal data. We expect that DEBM modelling will benefit individual prediction of symptom onset in the future, and may optimize selection of eligible mutation carriers for clinical trials.

REFERENCES

1. Seelaar, H., Rohrer, J.D., Pijnenburg, Y.A. et al., Clinical, genetic and pathological heterogeneity of frontotemporal dementia: a review. J Neurol Neurosurg Psychiatry, 2011. 82(5): p. 476-86.
2. van Swieten, J.C. and P. Heutink, Mutations in progranulin (GRN) within the spectrum of clinical and pathological phenotypes of frontotemporal dementia. Lancet Neurol, 2008. 7(10): p. 965-74.
3. Mann, D.M.A. and J.S. Snowden, Frontotemporal lobar degeneration: Pathogenesis, pathology and pathways to phenotype. Brain Pathol, 2017. 27(6): p. 723-736.
4. Woollacott, I.O. and J.D. Rohrer, The clinical spectrum of sporadic and familial forms of frontotemporal dementia. J Neurochem, 2016. 138 Suppl 1: p. 6-31.
5. Chitramuthu, B.P., H.P.J. Bennett, and A. Bateman, Progranulin: a new avenue towards the understanding and treatment of neurodegenerative disease. Brain, 2017. 140(12): p. 3081-3104.
6. Young, A.L., Marinescu, R.V., Oxtoby, N.P., et al., Uncovering the heterogeneity and temporal complexity of neurodegenerative diseases with Subtype and Stage Inference. Nat Commun, 2018. 9(1): p. 4273.
7. Jiskoot, L.C., Panman, J.L., Meeter, L.H., et al., Longitudinal multimodal MRI as prognostic and diagnostic biomarker in presymptomatic familial frontotemporal dementia. Brain, 2019. 142(1): p. 193-208.
8. Jiskoot, L.C., Panman, J.L., van Asseldonk, L., et al., Longitudinal cognitive biomarkers predicting symptom onset in presymptomatic frontotemporal dementia. J Neurol, 2018.
9. Meeter, L.H., Dopper, E.G.P., Jiskoot, L.C., et al., Neurofilament light chain: a biomarker for genetic frontotemporal dementia. Ann Clin Transl Neurol, 2016. 3(8): p. 623-36.
10. van der Ende, E.L., Meeter, L.H., Poos, J.M., et al., Serum neurofilament light chain in genetic frontotemporal dementia: a longitudinal, multicentre cohort study. Lancet Neurol, 2019. 18(12): p. 1103-1111.
11. Rohrer, J.D., Nicholas, J.M., Cash, D.M., et al., Presymptomatic cognitive and neuroanatomical changes in genetic frontotemporal dementia in the Genetic Frontotemporal dementia Initiative (GENFI) study: a cross-sectional analysis. Lancet Neurol, 2015. 14(3): p. 253-62.
12. Donohue, M.C., Jacqmin-Gadda, H., Le Goff, M., et al., Estimating long-term multivariate progression from short-term data. Alzheimers Dement, 2014. 10(5 Suppl): p. S400-10.
13. Venkatraghavan, V., Bron, E.E., Niessen, W.J., et al., A discriminative event based model for Alzheimer's disease progression modelling. Information Processing in Medical Imaging, 2017: p. 121-133.
14. Fonteijn, H.M., Modat, M., Clarkson, M.J., et al., An event-based model for disease progression and its application in familial Alzheimer's disease and Huntington's disease. Neuroimage, 2012. 60(3): p. 1880-9.
15. Venkatraghavan, V., Bron, E.E., Niessen, W.J., et al., Disease progression timeline estimation for Alzheimer's disease using discriminative event based modeling. Neuroimage, 2019. 186: p. 518-532.
16. Rascovsky, K., Hodges, J.R., Knopman, D., et al., Sensitivity of revised diagnostic criteria for the behavioural variant of frontotemporal dementia. Brain, 2011. 134(Pt 9): p. 2456-77.
17. Gorno-Tempini, M.L., Hillis, A.E., Weintraub, S., et al., Classification of primary progressive aphasia and its variants. Neurology, 2011. 76(11): p. 1006-14.
18. Parmera, J.B., Rodriguez, R.D., Studart Neto, A., et al., Corticobasal syndrome: A diagnostic conundrum. Dement Neuropsychol, 2016. 10(4): p. 267-275.
19. Panman, J.L., Jiskoot, L.C., Bouts, M., et al., Gray and white matter changes in presymptomatic genetic frontotemporal dementia: a longitudinal MRI study. Neurobiol Aging, 2019. 76: p. 115-124.
20. Knopman, D.S., Kramer, J.H., Boeve, B.F., et al., Development of methodology for conducting clinical trials in frontotemporal lobar degeneration. Brain, 2008. 131(Pt 11): p. 2957-68.
21. Cummings, J.L., The Neuropsychiatric Inventory: comprehensive assessment of psychopathology in dementia. Neurology, 1994. 44(12): p. 2308-14.
22. Mioshi, E., Hsieh, S., Savage, S., et al., Clinical staging and disease progression in frontotemporal dementia. Neurology, 2010. 74(20): p. 1591-7.
23. Barandiaran, M., Moreno, F., de Arriba, M., et al., Longitudinal Neuropsychological Study of Presymptomatic c.709-1G>A Progranulin Mutation Carriers. J Int Neuropsychol Soc, 2019. 25(1): p. 39-47.

24. Jiskoot, L.C., Boccheta, M., Nicholas, J.M., et al., Presymptomatic white matter integrity loss in familial frontotemporal dementia in the GENFI cohort: A cross-sectional diffusion tensor imaging study. Ann Clin Transl Neurol, 2018. 5(9): p. 1025-1036.
25. Jenkinson, M., Beckmann, C.F., Behrens, T.E., et al., Fsl. Neuroimage, 2012. 62(2): p. 782-90.
26. Collins, D.L., Holmes, C.J., Peters, T.M., et al., Automated 3-D model-based neuroanatomical segmentation. Human Brain Mapping, 1995. 3(3): p. 190-208.
27. Mori, S., Wakana, S., van Zijl, P.C.M., et al., MRI atlas of Human White Matter. 2005, Amsterdam, the Netherlands: Elsevier.
28. Menke, R.A., Gray, E., Lu, C.H., et al., CSF neurofilament light chain reflects corticospinal tract degeneration in ALS. Ann Clin Transl Neurol, 2015. 2(7): p. 748-55.
29. Tomimoto, H., White matter integrity and cognitive dysfunction: Radiological and neuropsychological correlations. Geriatr Gerontol Int, 2015. 15 Suppl 1: p. 3-9.
30. Hase, Y., Horsburgh, K., Ihara, M., et al., White matter degeneration in vascular and other ageing-related dementias. J Neurochem, 2018. 144(5): p. 617-633.
31. Hardy, C.J., Buckley A.H., Downey, L.E., et al., The Language Profile of Behavioral Variant Frontotemporal Dementia. J Alzheimers Dis, 2016. 50(2): p. 359-71.
32. Ash, S., Nevler, N., Phillips, J., et al., A longitudinal study of speech production in primary progressive aphasia and behavioral variant frontotemporal dementia. Brain Lang, 2019. 194: p. 46-57.
33. Nevler, N., Ash, S., Jester, C., et al., Automatic measurement of prosody in behavioral variant FTD. Neurology, 2017. 89(7): p. 650-656.
34. Mesulam, M.M., Primary Progressive Aphasia and the Left Hemisphere Language Network. Dement Neurocogn Disord, 2016. 15(4): p. 93-102.
35. Staffaroni, A.M., Ljubenkov, P.A., Kornak, J., et al., Longitudinal multimodal imaging and clinical endpoints for frontotemporal dementia clinical trials. Brain, 2019. 142(2): p. 443-459.
36. Grossman, M., The non-fluent/agrammatic variant of primary progressive aphasia. Lancet Neurol, 2012. 11(6): p. 545-55.
37. Rohrer, J.D. and H.J. Rosen, Neuroimaging in frontotemporal dementia. Int Rev Psychiatry, 2013. 25(2): p. 221-9.
38. Sudre, C.H., Boccheta, M., Cash, D., et al., White matter hyperintensities are seen only in GRN mutation carriers in the GENFI cohort. Neuroimage Clin, 2017. 15: p. 171-180.
39. Bonvicini, C., Milanesi, E., Pilotto, A., et al., Understanding phenotype variability in frontotemporal lobar degeneration due to granulin mutation. Neurobiol Aging, 2014. 35(5): p. 1206-11.

APPENDIX A. BIOMARKERS

Biomarker selection

For biomarker selection, we extensively searched for relevant literature about presymptomatic FTD-*GRN* in Pubmed. We reviewed all empirical studies that included at least a presymptomatic *GRN* mutation carrier group. Next, we determined which biomarkers were frequently reported as abnormal in previous empirical studies and included these biomarkers accordingly, restricted to fluid biomarkers, grey matter brain regions, white matter tracts, and cognition. The selected biomarkers were: serum NfL [1-3], MMSE [4-6], cognitive domains of language, attention and processing speed, executive functioning, and social cognition [5, 7-9]; left and right volumes of the insula, frontal lobe, parietal lobe and the temporal lobe [4, 6, 10-21]; white matter tracts: left and right fractional anisotropy of anterior thalamic radiation, superior longitudinal fasciculus, uncinate fasciculus, and forceps minor [10, 17-19, 22, 23]. Although the *GRN* mutation affects plasma progranulin protein levels, these levels were not selected as biomarker, as research has shown that these remain stable in both the presymptomatic and symptomatic stage [6, 24].

MRI processing and ROI calculation

An overview of MRI acquisition parameters is presented in Appendix Table 1. The standard voxel-based morphometry pipeline from FSL [25-27] was used to process T1-weighted images. In brief, the brain was extracted from the images, and we carefully checked the brain extraction for missing brain tissue and areas of non-brain tissue, and adjusted the image accordingly. We corrected RF inhomogeneities by bias field correction with a Markov random field model and subsequently segmented the brain in grey matter, white matter, and cerebrospinal fluid images [28]. A study specific grey matter template was created in standard space using a balanced set of subjects, and all grey matter segmentations were registered to this template with non-linear registration, and then corrected for any local expansion or contraction by modulation of the Jacobian warp field [26]. Last, an isotropic Gaussian kernel with a sigma of 3mm was applied for smoothing of the grey matter images. Total intracranial volume (TIV) was calculated as the sum of the volumes from grey matter, white matter and cerebrospinal fluid in standard space. The structures from the MNI-atlas were used as grey matter ROIs. We extracted volumetric measurements from the ROIs by registering the structural MNI-atlas [29] to the grey matter images in standard space, and multiplying the grey matter density of the ROI with the total volume of the ROI, resulting in the grey matter volume within the ROI. Left and right regions were considered separately.

Diffusion tensor images were corrected for motion artefacts and eddy currents by alignment to the b=0 image, and subsequently, the tensor was fitted at each voxel to create fractional anisotropy (FA) images. The FA images were processed with the tract-based spatial statistics

(TBSS) pipeline as implemented in FSL [30]. Using non-linear registration, the images were aligned to the FMRIB58_FA template and then averaged into a mean FA image. The mean FA image was thresholded at 0.2 and thinned into a white matter skeleton. All individual FA images were projected onto this skeleton, resulting in skeletonized FA data for each participant. The probabilistic tracts from the Johns Hopkins University atlas [31] were applied as white matter ROIs to the skeleton mask, and the masked ROIs were used to extract FA values from the individual tracts. Left and right tracts were considered separately.

Table A.1. MRI acquisition protocols

	Rotterdam 1	**Rotterdam 2**	**Brescia**	**Barcelona**
N (s/p/nc)	3/22/24	5/9/6	7/17/0	1/6/1
Scanner	Philips Achieva 3T	Philips Achieva 3T	Siemens Skyra	Siemens Trio Tim
Head Coil	8 channel SENSE	32 channel SENSE	32 channel	64 channel
T1 weighted imaging				
TR	9.8 ms	6.8 ms	2000 ms	2000 ms
TE	4.6 ms	3.1 ms	2.9 ms	2.9 ms
FOV	224x168 mm	256x256 mm	282x282 mm	282x282 mm
Voxel size	0.88x0.88x1.2 mm	1.1mm^3	1.1 mm^3	1.1mm^3
Flip angle	8°	8°	8°	8°
Slices	140	207	208	208
Diffusion tensor imaging				
TR	8250 ms	7000 ms	7300 ms	7300 ms
TE	80 ms	69 ms	90 ms	90 ms
FOV	256x256 mm	240x240 mm	240x240 mm	240x240 mm
Voxel size	2x2x2mm	2.5x2.5x2.5mm	2.5x2.5x2.5mm	2.5x2.5x2.5mm
Slices	70	59	59	59
Directions	60	68	68	68
B-values	0/1000 s/mm^2	0/1000 s/mm^2	0/1000 s/mm^2	0/1000 s/mm^2

Numbers are subjects included after quality check. Abbreviations: s = symptomatic, p = presymptomatic, nc = non-carrier, TR = repetition time, TE = echo time, FOV = field of view.

Cognitive assessment

The following cognitive tests were performed, depending on the protocol from the local site. For language, the Boston Naming Task [32] and semantic fluency (animals) [33] were used. Tests concerning attention and processing speed were the Trail making test part A [34], Stroop part 1 and 2 [35], symbol substitution [36], letter digit substitution task [37], and forward digit span [36]. For executive functioning, we used Trail making test part B [34], Stroop task part 3 [35], phonological fluency [33] and digit span backwards [36]. Tests for social cognition were the Ekman faces test [38], emotion recognition from the mini social cognition and emotional assessment (MINI-SEA) [39], and Happé cartoon task [40]. Raw scores from tests in which a higher score indicates worse performance were reversed (i.e. Trail making test, Stroop). We transformed all raw test scores to z-scores, based on the mean and standard deviation of the non-carriers. Subsequently, cognitive domains were

Table A.2. Availability and characteristics of cognitive data

	Symptomatic						Presymptomatic	
	Total (n=35)*		bvFTD (n=17)		nfvPPA (n=16)		N=56	
	N	*Mean ± SD*	*N*	*Mean ± SD*	*N*	*Mean ± SD*	*N*	*Mean ± SD*
MMSE	29	-3.07 ± 1.50	15	-3.26 ± 1.69	14	-2.87 ± 1.28	55	0.22 ± 1.01
Language	32	-2.86 ± 1.37	16	-2.69 ± 1.58	14	-3.00 ± 1.24	55	0.28 ± 1.09
Boston naming test	25	-1.97 ± 1.32	13	-1.75 ± 1.44	12	-2.21 ± 1.19	55	0.57 ± 1.37
Semantic fluency	31	-3.28 ± 1.38	15	-3.14 ± 1.57	14	-3.45 ± 1.30	55	0.00 ± 1.31
Attention, concentration and mental processing speed	33	-2.35 ± 1.17	16	-2.43 ± 1.32	15	-2.26 ± 1.12	55	-0.05 ± 0.75
TMT-A	32	-2.65 ± 1.62	16	-2.91 ± 1.63	14	-2.23 ± 1.66	55	-0.01 ± 0.92
Stroop card 1&2	17	-3.05 ± 2.18	10	-2.96 ± 2.20	7	-3.18 ± 2.32	55	0.14 ± 1.02
LDST	4	-2.06 ± 1.59	2	-2.09 ± 1.99	2	-2.03 ± 1.90	17	0.22 ± 0.70
Symbol substitution	17	-2.35 ± 1.41	7	-3.01 ± 1.13	10	-1.89 ± 1.45	22	0.00 ± 1.29
Digit span forward	31	-1.66 ± 1.05	15	-1.41 ± 1.29	14	-1.95 ± 0.74	55	-0.26 ± 0.95
Executive functioning	32	-2.33 ± 0.97	15	-2.23 ± 1.19	15	-2.37 ± 0.79	55	-0.03 ± 0.75
TMT-B	28	-2.63 ± 0.97	13	-2.50 ± 1.11	13	-2.69 ± 0.89	55	0.03 ± 0.79
Stroop card 3	14	-3.84 ± 2.29	8	-3.73 ± 2.50	6	-3.98 ± 2.20	55	-0.36 ± 1.05
Phonological fluency	29	-2.12 ± 0.95	14	-1.92 ± 1.02	15	-2.30 ± 0.87	55	0.30 ± 1.36
Digit span backwards	30	-1.65 ± 1.14	15	-1.61 ± 1.44	13	-1.61 ± 0.75	55	-0.08 ± 1.11
Social cognition	15	-1.87 ± 0.76	7	-2.15 ± 0.92	8	-1.62 ± 0.52	51	-0.10 ± 1.02
Ekman faces	3	-0.70 ± 0.60	2	-0.37 ± 0.18	1	-1.36 ± N/A	26	0.14 ± 0.89
Mini-SEA Emotion Recognition	10	-1.98 ± 0.83	3	-2.65 ± 1.13	7	-1.69 ± 0.52	22	-0.62 ± 0.98
HappeTOM	5	-2.07 ± 0.86	4	-2.32 ± 0.75	1	-1.05 ± N/A	28	0.42 ± 0.77
Happe non TOM	5	-1.65 ± 0.81	4	-1.81 ± 0.84	1	-1.03 ± N/A	28	0.34 ± 1.20

Abbreviations: bvFTD = behavioural variant frontotemporal dementia, nfvPPA = non-fluent variant primary progressive aphasia, MMSE = mini mental state examination, TMT = trail making test, LDST = letter digit substitution task, mini-SEA = mini social cognition and emotional assessment, TOM = theory of mind. Values are mean z-scores ± standard deviation based on non-carriers, uncorrected for confounding factors. * The two remaining participants presented with cortico-basal degeneration.

composed as the mean z-score of all available tests within that domain per individual, disregarding missing tests.

Biomarker statistics

Before modelling, we checked skewed distributions in the biomarkers with the following graphs and tests: histograms, q-q plots, skewness and kurtosis values (values between 2 and −2 indicate normality), Kolmogorov-Smirnov and Shapiro-Wilk's tests (values above 0.05 indicate normality). When three or more tests indicated skewness, the distributions were adjusted using log-transformations (log10), i.e. neurofilament light chain levels, MMSE, BNT, Trail Making Test, Stroop, facial emotion recognition. In the case of cognitive tests, log-transformation was performed before transforming raw scores to z-scores.

Biomarker characteristics and statistical differences between groups are presented in Table A.3. Symptomatic mutation carriers had higher NfL levels, lower grey matter volumes, impaired white matter microstructure, and worse cognitive functions than both presymptomatic mutation carriers and non-carriers in all selected biomarkers. Post-hoc analysis revealed that these differences in biomarkers were specifically driven by the bvFTD patients. For nfvPPA patients, we found higher NfL levels and worse cognitive performance than both presymptomatic mutation carriers and non-carriers. NfvPPA patients showed smaller grey matter volumes than both presymptomatic mutation carriers and non-carriers, especially in left-sided ROIs, and lower fractional anisotropy levels in the left anterior thalamic radiation, left uncinate fasciculus, and the forceps minor. The volume of the right frontal lobe was smaller in nfvPPA patients compared with presymptomatic mutation carriers. Furthermore, bvFTD patients had smaller volumes of the right frontal and temporal lobe than nfvPPA patients, and lower fractional anisotropy values in the forceps minor, left superior longitudinal fasciculus and right uncinate fasciculus. There were no differences in any of the selected biomarkers between presymptomatic mutation carriers and non-carriers.

Table A.3. Biomarker characteristics after correction for confounding factors

		Symptomatic			Presymptomatic
		Total	bvFTD	nfvPPA	
Neurofilament light chain		1.90 ± 0.25*	1.89 ± 0.23*	1.91 ± 0.28†	1.10 ± 0.22
GM volume	*Left frontal lobe*	-2.75 ± 1.8*	-3.42 ± 2.06*	-2.46 ± 1.40†	0.30 ± 0.65
	Right frontal lobe	-1.72 ± 1.79*	-2.76 ± 1.43*,‡	-0.93 ± 1.79§	0.30 ± 0.65
	Left insula	-2.32 ± 1.56*	-2.45 ± 1.79*	-2.35 ± 1.51†	-0.32 ± 0.95
	Right insula	-1.02 ± 1.13*	-1.47 ± 1.26*	-0.74 ± 0.98	-0.08 ± 0.84
	Left parietal lobe	-1.87 ± 1.11*	-2.18 ± 1.39*	-1.74 ± 0.84†	-0.03 ± 1.02
	Right parietal lobe	-1.19 ± 2.00*	-1.42 ± 2.08*	-0.89 ± 2.15	-0.06 ± 0.96
	Left temporal lobe	-2.97 ± 2.42*	-3.21 ± 2.59*	-2.98 ± 2.51†	-0.19 ± 0.96
	Right temporal lobe	-1.14 ± 2.66*	-2.22 ± 3.40*,‡	-0.12 ± 1.69	-0.08 ± 0.94
FA	*Left anterior thalamic radiation*	-2.28 ± 1.34*	-2.73 ± 1.60*	-1.77 ± 0.98†	-0.33 ± 0.95
	Right anterior thalamic radiation	-1.24 ± 1.23*	-1.78 ± 1.51*	-0.66 ± 0.66	-0.27 ± 0.77
	Forceps Minor	-3.00 ± 1.52*	-4.01 ± 1.52*,‡	-2.08 ± 0.96†	0.46 ± 0.93
	Left superior longitudinal fasciculus	-1.50 ± 1.39*	-2.42 ± 1.28*,‡	-0.61 ± 0.96	0.02 ± 0.88
	Right superior longitudinal fasciculus	-1.14 ± 1.12*	-1.47 ± 1.14*	-0.74 ± 1.06	-0.11 ± 0.60
	Left uncinate fasciculus	-2.63 ± 1.15*	-3.00 ± 1.43*	-2.29 ± 0.88†	-0.35 ± 0.86
	Right uncinate fasciculus	-1.92 ± 2.16*	-3.19 ± 2.07*,‡	-0.77 ± 1.74	-0.51 ± 1.12
MMSE		-2.71 ± 1.19*	-2.71 ± 1.28*	-2.71 ± 1.14†	0.06 ± 0.91
Attention and processing speed		-2.06 ± 1.09*	-2.11 ± 1.15*	-2.05 ± 1.12†	-0.22 ± 0.65
Executive functioning		-2.12 ± 0.88*	-2.00 ± 0.99*	-2.24 ± 0.82†	-0.14 ± 0.72
Language		-2.54 ± 1.23*	-2.35 ± 1.33*	-2.84 ± 1.17†	0.13 ± 0.97
Social cognition		-1.89 ± 0.64*	-2.13 ± 0.74*	-1.52 ± 0.42†	-0.19 ± 0.96

Abbreviations: bvFTD = behavioural variant frontotemporal dementia, nfvPPA = non-fluent variant primary progressive aphasia, GM volume = grey matter volume, FA = fractional anisotropy, MMSE = Mini Mental State Examination. Values are mean z-score (based on non-carriers) ± standard deviation, after correction for confounding factors of age, gender, MRI protocol, and years of education.

* Both the entire group of symptomatic mutation carriers and only bvFTD patients significantly differed from presymptomatic mutation carriers as well as non-carriers ($p<0.05$, corrected)

† Significant difference between nfvPPA patients and presymptomatic mutation carriers as well as non-carriers ($p<0.05$, corrected)

‡ Significant difference between bvFTD patients and nfvPPA patients ($p<0.05$, corrected)

¶ Significant difference between nfvPPA patients and presymptomatic mutation carriers ($p<0.05$, corrected)

REFERENCES

1. Meeter, L.H., et al., Neurofilament light chain: a biomarker for genetic frontotemporal dementia. Ann Clin Transl Neurol, 2016. 3(8): p. 623-36.
2. Rohrer, J.D., et al., Serum neurofilament light chain protein is a measure of disease intensity in frontotemporal dementia. Neurology, 2016. 87(13): p. 1329-36.
3. van der Ende, E.L., et al., Serum neurofilament light chain in genetic frontotemporal dementia: a longitudinal, multicentre cohort study. Lancet Neurol, 2019. 18(12): p. 1103-1111.
4. Rohrer, J.D., et al., Presymptomatic cognitive and neuroanatomical changes in genetic frontotemporal dementia in the Genetic Frontotemporal dementia Initiative (GENFI) study: a cross-sectional analysis. Lancet Neurol, 2015. 14(3): p. 253-62.
5. Jiskoot, L.C., et al., Longitudinal cognitive biomarkers predicting symptom onset in presymptomatic frontotemporal dementia. J Neurol, 2018.
6. Benussi, A., et al., Clinical and biomarker changes in presymptomatic genetic frontotemporal dementia. Neurobiol Aging, 2019. 76: p. 133-140.
7. Barandiaran, M., et al., Neuropsychological features of asymptomatic c.709-1G>A progranulin mutation carriers. J Int Neuropsychol Soc, 2012. 18(6): p. 1086-90.
8. Barandiaran, M., et al., Longitudinal Neuropsychological Study of Presymptomatic c.709-1G>A Progranulin Mutation Carriers. J Int Neuropsychol Soc, 2019. 25(1): p. 39-47.
9. Jiskoot, L.C., et al., Presymptomatic cognitive decline in familial frontotemporal dementia: A longitudinal study. Neurology, 2016. 87(4): p. 384-91.
10. Borroni, B., et al., Brain magnetic resonance imaging structural changes in a pedigree of asymptomatic progranulin mutation carriers. Rejuvenation Res, 2008. 11(3): p. 585-95.
11. Cash, D.M., et al., Patterns of gray matter atrophy in genetic frontotemporal dementia: results from the GENFI study. Neurobiol Aging, 2017. 62: p. 191-196.
12. Premi, E., et al., Subcortical and Deep Cortical Atrophy in Frontotemporal Dementia due to Granulin Mutations. Dement Geriatr Cogn Dis Extra, 2014. 4(1): p. 95-102.
13. Young, A.L., et al., Uncovering the heterogeneity and temporal complexity of neurodegenerative diseases with Subtype and Stage Inference. Nat Commun, 2018. 9(1): p. 4273.
14. Jacova, C., et al., Anterior brain glucose hypometabolism predates dementia in progranulin mutation carriers. Neurology, 2013. 81(15): p. 1322-31.
15. Popuri, K., et al., Gray matter changes in asymptomatic C9orf72 and GRN mutation carriers. Neuroimage Clin, 2018. 18: p. 591-598.
16. Moreno, F., et al., Distinctive age-related temporal cortical thinning in asymptomatic granulin gene mutation carriers. Neurobiol Aging, 2013. 34(5): p. 1462-8.
17. Dopper, E.G., et al., Structural and functional brain connectivity in presymptomatic familial frontotemporal dementia. Neurology, 2014. 83(2): p. e19-26.
18. Jiskoot, L.C., et al., Longitudinal multimodal MRI as prognostic and diagnostic biomarker in presymptomatic familial frontotemporal dementia. Brain, 2019. 142(1): p. 193-208.
19. Panman, J.L., et al., Gray and white matter changes in presymptomatic genetic frontotemporal dementia: a longitudinal MRI study. Neurobiol Aging, 2019. 76: p. 115-124.
20. Pievani, M., et al., Pattern of structural and functional brain abnormalities in asymptomatic granulin mutation carriers. Alzheimers Dement, 2014. 10(5 Suppl): p. S354-S363 e1.
21. Caroppo, P., et al., Lateral Temporal Lobe: An Early Imaging Marker of the Presymptomatic GRN Disease? J Alzheimers Dis, 2015. 47(3): p. 751-9.
22. Jiskoot, L.C., et al., Presymptomatic white matter integrity loss in familial frontotemporal dementia in the GENFI cohort: A cross-sectional diffusion tensor imaging study. Ann Clin Transl Neurol, 2018. 5(9): p. 1025-1036.
23. Olm, C.A., et al., Longitudinal structural gray matter and white matter MRI changes in presymptomatic progranulin mutation carriers. Neuroimage Clin, 2018. 19: p. 497-506.
24. Meeter, L.H., et al., Progranulin Levels in Plasma and Cerebrospinal Fluid in Granulin Mutation Carriers. Dement Geriatr Cogn Dis Extra, 2016. 6(2): p. 330-340.
25. Douaud, G., et al., Anatomically related grey and white matter abnormalities in adolescent-onset schizophrenia. Brain, 2007. 130(Pt 9): p. 2375-86.
26. Jenkinson, M., et al., Fsl. Neuroimage, 2012. 62(2): p. 782-90.
27. Smith, S.M., et al., Advances in functional and structural MR image analysis and implementation as FSL. Neuroimage, 2004. 23 Suppl 1: p. S208-19.

28. Zhang, Y., M. et al, Segmentation of brain MR images through a hidden Markov random field model and the expectation-maximization algorithm. IEEE Trans Med Imaging, 2001. 20(1): p. 45-57.
29. Collins, D.L., et al, Automated 3-D model-based neuroanatomical segmentation. Human Brain Mapping, 1995. 3(3): p. 190-208.
30. Smith, S.M., et al., Tract-based spatial statistics: voxelwise analysis of multi-subject diffusion data. Neuroimage, 2006. 31(4): p. 1487-505.
31. Mori, S., et al, MRI atlas of Human White Matter. 2005, Amsterdam, the Netherlands: Elsevier.
32. Kaplan, E., et al, Boston Naming Test. 1983, Philadelphia: Lea & Febiger.
33. Thurstone, L.L., et al, Primary Mental Abilities. 1962, Chicago: University of Chicago Press.
34. Army individual test battery. Manual of directions and scoring. 1944, Washington, DC: War Department, Adjunct General's Office.
35. Stroop, J., Studies of interference in serial verbal reaction. Journal of Experimental Psychology, 1935. 18: p. 643-662.
36. Wechsler, D., WAIS-III Technische Handleiding. 2005, Amsterdam: Harcourt Test Publishers.
37. Jolles, J., et al, Maastricht aging study: Determinants of cognitive aging. 1995, Maastricht: Neuropsych Publishers.
38. Ekman, P., et al., Pictures of facial affect 1976, Palo Alto, CA: Consulting Psychological Press.
39. Funkiewiez, A., et al., The SEA (Social cognition and Emotional Assessment): a clinical neuropsychological tool for early diagnosis of frontal variant of frontotemporal lobar degeneration. Neuropsychology, 2012. 26(1): p. 81-90.
40. Happe, F., H. et al, Acquired 'theory of mind' impairments following stroke. Cognition, 1999. 70(3): p. 211-40.

APPENDIX B – DISCRIMINATIVE EVENT BASED MODELLING

DEBM: Gaussian mixture modelling

DEBM uses Gaussian mixture modelling to transform biomarker values to posterior probabilities of them being abnormal. This is done by assuming the probability density functions of normal and abnormal values are represented by Gaussians $N(\mu_{\sim E}, \sigma_{\sim E})$ and $N(\mu_E, \sigma_E)$ respectively, where the occurrence of the biomarker abnormality event is denoted by E and the absence of such an event is denoted by $\sim E$.

Gaussian mixture modelling is an optimisation task to estimate these normal and abnormal Gaussians as well as the mixing parameter based on maximum log-likelihood, where the log-likelihood for biomarker B is computed as the summation over all *GRN* mutation carriers in the dataset as follows:

$$L_B = \sum_{\forall j \in Carriers} \log f(B_j)$$

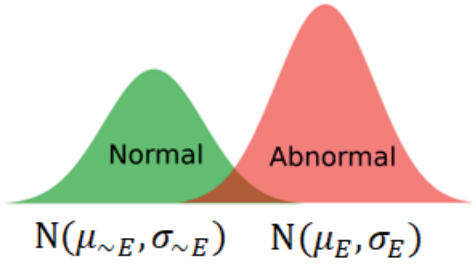

Figure B.1:
Illustrations of the Gaussian probability density functions for normal and abnormal values of biomarker B

Here, the likelihood $f(B)$ is computed as follows:

$$f(B) = \theta_{\sim E} p(B|\mu_{\sim E}, \sigma_{\sim E}) + \theta_E p(B|\mu_E, \sigma_E),$$

Where $\theta_{\sim E} + \theta_E = 1$, and the mixing parameters $\theta_{\sim E}$ and θ_E show the relative proportions of the two Gaussians in the dataset. The abnormal Gaussian is initialized using the mean and standard deviation of the symptomatic subjects, while the normal Gaussian is initialized using the non-carriers. Since non-carriers are healthy controls, we fix $\mu_{\sim E}$ and $\sigma_{\sim E}$ to their initialized values and only optimize the remaining parameters in the Gaussian mixture model. The mixing parameter and the Gaussian parameters are optimized alternately until convergence as detailed previously,[1].

For imaging-biomarkers with left and right counter parts, we propose a novel modification to the Gaussian mixture model optimization called Siamese Gaussian mixture model (Siamese GMM). We propose to jointly optimize the parameters of these biomarkers, by taking advantage of symmetry in the brain. The log-likelihood for the joint optimization for the imaging biomarkers $\boldsymbol{I^L}$ and $\boldsymbol{I^R}$is given below:

$$\boldsymbol{L_I = \sum_{\forall j \in Carriers} \log f\left(I^L{}_j\right) + \log f\left(I^R{}_j\right)}$$

where $\boldsymbol{f\left(I^L{}_j\right)}$ and $\boldsymbol{f\left(I^R{}_j\right)}$ are expressed mathematically as:

$$\boldsymbol{f\left(I^L{}_j\right) = \theta^L_{\sim E} p\left(I^L{}_j \middle| \mu_{\sim E}, \sigma_{\sim E}\right) + \theta^L_E p\left(I^L{}_j \middle| \mu_E, \sigma_E\right)}$$

$$\boldsymbol{f\left(I^R{}_j\right) = \theta^R_{\sim E} p\left(I^R{}_j \middle| \mu_{\sim E}, \sigma_{\sim E}\right) + \theta^R_E p\left(I^R{}_j \middle| \mu_E, \sigma_E\right)}$$

$\boldsymbol{\theta^L_{\sim E} + \theta^L_E = 1}$ and $\boldsymbol{\theta^R_{\sim E} + \theta^R_E = 1}$. The mixing parameters ($\boldsymbol{\theta^L_{\sim E}, \theta^L_E, \theta^R_{\sim E}, \theta^R_E}$) and the abnormal Gaussian parameters ($\boldsymbol{\mu_E}$, $\boldsymbol{\sigma_E}$) are again optimized alternately until convergence,[1]. This joint optimization of the left and right counter parts by sharing the normal and abnormal Gaussians reduces the number of parameters to be optimized, and thus improves the robustness. In case of asymmetrical atrophy patterns, where one of the biomarkers is stronger than the other, the joint optimization also helps in making the GMM more stable for the weaker biomarker.

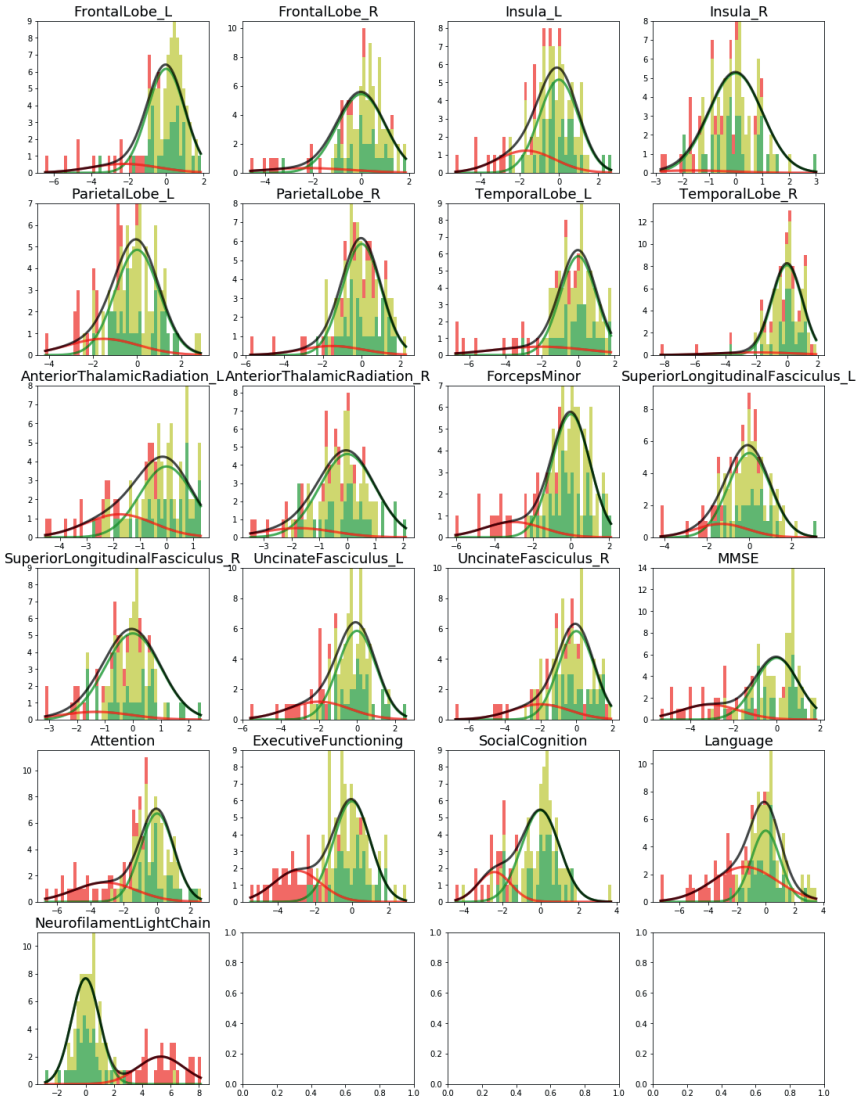

Figure B.2. Gaussian mixture modelling distributions. The histogram bins are divided in three colours, where the green part shows the proportion of non-carriers, the yellow part shows the proportion of presymptomatic carriers and the red part shows the proportion of symptomatic carriers. The Gaussians shown here are the ones that were estimated using Gaussian mixture modelling, where the green Gaussian is the normal one estimated using non-carriers and the red Gaussian is the abnormal one estimated using the carriers. The amplitudes of these Gaussians are based on the estimated mixing parameter. The grey curve shows the total estimated distribution, which is the summation of green and red Gaussians.

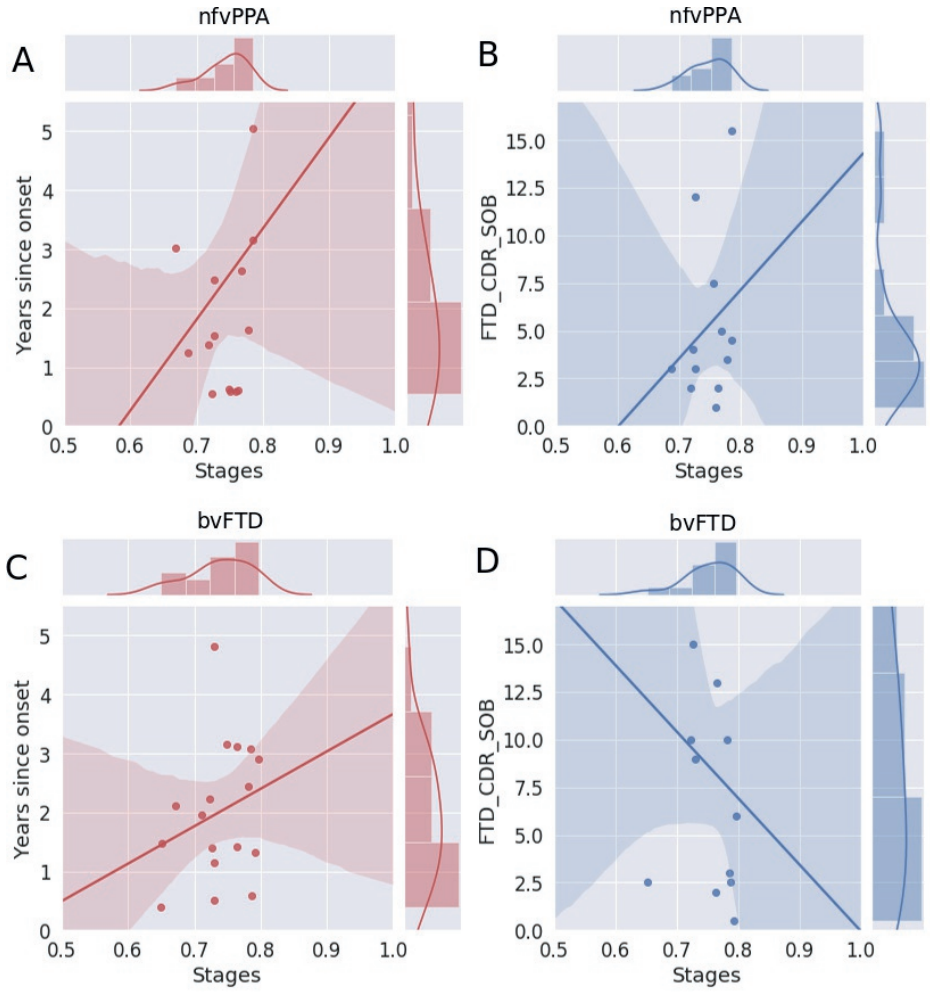

Figure B.3. Correlation of disease severity (as estimated by non-imaging DEBM using cross-validation) with years since onset and FTD-CDR-SOB. The 2D scatter plots in figures A and C show the correlations of disease severity with years since onset, for symptomatic nfvPPA and bvFTD subjects respectively. The 2D scatter plot in figures B and D show the correlations of disease severity with FTD-CDR-SOB. The plot on top of each subfigure shows the probability density function of the disease stages. The plots on the right of figures A and C show the probability density functions of years since symptom onset. The plots on the right of figures B and D show the probability density function of FTD-CDR-SOB.

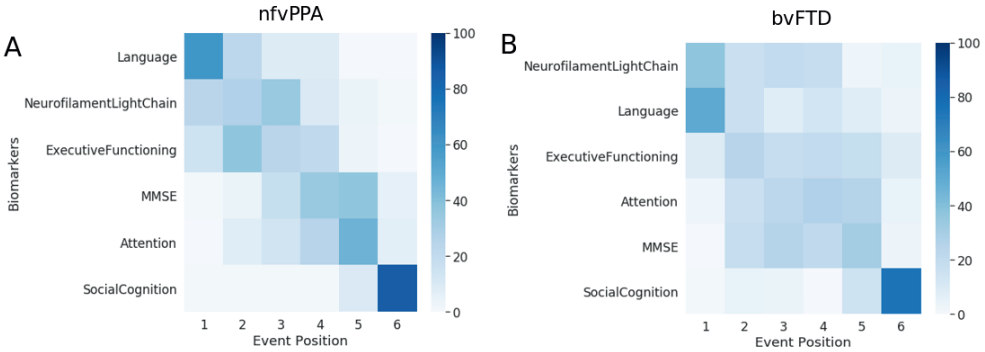

Figure B.4. Cascade of non-imaging biomarker changes in nfvPPA (A) and bvFTD (B) subjects along with the uncertainty associated with it. The biomarkers are ordered based on the position in the estimated cascade. The color-map is based on the number of times a biomarker is at a position in 100 repetitions of bootstrapping.

REFERENCES

1. Venkatraghavan, V., et al, Disease progression timeline estimation for Alzheimer's disease using discriminative event based modeling. Neuroimage, 2019. 186: p. 518-532.

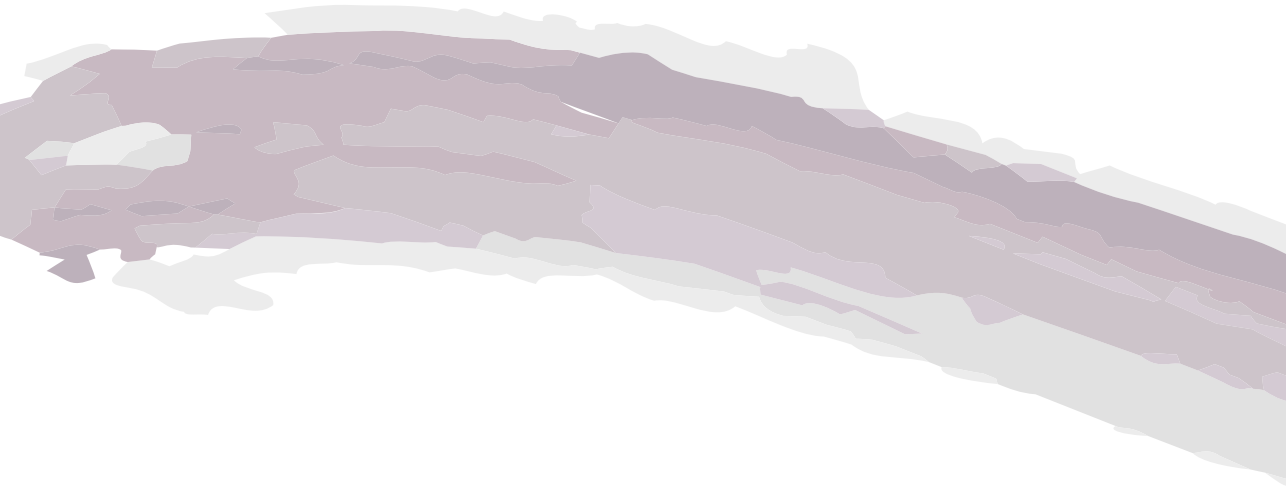

Chapter 2.2

Cognition and gray and white matter characteristics of presymptomatic *C9orf72* repeat expansion

Papma, J.M.*
Jiskoot, L.C*.
Panman, J.L.
Dopper, E.G.P.
den Heijer, T.
Donker Kaat, L.
Pijnenburg, Y.A.L.
Meeter, L.H.
van Minkelen, R.
Rombouts, S.A.R.B.
van Swieten, J.C.

* these authors contributed equally to this work

Neurology, 2017

ABSTRACT

Objective: To investigate cognitive function, gray matter volume, and white matter integrity in the presymptomatic stage of chromosome 9 open reading frame 72 repeat expansion (*C9orf72RE*).

Methods: Presymptomatic *C9orf72RE* carriers (n=18) and first-degree family members without a pathogenic expansion (healthy controls HC, n=15) underwent a standardized protocol of neuropsychological tests, T1-weighted MRI, and diffusion tensor imaging within our cohort study of autosomal dominant frontotemporal dementia (FTD). We investigated group differences in cognitive function, gray matter volume through voxel-based morphometry, and white matter integrity by means of tract-based spatial statistics. We correlated cognitive change with underlying gray or white matter.

Results: Our data demonstrate lower scores on letter fluency, Stroop card I, and Stroop card III, accompanied by white matter integrity loss in tracts connecting the frontal lobe, the thalamic radiation, and tracts associated with motor functioning in presymptomatic *C9orf72RE* compared with HC. In a subgroup of *C9orf72RE* carriers above 40 years of age, we found gray matter volume loss in the thalamus, cerebellum, and parietal and temporal cortex. We found no significant relationship between subtle cognitive decline and underlying gray or white matter.

Conclusions: This study demonstrates that a decline in cognitive functioning, white matter integrity, and gray matter volumes are present in presymptomatic *C9orf72RE* carriers. These findings suggest that neuropsychological assessment, T1-weighted MRI, and diffusion tensor imaging might be useful to identify early biomarkers in the presymptomatic stage of FTD or amyotrophic lateral sclerosis.

INTRODUCTION

The pathogenic chromosome 9 open reading frame 72 repeat expansion (*C9orf72RE*) underlies the majority of familial frontotemporal dementia (FTD) and amyotrophic lateral sclerosis (ALS) [1]. The clinical presentation is variable, comprising behavioral variant FTD (bvFTD) or ALS as well as prominent neuropsychiatric symptoms and episodic memory disorders [2–4]. In accordance, neuroimaging studies have shown a variable pattern of both cortical and subcortical gray matter atrophy involving frontal, temporal, and parietal regions, the cerebellum, and the thalamus [5–10]. Scarce diffusion tensor imaging (DTI) studies indicated white matter degeneration localized in the cingulum, corticospinal tract, corpus callosum, and cerebellar peduncle in *C9orf72RE* patients [8,11–13]. The field of disease-modifying treatment in FTD and ALS, and particularly in *C9orf72RE* related disease [14], shows important progress. Ideally, a therapy would be instituted early in the disease process, when neurodegeneration is still limited. This increases the need for markers that identify early disease-related changes and track disease progression. When studying early markers in autosomal dominant disease, the presymptomatic stage offers unique opportunities [15–18]. Studies into the presymptomatic stage of *C9orf72RE*-associated FTD or ALS are scarce, but have shown evidence for behavioral changes [17], and gray matter volume loss in temporal, parietal, frontal, and cerebellar regions [17,18], though this was contradicted by an absence of atrophy in a study of 7 presymptomatic *C9orf72RE* carriers [10]. In order to expand the knowledge on biomarkers for early-stage *C9orf72RE*, the present study examines presymptomatic cognition and gray and white matter through neuropsychological assessment, T1-weighted MRI, and DTI in a standardized cohort study of autosomal dominant FTD [15,16]. We furthermore relate presymptomatic *C9orf72RE* cognitive changes to underlying gray or white matter to enable early anatomical pinpointing of the clinical heterogeneity in *C9orf72RE*.

METHODS

Participants. Between July 2013 and January 2017, we recruited 33 healthy at-risk first-degree family members of 12 Dutch pedigrees with an autosomal dominant inheritance pattern and the *C9orf72RE*. The clinical diagnosis in affected family members was bvFTD in 7 families, bvFTD and FTD-ALS in 3 families, bvFTD and ALS in 1 family, and FTDALS in 1 family (Appendix Table A1). All participants underwent a standardized workup including MRI of the brain [15], neuropsychological assessment [16], neuropsychiatric and behavioral questionnaires, physical and neurologic examination, and a structured interview with a knowledgeable informant (e.g., siblings, spouses) covering functional, cognitive, behavioral, or neuropsychiatric changes in daily living. We defined participants as presymptomatic

when established criteria for FTD or ALS were not fulfilled [19,20], i.e., an absence of cognitive disorders on neuropsychological testing, an absence of significant behavioral/ neuropsychiatric changes (see Rascovsky et al., [20]) reported during a structured interview with knowledgeable informants or questionnaires, and an absence of signs of motor neuron disease during neurologic examination. Two participants were included in the Genetic Frontotemporal Dementia Initiative (GENFI) cohort study [17].

Genetic analysis. Venipuncture for DNA isolation was performed at study entry. The presence of the GGGGCC hexanucleotide repeat expansion in *C9orf72* was established by long-range PCR and tandem repeat-primed PCR analyses, as described before [1]. The presence of more than 30 repeats in *C9orf72* was considered pathogenic in this research setting, as this is rare in the healthy population [21]. Based on this analysis, we assigned the participants to the *C9orf72RE* carrier (n=18) or healthy control (HC) group (n=15). Standard protocol approvals, registrations, and patient consents. Investigators and participants were blind to the genetic status of the participants, unless participants underwent predictive testing (2 participants). The study was approved by the Medical and Ethical Review Committee of the Erasmus Medical Center and written informed consent was obtained from all participants.

Neuropsychological assessment. Trained neuropsychologists (L.C.J., J.L.P.) administered a standardized battery of neuropsychological tests and neuropsychiatric and behavioral questionnaires. The battery [16] covered the following cognitive domains: global cognitive functioning using Mini-Mental State Examination (MMSE) and Frontal Assessment Battery (FAB); language through the 60-item Boston Naming Test, Semantic Association Test verbal subtask, categorical (animals) and letter fluency; attention using the Trail Making Test (TMT) A, Stroop color word test card I and II (Stroop I and II), and Letter Digit Substitution Test; executive functioning by means of TMT B and Stroop III; the memory domain using the Dutch version of the Rey Auditory Verbal Learning Test learning and recall, and Wechsler Adult Intelligence Scale (WAIS)–III digit span total; visuoconstruction using Royall clock drawing test and WAIS-III block design; and social cognition through the Happé cartoon task and Ekman 60 Faces Test. We standardized all raw neuropsychological test scores by converting them to z scores (individual test score minus mean of HC, divided by SD of HC) and created composite domain scores. The presence of neuropsychiatric and behavioral symptoms was investigated using Beck Depression Inventory (BDI) [16], Neuropsychiatric Inventory (NPI) [22], and Cambridge Behavioural Inventory–Revised (CBI-R) [23].

MRI acquisition and preprocessing. We acquired whole brain T1-weighted MRI and DTI scans on a Philips (Best, the Netherlands) 3.0T Achieva MRI scanner, using an 8-channel or 32-channel (in 5 cases) SENSE head coil, with the same scanning measures as described in our previous study [15]. FSL was used for imaging analyses, i.e., voxel-based morphometry (VBM) for T1-weighted images and tract-based spatial statistics (TBSS) for DTI (FMRIB's

Software Library; fmrib.ox.ac.uk). We performed preprocessing of T1-weighted images through brain extraction followed by tissue segmentation and alignment to Montreal Neurological Institute 152 standard space using nonlinear registration. A study-specific template with a balanced set of *C9orf72RE* carriers and HC was created and native gray matter images were nonlinearly re-registered to this template. The registered partial volume images were modulated to correct for local expansion or contraction by dividing by the Jacobian of the warp field. These modulated gray matter images were smoothed with an isotropic Gaussian kernel with a sigma of 4 mm, corresponding with a full width at half maximum kernel of 9 mm. We corrected diffusion tensor images for motion artefacts and eddy current by alignment to the b0 image using the FMRIB Diffusion Toolbox. Images were nonlinearly registered to a study-specific template. The tensor was fitted at each voxel using DTIFIT to create fractional anisotropy (FA) images. We created and thinned a mean FA image to obtain a skeleton containing the center of all tracts. Individual FA data were projected onto this skeleton, resulting in skeletonized FA data for each participant, fed into voxel-wise statistics. Mean diffusivity (MD), radial diffusivity (RD), and axial diffusivity (AxD) were then projected onto the white matter skeleton, using the skeleton projection vectors estimated in the FA analysis.

Neuroimaging analysis. We performed permutation-based testing using 5,000 permutations, and created 2 separate models for 2-sample t tests (carriers vs HC) for gray matter volume or white matter diffusion measures, with age, sex, and when applicable head coil as covariates. Due to an acquisition artefact, one DTI scan could not be used in our analyses (carrier). In FSL, we performed 2 separate within-group correlation analyses between z scores of neuropsychological tests differing between carriers and HC at $p<0.05$, gray matter or white matter. In these cognition–neuroimaging correlation analyses, an additional covariate for education was added. The significance level was set at $p<0.05$ (2-tailed), corrected for multiple comparisons (family-wise error [FWE]), using threshold-free cluster enhancement. We used the Harvard–Oxford cortical structural atlas and the Johns Hopkins University DTI-based white matter atlas implemented in FSL.

Neuropsychological and neuroimaging analyses in carriers and HC >40 years of age. We performed group comparisons in a subgroup of carriers and HC >40 years of age, i.e., closer to clinical onset age (n=13 *C9orf72RE* carriers, and n=11 HC) [17,24] for neuropsychological tests and gray and white matter analyses. Due to an acquisition artefact, one DTI scan could not be used in the analysis (i.e., n=12 *C9orf72RE* carriers).

Statistical analysis. Statistical analyses on neuropsychological and demographic data were performed with SPSS Statistics 21.0 (SPSS Inc., Chicago, IL). We analyzed demographic data using 2-sample t tests or Pearson x2 tests. We found a left skewed distribution for the Royall clock drawing test, MMSE, and FAB, and a right-skewed distribution for the NPI, BDI,

and CBI-R. We reported the median and interquartile ranges and performed Mann-Whitney U tests. In order to meet criteria for normality, we replaced one extreme outlier in the TMT-B by the highest test scores (88 seconds) added up with 10 seconds. Given the left-skewed distribution of the Royall clock drawing test, the domain visuoconstruction consisted only of z scores of WAIS-III block design. Z-scores for neuropsychological data were compared between groups by means of one-way analysis of covariance with age, sex, and education level as covariates. We set the significance level at $p<0.05$ (2-tailed) across all comparisons, with Bonferroni correction for multiple comparisons.

RESULTS

Demographic data. In *C9orf72RE* carriers and HC, the age range was distributed equally, with respectively 5 and 4 participants <40 years. MMSE, FAB, and neuropsychiatric or behavioral measures did not differ between groups (table 1). For details on the presence of neuropsychiatric symptoms on NPI, see Appendix table A2. Physical and neurologic examination in our participants did not show abnormalities, specifically signs of motor neuron disease.

Neuropsychological assessment. None of the participants performed at disorder level (i.e., ≥2 SD below normative data mean). *C9orf72RE* carriers had lower scores than HC on letter fluency, Stroop I, and Stroop III (see table 2). In the subgroup analysis of presymptomatic *C9orf72RE* carriers and HC over 40 years of age, we found no between-group differences (see table e-3). At a Bonferroni-corrected threshold, there were no differences between groups for neuropsychological tests or composite domain scores.

Gray matter volume and white matter integrity. Whole-brain TBSS analyses demonstrated lower FA and higher RD in *C9orf72RE* carriers compared with HC within the right superior corona radiata, the right inferior longitudinal fasciculus, the right uncinated fasciculus, the bilateral anterior thalamic radiation, the corticospinal tract, and the right internal and external capsule (figure 1 and table 3). In the subgroup analysis over 40 years of age, we found no differences for white matter measures at a threshold of FWE ($p<0.05$). We did find results for FA at a less stringent threshold of FWE ($p<0.15$) (figure 2 and table 3). Whole-group VBM analyses revealed no gray matter volume differences between *C9orf72RE* carriers and HC. When we confined our analyses to a subgroup >40 years of age, *C9orf72RE* carriers showed lower gray matter volume in the right inferior temporal gyrus, right cerebellum (VI), left postcentral and precentral gyrus, the left superior parietal lobe, and the left thalamus compared with HC (figure 2 and table 3). Vice versa, we found no gray or white matter changes in HC compared with *C9orf72RE* carriers.

Relationship between neuropsychological assessment and gray or white matter. We found no

Table 1. Demographic data of *C9orf72RE* carriers and HC

	C9orf72RE carriers (n=18)	HC (n=15)	**P value**
Age (years)	45.8 (13.8)	47.8 (13.3)	0.689
Sex, female (%)	15 (83.3)	8 (53.3)	0.062
Education (Verhage[1])	5.6 (0.8)	5.5 (0.8)	0.784
Mean age of family onset (years)	53.0 (5.3)	53.5 (4.6)	0.804
Presence of motor neuron disease signs (%)*	0 (0.0)	0 (0.0)	-
MMSE	30.0 (1)	29.5 (1)	0.630
FAB	17.0 (1)	17.5 (2)	0.602
NPI*	0 (1)	0 (0)	0.655
BDI*	3.0 (13)	3.0 (8)	0.455
CBI-R*	1 (6)	0 (5)	0.455

Values indicate: mean ± standard deviation, number (percentage), or in case of MMSE, FAB, NPI, BDI, CBI-R: median (interquartile range). Abbreviations: MMSE, Mini-Mental State Examination; FAB, Frontal Assessment Battery; NPI, Neuropsychiatric Inventory; BDI, Beck Depression Inventory; CBI-R, Cambridge Behavioural Inventory Revised. *Missing data for presence of motor neuron disease signs in one HC, for FAB in one carrier, for NPI in one carrier, for BDI in one carrier, for CBI-R in one HC. [1]Dutch educational system categorized into levels from 1 = less than 6 years of primary education to 7 = academic schooling. P value by means of 2-sample t-test or chi-square test. MMSE, FAB, NPI, BDI and CBI-R data was not normally distributed and P-values were calculated by means of Mann-Whitney U test.

correlation between letter fluency, Stroop I, or Stroop III and gray or white matter volumes within the whole group of *C9orf72RE* carriers or HC.

DISCUSSION

In this study, we demonstrate lower cognitive test performance for letter fluency, Stroop I, and Stroop III, and white matter integrity loss within the superior corona radiata, the inferior longitudinal fasciculus, the uncinate fasciculus, the anterior thalamic radiation, the corticospinal tract, and the internal and external capsule in presymptomatic *C9orf72RE* carriers compared with HC. Gray matter volume loss was found in a subgroup of presymptomatic carriers over 40 years of age, in the thalamus, cerebellum, and parietal and temporal regions.

We found no correlation between subtle cognitive changes and underlying gray and white

Table 2. Neuropsychological data of *C9orf72RE* carriers and HC

Domain	Neuropsychological test	C9orf72RE carriers (n=18)	HC (n=15)	C9orf72RE carriers (n=18)	P value
		Raw scores	Raw scores	Z-scores	
Language	BNT	53.8 (3.7)	54.0 (3.9)	-0.04 (0.94)	0.850
	SAT	27.7 (1.0)	28.3 (1.0)	-0.62 (0.98)	0.428
	Animal fluency	25.9 (5.6)	27.8 (7.5)	-0.25 (0.74)	0.237
	Letter fluency	37.3 (9.1)	40.9 (12.2)	-0.30 (0.75)	0.026
	Total Language	-	-	-0.30 (0.47)	0.101
Memory	RAVLT learning	49.7 (7.9)	50.9 (10.9)	-0.11 (0.73)	0.476
	RAVLT recall	10.6 (2.3)	9.0 (4.0)	0.39 (0.56)	0.248
	Digit Span	16.3 (3.7)	17.9 (5.1)	-0.31 (0.72)	0.159
	Total Memory	-	-	-0.01 (0.45)	0.605
Attention and mental processing speed	TMT A*	32.1 (8.2)	28.2 (7.8)	-0.50 (1.06)	0.247
	Stroop I*	45.7 (6.9)	41.8 (4.9)	-0.80 (1.43)	0.041
	Stroop II*	58.1 (11.2)	51.5 (8.3)	-0.79 (1.34)	0.096
	LDST	33.4 (6.0)	35.8 (8.2)	-0.29 (0.73)	0.255
	Total Attention	-	-	-0.81 (1.22)	0.069
Executive function	TMT B*	62.9 (18.1)	54.1 (12.4)	-0.71 (1.47)	0.283
	Stroop III*	92.8 (21.9)	77.7 (16.7)	-0.90 (1.31)	0.048
	Total Executive Functioning	-	-	-0.81 (1.22)	0.060
Social cognition†	Ekman faces	47.1 (4.7)	45.7 (7.6)	0.19 (0.62)	0.760
	Happé ToM	24.0 (7.5)	22.5 (3.5)	-0.20 (0.47)	0.100
	Total Social Cognition	-	-	-0.01 (0.50)	0.448
Visuo-construction	Clock drawing	13.0 (1.0)	13.0 (1.0)	-	0.464
	Block Design	34.7 (13.9)	40.6 (13.8)	-0.43 (1.01)	0.091
	Total Visuoconstruction	-	-	-0.43 (1.01)	0.091

Values indicate: uncorrected mean (standard deviation), or in case of Clock drawing median (interquartile range). Abbreviations: BNT, Boston Naming Test; SAT, Semantic Association Test; TMT, Trail Making Test; LDST, Letter Digit Substitution Test; RAVLT, Rey Auditory Verbal Learning Test. Average Z-scores for HC were not reported as these were equal to zero per definition. *Higher scores indicate worse performance, Z-scores are inverted. † Missing data for social cognition tests for one carrier. P value on Z-score comparisons of *C9orf72RE* carriers and HC, corrected for age, sex and education.

Figure 1. Differences in white matter integrity between the whole group of *C9orf72RE* carriers and HC.

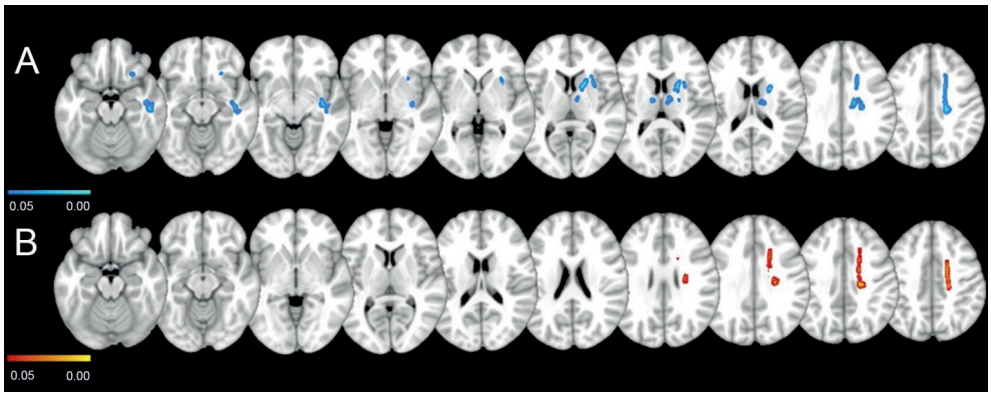

(A) White matter results for FA, for the contrast carriers < HC in the entire cohort. (B) White matter results for RD, for the contrast carriers > HC in the entire cohort. Results are corrected for multiple comparisons (color bars represent family-wise error $p<0.05$) using threshold-free cluster enhancement.

matter substrates in presymptomatic *C9orf72RE*. While participants in our study performed within the normative range of neuropsychological tests by definition, our results indicated a subtle decline in language (letter fluency), attention (Stroop I), and executive function (Stroop III) in presymptomatic *C9orf72RE* carriers compared with HC. These findings did not survive correction for multiple comparisons, but are in line with observations in symptomatic *C9orf72RE* patients with FTD, showing a typical FTD profile with language impairment, attention deficits, and executive dysfunction [2,3]. Also, approximately 50% of symptomatic *C9orf72RE* patients with ALS developed executive dysfunction during the course of their disease [25]. In the present study we found no evidence for presymptomatic memory decline, neuropsychiatric or behavioral symptoms in *C9orf72RE* [4,5,25,26]. Therefore, our presymptomatic phenotypic profile contradicts the results of 2 other studies in presymptomatic *C9orf72RE* FTD and ALS relatives, in which behavioral changes were found present up to 15 years before estimated symptom onset [17], and cognitive decline was absent [17,18]. These presymptomatic phenotypic differences may relate to the diversity in emerging clinical phenotype (i.e., ALS, FTD, or FTD-ALS), reflect the large clinical heterogeneity observed in *C9orf72RE* [21], or relate to differences in disease stage. Interestingly, the latter explanation was contradicted by our nonsignificant results in the subgroup analysis in carriers and HC >40 years of age, i.e., approaching symptom onset. While these results could reflect a lack of power, it may also be suggested that cognitive deficits in *C9orf72RE* are long present, and do not merely mark clinical onset. If true, this would contradict findings and hypotheses on cognitive decline emerging only years before symptom onset in presymptomatic *MAPT*

Table 3. GM volume clusters and white matter tracts in *C9orf72RE* compared with HC

	Cluster size	P-value	X	Y	Z	L/R	Peak voxel location
Grey matter volume differences in whole group							
-	-	-	-	-	-	-	-
White matter integrity differences in whole group							
FA: Carriers < HC	783	0.040	20	-22	38	R	Superior corona radiata
	379	0.044	48	-12	-26	R	Inferior longitudinal fasciculus
	194	0.042	16	9	6	R	Anterior limb internal capsule
	97	0.045	10	-10	13	R	Anterior thalamic radiation
	67	0.048	30	10	8	R	External capsule
	36	0.048	29	22	-19	R	Uncinate fasciculus
	24	0.047	-11	-9	12	L	Anterior thalamic radiation
RD: Carriers > HC	672	0.044	20	-21	38	R	Superior corona radiata, corticospinal tract
Grey matter volume differences > 40 years of age							
Carriers < HC	928	0.014	52	-40	-16	R	Inferior temporal gyrus (temporo-occipital part)
	198	0.035	26	-50	-30	R	Cerebellum (VI)
	104	0.039	-52	-24	44	L	Postcentral gyrus
	66	0.014	-36	-56	48	L	Superior parietal lobule
	39	0.044	-60	-6	40	L	Precentral gyrus
	38	0.033	-14	-24	4	L	Thalamus
White matter integrity differences > 40 years of age at a lower threshold							
FA: Carriers < HC	951	0.111	7	20	18	R	Forceps minor
	115	0.138	-14	-44	12	L	Forceps major
	46	0.145	-23	-58	14	L	Forceps major
	23	0.148	33	-25	4	R	Inferior fronto-occipital fasciculus
	23	0.147	-44	-9	-14	L	Inferior longitudinal fasciculus
	20	0.146	48	-16	-20	R	Inferior longitudinal fasciculus

Results are corrected for multiple comparisons (FWE) using threshold-free cluster enhancement at $p<0.05$. White matter integrity differences > 40 years of age were found at a threshold FWE $p<0.15$.

Figure 2. Differences in white matter integrity between *C9orf72RE* carriers and HC for subgroup analysis > 40 years of age.

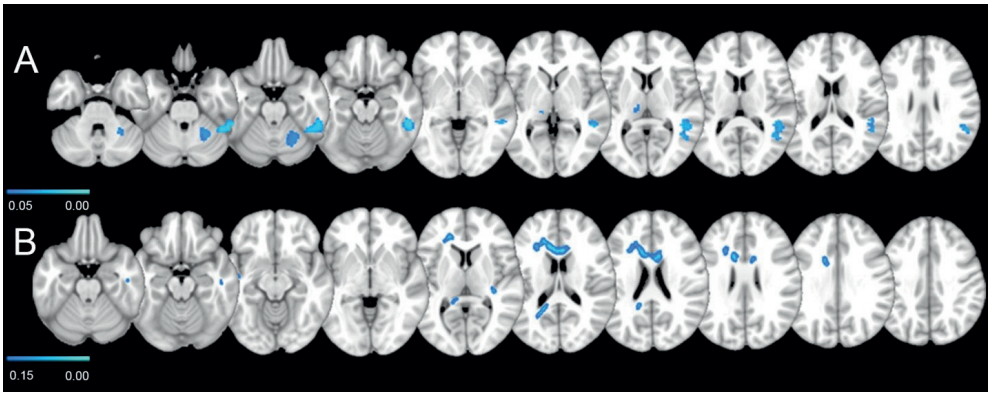

(A) Gray matter results for the contrast carriers < HC. B: White matter results for RD, for the contrast carriers > HC. Results are corrected for multiple comparisons (color bars represent family-wise error $p<0.05$ in grey matter analysis and $p<0.15$ in white matter analysis) using threshold-free cluster enhancement.

and *GRN* [16,17]. In our study, presymptomatic *C9orf72RE* carriers demonstrated white matter integrity loss reflected by lower FA and higher RD, within tracts connecting regions of significant gray matter loss in symptomatic FTD or ALS, such as the frontal lobe in case of the inferior longitudinal fasciculus and the uncinated fasciculus [11], the thalamus in case of the thalamic radiation [5], and motor regions in case of the corticospinal tract, corona radiata, and internal/external capsule [27]. The uncinate fasciculus and inferior longitudinal fasciculus are tracts typically associated with bvFTD [28], while FA reduction in white matter within the frontal and cingulate gyrus or internal capsule was reported in ALS [29]. Our results of decreased FA and higher RD are concordant with the scarce DTI studies in symptomatic *C9orf72RE*. Patients with *C9orf72RE* ALS showed FA, RD, and MD change in frontotemporal white matter and bilateral thalamic tracts [8]. In *C9orf72RE* FTD, decreased FA and increased AxD was found in the corpus callosum, cingulum bundle [11], and right and left superior cerebellar peduncle [12]. It has been demonstrated repeatedly that early white matter integrity alterations precede gray matter changes in FTD [15,30,31]. In accordance, our study shows white matter integrity loss in the entire group of *C9orf72RE* carriers, while gray matter volume loss was confined to a subgroup of presymptomatic carriers over 40 years of age. However, white matter integrity was not encountered in the >40 subgroup at a stringent threshold. Since a less stringent threshold did show results in frontal white matter, the lack of results in the subgroup could be explained as a lack of power, considering the small sample size in the subgroup analyses, and the fact that one extra DTI scan was not available due to an acquisition artefact. Longitudinal follow-up of preclinical cohorts of *C9orf72RE* carriers, as well as the use of different analysis techniques (e.g., cortical thickness

analysis), will have to elucidate the sequential order of gray and white matter change in *C9orf72RE* specifically. The finding of atrophy in the smaller group of older presymptomatic carriers, closer to clinical onset [32], contradicts the view that atrophy in *C9orf72RE* reflects developmental abnormalities [21], as in that case gray matter loss should be detectable across our entire cohort. This was supported by a presymptomatic *C9orf72RE* study showing gray matter abnormalities up to 25 years before symptom onset [17].

Pathologic and T1-weighted MRI studies suggest a symmetric cortico-thalamo-cerebellar network impairment to underlie symptomatic *C9orf72RE* [2,6,9,12,33]. In the present study, we show that this pattern is already present in presymptomatic *C9orf72RE* carriers at risk for conversion. We found gray matter volume loss in the cerebellum (lobule VI) and thalamus, inferior temporal gyrus, postcentral gyrus, and superior parietal lobe. Cerebellar and thalamic pathology are increasingly recognized to contribute to cognition, behavior, and neuropsychiatric (dys)functioning, through their role as relay station [34]. The thalamus is involved in multiple functional networks, and has been related to *C9orf72RE* symptomatology by undermining salience network connectivity [7], compromised in bvFTD. Lobules VI and VII of the cerebellum are considered the cognitive cerebellum [35], and showed atrophy in both bvFTD and ALS [36], In correlation analyses, however, particularly the superior cerebellum has been related to cognitive functioning in bvFTD [36]. Postcentral gyrus thinning, i.e., the primary somatosensory cortex, is associated with ALS, and inferior temporal gyrus thinning was related to faster clinical progression in a longitudinal study in ALS [37]. The precentral gyrus and superior parietal lobe were previously identified as regions associated with symptomatic *C9orf72RE* [9,26], as more widespread atrophy was shown to underlie *C9orf72RE* compared with other FTD mutations, specifically *MAPT* mutation carriers [9].

In this study, subtle cognitive changes did not correlate with underlying gray or white matter in *C9orf72RE* carriers or HC. Possible explanations lie in the lack of power to detect such an association, or the heterogeneity in our cohort with respect to emerging phenotype (i.e., FTD or ALS), which could complicate pinpointing clinical features. On the basis of the present results, it is difficult to predict the clinical outcome of individual patients, as we identified group level results indicative for both FTD and ALS phenotypes. Longitudinal studies extending into the symptomatic stage may further elucidate the most sensitive biomarkers for different phenotypes.

Important strengths of this study are the standardized protocol with single-center MRI and neuropsychological evaluation, as well as the use of a well-matched control group. Important drawbacks are the small sample of presymptomatic *C9orf72RE* carriers and the fact that our diffusion-weighted field of view did not include cerebellar white matter. Finally, we cannot account for incomplete penetrance associated with *C9orf72RE* in the presymptomatic stage. We did account for incomplete age-related penetrance, i.e., ages at onset fluctuating

between 40 and 90 years [24], by performing analyses in a subgroup >40 years of age.

Our data demonstrate a presymptomatic *C9orf72RE* stage characterized by a subtle decline in attention, executive functioning, and language, and white matter changes in tracts connecting the frontal lobe, the thalamic radiation, and tracts associated with motor functioning. Gray matter loss was demonstrated in a subgroup of *C9orf72RE* carriers over 40 years of age. We found no correlation between subtle cognitive change and underlying white or gray matter substrates. This study expands on the knowledge of the presence of disease-related changes in presymptomatic *C9orf72RE* carriers [17,18]. In the future, larger but foremost longitudinal studies may confirm cognitive and gray and white matter abnormality patterns in presymptomatic *C9orf72RE*, and elucidate the sequential order of these potential markers in the *C9orf72RE* disease evolution.

REFERENCES

1. DeJesus-Hernandez M, Mackenzie IR, Boeve BF, et al. Expanded GGGGCC hexanucleotide repeat in noncoding region of C9ORF72 causes chromosome 9p-linked FTD and ALS. Neuron 2011;72:245–256.
2. Boeve BF, Boylan KB, Graff-Radford NR, et al. Characterization of frontotemporal dementia and/or amyotrophic lateral sclerosis associated with the GGGGCC repeat expansion in C9ORF72. Brain 2012;135:765–783.
3. Simon-Sanchez J, Dopper EG, Cohn-Hokke PE, et al. The clinical and pathological phenotype of C9ORF72 hexanucleotide repeat expansions. Brain 2012;135:723–735.
4. Murray ME, DeJesus-Hernandez M, Rutherford NJ, et al. Clinical and neuropathologic heterogeneity of c9FTD/ALS associated with hexanucleotide repeat expansion in C9ORF72. Acta Neuropathol 2011;122:673–690.
5. Mahoney CJ, Beck J, Rohrer JD, et al. Frontotemporal dementia with the C9ORF72 hexanucleotide repeat expansion: clinical, neuroanatomical and neuropathological features. Brain 2012;135:736–750.
6. Sha SJ, Takada LT, Rankin KP, et al. Frontotemporal dementia due to C9ORF72 mutations: clinical and imaging features. Neurology 2012;79:1002–1011.
7. Lee SE, Khazenzon AM, Trujillo AJ, et al. Altered network connectivity in frontotemporal dementia with C9orf72 hexanucleotide repeat expansion. Brain 2014;137:3047–3060.
8. Bede P, Bokde AL, Byrne S, et al. Multiparametric MRI study of ALS stratified for the C9orf72 genotype. Neurology 2013;81:361–369.
9. Whitwell JL, Weigand SD, Boeve BF, et al. Neuroimaging signatures of frontotemporal dementia genetics: C9ORF72, tau, progranulin and sporadics. Brain 2012; 135:794–806.
10. Floeter MK, Bageac D, Danielian LE, Braun LE, Traynor BJ, Kwan JY. Longitudinal imaging in C9orf72 mutation carriers: relationship to phenotype. Neuroimage Clin 2016;12:1035–1043.
11. Mahoney CJ, Ridgway GR, Malone IB, et al. Profiles of white matter tract pathology in frontotemporal dementia. Hum Brain Mapp 2014;35:4163–4179.
12. Mahoney CJ, Simpson IJ, Nicholas JM, et al. Longitudinal diffusion tensor imaging in frontotemporal dementia. Ann Neurol 2015;77:33–46.
13. Westeneng HJ, Walhout R, Straathof M, et al. Widespread structural brain involvement in ALS is not limited to the C9orf72 repeat expansion. J Neurol Neurosurg Psychiatry 2016;87:1354–1360.
14. Jiang J, Cleveland DW. Bidirectional transcriptional inhibition as therapy for ALS/FTD caused by repeat expansion in C9orf72. Neuron 2016;92:1160–1163.
15. Dopper EG, Rombouts SA, Jiskoot LC, et al. Structural and functional brain connectivity in presymptomatic familial frontotemporal dementia. Neurology 2014;83: e19–e26.
16. Jiskoot LC, Dopper EG, Heijer T, et al. Presymptomatic cognitive decline in familial frontotemporal dementia: a longitudinal study. Neurology 2016;87:384–391.
17. Rohrer JD, Nicholas JM, Cash DM, et al. Presymptomatic cognitive and neuroanatomical changes in genetic frontotemporal dementia in the Genetic Frontotemporal Dementia Initiative (GENFI) study: a cross-sectional analysis. Lancet Neurol 2015;14:253–262.
18. Walhout R, Schmidt R, Westeneng HJ, et al. Brain morphologic changes in asymptomatic C9orf72 repeat expansion carriers. Neurology 2015;85:1780–1788.
19. Brooks BR, Miller RG, Swash M, Munsat TL, World Federation of Neurology Research Group on Motor Neuron Diseases. El Escorial revisited: revised criteria for the diagnosis of amyotrophic lateral sclerosis. Amyotroph Lateral Scler Other Motor Neuron Disord 2000;1:293–299.
20. Rascovsky K, Hodges JR, Knopman D, et al. Sensitivity of revised diagnostic criteria for the behavioural variant of frontotemporal dementia. Brain 2011;134:2456–2477.
21. Rohrer JD, Isaacs AM, Mizielinska S, et al. C9orf72 expansions in frontotemporal dementia and amyotrophic lateral sclerosis. Lancet Neurol 2015;14:291–301.
22. Cummings JL. The neuropsychiatric inventory: assessing psychopathology in dementia patients. Neurology 1997; 48:S10–S16.
23. Wedderburn C, Wear H, Brown J, et al. The utility of the Cambridge Behavioural Inventory in neurodegenerative disease. J Neurol Neurosurg Psychiatry 2008;79:500–503.
24. Murphy NA, Arthur KC, Tienari PJ, Houlden H, Chio A, Traynor BJ. Age-related penetrance of the C9orf72 repeat expansion. Sci Rep 2017;7:2116.
25. Patel AN, Sampson JB. Cognitive profile of C9orf72 in frontotemporal dementia and amyotrophic

lateral sclerosis. Curr Neurol Neurosci Rep 2015;15:59.
26. Mahoney CJ, Downey LE, Ridgway GR, et al. Longitudinal neuroimaging and neuropsychological profiles of frontotemporal dementia with C9ORF72 expansions. Alzheimers Res Ther 2012;4:41.
27. Agosta F, Galantucci S, Riva N, et al. Intrahemispheric and interhemispheric structural network abnormalities in PLS and ALS. Hum Brain Mapp 2014;35:1710–1722.
28. Bhogal P, Mahoney C, Graeme-Baker S, et al. The common dementias: a pictorial review. Eur Radiol 2013;23:3405–3417.
29. Li J, Pan P, Song W, Huang R, Chen K, Shang H. A meta-analysis of diffusion tensor imaging studies in amyotrophic lateral sclerosis. Neurobiol Aging 2012;33:1833–1838.
30. Borroni B, Alberici A, Premi E, et al. Brain magnetic resonance imaging structural changes in a pedigree of asymptomatic progranulin mutation carriers. Rejuvenation Res 2008;11:585–595.
31. Gordon E, Rohrer JD, Fox NC. Advances in neuroimaging in frontotemporal dementia. J Neurochem 2016;138 (suppl 1):193–210.
32. Van Mossevelde S, van der Zee J, Gijselinck I, et al. Clinical evidence of disease anticipation in families segregating a C9orf72 repeat expansion. JAMA Neurol 2017;74:445–452.
33. Troakes C, Maekawa S, Wijesekera L, et al. An MND/ALS phenotype associated with C9orf72 repeat expansion: abundant p62-positive, TDP-43-negative inclusions in cerebral cortex, hippocampus and cerebellum but without associated cognitive decline. Neuropathology 2012;32:505–514.
34. Middleton FA, Strick PL. Basal ganglia and cerebellar loops: motor and cognitive circuits. Brain Res Brain Res Rev 2000;31:236–250.
35. Stoodley CJ, Schmahmann JD. Evidence for topographic organization in the cerebellum of motor control versus cognitive and affective processing. Cortex 2010;46:831–844.
36. Tan RH, Devenney E, Dobson-Stone C, et al. Cerebellar integrity in the amyotrophic lateral sclerosis frontotemporal dementia continuum. PLoS One 2014;9:e105632.
37. Verstraete E, Veldink JH, Hendrikse J, Schelhaas HJ, van den Heuvel MP, van den Berg LH. Structural MRI reveals cortical thinning in amyotrophic lateral sclerosis. J Neurol Neurosurg Psychiatry 2012;83:383–388.

APPENDIX

Table A1. Carrier and HC distribution for autosomal dominant *C9orf72RE* families

Family number and diagnosis	*C9orf72RE* carriers	HC	Total
Family 1 – bvFTD	3 (16.7)	2 (13.3)	5 (15.2)
Family 2 - bvFTD	1 (5.6)	0 (0.0)	1 (3.0)
Family 3 – FTD-ALS	1 (5.6)	0 (0.0)	1 (3.0)
Family 4 - bvFTD	3 (16.7)	5 (33.3)	8 (24.2)
Family 5 – bvFTD and ALS	1 (5.6)	0 (0.0)	1 (3.0)
Family 6 - bvFTD	1 (5.6)	0 (0.0)	1 (3.0)
Family 7 – bvFTD and FTD-ALS	4 (22.2)	4 (26.7)	8 (24.2)
Family 8 – bvFTD and ALS	1 (5.6)	2 (13.3)	3 (9.1)
Family 9 – bvFTD and FTD-ALS	1 (5.6)	0 (0.0)	1 (3.0)
Family 10 – bvFTD and FTD-ALS	1 (5.6)	0 (0.0)	1 (3.0)
Family 11 - bvFTD	0 (0.0)	1 (6.7)	1 (3.0)
Family 12 - bvFTD	1 (5.6)	1 (6.7)	2 (6.1)
Total	18	15	33

Values indicate: number (valid percentage).

Table A2. Neuropsychiatric Inventory, presence of symptoms

	C9orf72RE carriers (n=17)*	HC (n=15)
Delusions	0 (0)	0 (0)
Hallucinations	1 (5.9)	0 (0)
Agitation/Agression	1 (5.9)	0 (0)
Depression/Dysphoria	2 (11.8)	2 (13.3)
Anxiety	0 (0)	0 (0)
Elation/Euphoria	1 (5.9)	0 (0)
Apathy/Indifference	0 (0)	0 (0)
Disinhibition	1 (5.9)	0 (0)
Irritability/Lability	2 (11.8)	1 (6.7)
Aberrant motor behavior	0 (0)	0 (0)
Sleep and nighttime behavior disorders	0 (0)	0 (0)
Appetite and eating changes	0 (0)	1 (6.7)

Values indicate: number (valid percentage). *Missing data for NPI in one carrier.

Table A3. Neuropsychological data of *C9orf72RE* carriers and HC >40 years of age

Domain	Neuropsychological test	C9orf72RE carriers (n=13) Raw scores	HC (n=11) Raw scores	C9orf72RE carriers (n=13) Z-scores	P value
Language	SAT	27.9 (1.1)	28.3 (1.1)	-0.38 (0.97)	0.815
	Animal fluency	25.3 (6.4)	26.2 (6.7)	-0.13 (0.95)	0.504
	Letter fluency	36.1 (8.7)	38.5 (13.1)	-0.18 (0.67)	0.227
	Total Language	-	-	-0.15 (0.52)	0.656
Memory	RAVLT learning	46.6 (7.1)	48.7 (11.4)	-0.19 (0.63)	0.563
	RAVLT recall	9.6 (1.6)	7.7 (3.9)	0.48 (0.41)	0.121
	Digit Span	16.5 (4.2)	16.6 (4.5)	-0.00 (0.92)	0.853
	Total Memory		-	0.10 (0.41)	0.803
Attention and mental processing speed	TMT A*	34.2 (8.4)	30.7 (6.6)	-0.53 (1.28)	0.658
	Stroop I*	45.5 (6.9)	43.1 (4.9)	-0.50 (1.40)	0.238
	Stroop II*	59.7 (11.7)	53.3 (7.6)	-0.84 (1.53)	0.221
	LDST	32.6 (5.7)	33.5 (7.7)	-0.11 (0.73)	0.718
	Total Attention	-	-	-0.50 (1.03)	0.267
Executive function	TMT B*	68.9 (15.7)	58.0 (11.5)	-0.95 (1.37)	0.133
	Stroop III*	99.9 (21.6)	80.5 (16.7)	-1.16 (1.30)	0.083
	Total Executive Functioning	-	-	-1.06 (1.12)	0.074
Social cognition†	Ekman faces	45.8 (4.6)	45.3 (8.8)	0.06 (0.53)	0.752
	Happé ToM	21.0 (2.5)	20.8 (6.0)	0.03 (0.42)	0.829
	Total Social Cognition	-	-	0.05 (0.43)	0.980
Visuoconstruction	Clock drawing	13 (1)	13 (1)	-	0.910
	Block Design	30.7 (13.0)	36.3 (13.3)	-0.42 (0.98)	0.409
	Total Visuoconstruction	-	-	-0.42 (0.98)	0.409

Values indicate: uncorrected mean (standard deviation), or in case of Clock drawing median (interquartile range). Abbreviations: BNT, Boston Naming Test; SAT, Semantic Association Test; TMT, Trail Making Test; LDST, Letter Digit Substitution Test; RAVLT, Rey Auditory Verbal Learning Test. Average Z-scores for HC were not reported as these were equal to zero per definition. *Higher scores indicate worse performance, Z-scores are inverted. † Missing data for social cognition tests for one carrier. P value on Z-score comparisons of C9orf72RE carriers and HC, by means of univariate ANCOVA corrected for age, sex and education. In case of Clock drawing P value by means of Mann-Whitney U test. At bonferroni correction $p<0.002$ there are no significant results.

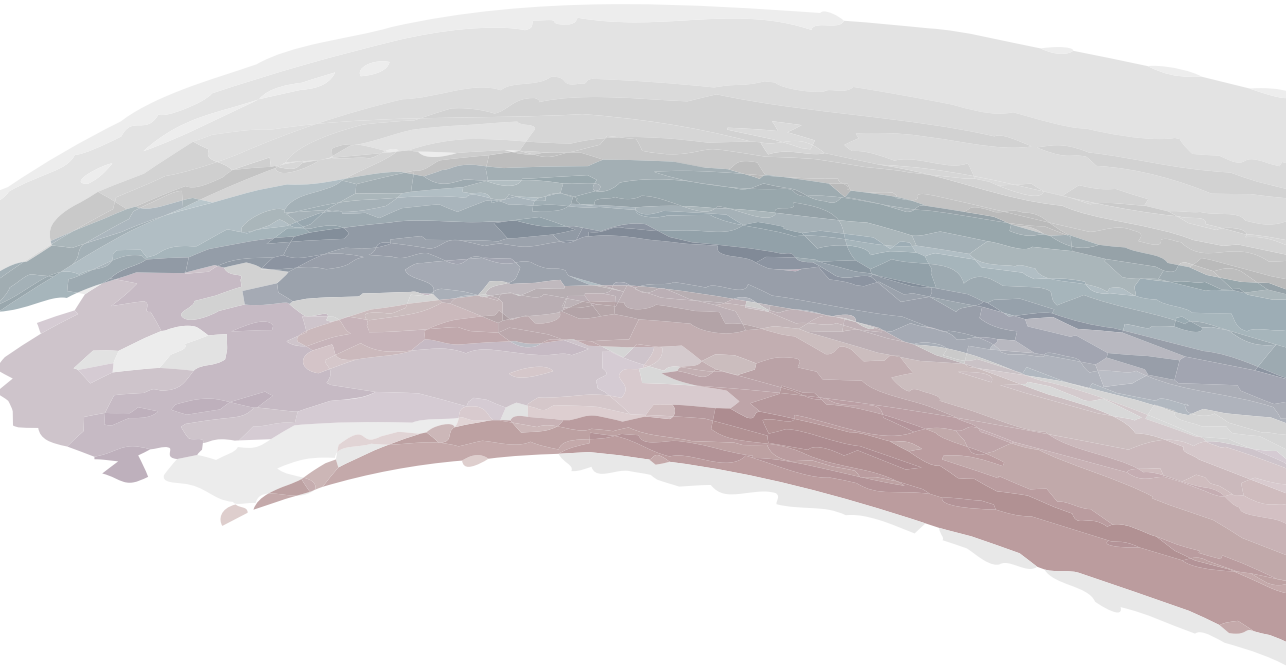

CHAPTER 3

LONGITUDINAL NEUROIMAGING TRAJECTORIES IN THE FTD-RISC STUDY

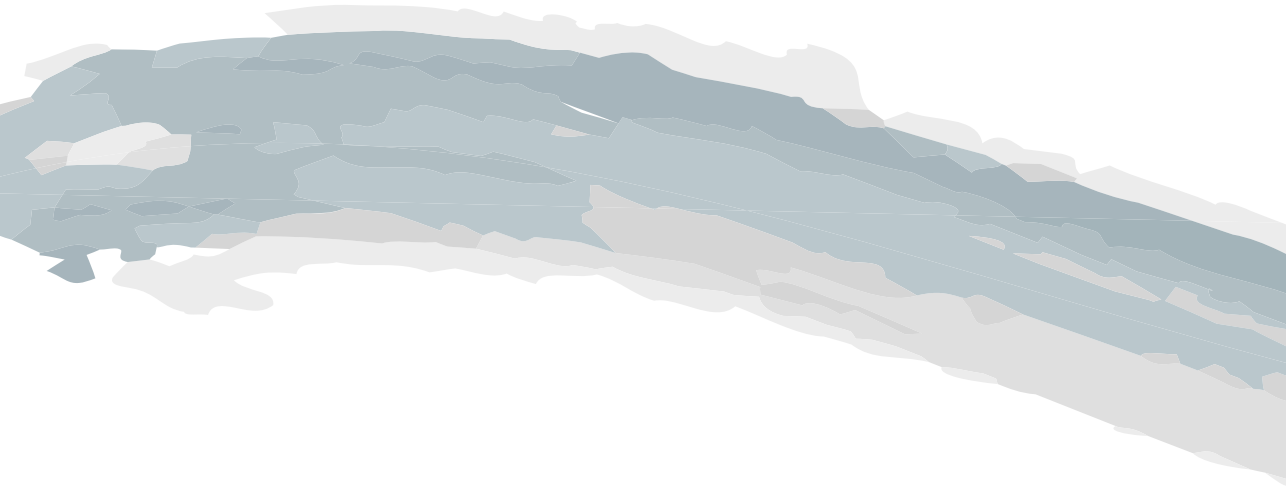

Chapter 3.1

Gray and white matter changes in presymptomatic frontotemporal dementia: a longitudinal MRI study

Panman, J.L.
Jiskoot, L.C.
Bouts, M.J.R.J.
Meeter, L.H.H.
van der Ende, E.L.
Poos, J.M.
Feis, R.A.
Kievit, A.J.A.
van Minkelen, R.
Dopper, E.G.P.
Rombouts, S.A.R.B.
van Swieten, J.C.
Papma, J.M.

Neurobiology of Aging, 2019

ABSTRACT

In genetic frontotemporal dementia, cross-sectional studies have identified profiles of presymptomatic neuroanatomical loss for *C9orf72* repeat expansion, *MAPT* and *GRN* mutations. In this study we characterize longitudinal gray matter (GM) and white matter (WM) brain changes in presymptomatic FTD. We included healthy carriers of *C9orf72* repeat expansion (n=12), *MAPT* (n=15), *GRN* (n=33) mutations, and related non-carriers (n=53), that underwent MRI at baseline and two-year follow-up. We analyzed cross-sectional baseline, follow-up, and longitudinal GM and WM changes using voxel-based morphometry and cortical thickness analysis in SPM, and tract-based spatial statistics in FSL. Compared to non-carriers, *C9orf72* repeat expansion carriers showed lower GM volume in the cerebellum and insula, and WM differences in the anterior thalamic radiation, at baseline and follow-up. *MAPT* mutation carriers showed emerging GM temporal lobe changes, and longitudinal WM degeneration of the uncinate fasciculus. *GRN* mutation carriers did not show presymptomatic neurodegeneration. This study shows distinct presymptomatic cross-sectional and longitudinal patterns of GM and WM changes across *C9orf72* repeat expansion, *MAPT*, and *GRN* mutation carriers compared with non-carriers.

INTRODUCTION

Hereditary frontotemporal dementia (FTD) is a neurodegenerative disorder, predominantly caused by autosomal dominant genetic mutations in the *MAPT* and *GRN* genes, or a repeat expansion in the *C9orf72* gene [1, 2]. Increasing evidence confirms the presence of pathophysiological and subsequent neuroanatomical changes in the presymptomatic stage of genetic FTD and amyotrophic lateral sclerosis (ALS) [3-20]. Previous MRI studies have revealed gene-specific neuroimaging profiles in healthy carriers of pathogenic FTD mutations (hereafter referred as 'presymptomatic mutation carriers') [3-7, 11, 15, 16, 18, 19]. In presymptomatic *MAPT* mutation carriers, lower gray matter (GM) volume in the anterior temporal lobes has been found [6, 18], as well as lower fractional anisotropy (FA) in the white matter (WM) of the right uncinate fasciculus when using region of interest analyses [7]. In presymptomatic *GRN* mutation carriers, subtle GM differences in the insula, temporal and frontal lobes were shown [5, 6, 16, 18], and WM differences in the uncinate fasciculus and inferior fronto-occipital fasciculus [4, 7]. Presymptomatic *C9orf72* repeat expansion carriers were characterized by lower GM volume of the insula, thalamus and cerebellum [3, 6, 11, 15, 18], and cortical thinning of the temporal lobe [19]. These changes were already shown up to 25 years before estimated symptom onset [18]. WM loss in presymptomatic *C9orf72* repeat expansion carriers included the corticospinal tract, anterior thalamic radiation, inferior longitudinal fasciculus, and the uncinate fasciculus [3, 15].

Though cross-sectional MRI studies in presymptomatic FTD indicate that the disease process starts several years before clinical symptom onset, studies that examine longitudinal presymptomatic GM and WM changes in specific mutations are scarce [18, 21]. Understanding longitudinal presymptomatic FTD related brain changes is important, as it enables both the identification of vulnerable brain regions as well as the timeframe and progression of brain changes, with important implications for disease management and treatment [21]. Progression of gray and white matter changes in presymptomatic FTD carriers may follow a gradual trajectory, similar to the presymptomatic stage of other neurodegenerative diseases like Alzheimer's disease (AD), shown in the Dominant Inherited Alzheimer Network (DIAN) study [18, 22-24], but could also deviate from findings in AD. For example, remarkable early brain changes have been found in *C9orf72* repeat expansion carriers which may indicate that *C9orf72* repeat expansion associated pathology knows an early start and progresses in a very slow manner [15, 18], or could even exist as a neurodevelopmental disorder [11, 19]. On the other hand, previous research demonstrated that atrophy rates during the symptomatic stage of FTD are twice as high compared with Alzheimer's disease patients [25-27], with the fastest atrophy rates in FTD-*GRN* patients [28, 29]. An interesting issue therefore, is whether *GRN* pathology spreads in the last years before symptom onset with a much faster, more explosive rate [10, 12]. In the current

study, we aimed to investigate longitudinal GM and WM brain changes in the presymptomatic stage of FTD, with a specific focus on FTD genotypic patterns. Some previous studies have used voxel-based morphometry (VBM) [4, 6, 7, 15, 20] and others used cortical thickness estimation for GM analyses in presymptomatic FTD [3, 5, 11, 16, 19]. In this study, we used both methods, and additional tract-based spatial statistics (TBSS) for DTI analysis, in order to grasp the full extent of presymptomatic GM and WM differences. Furthermore, in normal brain aging [30], and Parkinson's disease [31], differences between results from VBM and cortical thickness in the same sample have been demonstrated, indicating that both methods could be complementary [30, 31]. We performed a two-year follow-up study in which we investigated cross-sectional and longitudinal structural neuroimaging profiles using whole brain VBM, cortical thickness analysis and TBSS in presymptomatic carriers between the *C9orf72* repeat expansion, and *GRN* or *MAPT* mutation carriers and non-carriers.

METHODS

Study procedure and ethical approval. In the FTD Risk Cohort (FTD-RisC), we investigated first-degree relatives of FTD patients with one of the three major autosomal pathogenic mutations (*C9orf72, MAPT, GRN*), as previously described in our baseline study papers [7, 15]. In this study, every two years, participants underwent MRI of the brain, neurological examination, and neuropsychological assessment [9, 10]. Knowledgeable informants (e.g. spouses, siblings) completed questionnaires and were interviewed on changes in cognition and/or behavior. Genotyping was performed at baseline study visit [7, 15]. As a result, participants were labeled as either mutation carrier or non-carriers. All clinical investigators and participants were blinded for the participants' genetic status, unless participants underwent predictive testing. The FTD-RisC study was approved by the Medical and Ethical Review Committee of the Erasmus Medical Center, and written informed consent has been obtained from all participants.

Subject inclusion. For the present study, we selected all presymptomatic participants, either mutation carriers, or healthy non-carrier family members, with a baseline and two-year follow-up MRI scan (n = 113). We defined participants as presymptomatic based on (1) not fulfilling established criteria for possible FTD, primary progressive aphasia (PPA) or ALS [32-34], (2) the absence of cognitive or behavioral disorders on extensive neuropsychological assessment or the Neuropsychiatric Inventory (NPI-Q [35]), as described previously [7, 9, 10, 15], (3) the absence of signs of motor neuron disease on neurological examination, (4) the presence of normal cognitive functioning and behavior as reported by the participant and knowledgeable informant. The Frontotemporal Dementia – Clinical Rating Scale sum of boxes (FTD-CDR), Mini Mental State Examination (MMSE) and NPI-Q were reported as functional,

cognitive and behavioral screening instruments, respectively. The neuropsychological assessment included tests considering language, attention, executive functioning, memory, visuoconstruction, and social cognition, for specifics see Jiskoot et al., [10] and appendix A.

MRI acquisition. All participants underwent 3T T1-weighted and diffusion tensor imaging (DTI) at baseline and two-year follow-up using a standardized protocol (Philips Achieva – Philips Medical Systems, Best, the Netherlands). T1-weighted images were acquired with the following scanning parameters: repetition time (TR) = 9.8ms, echo time (TE) = 4.6 ms, flip angle = 8º, 140 slices, voxel size = 0.88x0.88x1.20 mm3. DTI was performed using single shot echo planar imaging with 61 non-collinear gradient directions (1 b=0, 60 b = 1000 s/mm2, TR = 8250ms, TE = 80ms, flip angle = 90º, 70 axial slices, voxel size = 2x2x2 mm3). While MRI sequence parameters were fixed over time, during follow up, a routine software update by the manufacturer was installed at our MRI site, dated 17-09-2015 (Appendix B). MRI-images were visually checked for gross neurological pathology and artifacts, and excluded from analysis when image quality proved insufficient.

Voxel-based morphometry. Whole-brain T1-weighted images were preprocessed using the longitudinal processing stream within the Computation Anatomy Toolbox (CAT) of the Statistical Parametric Mapping software (SPM12; the Wellcome Trust Center for Neuroimaging, London, UK) running in Matlab 2016b (Mathworks, Natick, MA, USA). First, longitudinal images from all subjects were rigidly aligned within-subjects and the images were segmented into grey and white matter and cerebrospinal fluid based on tissue probability. Afterwards, segmented tissue images were aligned to standard space. Using diffeomorphic image registration (DARTEL) [36], we created a study-specific grey matter template in standard space, and grey matter segmentations from all subjects were warped and normalized to this template. After registration and normalization, grey matter images were smoothed using a full width at half maximum (FWHM) kernel of 8 mm to correct for individual brain differences. We performed cross-sectional VBM analysis of variance (ANOVA) at baseline and follow-up to compare mutation groups (*C9orf72, GRN and MAPT*) with non-carriers and with each other, at both time points separately. Follow-up GM volume images were subtracted from their corresponding baseline maps and a longitudinal ANOVA was performed to determine the amount of change in grey matter over time between groups [37]. Statistical analysis was performed using a full factorial model with age, sex, scanner update and baseline total intracranial volume (TIV) as covariates. TIV in mm3 was estimated through the segmentation and tissue volume calculation of the GM, WM and cerebrospinal fluid. The statistical threshold was set at $p<0.05$ at cluster level, corrected for multiple comparisons using family wise error (FWE). We also explored clusters showing trends towards significant difference at $p^{FWE}<0.1$.

Cortical thickness. We extended the standard brain segmentation protocol from the CAT

toolbox in SPM12 as mentioned above with surface based cortical thickness estimation for baseline and follow-up images, using projection-based thickness [38]. For statistical analysis, we used the same models as for the VBM analysis, and performed cross-sectional baseline and follow-up analyses, to compare the effect of mutation group (*C9orf72, GRN, MAPT*) with non-carriers and each other. We performed an analysis of variance (ANOVA) with age, sex and scanner update (for follow up analysis) as covariates, and thresholded at $p^{FWE}<0.05$ at cluster level. We also explored clusters showing trends towards significant difference at $p^{FWE}<0.1$. For the longitudinal analysis, follow-up cortical thickness images were subtracted from their corresponding baseline maps, and a longitudinal ANOVA was performed to determine the amount of change in thickness over time for each participant, also at $p^{FWE}<0.05$, corrected for age, sex and scanner update. However, as recommended, the cortical thickness analyses were not adjusted for baseline TIV (http://www.neuro.uni-jena.de/cat12/CAT12-Manual.pdf).

Tract-based spatial statistics. Diffusion weighted images were preprocessed using TBSS as described previously [7, 15]. We used the FMRIB58_FA derived skeleton instead of a study-specific skeleton to allow for comparisons across baseline, follow-up and longitudinal analyses. Skeletonized FA and mean diffusivity (MD) images were fed into voxel-wise group statistics for cross-sectional baseline and follow-up analyses, to investigate the effect of mutation group. For the longitudinal analysis, follow-up FA and MD images were subtracted from their corresponding baseline maps, to determine the amount of change in white matter integrity over time for each participant, and compared between groups with an ANOVA. Comparisons were performed using permutation-based testing (5,000 permutations), with age, gender, the scanner update and baseline TIV as covariates. The statistical threshold was set at $p^{FWE}<0.05$.

Statistical analyses. Other statistical analyses were performed using SPSS Statistics 24.0 for Windows (SPSS Inc., Chicago, IL, USA). Group differences in sex were analyzed using Pearson $\chi 2$ tests. Age at time of MRI scan was compared by means of one-way ANOVA. Because of a skewed distribution, the MMSE and NPI-Q scores were analyzed with a Kruskal-Wallis test. Composite cognitive domain scores for language, attention, executive functioning, memory, visuoconstruction, and social cognition were computed and evaluated between groups as described previously [10], and reported in Appendix A. As the distribution of neuropsychological test data was predominantly skewed, we applied Kruskal-Wallis tests, with post-hoc Mann-Whitney-U tests for composite cognitive domain scores. We applied a significance level of $p<0.05$ with post-hoc Bonferroni comparisons for all statistical analyses.

RESULTS

Subjects. DNA sequencing assigned participants either to the *C9orf72* repeat expansion carrier (n=12), *MAPT* mutation carrier (n=15), *GRN* mutation carrier (n=33), or in the case of mutation-negative family members, to the non-carrier group (n=53). One presymptomatic *MAPT* mutation carrier was excluded from GM analysis due to a large cerebellar cyst, and one presymptomatic *C9orf72* repeat expansion carrier was excluded due to registration and reconstruction errors. GM analysis was carried out in 11 *C9orf72* repeat expansion, 14 *MAPT*, and 33 *GRN* mutation carriers, and 53 non-carriers, and WM analysis in 12 *C9orf72* repeat expansion, 14 *MAPT*, and 28 *GRN* mutation carriers, and 50 non-carriers. Nine subjects were excluded from DTI analysis due to signal dropout (n=6) and motion artifacts (n=3). All participants were presymptomatic at both baseline and follow up visit, with FTD-CDR = 0 at both time points (table 1). An overview of demographic characteristics is presented in Table 1. *MAPT* mutation carriers were significantly younger than non-carriers and *GRN* mutation carriers. Other subject characteristics were similar across groups, including screening measures for clinical symptoms such as the MMSE and NPI-Q. None of the participants scored below two standard deviations on neuropsychological tests. At baseline, all groups performed similar on composite cognitive domains (Appendix A). At follow-up, *C9orf72* repeat expansion carriers and non-carriers performed significantly worse than *GRN* mutation carriers on social cognition (Appendix A).

C9orf72 repeat expansion carriers versus non-carriers. Cross-sectional VBM analysis at baseline showed lower GM volume in the cerebellum, insula, left frontal, and left planum temporale in C9orf72 repeat expansion carriers compared to non-carriers (Fig1A, Appendix C.1), while cortical thickness analysis showed thinning in the right postcentral gyrus and a trend towards thinning of the left precentral gyrus (at p^{FWE}=0.060). Cross-sectional VBM analysis at two-year follow-up showed lower GM volume in C9orf72 repeat expansion carriers compared to non-carriers in the thalamus, cerebellum, and several bilateral cortical regions, i.e. orbitofrontal and insular cortex, and the postcentral gyrus (Fig1A, Appendix C.1). In addition, cortical thickness analysis showed cortical thinning in bilateral precentral gyrus and right superior parietal lobule in *C9orf72* repeat expansion carriers compared to non-carriers (Fig1B, Appendix C.2). Longitudinal VBM and cortical thickness analyses did not reveal any significant changes in C9orf72 repeat expansion carriers. Furthermore, there were no brain regions where non-carriers showed lower GM volume or cortical thinning compared to C9orf72 carriers at baseline, follow up or longitudinally.

Cross-sectional analyses at baseline revealed lower FA in *C9orf72* repeat expansion carriers in frontotemporal tracts compared to non-carriers, predominantly located in the bilateral corticospinal tract and anterior thalamic radiation, the right inferior fronto-occipital

Table 1. Demographic characterization

Variable	Non carriers	*MAPT*	*GRN*	*C9orf72*	p-value
Subjects (Male)	53 (24)	15 (9)	33 (11)	12 (2)	0.094
Mean age (SD)	50.72 (10.73)	41.77 (9.50)	52.10 (7.53)	49.70 (12.36)	0.010*
< 35	3	2	0	1	
35-50	18	11	13	6	
50-65	29	1	18	4	
65+	3	1	2	1	
Baseline					
MMSE	29.13 (1.21)	29.47 (0.64)	29.09 (1.40)	29.58 (0.67)	0.657
NPI-Q	0.19 (0.54)	1.50 (3.75)	0.70 (1.42)	0.55 (1.21)	0.401
Follow up					
MMSE	29.26 (1.23)	28.80 (2.11)	28.84 (1.57)	29.25 (0.96)	0.580
NPI-Q	0.42 (0.88)	2.08 (5.77)	0.18 (0.48)	1.18 (1.66)	0.128

Abbreviations: MMSE; Mini-Mental State Examination; NPI-Q: Neuropsychiatric Inventory Questionnaire; SD: standard deviation. Scores for MMSE and NPI-Q are presented as mean scores (SD). *MAPT mutation carriers significantly younger than non-carriers and GRN mutation carriers.

fasciculus, and superior longitudinal fasciculus (Fig2A, Appendix C.3), and higher MD in almost the entire skeleton when compared to non-carriers (Fig2B, Appendix C.3). At follow-up, we found lower FA and increased MD in the same tracts as baseline analyses, although to a lesser extent (Fig2B, Appendix C.3). We did not find any significant longitudinal changes in the WM (both FA and MD) of *C9orf72* repeat expansion carriers compared to non-carriers, or vice versa.

MAPT mutation carriers versus non-carriers. Cross-sectional VBM and cortical thickness analyses at baseline showed no GM volume differences in *MAPT* mutation carriers compared with non-carriers. VBM analysis at follow-up, showed lower GM volume in the left temporal pole of *MAPT* mutation carriers (Fig3A, Appendix C.1), and cortical thickness analysis at follow-up showed a trend towards cortical thinning of the right inferior temporal lobe (at pFWE=0.072; Fig3B, Appendix C.2). Longitudinal analysis showed significant GM volume decline in the hippocampus compared to non-carriers (Fig3A, Appendix C.1), whereas cortical thickness analysis did not pick up any longitudinal changes. Non-carriers did not show areas of GM volume decline or cortical thinning compared to *MAPT* mutation carriers.

Baseline or follow-up cross-sectional analyses did not show any significant WM differences in *MAPT* mutation carriers. Longitudinal analyses showed significant lower FA in the left

Figure 1. Gray matter differences in *C9orf72* repeat expansion carriers

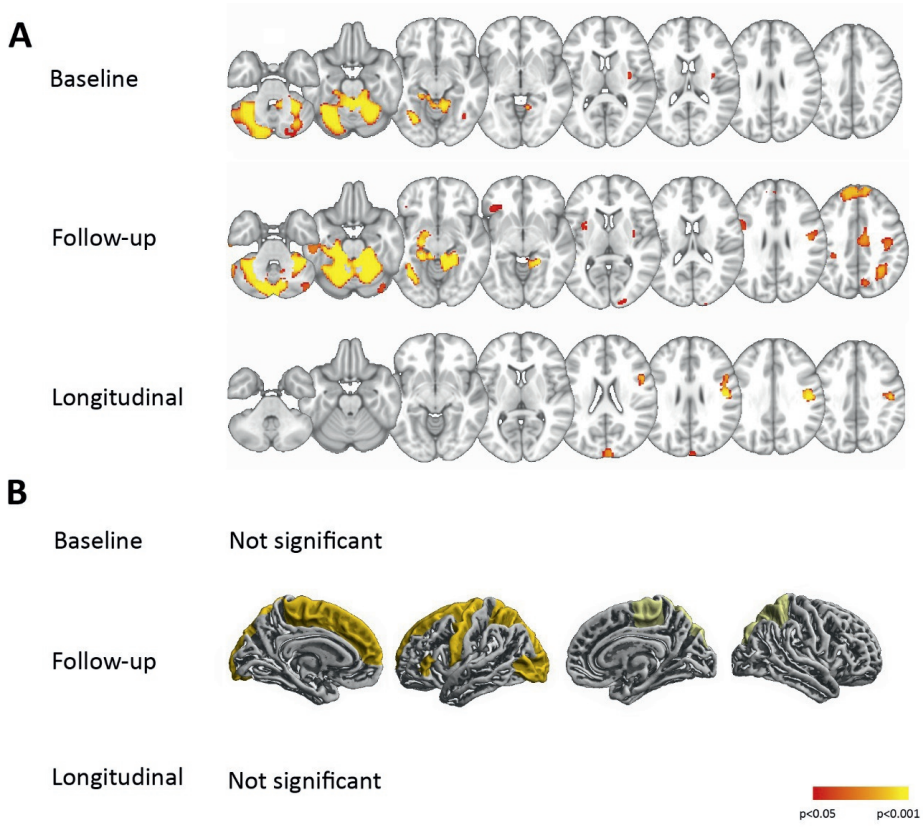

A. VBM comparisons, $p^{FWE} < 0.05$. GM of *C9orf72* repeat expansion carriers compared to non-carriers. B Cortical thickness analysis, $p^{FWE} < 0.05$. Thinning in *C9orf72* repeat expansion carriers compared to non-carriers. Abbreviations: GM: gray matter, VBM: voxel-based morphometry.

uncinate fasciculus, the left anterior thalamic radiation and the left inferior fronto-occipital fasciculus of *MAPT* mutation carriers compared to non-carriers (Fig4, Appendix C.3). There were no significant changes in MD over time in *MAPT* mutation carriers compared to non-carriers.

GRN mutation carriers versus non-carriers. *GRN* mutation carriers did not show GM volume or cortical thickness differences compared with non-carriers at baseline, follow-up or in longitudinal analyses. In addition, non-carriers did not show any loss of GM volume or cortical thinning compared to *GRN* mutation carriers. Furthermore, we did not find significant differences in FA or MD between *GRN* mutation carriers and non-carriers.

Comparisons between mutation groups. *C9orf72* repeat expansion carriers showed lower

Figure 2. White matter differences in *C9orf72* repeat expansion carriers.

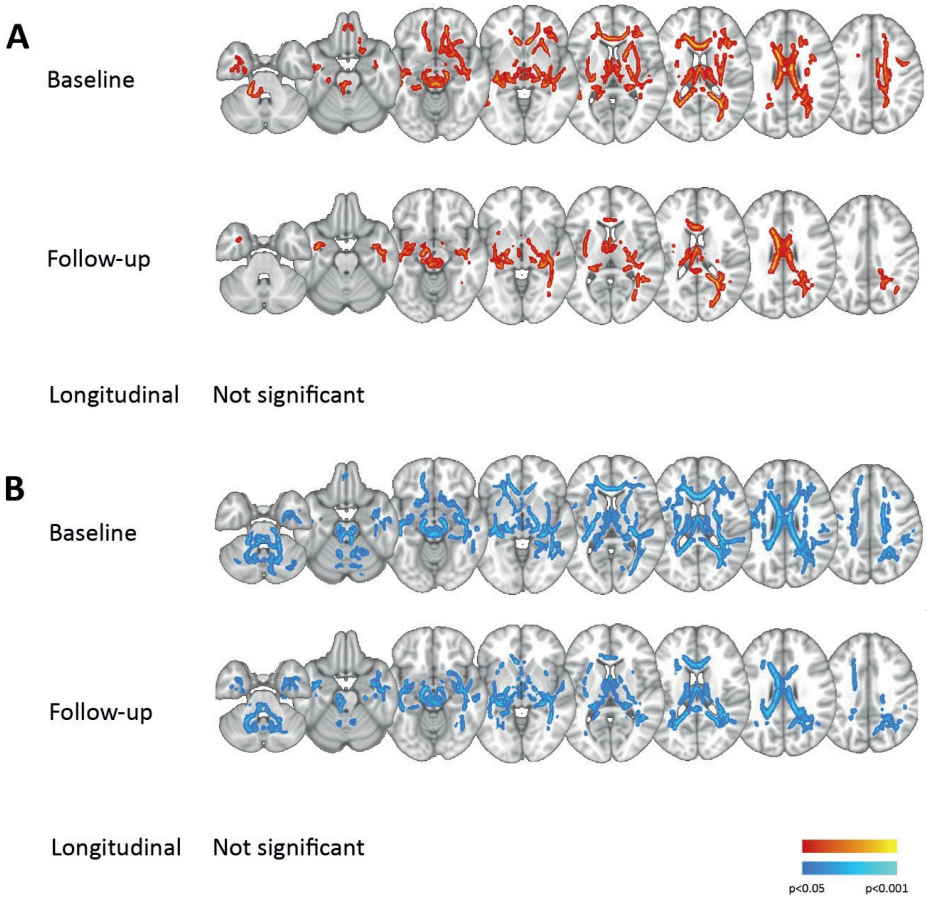

A: Lower FA in *C9orf72* repeat expansion carriers compared to non-carriers, $p^{FWE} < 0.05$. B: Higher MD in *C9orf72* repeat expansion carriers compared to non-carriers, $p^{FWE} < 0.05$. Abbreviations: FA: fractional anisotropy, MD: mean diffusivity

GM volume in the cerebellum, thalamus and insula in at both baseline and follow up when compared to *MAPT* mutation carriers (Appendix C.1). Compared to *GRN* mutation carriers, *C9orf72* repeat expansion carriers had lower GM volume in the cerebellum, thalamus, insula and frontal cortical regions at baseline and follow up (Appendix C.1). Additionally, cortical thickness analyses showed thinning in *C9orf72* repeat expansion carriers compared to *GRN* mutation carriers in the precentral and postcentral gyrus, at baseline and follow up (Appendix C.2).

We did not find longitudinal VBM or cortical thickness changes in *C9orf72* repeat expansion carriers compared to *GRN* or *MAPT* mutation carriers. We found thinning of the right temporal

Figure 3. Gray matter changes in *MAPT* carriers.

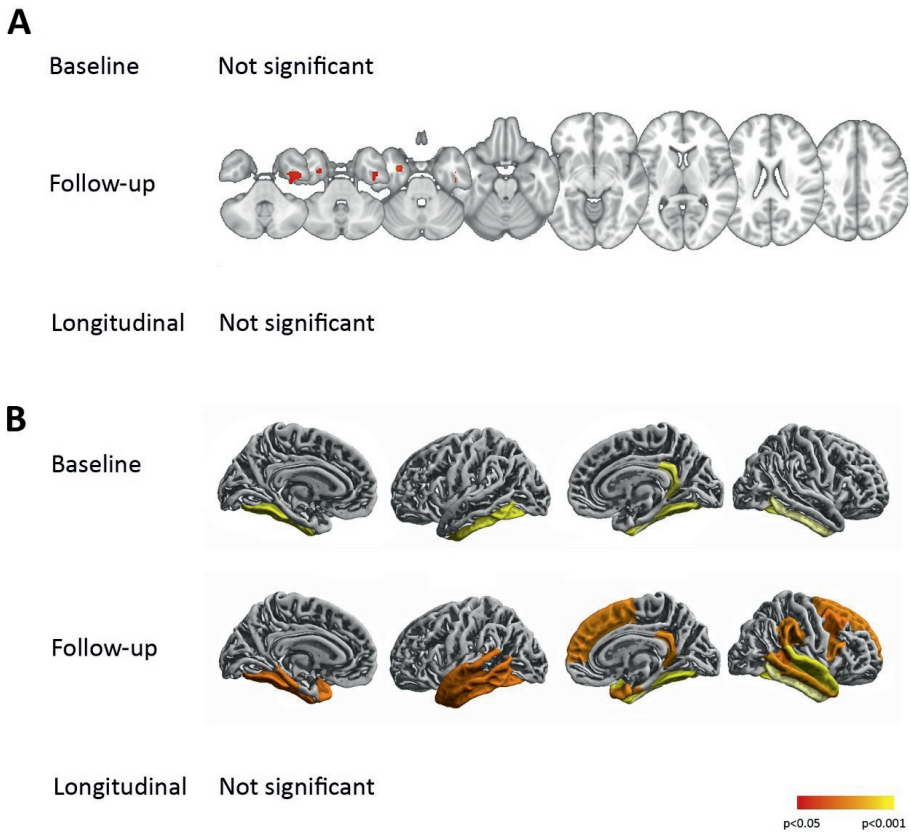

A. VBM comparisons, $p^{FWE} < 0.05$. GM of *MAPT* carriers compared to non-carriers. B Cortical thickness analysis, $p^{FWE} < 0.05$. Thinning in *MAPT* carriers compared to non-carriers. Abbreviations: GM: gray matter, VBM: voxel-based morphometry.

pole in *MAPT* mutation carriers compared to *GRN* mutation carriers at follow up (Appendix C.2), but not at baseline or longitudinally. There were no VBM or cortical thickness changes in *MAPT* mutation carriers compared to *C9orf72* repeat expansion carriers, or changes in *GRN* mutation carriers compared to *MAPT* mutation carriers or *C9orf72* repeat expansion carriers at baseline, follow up or longitudinally.

C9orf72 repeat expansion carriers had lower FA and higher MD in the bilateral anterior thalamic radiation and forceps minor and major, right uncinate and inferior fronto-occipital fasciculus and corticospinal tract at baseline compared to *MAPT* mutation carriers, (Appendix C.3). At follow up, *C9orf72* repeat expansion carriers had lower FA in the bilateral anterior thalamic radiation, right temporal and left frontal tracts compared to *MAPT* mutation carriers,

Figure 4. Longitudinal FA degeneration in *MAPT* carriers

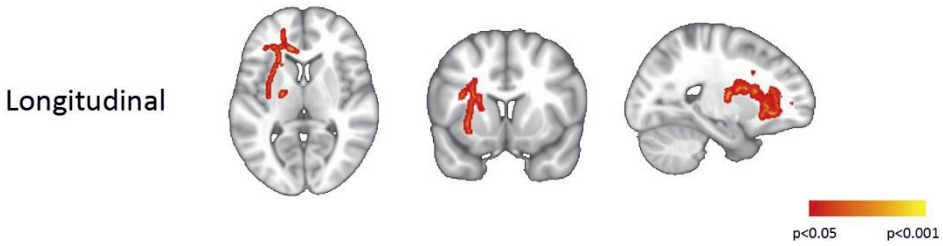

Longitudinal fractional anisotropy (FA) degeneration in *MAPT* mutation carriers compared to non-carriers, $p^{FWE} < 0.05$

without differences in MD at follow up. Compared to *GRN* mutation carriers, we found higher MD in *C9orf72* repeat expansion carriers in bilateral temporal and parietal tracts at baseline, and in the right superior longitudinal and inferior fronto-occipital fasciculus at follow up (Appendix C.3). We did not find differences in FA between *C9orf72* repeat expansion carriers and *GRN* mutation carriers.

Longitudinal analysis did not reveal any significant differences in FA or MD between *C9orf72* repeat expansion carriers and *MAPT* or *GRN* mutation carriers. Compared to *GRN* mutation carriers, we found a longitudinal decline of FA in *MAPT* mutation carriers in left frontal tracts, predominantly in the uncinate and inferior fronto-occipital fasciculus (Appendix C.3) No other FA or MD changes were found in *MAPT* mutation carriers at baseline or follow up compared to *GRN* mutation carriers or *C9orf72* repeat expansion carriers. Compared to *MAPT* mutation carriers, *GRN* mutation carriers had lower FA at follow up in left frontal tracts, predominantly the forceps major, but not at baseline or longitudinal analyses (Appendix C.3). We did not find changes in FA or MD in *GRN* mutation carriers compared to *C9orf72* repeat expansion carriers.

DISCUSSION

In this longitudinal MRI study, we found presymptomatic GM and WM changes in *C9orf72* repeat expansion carriers and *MAPT* mutation carriers at cross-sectional and longitudinal analyses, but not in *GRN* mutation carriers. Compared with non-carriers, presymptomatic *C9orf72* repeat expansion carriers showed prominent lower GM volume in the cerebellum, thalamus, insula, and cortical frontal and temporal regions, seemingly stable over time. WM differences in *C9orf72* repeat expansion carriers were found in subcortical and posterior tracts, particularly the anterior thalamic radiation. *MAPT* mutation carriers were characterized by left-sided GM volume loss and right-sided cortical thinning in the temporal lobe at follow

up, and longitudinal WM changes in predominantly left-sided frontotemporal tracts when compared with non-carriers.

Our longitudinal findings indicate that the presymptomatic stage of *C9orf72* repeat expansion is characterized by a stable lower GM volume in the cerebellum, thalamus, insula and several frontal and temporal regions [18].The prominent cerebellar atrophy was in line with other presymptomatic cross-sectional studies [3, 6, 15], though the study of Rohrer et al. [18] suggested a temporal ordering of presymptomatic changes with atrophy in the thalamus, insula, occipital, frontal and temporal lobe preceding cerebellar atrophy, already 25 years before estimated symptom onset. Due to methodological differences (e.g. mixed effect models based on region of interest data vs. whole brain analyses, percentage of total intracranial volume vs. absolute measures, and the use of estimated years of onset), it is difficult to compare our findings to the GENFI consortium paper. However, it is important to appreciate the fact that *C9orf72* repeat expansion mutation carriers seem to show remarkable early GM changes [3, 18, 19]. This has been explained previously as either following a trajectory with an early onset and very slow progression of atrophy [18], or as a neurodevelopmental disorder [11, 19]. Though our results agree with early GM and WM differences in presymptomatic *C9orf72* repeat expansion carriers compared with non-carriers, we cannot comment on the underlying mechanism. Stable lower GM volume may indicate a neurodevelopmental process, but could also mean that our two year follow up period is not sufficient to detect very slow progressive brain changes.

Our findings of extensive subcortical WM differences at baseline between *C9orf72* repeat expansion carriers and non-carriers are in line with previous studies, indicating early involvement of the thalamic radiation in symptomatic *C9orf72* carriers, with both the ALS and FTD phenotype [39-41]. Furthermore, in this study we showed that these WM differences remain relatively stable during a two-year period. Functional connectivity loss in presymptomatic *C9orf72* repeat expansion carriers has been found in the thalamus and the salience network [11]. Decreasing WM connections in the thalamus in *C9orf72* repeat expansion may underlie functional connectivity and neuronal loss in areas related to the salience network, such as the insula and orbitofrontal cortex [42, 43], which is strongly associated with FTD [42, 44].

The GM and WM regions that were affected in our cross-sectional analyses in *C9orf72* repeat expansion carriers were in accordance with expected pathology in FTD and ALS [8], e.g. orbitofrontal, temporal and insula atrophy are associated with behavioural variant FTD [2, 13, 45], and changes in the precentral and postcentral gyrus may eventually underlie ALS [46, 47]. Our results of subcortical WM loss could well fit both FTD and ALS phenotypes of the *C9orf72* repeat expansion [39-41]. When performing MRI group analysis in specifically presymptomatic *C9orf72* repeat expansion carriers, it is important to keep in mind the

heterogeneity in disease phenotype, e.g. FTD or ALS, memory or psychiatric disorders [8]. In line with this reasoning, the location of emerging presymptomatic GM volume loss might predict the disease phenotype of an individual *C9orf72* repeat expansion carrier. And, both the onset of pathophysiological changes as well as the affected brain regions may be highly variable across patients, which complicates comparisons between cross-sectional group analyses and claims on the onset of neurodegeneration. The mean disease onset in *C9orf72* repeat expansion carriers has been reported at 50 years of age, ranging from early adulthood to old-age – e.g. 27 to 83 years, and large intra-family heterogeneity in disease onset and phenotype is common [48, 49]. Therefore, the disease trajectory of *C9orf72* repeat expansion carriers may be elucidated by longer follow up periods and longitudinal modelling with both presymptomatic and symptomatic carriers with different phenotypes.

At follow up, we found cortical GM thinning in the right temporal lobe in presymptomatic *MAPT* mutation carriers, and GM volume loss in the left temporal pole and parahippocampal gyrus, which is line with previous cross-sectional presymptomatic *MAPT* studies [6, 7, 18], and resembles the atrophy pattern found in symptomatic *MAPT* carriers 28, [45, 50, 51]. Furthermore, GM volume in the right hippocampus significantly decreased over time. In addition, we found longitudinal WM changes in left-sided frontotemporal association tracts including the uncinate fasciculus, which connects structures of the limbic system in the temporal lobe with the orbitofrontal cortex, and has been indicated to underlie inhibition and impulse control [52, 53]. Although our results are somewhat contradicting in asymmetry, and involve left or right hemispheres in VBM and cortical thickness analyses, this may suggest emerging pathophysiological changes in both temporal lobes of *MAPT* mutation carriers. Therefore, as previously proposed, VBM and cortical thickness analyses may be applied as complementary methods [30, 31]. VBM relies on a mixture of measurements in cortical thickness, cortical surface areas and folding of the gyri [36]. When used together, voxel-based cortical thickness analysis could aid understanding of underlying GM differences, especially in age-related brain changes [30, 54]. Even though the *MAPT* mutation carriers were younger (mean age: 41.77) than non-carriers (mean age: 50.72) and *GRN* mutation carriers (mean age: 52.10), mean onset in *MAPT* mutations has been reported at 55 [48], and ranges till before 40 in some families [2]. Therefore, the majority of our *MAPT* mutation carriers are likely within one or two decades before symptom onset. The present findings combined with previous functional MRI, cognitive and GM studies [9, 18, 20] indicate that GM and WM loss in presymptomatic *MAPT* carriers gradually progressed in a period of five to ten years before symptom onset, starting in the temporal lobe, followed by slowly progressive cognitive decline.

The absence of any significant changes in a relatively large cohort of presymptomatic *GRN* mutation carriers compared to non-carriers in the present study is a remarkable finding,

supported by previous cross-sectional studies [6, 7]. One may argue that in a voxel-based group-wise analysis subtle changes may remain undetected due to the typical, but in the presymptomatic stage, not yet visible asymmetrical left or right-sided atrophy in *GRN* mutation carriers [6, 50]. Yet, Rohrer et. al [18] found GM volume decline 15 years before expected age of onset with linear mixed modelling in *GRN* mutation carriers when combining the right and left insula. An alternative explanation might be that pathophysiological changes due to *GRN* mutation carriers spread quite rapidly, with extensive damage in a short period before symptom onset [6]. Such hypothesis may be supported by the rapid decrease in cognitive functioning and strong increase in CSF NfL levels in the short transitional stage from presymptomatic till symptom onset in *GRN* mutation carriers [10, 13], accompanied by quickly expanding atrophy on T1-weighted imaging, starting eighteen months before symptom onset [55]. Since the asymmetric left or right-sided pattern of atrophy differs in patients even from the same families [45, 51, 56], and therefore group-wise neuroimaging analyses in presymptomatic carriers may result in a less useful biomarker for *GRN* mutation carriers, other biomarkers that measure pathological changes may be necessary. In *GRN* mutation carriers, mean symptom onset may be 65 years, but fluctuates within families up to 20 years [2, 48]. Rapid changes over time implicate that 6- to 12 months monitoring from susceptible ages, e.g. from ~45 years onward may be indicated in *GRN* mutation carriers [2, 56, 57], to enable prescription of – future – pharmacological treatment before onset of the neurodegenerative process.

Key strengths of our study are the longitudinal measurements in a large cohort of presymptomatic FTD mutation carriers, and the single-center standardized MRI protocol with stable sequence parameters over time. Longitudinal multimodal imaging adds significant value over cross-sectional or unimodal imaging, as it enables insight into the profile and trajectory of brain changes. However, our current cross-sectional baseline findings in *C9orf72* repeat expansion carriers were not completely compliant with previous baseline findings of our group [15], and can be explained by the current increased control group that could have led to an increase in statistical power. Especially for the *C9orf72* repeat expansion and *MAPT* mutation group, our sample size was quite small, and results in these mutation groups may have been driven by individual carriers. Region of interest (ROI) analyses could overcome some of the power problems, as it significantly reduces the strictness of the multiple comparisons correction, however with the risk that unexpected brain regions may be overlooked. Before choosing predefined ROI's, explorative whole brain analyses in the presymptomatic stage are necessary– which we aimed to accomplish with our present study. Furthermore, when using mixed effects models and longer follow up periods, ROI based analysis could elucidate on the rate of brain changes and the acceleration related to time towards symptom onset or increasing age, as for example in the GENFI study [18]. However, using estimated years to onset in longitudinal mixed effects models

may be disadvantageous, as large intra-familiar heterogeneity in age at disease onset has been reported in genetic FTD mutations [2, 48, 49]. Our follow-up and longitudinal results may have been slightly compromised by a software upgrade on our MRI scanner [58-60]. To account for possible signal changes, we added a covariate to our statistical analyses, minimizing the potential effects of the scanner update.

In conclusion, this study shows distinct presymptomatic GM and WM alterations across *C9orf72* repeat expansion, and *MAPT* and *GRN* mutations carriers. Presymptomatic neuroanatomical changes in *C9orf72* repeat expansion carriers, in particular affecting the cerebellum and subcortical grey and white matter, may be present early in the disease process and our results point towards a possible neurodevelopmental disorder. In *MAPT* mutation carriers, our results suggest gradual progression of neurodegeneration, starting with GM volume loss, cortical thinning and WM integrity loss in the temporal lobes. Rapid pathophysiological and neuroanatomical progression may reflect the trajectory before symptom onset in *GRN* mutation carriers, as we found no cross-sectional and longitudinal changes in a relatively large group of presymptomatic *GRN* mutation carriers. Complicating factors when performing longitudinal group analyses in presymptomatic FTD mutation carriers are an asymmetric pattern of atrophy and heterogeneity in pathophysiology, phenotype and onset-age. Other studies may confirm and elaborate on our longitudinal findings, increasing insight in the timing and progression of genotype- and phenotype-related presymptomatic neurodegeneration in genetic FTD.

REFERENCES

1. Renton, A.E., Majounie, E., Waite, A., et al. 2011. A hexanucleotide repeat expansion in C9ORF72 is the cause of chromosome 9p21-linked ALS-FTD. Neuron 72(2), 257-68.
2. Seelaar, H., Rohrer, J.D., Pijnenburg, Y.A., et al. 2011. Clinical, genetic and pathological heterogeneity of frontotemporal dementia: a review. J Neurol Neurosurg Psychiatry 82(5), 476-86.
3. Bertrand, A., Wen, J., Rinaldi, D., et al. 2017. Early Cognitive, Structural, and Microstructural Changes in Presymptomatic C9orf72 Carriers Younger Than 40 Years. JAMA Neurol.
4. Borroni, B., Alberici, A., Premi, E., et al. 2008. Brain magnetic resonance imaging structural changes in a pedigree of asymptomatic progranulin mutation carriers. Rejuvenation Res 11(3), 585-95.
5. Caroppo, P., Habert, M.O., Durrleman, S., et al. 2015. Lateral Temporal Lobe: An Early Imaging Marker of the Presymptomatic GRN Disease? J Alzheimers Dis 47(3), 751-9.
6. Cash, D.M., Bocchetta, M., Thomas, D.L., et al. 2017. Patterns of gray matter atrophy in genetic frontotemporal dementia: results from the GENFI study. Neurobiol Aging 62, 191-6.
7. Dopper, E.G., Rombouts, S.A., Jiskoot, L.C., et al. 2014. Structural and functional brain connectivity in presymptomatic familial frontotemporal dementia. Neurology 83(2), e19-26.
8. Floeter, M.K., Bageac, D., Danielian, L.E., et al. 2016. Longitudinal imaging in C9orf72 mutation carriers: Relationship to phenotype. Neuroimage Clin 12, 1035-43.
9. Jiskoot, L.C., Dopper, E.G., Heijer, T., et al. 2016. Presymptomatic cognitive decline in familial frontotemporal dementia: A longitudinal study. Neurology 87(4), 384-91.
10. Jiskoot, L.C., Panman, J.L., van Asseldonk, L., et al. 2018. Longitudinal cognitive biomarkers predicting symptom onset in presymptomatic frontotemporal dementia. J Neurol.
11. Lee, S.E., Sias, A.C., Mandelli, M.L., et al. 2017. Network degeneration and dysfunction in presymptomatic C9ORF72 expansion carriers. Neuroimage Clin 14, 286-97.
12. Meeter, L.H., Dopper, E.G., Jiskoot, L.C., et al. 2016. Neurofilament light chain: a biomarker for genetic frontotemporal dementia. Ann Clin Transl Neurol 3(8), 623-36.
13. Meeter, L.H., Kaat, L.D., Rohrer, J.D., et al. 2017. Imaging and fluid biomarkers in frontotemporal dementia. Nat Rev Neurol 13(7), 406-19.
14. Meeter, L.H., Gendron, T.F., Sias, A.C., et al. 2018. Poly(GP), neurofilament and grey matter deficits in C9orf72 expansion carriers. Annals of Clinical and Translation Neurology, 15.
15. Papma, J.M., Jiskoot, L.C., Panman, J.L., et al. 2017. Cognition and gray and white matter characteristics of presymptomatic C9orf72 repeat expansion. Neurology 89(12), 1256-64.
16. Pievani, M., Paternico, D., Benussi, L., et al. 2014. Pattern of structural and functional brain abnormalities in asymptomatic granulin mutation carriers. Alzheimers Dement 10(5 Suppl), S354-S63 e1
17. Rohrer, J.D., Warren, J.D., Fox, N.C., et al. 2013. Presymptomatic studies in genetic frontotemporal dementia. Rev Neurol (Paris) 169(10), 820-4.
18. Rohrer, J.D., Nicholas, J.M., Cash, D.M., et al. 2015. Presymptomatic cognitive and neuroanatomical changes in genetic frontotemporal dementia in the Genetic Frontotemporal dementia Initiative (GENFI) study: a cross-sectional analysis. Lancet Neurol 14(3), 253-62.
19. Walhout, R., Schmidt, R., Westeneng, H.J., et al. 2015. Brain morphologic changes in asymptomatic C9orf72 repeat expansion carriers. Neurology 85(20), 1780-8.
20. Whitwell, J.L., Josephs, K.A., Avula, R., et al. 2011a. Altered functional connectivity in asymptomatic MAPT subjects: a comparison to bvFTD. Neurology 77(9), 866-74.
21. Schuster, C., Elamin, M., Hardiman, O., et al. 2015. Presymptomatic and longitudinal neuroimaging in neurodegeneration--from snapshots to motion picture: a systematic review. J Neurol Neurosurg Psychiatry 86(10), 1089-96.
22. Bateman, R.J., Xiong, C., Benzinger, T.L., et al. 2012. Clinical and biomarker changes in dominantly inherited Alzheimer's disease. N Engl J Med 367(9), 795-804
23. Benzinger, T.L., Blazey, T., Jack, C.R. Jr., et al. 2013. Regional variability of imaging biomarkers in autosomal dominant Alzheimer's disease. Proc Natl Acad Sci U S A 110(47), E4502-9
24. Kinnunen, K.M., Cash, D.M., Poole, T., et al. 2018. Presymptomatic atrophy in autosomal dominant Alzheimer's disease: A serial magnetic resonance imaging study. Alzheimers Dement 14(1), 43-53.
25. Frings, L., Yew, B., Flanagan, E., et al, M. 2014. Longitudinal grey and white matter changes in frontotemporal dementia and Alzheimer's disease. PLoS One 9(3), e90814.
26. Krueger, C.E., Dean, D.L., Rosen, H.J., et al. 2010. Longitudinal rates of lobar atrophy in

frontotemporal dementia, semantic dementia, and Alzheimer's disease. Alzheimer Dis Assoc Disord 24(1), 43-8.
27. Whitwell, J.L. 2010. Progression of atrophy in Alzheimer's disease and related disorders. Neurotox Res 18(3-4), 339-46
28. Whitwell, J.L., Boeve, B.F., Weigand, S.D., et al. 2015. Brain atrophy over time in genetic and sporadic frontotemporal dementia: a study of 198 serial magnetic resonance images. Eur J Neurol 22(5), 745-52.
29. Whitwell, J.L., Weigand, S.D., Gunter, J.L., et al. 2011b. Trajectories of brain and hippocampal atrophy in FTD with mutations in MAPT or GRN. Neurology 77(4), 393-8.
30. Hutton, C., Draganski, B., Ashburner, J., et al. 2009. A comparison between voxel-based cortical thickness and voxel-based morphometry in normal aging. Neuroimage 48(2), 371-80.
31. Gerrits, N.J., van Loenhoud, A.C., van den Berg, S.F., et al. 2016. Cortical Thickness, Surface Area and Subcortical Volume Differentially Contribute to Cognitive Heterogeneity in Parkinson's Disease. PLoS One 11(2), e0148852
32. Rascovsky, K., Hodges, J.R., Knopman, D., et al. 2011. Sensitivity of revised diagnostic criteria for the behavioural variant of frontotemporal dementia. Brain 134(Pt 9), 2456-77.
33. Gorno-Tempini, M.L., Hillis, A.E., Weintraub, S., et al. 2011. Classification of primary progressive aphasia and its variants. Neurology 76(11), 1006-14.
34. Ludolph, A., Drory, V., Hardiman, O., et al. 2015. A revision of the El Escorial criteria - 2015. Amyotroph Lateral Scler Frontotemporal Degener 16(5-6), 291-2.
35. Cummings, J.L. 1997. The Neuropsychiatric Inventory: assessing psychopathology in dementia patients. Neurology 48(5 Suppl 6), S10-6
36. Ashburner, J., Friston, K.J. 2000. Voxel-based morphometry--the methods. Neuroimage 11(6 Pt 1), 805-21
37. Dopper, E.G., Chalos, V., Ghariq, E., et al. 2016. Cerebral blood flow in presymptomatic MAPT and GRN mutation carriers: A longitudinal arterial spin labeling study. Neuroimage Clin 12, 460-5.
38. Dahnke, R., Yotter, R.A., Gaser, C. 2013. Cortical thickness and central surface estimation. Neuroimage 65, 336-48.
39. Bede, P., Bokde, A.L., Byrne, S., et al. 2013. Multiparametric MRI study of ALS stratified for the C9orf72 genotype. Neurology 81(4), 361-9.
40. Mahoney, C.J., Beck, J., Rohrer, J.D., et al. 2012. Frontotemporal dementia with the C9ORF72 hexanucleotide repeat expansion: clinical, neuroanatomical and neuropathological features. Brain 135(Pt 3), 736-50.
41. Schonecker, S., Neuhofer, C., Otto, M., et al. 2018. Atrophy in the Thalamus But Not Cerebellum Is Specific for C9orf72 FTD and ALS Patients - An Atlas-Based Volumetric MRI Study. Front Aging Neurosci 10, 45.
42. Seeley, W.W. 2010. Anterior insula degeneration in frontotemporal dementia. Brain Struct Funct 214(5-6), 465-75.
43. Uddin, L.Q. 2015. Salience processing and insular cortical function and dysfunction. Nat Rev Neurosci 16(1), 55-61.
44. Zhou, J., Greicius, M.D., Gennatas, E.D., et al. 2010. Divergent network connectivity changes in behavioural variant frontotemporal dementia and Alzheimer's disease. Brain 133(Pt 5), 1352-67.
45. Gordon, E., Rohrer, J.D., Fox, N.C. 2016. Advances in neuroimaging in frontotemporal dementia. J Neurochem 138 Suppl 1, 193-210.
46. Chio, A., Pagani, M., Agosta, F., et al. 2014. Neuroimaging in amyotrophic lateral sclerosis: insights into structural and functional changes. Lancet Neurol 13(12), 1228-40.
47. Turner, M.R., Agosta, F., Bede, P., et al. 2012. Neuroimaging in amyotrophic lateral sclerosis. Biomark Med 6(3), 319-37.
48. Olszewska, D.A., Lonergan, R., Fallon, E.M., et al. 2016. Genetics of Frontotemporal Dementia. Curr Neurol Neurosci Rep 16(12), 107
49. Van Mossevelde, S., van der Zee, J., Gijselinck, I., et al. 2017. Clinical Evidence of Disease Anticipation in Families Segregating a C9orf72 Repeat Expansion. JAMA Neurol 74(4), 445-52.
50. Rohrer, J.D., Ridgway, G.R., Modat, M., et al. 2010. Distinct profiles of brain atrophy in frontotemporal lobar degeneration caused by progranulin and tau mutations. Neuroimage 53(3), 1070-6.
51. Whitwell, J.L., Weigand, S.D., Boeve, B.F., et al. 2012. Neuroimaging signatures of frontotemporal dementia genetics: C9ORF72, tau, progranulin and sporadics. Brain 135(Pt 3), 794-806.

52. Hornberger, M., Geng, J., Hodges, J.R. 2011. Convergent grey and white matter evidence of orbitofrontal cortex changes related to disinhibition in behavioural variant frontotemporal dementia. Brain 134(Pt 9), 2502-12
53. Olson, I.R., Von Der Heide, R.J., Alm, K.H., et al. 2015. Development of the uncinate fasciculus: Implications for theory and developmental disorders. Dev Cogn Neurosci 14, 50-61
54. Pereira, J.B., Ibarretxe-Bilbao, N., Marti, M.J., et al. 2012. Assessment of cortical degeneration in patients with Parkinson's disease by voxel-based morphometry, cortical folding, and cortical thickness. Hum Brain Mapp 33(11), 2521-34.
55. Rohrer, J.D., Warren, J.D., Barnes, J., et al. 2008. Mapping the progression of progranulin-associated frontotemporal lobar degeneration. Nat Clin Pract Neurol 4(8), 455-60
56. van Swieten, J.C., Heutink, P. 2008. Mutations in progranulin (GRN) within the spectrum of clinical and pathological phenotypes of frontotemporal dementia. Lancet Neurol 7(10), 965-74
57. Onyike, C.U., Diehl-Schmid, J. 2013. The epidemiology of frontotemporal dementia. Int Rev Psychiatry 25(2), 130-7.
58. Shuter, B., Yeh, I.B., Graham, S., et al. 2008. Reproducibility of brain tissue volumes in longitudinal studies: effects of changes in signal-to-noise ratio and scanner software. Neuroimage 41(2), 371-9.
59. Takao, H., Hayashi, N., Kabasawa, H., et al. 2012. Effect of scanner in longitudinal diffusion tensor imaging studies. Hum Brain Mapp 33(2), 466-77.
60. Takao, H., Hayashi, N., Ohtomo, K. 2013. Effects of the use of multiple scanners and of scanner upgrade in longitudinal voxel-based morphometry studies. J Magn Reson Imaging 38(5), 1283-91.

APPENDIX A

Table A.1 Composite cognitive domain scores

	C9orf72	*GRN*	*MAPT*	p-value
BASELINE				
Language	-0.089 (0.599)	0.001 (0.947)	0.221 (0.797)	0.812
Attention	-0.130 (0.674)	-0.014 (0.905)	0.302 (0.571)	0.391
Executive functioning	-0.117 (0.850)	0.051 (0.966)	0.313 (0.616)	0.417
Memory	0.322 (0.433)	0.090 (0.918)	0.107 (1.536)	0.263
Visuoconstruction	-0.288 (1.269)	0.008 (2.096)	0.239 (1.700)	0.796
Social cognition	-0.163 (0.485)	0.305 (0.694)	0.328 (0.703)	0.055
FOLLOW UP				
Language	-0.088 (0.655)	0.104 (0.771)	-0.099 (0.804)	0.832
Attention	-0.298 (0.814)	-0.046 (0.880)	0.343 (0.528)	0.190
Executive functioning	-0.237 (0.841)	0.164 (0.781)	0.168 (0.623)	0.578
Memory	0.008 (1.137)	-0.030 (1.030)	-0.172 (1.944)	0.847
Visuoconstruction	-0.636 (1.166)	-0.069 (0.838)	0.099 (0.810)	0.315
Social cognition	-0.457 (0.848)	0.407 (0.763)	0.123 (0.803)	0.018*

Non-parametric Kruskal Wallis tests between mutation groups and non-carriers. Post-hoc Mann-Whitney-U tests demonstrated that *GRN* mutation carriers performed significantly better at social cognition tasks than non-carriers and *C9orf72* repeat expansion carriers at follow up.

APPENDIX B

Table B.1 Distribution of scans with respect to the software update

	Non-carriers	***C9orf72***	***MAPT***	***GRN***
Baseline scan before update	53	12	15	33
Baseline scan after update	0	0	0	0
Follow-up scan before update	37	2	13	29
Follow-up scan after update	16	10	2	4

APPENDIX C

Table C.1 Significant whole brain VBM clusters

	pFWE	cluster size	MNI space			hemisphere	Peak voxel
			x	y	z		
BASELINE							
C9orf72 < non-carrier	0.000	2873	33	-6	11	right	insula
	0.000	3990	30	-57	-23	right	VI Cerebellum
	0.000	3281	-30	3	8	left	insula
	0.000	1993	-36	-50	-27	left	VI Cerebellum
	0.017	890	-45	-35	6	left	planum temporale
	0.050	659	-24	36	-14	left	orbitofrontal cortex
C9orf72 < *GRN*	0.000	4329	33	-59	-26	right	VI Cerebellum
	0.000	3049	33	-6	12	right	insula
	0.000	2406	-18	-62	-32	left	VI Cerebellum
	0.000	3230	-30	5	9	left	insula
	0.005	1196	5	24	-15	right	subcallosal cortex
	0.010	1018	54	-8	39	right	postcentral gyrus
	0.015	923	-21	51	-11	left	frontal pole
	0.052	652	-45	-35	15	left	planum temporale
C9orf72 < *MAPT*	0.000	2357	33	-3	15	right	insula
	0.000	3615	21	-48	-23	right	V cerebellum
	0.000	1942	-23	-60	-23	left	VI Cerebellum
	0.002	1420	-45	-35	14	left	planum temporale
	0.003	1320	-27	11	11	left	insula
FOLLOW UP							
MAPT < non-carrier	0.019	914	-23	-8	-38	left	parahippocampal gyrus
C9orf72 < non-carrier	0.000	9839	21	-42	-17	right	V cerebellum
	0.002	1483	-36	-30	51	left	postcentral gyrus
	0.015	963	-8	18	-9	left	subcallosal cortex
	0.023	864	42	-5	6	right	insula
	0.039	745	53	-9	41	right	postcentral gyrus
	0.041	734	45	-33	11	right	supramarginal gyrus
	0.042	731	-51	-3	-11	left	superior temporal gyrus
	0.044	718	-18	47	32	left	frontal pole
C9orf72 < *GRN*	0.000	3006	21	-42	-15	right	V cerebellum
	0.002	1502	-24	-32	59	left	postcentral gyrus

	0.011	1045	-15	-35	0	left	thalamus
	0.015	959	6	30	-15	right	subcallosal cortex
	0.021	882	53	-9	41	right	postcentral gyrus
C9orf72 < *MAPT*	0.000	3020	21	-47	-17	right	V cerebellum
	0.011	1049	-6	-27	6	left	thalamus
LONGITUDINAL							
MAPT < non-carrier	0.049	905	36	-23	-11	right	hippocampus

Significant clusters in whole brain voxel-based morphometry (VBM) analysis. Clusters below 20 voxels are not reported.

Table C.2. Significant whole brain cortical thickness clusters

	pFWE	cluster size	MNI space			hemisphere	Peak voxel
			x	y	z		
BASELINE							
C9orf72 < non-carrier	0.021	162	-17	-18	67	left	precentral gyrus
	0.06	122	33	-36	56	right	postcentral gyrus
C9orf72 < *GRN*	0.012	183	-17	-18	-67	left	precentral gyrus
	0.026	154	-4	-42	62	left	postcentral gyrus
FOLLOW UP							
MAPT < non-carrier	0.072	116	45	-14	-36	right	inferior temporal gyrus
C9orf72 < control	0.001	290	19	-49	63	right	superior parietal lobule
	0.012	185	-20	-20	72	left	precentral gyrus
	0.024	159	5	-30	54	right	precentral gyrus
MAPT < *GRN*	0.050	130	48	10	-36	right	temporal pole
C9orf72 < *GRN*	0.000	451	-21	-20	72	left	precentral gyrus
	0.000	336	5	-19	63	right	precentral gyrus
	0.040	139	20	-49	60	right	superior parietal lobule
	0.076	114	-4	-42	62	left	postcentral gyrus
LONGITUDINAL							
No supratreshold clusters							

Significant clusters in whole brain cortical thickness analysis. Clusters below 20 voxels are not reported.

Table C.3. Significant whole brain TBSS clusters

		pFWE	Cluster size	MNI Space			Hemis-phere	Peak Voxel
				X	Y	Z		
BASELINE								
FA	*C9orf72* < Non-carrier	0.004	25256	-3	23	14	left	Genu of corpus callosum
	C9orf72 < *MAPT*	0.023	2601	27	-54	18	right	forceps major
		0.030	1897	-10	20	20	left	cingulum (cingulate)
		0.034	1662	13	-17	85	right	anterior thalamic radiation
		0.032	831	30	-9	15	right	superior longitudinal fasciculus
		0.046	293	6	-27	-12	right	anterior thalamic radiation
		0.049	22	-32	-19	2	left	superior longitudinal fasciculus
MD	*C9orf72* > Non-carrier	0.002	36898	-6	28	10	left	genu of corpus callosum
	C9orf72 < *GRN*	0.005	21350	9	30	7	right	forceps minor
		0.049	123	13	-33	-40	right	corticospinal tract
		0.049	96	30	-48	-39	right	corticospinal tract
	C9orf72 < *MAPT*	0.013	20561	27	-49	20	right	inferior fronto occipital fasciculus
		0.048	222	41	-13	-22	right	inferior longitudinal fasciculus
		0.048	119	38	-66	-12	right	inferior longitudinal fasciculus
		0.049	49	-21	-3	34	left	superior longitudinal fasciculus
		0.049	32	-24	9	33	left	superior longitudinal fasciculus, temporal part
		0.049	21	-28	-1	19	left	superior longitudinal fasciculus

FOLLOW UP								
FA	*C9orf72* < Non-carrier	0.021	4864	49	-18	-20	right	inferior longitudinal fasciculus
		0.026	4086	-4	-3	4	left	anterior thalamic radiation
		0.033	1886	7	12	22	right	body of corpus callosum
		0.046	173	11	1	1	right	anterior thalamic radiation
		0.049	83	-1	-39	10	left	splenium of corpus callosum
	GRN < MAPT	0.045	495	-17	38	29	left	forceps minor
		0.048	50	-33	-6	6	left	superior longitudinal fasciculus
		0.048	33	-16	54	4	left	forceps minor
	C9orf72 < MAPT	0.031	1723	28	-49	26	right	superior longitudinal fasciculus
		0.043	1055	25	-33	1	right	anterior thalamic radiation
		0.046	874	-13	16	24	left	cingulum (cingulate)
		0.035	636	-34	-6	1	left	superior longitudinal fasciculus
		0.049	154	-36	37	-5	left	Uncinate fasciculus
		0.048	143	-27	21	25	left	Uncinate fasciculus
		0.048	40	10	1	0	right	anterior thalamic radiation
MD	*C9orf72* > Non-carrier	0.018	22491	-20	-35	7	left	anterior thalamic radiation
		0.041	1001	18	-58	-37	right	corticospinal tract
		0.044	620	-25	-42	-5	left	cingulum (hippocampus)
		0.048	69	50	-38	44	right	superior longitudinal fasciculus
	C9or7f2 > GRN	0.044	690	33	-42	15	right	inferior fronto occipital fasciculus
		0.049	157	47	-14	-22	right	inferior longitudinal fasciculus

LONGITUDINAL								
FA	*MAPT* < Non-carrier	0.030	1539	-28	37	18	left	Anterior thalamic radiation
		0.037	1399	-22	15	15	left	Anterior thalamic radiation
		0.045	52	-17	20	-9	left	Uncinate fasciculus
	MAPT < *GRN*	0.025	2146	-21	6	17	left	anterior thalamic radiation
		0.047	24	-21	-11	7	left	corticospinal tract

Significant clusters in whole brain TBSS analysis. FA = fractional anisotropy, MD = mean diffusivity. Clusters below 20 voxels are not reported.

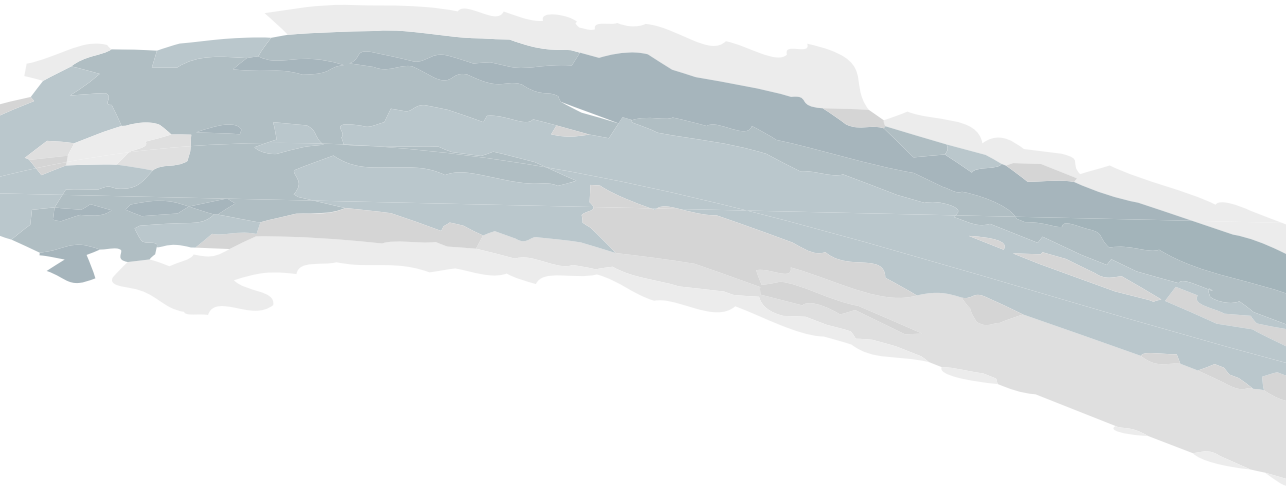

Chapter 3.2

Longitudinal multimodal MRI as prognostic and diagnostic biomarker in presymptomatic familial frontotemporal dementia

Jiskoot, L.C.
Panman, J.L.
Meeter, L.H.H.
Dopper, E.G.P.
Donker Kaat, L.
Franzen, S.
van der Ende, E.L.
van Minkelen, R.
Rombouts, S.A.R.B.
Papma, J.M.
van Swieten, J.C.

Brain, 2019

ABSTRACT

Developing and validating sensitive biomarkers for the presymptomatic stage of familial frontotemporal dementia is an important step in early diagnosis and for the design of future therapeutic trials. In the longitudinal Frontotemporal Dementia Risk Cohort, presymptomatic mutation carriers and non-carriers from families with familial frontotemporal dementia due to microtubule-associated protein tau (*MAPT*) and progranulin (*GRN*) mutations underwent a clinical assessment and multimodal MRI at baseline, 2-, and 4-year follow-up. Of the cohort of 73 participants, eight mutation carriers (three *GRN*, five *MAPT*) developed clinical features of frontotemporal dementia ('converters'). Longitudinal whole-brain measures of white matter integrity (fractional anisotropy) and grey matter volume in these converters (n = 8) were compared with healthy mutation carriers ('non-converters'; n = 35) and non-carriers (n = 30) from the same families. We also assessed the prognostic performance of decline within white matter and grey matter regions of interest by means of receiver operating characteristic analyses followed by stepwise logistic regression. Longitudinal whole-brain analyses demonstrated lower fractional anisotropy values in extensive white matter regions (genu corpus callosum, forceps minor, uncinate fasciculus, and superior longitudinal fasciculus) and smaller grey matter volumes (prefrontal, temporal, cingulate, and insular cortex) over time in converters, present from 2 years before symptom onset. White matter integrity loss of the right uncinate fasciculus and genu corpus callosum provided significant classifiers between converters, non-converters, and non-carriers. Converters' within-individual disease trajectories showed a relatively gradual onset of clinical features in *MAPT*, whereas *GRN* mutations had more rapid changes around symptom onset. *MAPT* converters showed more decline in the uncinate fasciculus than *GRN* converters, and more decline in the genu corpus callosum in *GRN* than *MAPT* converters. Our study confirms the presence of spreading predominant frontotemporal pathology towards symptom onset and highlights the value of multimodal MRI as a prognostic biomarker in familial frontotemporal dementia.

INTRODUCTION

Frontotemporal dementia (FTD) is the second most common presenile dementia disorder (onset <65 years), with a clinical profile of behavioural disturbances and/or language deterioration [behavioural variant (bv)FTD or primary progressive aphasia (PPA)] [1-3]. FTD can have an autosomal dominant inheritance pattern, with mutations in the *GRN* or *MAPT* genes and the *C9orf72* repeat expansion as its three major causes [4]. Structural neuroimaging studies in symptomatic FTD have shown predominant grey matter volume loss of the prefrontal cortex, anterior temporal lobe, insula and anterior cingulate cortex early in the disease course, with atrophy increasing as the disease progresses [5-8]. Studies now also suggest white matter integrity loss as a hallmark of FTD, exceeding grey matter atrophy in location and severity [1-3, 9].The uncinate fasciculus, connecting the orbitofrontal cortex, temporal pole, insula and amygdala, has been suggested as the key target of network-led neurodegeneration early in the disease process [10, 11; see also the literature review in the Supplementary material].

Comparable to studies in presymptomatic familial Alzheimer's [12-14] and Huntington's disease [15, 16], converging evidence from studies in familial FTD also demonstrates the presence of a presymptomatic stage, reflected in early changes in neuroimaging, cognition, blood, and CSF [17-23]. White matter integrity loss of the uncinate fasciculus was found in the presymptomatic stage of both *MAPT* [18, 22], and *GRN* mutation carriers [17]. Studies demonstrated gene-specific white matter integrity loss in the forceps minor in *MAPT* [18], and the inferior fronto-occipital fasciculus [17], and internal capsule [22] in *GRN*. Grey matter volume loss was found in, amongst others, the frontal, temporal, insular, and cingulate cortices [19, 24, 25]. Cognitive and structural neuroimaging changes were identified from 5 to 10 years before estimated onset, respectively, with the first changes in *MAPT* being naming deficits and grey matter volume loss of the temporal lobe (hippocampus and amygdala), and the first changes in *GRN* being working memory deficits and grey matter volume loss of the insula [19]. Although these results suggest a pathophysiological cascade of events in the presymptomatic stage of familial FTD, interpretation of these changes is hampered by the fact that analyses are based on cross-sectional data, and therefore do not represent individual longitudinal trajectories [12, 26]. Moreover, these studies make use of estimated years to symptom onset as a proxy for actual symptom onset, which is commonly used in familial Alzheimer's disease [12, 14, 27]. Estimated years to onset is, however, far less accurate in familial FTD, given the large variation in age at onset between and within families [28]. Recent longitudinal analyses on 4-year follow-up neuropsychological assessment data [21] demonstrated subtle cognitive decline, starting 2 years prior to the development of clinical symptoms, suggesting a more sudden onset rather than a gradual acceleration when approaching the symptomatic disease stage. Longitudinal neuroimaging

studies describing the trajectories of white matter integrity and grey matter volume loss in the presymptomatic stage of *MAPT* and *GRN* mutations are still lacking, but could provide valuable information on (i) imaging-based disease staging; (ii) characterization of disease trajectories; (iii) validation of prognostic biomarkers; and (iv) establishing the sensitivity of various neuroimaging techniques in early disease stages [26].

In this study, we investigated longitudinal changes in grey matter volume and white matter integrity over a 4-year follow-up period in mutation carriers that developed clinical features of FTD in this time window (converters), presymptomatic mutation carriers (non-converters), and non-carriers from Dutch FTD families with *GRN* or *MAPT* mutations. The study aims are threefold: (i) to investigate cross-sectional and longitudinal changes in white matter integrity and grey matter volume between converters, non-converters and non-carriers from 4 years before to symptom onset; (ii) to explore converters' within-individual trajectories; and (iii) to determine the prognostic value of longitudinal decline in multimodal neuroimaging parameters in predicting symptom onset, and to establish the best combination of multimodal neuroimaging parameters.

METHODS

Participants. A cohort of 83 participants with 50% risk of developing familial FTD, recruited between December 2009 and October 2012 from large Dutch families with *MAPT* or *GRN* mutations [18, 20, 21, 29], were followed on a 2-year basis over a time period of 4 years. DNA genotyping assigned participants either to the mutation carrier or non-carrier group: 43 mutation carriers (30 *GRN*, 13 *MAPT*) and 40 non-carriers (31 *GRN* family members, nine *MAPT* family members). At study entry, participants were asymptomatic according to established diagnostic criteria for bvFTD [30] or PPA [31], with FTD Clinical Dementia Rating–sum of boxes (FTD-CDR-SB) scores of 0 [32]. The study selection of mutation carriers was based on the presence of at least one follow-up MRI scan. We excluded 10 non-carriers who had not undergone all three study visits to ascertain stability of the data points, leaving 73 eligible participants in the final dataset (Fig. 1).

Standard protocol approvals, registrations, and patient consents. The clinical investigators and participants were blind for the participants' genetic status, except for those that underwent predictive testing at their own request. For converters, we offered genetic counselling to the patient and family members, and we unblinded the genetic status to confirm the presence of the pathogenic mutation. All participants gave written informed consent at study entry. The study was approved by the Medical and Ethical Review Committee of the Erasmus Medical Center.

Figure 1. Study design.

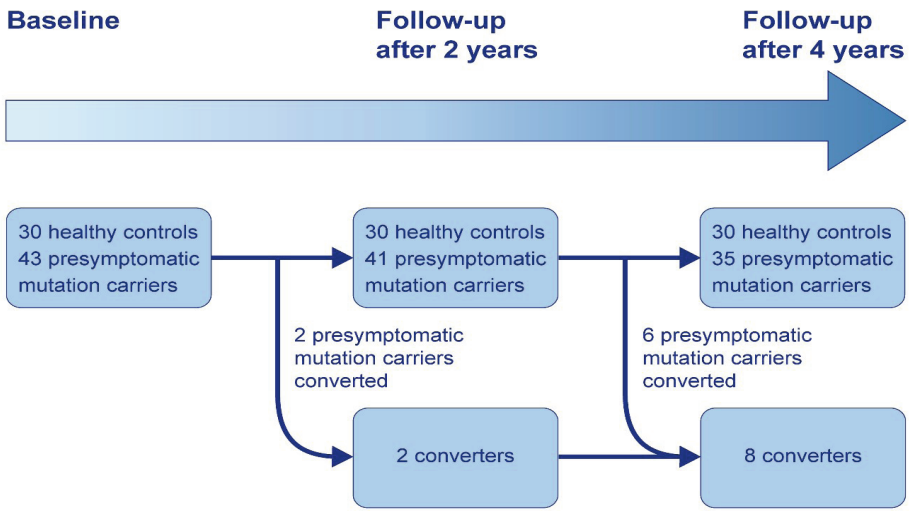

A schematic timeline of the 4-year follow-up of presymptomatic mutation carriers, converters and non-carriers within FTD-RisC. Eight mutation carriers converted to clinical FTD within the study window; two between baseline and follow-up after 2 years, and six between follow-up after 2 and 4 years. For the data analysis, the data were restructured into three new time points: 4 years before symptom onset, 2 years before symptom onset, and symptom onset.

Clinical assessment. Every 2 years, all participants underwent a standardized clinical assessment consisting of a brain MRI, medical history, neurological examination, and an extensive neuropsychological test battery. Knowledgeable informants (e.g. siblings, spouses) were asked about functional, cognitive, behavioural and/or neuropsychiatric changes by means of a structured interview, FTD-CDR-SB [32], and the Neuropsychiatric Inventory (NPI-Q), a well-validated questionnaire for neuropsychiatric features [33], either during the study visit or afterwards in a telephone interview. Participants' depressive features were rated every study visit by means of the BDI [34]. Neuropsychological testing consisted of screening tests for global cognition—the Mini-Mental State Examination (MMSE; [35]) and Frontal Assessment Battery (FAB; [36])—and tests within the domains of language, attention and mental processing speed, executive function, memory, visuoconstruction, and social cognition (see Jiskoot et al., [20, 21] for the full battery).

Converters. Eight mutation carriers developed clinical features of FTD, five carrying an *MAPT* mutation and three carrying a *GRN* mutation. Using the information from the above-mentioned clinical assessment in a multidisciplinary consensus meeting of the Erasmus MC

FTD Expertise Centre, we deemed mutation carriers to be converters (either bvFTD or PPA) if they met the following criteria: (i) progressive deterioration of behaviour and/or language by observation or history (as provided by a knowledgeable informant); (ii) significant functional decline (evidenced by FTD-CDR-SB scores >1 at the first or second follow-up visit); and (iii) cognitive deficits [<1 standard deviation (SD) in at least one domain] on neuropsychological assessment. The frontal and/or temporal atrophy on MRI in six converters (five *MAPT*, one *GRN*), together with progressive behaviour deterioration, functional decline, and cognitive deficits, met the international diagnostic consensus criteria (A–C) for probable bvFTD [30]. The presence of predominant left posterior fronto-insular atrophy on MRI in two converters (both *GRN*), in combination with a non-fluent, halting speech, sound errors and agrammatism, impaired comprehension of syntactically complex sentences and spared single-word comprehension and object knowledge met the clinical diagnostic criteria for imaging-supported non-fluent/agrammatic variant PPA (nfvPPA; [31]). The mutation carriers without clinical features of FTD (FTD-CDR-SB of 0 at all study visits) are referred to as 'non-converters' (n = 35). See Supplementary Table 1 and Supplementary material for demographic, neuroimaging, clinical and neuropsychological data of the converters, and Fig. 1 for converters' symptom onset within the study time-window.

Study design. The converters were compared to non-converters and non-carriers at three time points: baseline, follow-up after 2 and 4 years, presented as:

(i) 4 years before symptom onset: clinical and MRI data were available in six converters, as two developed symptoms between baseline and first follow-up visit, and therefore no data 4 years prior to symptom onset were available. Data were compared to baseline data of non-converters and non-carriers.

(ii) 2 years before symptom onset: clinical and MRI data were available for eight converters and compared to data of the 2-year follow-up of non-converters and non-carriers. Seven of the eight converters had reliable diffusion tensor imaging (DTI) data, while one converter (*MAPT*) was excluded due to insufficient data quality.

(iii) After symptom onset: clinical and MRI data were available from eight converters, and were compared to data of the follow-up after 4 years of non-converters and non-carriers. DTI data of seven converters were reliable, while one converter (*MAPT*) was excluded due to insufficient data quality.

Image acquisition and (pre)processing. On each study visit, we acquired volumetric T1-weighted and diffusion tensor images on a Philips 3T Achieva MRI scanner (Philips Medical Systems) using an 8-channel SENSE head coil. Images were preprocessed by means of standard FMRIB Software Library (FSL; version 5.0.6) voxel-based morphometry (VBM) and tract-based spatial statistics (TBSS) preprocessing tools (http://www.fmrib.ox.ac.uk/fsl).

See the Supplementary material for specific image acquisition parameters and preprocessing pipelines. The resulting images were fed into whole-brain voxel-wise statistics and region of interest analyses (see below).

Whole-brain voxel-wise statistics: TBSS and VBM. We investigated cross-sectional white matter diffusion (fractional anisotropy) and grey matter volume differences between converters, non-converters and non-carriers at the three time points by means of permutation-based testing using 5000 permutations, applying one-way ANCOVAs with age and gender as covariates. Change over time maps were generated by subtracting the white matter and grey matter maps calculated at the post-symptom onset visit from the maps calculated at the 4 years before symptom onset visit in FSL. Using TFCE in Randomise, the significance level was set at family-wise error-corrected $P<0.05$. As the field of view of the diffusion tensor images provided incomplete coverage of the lower brain areas including the cerebellum, the cerebellum was masked out from the TBSS analyses. In one of the converters we found a large (asymptomatic) cerebellar cyst, we therefore performed the VBM analyses in two steps, ascertaining that this subject did not significantly affect the results in the cerebellum: (i) the entire group with the cerebellum included in all subjects; and (ii) the analysis excluding the above-mentioned converter.

Region of interest selection. Based on an extensive literature search into white matter and grey matter changes in FTD (Supplementary material and Supplementary Table 2), we selected the following white matter regions of interest: uncinate fasciculus, superior longitudinal fasciculus, inferior longitudinal fasciculus, inferior fronto-occipital fasciculus, genu, body and splenium of the corpus callosum, fornix, cingulum bundle, and forceps minor. The John Hopkins University 1-mm atlas in FSL was used to parcel the entire white matter into predefined regions of interest (http://fsl.fmrib.ox.ac.uk/fsl/fslwiki/Atlases; [37]). Using FSL tools, the regions of interest were restricted to voxels included in the mean fractional anisotropy skeleton mask, after which they were applied to the fractional anisotropy skeleton, giving left and right fractional anisotropy values per tract for each participant. The Harvard-Oxford 2-mm structural Atlas in FSL was applied to each subjects' native space grey matter segmentation, after which the mean voxel grey matter partial volume estimation per region (48 left, 48 right regions of interest) was multiplied with the total volume of the image (in mm3/1000), giving the grey matter per region in millilitres. For the grey matter regions of interest, we selected the following regions: frontal lobe, prefrontal cortex, anterior temporal lobe, total temporal lobe, anterior cingulate cortex, total cingulate cortex, and insular cortex. The total cortical lobes and cingulate were the sum of all regions belonging to that area. The insula and anterior cingulate cortex were taken directly from the atlas. The prefrontal region of interest was the sum of the frontal pole, orbitofrontal cortex, and superior, middle and inferior frontal gyrus. The anterior temporal

region of interest was the sum of the temporal pole and the anterior divisions of the superior, middle and inferior temporal gyrus. All grey matter regions of interest were corrected for head size by expressing it as a percentage of the total intracranial volume in ml (%TIV), as automatically calculated in SPM12 (Wellcome Trust Centre for Neuroimaging, UCL, London, UK) running in MATLAB (version R2013b).

Statistical analysis. Statistical analyses were performed using SPSS Statistics 21.0 (IBM Corp., Armonk, NY) and GraphPad Prism 7 (La Jolla, California, USA). The significance level was set at $P<0.05$ (two-tailed) across all comparisons. We compared baseline demographic data between groups by means of one-way ANOVA, with Bonferroni post hoc testing. Between-group differences in sex were analysed using Pearson 2 tests. We analysed longitudinal data points of global cognition and questionnaires using linear mixed models. We investigated the classification abilities of region of interest white matter integrity and grey matter volume loss to discriminate between converters, non-converters and non-carriers by determining the area under the curve with 95% confidence intervals obtained by receiver operating characteristic analyses, with optimal cutoff levels at the highest Youden's index (sensitivity + specificity – 1). First, for ease of interpretation, we standardized all raw fractional anisotropy and grey matter volumes by converting them into z-scores per time point (i.e. raw score minus the mean of non-carriers, divided by the standard deviation of non-carriers). Then, we calculated delta z-scores between time points per region of interest (after onset minus 4 years before symptom onset). To assess the performance of combinations of neuroimaging parameters, we performed logistic regression analyses, taking group (converter versus non-converter and converter versus non-carrier) as dependent variable and the delta z-scores as independent variables. The models were selected with a forward stepwise method according to the likelihood ratio test and by applying the standard P-values for variable inclusion (0.05) and exclusion (0.10), with age and gender as covariates. Goodness of fit was evaluated with the Hosmer-Lemeshow 2 test. Nagelkerke R2 is reported as measure of effect size. To examine the converters' within-individual trajectories, we converted the raw clinical data scores to z-scores (i.e. individual test score minus the baseline mean of the non-carriers, divided by the baseline standard deviation of non-carriers) per time point. We calculated composite z-scores for cognitive domains by calculating z-scores per test and averaging the z-scores of the individual tests per domain (see Jiskoot et al., [20, 21] for the neuropsychological assessment battery).

Data availability. The data that support the findings of this study are available on request from the corresponding author. The data are not publicly available as they contain information that could compromise the privacy of research participants (e.g. their mutation carriership).

RESULTS

Demographics and clinical data. Demographic and clinical data of converters, non-converters and non-carriers are shown in Table 1. The mean familial age at symptom onset in converters was lower than in non-converters and non-carriers (both P = 0.006). After symptom onset, converters had lower MMSE scores than non-converters and non-carriers (both P<0.001) and significantly more neuropsychiatric features, reflected in higher BDI (P = 0.031 and P = 0.054, respectively) and NPI-Q (P = 0.075 and P = 0.011, respectively) scores. In longitudinal analyses, converters showed a significant decrease in MMSE over time (P = 0.002). Changes in global cognition or neuropsychiatric features did not reach statistical significance in non-converters and non-carriers, although somewhat higher NPI-Q scores were found in non-converters at 2- and 4-year follow-up.

Cross-sectional whole brain white matter integrity and grey matter volume loss. Four years before symptom onset, converters did not show any differences in fractional anisotropy or grey matter volume compared to non-converters and non-carriers [Table 2 and Fig. 2A(i)]. Two years before symptom onset, converters had lower fractional anisotropy values in the uncinate fasciculus, superior longitudinal fasciculus, inferior fronto-occipital fasciculus, inferior longitudinal fasciculus, corpus callosum, forceps minor, cingulum, anterior thalamic radiation and anterior corona radiata than both the other two groups [Table 2, Fig. 2A(ii) and B(ii)]. Lower grey matter volumes were found in the bilateral frontal and temporal lobes, insula and cingulate cortex, extending to the parietal lobe and cerebellum of converters compared to non-converters and non-carriers [Table 2 and Fig. 2A(ii)]. After symptom onset, converters had lower fractional anisotropy values across all white matter tracts [Table 2 and Fig. 2A(ii)], and lower grey matter volumes of large areas covering the frontal and temporal cortices, but also subcortical areas (e.g. thalamus) and cerebellum, with relative sparing of the parietal and occipital lobes in comparison to non-converters [Table 2 and Fig. 2A(ii)]. The differences were in similar locations, but more extensive in comparison to non-carriers [Table 2 and Fig. 2B(ii)]. The results were not affected by the converter with the cerebellar cyst, as exclusion did not change the abovementioned findings. No significant differences in fractional anisotropy or grey matter volumes were found between non-converters and non-carriers at any time point (Table 2).

Longitudinal whole brain white matter integrity and grey matter volume loss. Converters demonstrated longitudinal decline of fractional anisotropy in the genu corpus callosum and forceps minor over time compared to non-converters (Table 2 and Fig. 3A); this was even more extensive (left uncinate fasciculus, left superior longitudinal fasciculus and posterior corpus callosum) when compared to non-carriers (Table 2 and Fig. 3A). The longitudinal trajectories of the right uncinated fasciculus and genu corpus callosum are shown in Fig. 4A.

Table 1. Demographics and clinical data

Demographics		**Converters**	**Non-converters**	**Non-carriers**	***p*-value**
		(n=8)	**(n=35)**	**(n=30)**	
Age at study entry, y		49.5 ± 9.6	50.3 ± 10.2	50.6 ± 10.7	0.966
Sex, female (%)		4 (50)	21 (60)	19 (63.3)	0.790
Education (Verhage)[1]		6.0 ± 0.6	5.5 ± 1.0	5.4 ± 1.0	0.365
Gene, *GRN* (%)		3 (37.5)	27 (77.1)	24 (80)	0.050
Onset age family, y		52.4 ± 7.0	59.2 ± 5.5	59.4 ± 4.7	0.005
Years from estimated onset at study entry		5.0 ± 4.7	8.9 ± 8.1	N/A	0.596
Clinical data	**Years to onset**				
MMSE	**4**	29.3 ± 0.8	29.2 ± 1.5	29.4 ± 0.9	0.685
	2	29.1 ± 1.1	28.8 ± 1.9	29.4 ± 1.1	0.288
	0	26.3 ± 3.3	29.3 ± 1.2	29.4 ± 0.9	<0.001
FAB*	**4**	-	-	-	-
	2	17.3 ± 0.8	17.5 ± 0.9	17.5 ± 0.8	0.888
	0	15.7 ± 1.6	17.1 ± 1.1	16.9 ± 1.4	0.057
BDI	**4**	1.3 ± 1.6	3.5 ± 4.8	4.0 ± 4.3	0.414
	2	3.1 ± 3.9	3.2 ± 4.2	3.7 ± 4.1	0.897
	0	9.6 ± 10.5	3.0 ± 6.6	3.5 ± 4.3	0.032
NPI-Q*	**4**	-	-	-	-
	2	0.1 ± 0.4	2.9 ± 13.6	0.7 ± 1.3	0.638
	0	13.6 ± 16.4	3.9 ± 12.2	0.8 ± 1.5	0.015

Values indicate: mean ± standard deviation. Abbreviations: GRN, *progranulin*; MMSE, Mini-Mental State Examination; FAB, Frontal Assessment Battery; BDI, Beck's Depression Inventory; NPI-Q, Neuropsychiatric Inventory. [1]Dutch educational system categorized into levels from 1 = less than 6 years of primary education to 7 = academic schooling [Verhage *et al.*, 1964]. *Data only available on follow-up visits.

Furthermore, converters had significant grey matter volume loss of the prefrontal cortex, cingulate cortex, insula, temporal poles and inferior temporal gyrus in comparison to non-converters (Table 2 and Fig. 3B), again with more extensive grey matter volume loss (most of the frontal and temporal lobes, extending to the occipital cortex and cerebellum) compared to non-carriers (Table 2 and Fig. 3B). These results were also not affected by the converter with the cerebellar cyst, as exclusion did not change the above-mentioned findings. There were no significant differences in fractional anisotropy or grey matter volume loss between non-converters and non-carriers (Table 2).

Within-individual trajectories in converters. We further assessed the converters' within-

Table 2. Whole brain comparisons (TBSS, VBM) between converters, non-converters and non-carriers

	WM/GM	Cluster	Size	*p*	MNI coordinates			L/R	Area (peak voxel)
					x	y	z		
Converters vs. non-converters									
4 years before symptom onset	WM	-	-	ns	-	-	-	-	-
	GM	-	-	ns	-	-	-	-	-
2 years before symptom onset	WM	1	21781	0.004	15	42	-12	R	IFOF, UF, forceps minor
		2	1882	0.023	34	1	-32	R	cingulum
		3	144	0.047	48	-36	-4	R	SLF
		4	66	0.049	-48	-10	22	L	SLF
		5	19	0.050	-56	0	15	L	SLF
	GM	1	27122	<0.001	10	12	-28	R	orbitofrontal cortex
		2	4660	0.004	-40	2	-26	L	planum temporale
after symptom onset	WM	1	61066	<0.001	35	-8	-37	R	ILF
	GM	1	88222	<0.001	50	-12	-46	R	inferior temporal gyrus
longitudinal decline	WM	1	894	0.047	-3	153	84	n/a	gCC
	GM	1	18601	0.001	-30	22	2	L	insula
		2	6318	0.001	44	-32	-26	R	inferior temporal gyrus
Converters vs. non-carriers									
4 years before symptom onset	WM	-	-	ns	-	-	-	-	-
	GM	-	-	ns	-	-	-	-	-
2 years before symptom onset	WM	1	21781	0.004	15	42	-12	R	IFOF, UF, forceps minor
		2	1882	0.023	34	1	-32	R	cingulum
		3	144	0.047	48	-36	-4	R	SLF
		4	66	0.049	-48	-10	22	L	SLF
		5	19	0.050	-56	0	15	L	SLF
	GM	1	23126	<0.001	40	-38	-30	R	fusiform gyrus
		2	538	0.021	-16	50	32	L	frontal pole
after symptom onset	WM	1	62308	<0.001	14	50	-15	R	IFOF, UF
	GM	1	81558	<0.001	42	-10	-48	R	inferior temporal gyrus
		2	439	0.030	-14	-62	44	L	precuneus
		3	150	0.036	-18	-78	-4	L	lingual gyrus
		4	41	0.047	20	-86	-4	R	occipital fusiform gyrus

longitudinal decline	WM	1	914	0.026	-2	153	84	n/a	gCC
	GM	1	25216	0.001	-44	6	-30	L	temporal pole
		2	11300	0.001	46	-32	28	R	inferior temporal gyrus
		3	1165	0.014	18	-88	12	R	occipital pole
		4	391	0.029	-34	-70	22	L	lateral occipital cortex
		5	82	0.046	-20	-90	-4	L	occipital pole
Non-converters vs. non-carriers									
4 years before symptom onset	WM	-	-	ns	-	-	-	-	-
	GM	-	-	ns	-	-	-	-	-
2 years before symptom onset	WM	-	-	ns	-	-	-	-	-
	GM	-	-	ns	-	-	-	-	-
after symptom onset	WM	-	-	ns	-	-	-	-	-
	GM	-	-	ns	-	-	-	-	-
longitudinal decline	WM	-	-	ns	-	-	-	-	-
	GM	-	-	ns	-	-	-	-	-

Abbreviations: TBSS, Tract-Based Spatial Statistics; VBM, Voxel-Based Morphometry; MNI, Montreal Neurological Institute; R, right; L, left; gCC, genu corpus callosum; IFOF, inferior fronto-occipital fasciculus; UF, uncinate fasciculus; SLF, superior longitudinal fasciculus; ILF, inferior longitudinal fasciculus; ns, non-significant; n/a, not applicable. Clusters >50 voxels have been reported. $P<0.05$, FWE-corrected for multiple comparisons.

individual progression of global cognitive (MMSE, FAB), neuropsychiatric (NPI-Q), neuropsychological (language, executive function, social cognition, attention, memory) and neuroimaging (frontal and temporal lobe volume) measures (Fig. 5). Furthermore, a brief description of the clinical disease trajectories, including the onset of behavioural, neuropsychiatric, cognitive and neuroimaging changes can be found in the Supplementary material. As Figures 4A, 5 and the Supplementary material show, most *MAPT* converters had a relatively gradual onset of symptoms, reflected in slowly progressive clinical features and cognitive disturbances, but a steep increase of neuropsychiatric and grey matter volume loss. The *GRN* converters demonstrated more rapid changes in all biomarkers around symptom onset. With respect to cognition, *MAPT* converters demonstrated decline in all domains, namely language, attention, executive function, social cognition, and memory, while *GRN* converters declined most on attention and executive function (Supplementary Table 1 and Fig. 5). With respect to grey matter atrophy, visual inspection showed a disproportional volume loss of the (right) temporal lobes in *MAPT* converters, and relatively more volume loss of the (left) frontal lobes in *GRN* converters (Fig. 5). Visual inspection of the white matter trajectories suggested more fractional anisotropy decline in the uncinated

Figure 2. Cross-sectional whole brain grey matter volume and white matter integrity differences between converters, non-converters and non-carriers

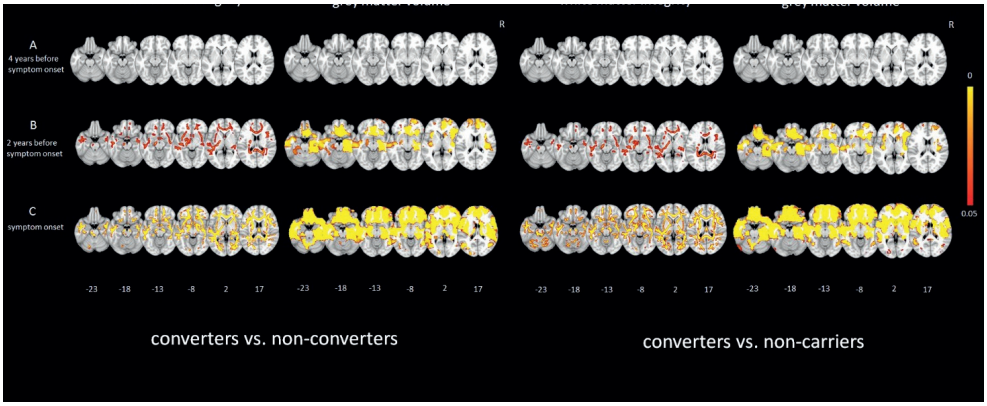

Maps illustrate significant differences in white matter integrity (FA; left) and grey matter volume (right) between converters and non-converters (Figure 2.1) and between converters and non-carriers (Figure 2.2) at 4 years before onset (A), 2 years before onset (B), and at symptom onset (C). FA thresholded (p<0.05) statistical images were thickened using tbss_fill in FSL for better visibility. Colour bars represent p-values.

Figure 3. Longitudinal whole brain grey matter volume and white matter integrity differences between converters, non-converters and non-carriers

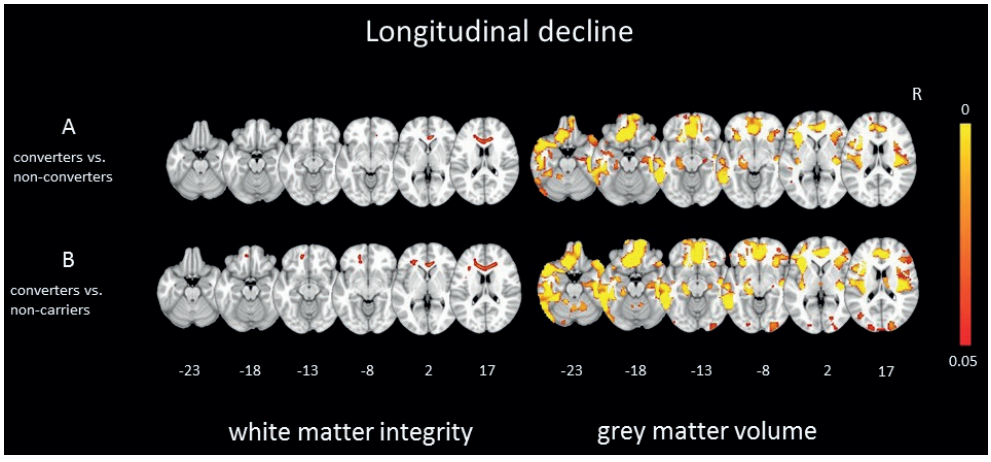

Maps illustrate significant differences in white matter integrity (left) and grey matter volume (right) between converters and non-converters (A) and between converters and non-carriers (B). FA thresholded (p<0.05) statistical images were thickened using tbss_fill in FSL for better visibility. Colour bars represent p-values.

fasciculus in *MAPT* converters than *GRN* converters, and more decline in the genu corpus callosum in *GRN* converters than *MAPT* converters (Fig. 4A). As most converters with bvFTD had an underlying *MAPT* mutation, similar patterns of decline were found; comparably, all

converters with nfvPPA had an underlying *GRN* mutation, and therefore showed similar patterns of decline to *GRN* converters (Figs 4A and 5). A steep increase of neuropsychiatric symptoms was noted in most bvFTD converters (converter 1, 2, 4 and 8), but not in nfvPPA converters (Supplementary material and Fig. 5).

Classification. Between converters and non-converters, longitudinal decline in the white matter integrity of the right uncinated fasciculus and genu corpus callosum provided significant classifiers (Table 3 and Fig. 4B). Decline in the genu corpus callosum provided the best fit for classifying between converters and non-converters ($X^2 = 0.738$; $P<0.001$). The model correctly classified 85.0% of cases. Between converters and non-carriers, longitudinal decline of the right uncinate fasciculus, genu corpus callosum, forceps minor, right inferior fronto-occipital fasciculus, right insula, and left anterior temporal lobe, provided significant classifiers (Supplementary Table 3 and Fig. 4B). Decline in the genu corpus callosum and right inferior longitudinal fasciculus provided the best fit for classifying between converters and non-carriers ($X^2 = 1.000$; $P<0.001$). The model correctly classified 100% of cases.

DISCUSSION

Our study is the first 4-year longitudinal study examining different neuroimaging modalities in a large cohort of at-risk participants from families with FTD due to *MAPT* or *GRN* mutations. Eight mutation carriers developed clinical features of FTD ('converters'). Cross-sectional analyses demonstrated extensive loss of white matter integrity and grey matter volume in converters, present from 2 years before symptom onset. Longitudinal analyses demonstrated the largest decline over time in the genu corpus callosum, uncinate fasciculus, forceps minor, and superior longitudinal fasciculus, as well as the prefrontal and cingulate cortex, insula, temporal pole and inferior temporal gyrus. Classifiers between converters, non-converters and non-carriers were white matter integrity loss of the right uncinated fasciculus and genu corpus callosum. Decline in the genu corpus callosum and right inferior longitudinal fasciculus provided the best measures for classifying between converters and non-converters. Analogous to other cohort studies in familial FTD [19], Alzheimer's disease [12-14], and Huntington's disease [15, 16], the transition period between presymptomatic and symptomatic disease stage, the time point of pathophysiological changes, type of progression and topographical order of neuroimaging changes, and genotype versus phenotype-specific patterns may give significant insights into the exact disease process of FTD; these are addressed below.

One of the key benefits of our study is the use of actual onset age in converters. Looking in more detail at symptom onset, converters with *GRN* mutations had a more sudden start of symptoms, while subtle behavioural and cognitive changes evolved over years in a few *MAPT*

Figure 4.1

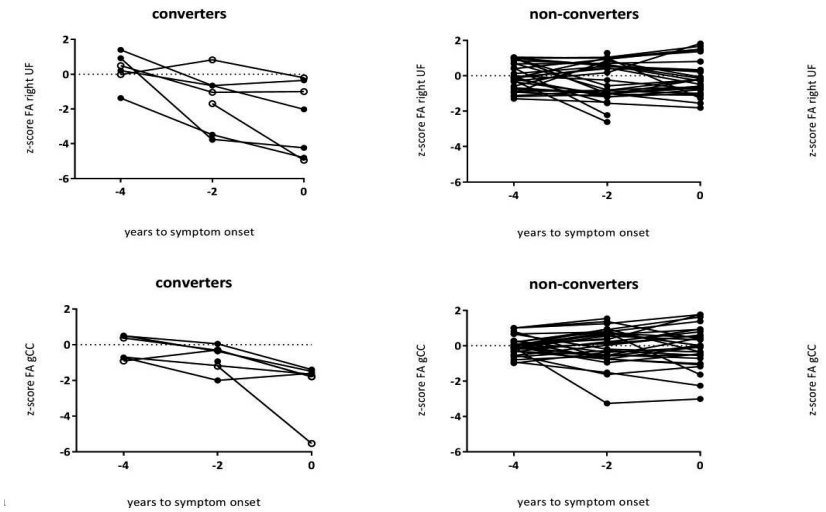

Figure 4.2

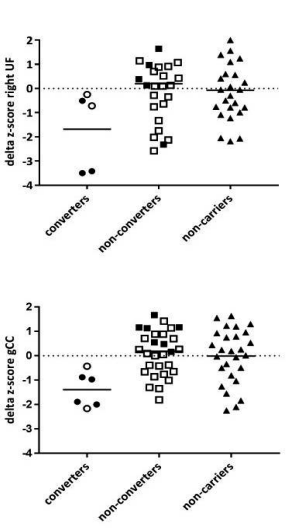

(4.1) Longitudinal trajectories of white matter integrity (FA) loss (z-score) in the right uncinate fasciculus (UF; top) and genu of the corpus callosum (gCC; bottom) in converters, non-converters and non-carriers. In converters, individual trajectories are drawn due to different sample sizes per time-point. White circles represent *GRN* converters; black circles represent *MAPT* converters. The significant decline of FA values between 2 years before symptom onset and symptom onset in converters is indicated with a bar (*). NB: Data points for two converters (one *MAPT*, one *GRN*) are missing at 4 years before symptom onset, as they converted between baseline and first follow-up, and therefore do not have the 4 years before symptom onset scan available. DTI data were of unsatisfactory quality for one (*MAPT*) converter 4 years before symptom onset (only UF), and another (*MAPT*) converter 2 years before symptom onset (both UF and gCC) – and therefore excluded. Data were unavailable at symptom onset for one converter (*MAPT*) as the scan session was terminated prematurely.

(4.2) Classification between converters, non-converters and non-carriers using the z-score delta fractional anisotropy (FA) of the right uncinate fasciculus (UF; top) and the genu of the corpus callosum (gCC; bottom). The dashed line represents the optimal cut-off to separate converters and non-converters (UF: delta FA=-0.51; sensitivity=100%, specificity=62.5% – gCC: delta FA=-0.85; sensitivity=100%, specificity=81.3%). The optimal cut-off between converters and non-carriers (not shown) is -0.39 (sensitivity= 100%, specificity= 69.6%) and -0.87 (sensitivity=100%, specificity=91.3%) for the UF and gCC respectively. White circles represent *GRN* converters; black circles represent *MAPT* converters. NB: deltas for two converters (one *MAPT*, one *GRN*) are missing, as they converted between baseline and first follow-up, and therefore do not have the 4 years before symptom onset scan available. DTI data of the UF for one (*MAPT*) converter was excluded due to unsatisfactory quality.

mutation carriers. Conversion was based on onset of clinical features of FTD (behavioural and/or language deterioration), significant functional decline, and neurocognitive deficits. All eight converters met the diagnostic criteria for probable bvFTD [30], or imaging-supported PPA [31], as they had frontal and/or temporal atrophy consistent with patterns described in early-stage symptomatic *MAPT*- and *GRN*-related FTD [38-41]. Although the present study does not include *C9orf72*-related FTD, it is important to recognize that symptomatic mutation carriers initially can have relatively normal structural imaging [42, 43] or atrophy patterns are less pronounced than in sporadic bvFTD [44]; therefore using frontal and/or temporal MRI abnormalities as core criteria in defining clinical conversion could miss a proportion of mutation carriers if generalized to a cohort including *C9orf72*. The exact timing of conversion was difficult to pinpoint due to a transitional stage of subtle behavioural or language impairment [30, 31], in line with the 'questionably/mildly symptomatic mutation carriers' described by Kinnunen et al. [14].

Analogous to the mild cognitive impairment (MCI) phase in Alzheimer's disease, several terms have been opted for this time period in FTD, such as 'pre-bvFTD' [45], 'prodromal frontotemporal dementia [FTD]' [46], 'frontotemporal MCI' [47] and the more broadly defined 'Mild Behavioural Impairment' [48]. However, they do not capture the entire range of possible clinical features in presymptomatic familial FTD, including early stage PPA. This emphasizes the need for additional clinical, neuroimaging, or fluid biomarkers. As a first step, incorporating neuropsychiatric measures into the definition of the transitional period of FTD could be considered, as subtle neuropsychiatric changes were found in presymptomatic mutation carriers in this and in previous studies [19, 49].

The most interesting findings of our study are the longitudinal changes in grey and white matter integrity 2 years before actual symptom onset, suggesting a specific 'changepoint' when approaching symptom onset. A similar pattern was demonstrated regarding neuropsychological biomarkers in the same cohort [21], with a sudden onset of cognitive decline in e.g. language, executive function, social cognition and memory from 2 years before symptom onset. Previous studies using estimated years to onset as a proxy demonstrated similar changes in grey matter volume [19], white matter integrity [22] and cognition [20], albeit earlier in the presymptomatic period, i.e. 5–10 years before estimated symptom onset. The discrepancy between the findings in our study and those in the larger GENFI study may be explained by the smaller and different samples (e.g. inclusion of *C9orf72* mutation carriers, all mutation carriers combined in one group), differences in analysis method (mixed-effects models versus ANCOVAs on changes over time maps, percentage of total intracranial volume versus corrected absolute volume), and the use of estimated years to onset versus actual symptom onset. Furthermore, when using cross-sectional data, inferences depend on the assumption that biomarker trajectories are similar across

Figure 5. Within-individual trajectories of clinical and neuroimaging changes in converters.

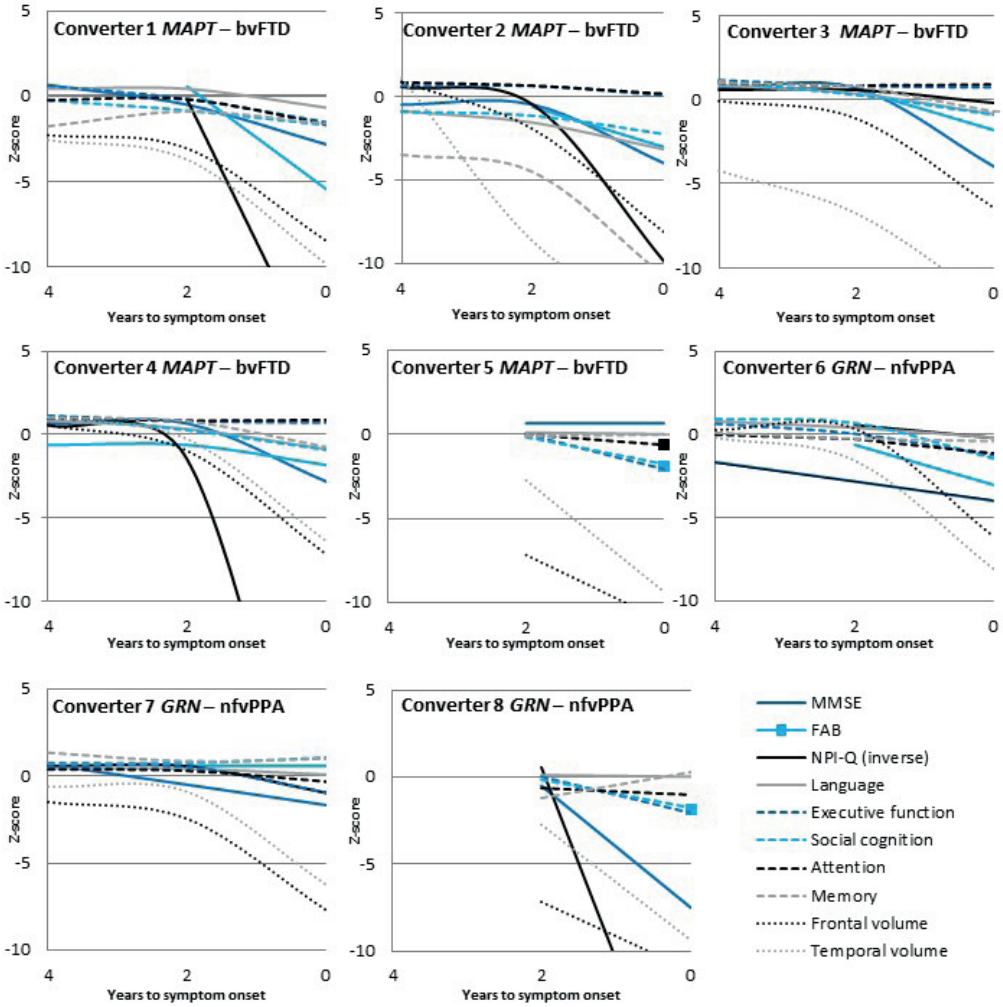

Raw data for each marker were first converted to z-scores by standardization to the baseline data of non-carriers. Each subplot (labelled with the converters number) presents the longitudinal global cognitive, neuropsychological and grey matter neuroimaging values (z-scores, y-axis) from 4 years to symptom onset to symptom onset (x-axis). The grey matter volumes of the most affected hemisphere are displayed (i.c. right side in converters with bvFTD, left side in all converters with nfvPPA). Coloured asterisks denote significant longitudinal decline (≥1 standard deviation) over time. Abbreviations: MMSE, Mini-Mental State Examination; FAB, Frontal Assessment Battery; *MAPT*, microtubule-associated protein tau; *GRN*, progranulin; bvFTD, behavioural variant frontotemporal dementia; nfvPPA, non-fluent variant primary progressive aphasia.

patients [13], while in this study we were able to show that within-individual trajectories can differ. An interesting issue is the type of change (e.g. stepped change, linear) and rate of progression (e.g. gradual, accelerated) occurring after this change-point, and a study with a larger cohort of converters with longer follow-up will certainly shed more light on this matter.

Table 3a. Diagnostic performance of white matter integrity and grey matter volume loss between converters and non-converters.

	L/R	AUC [95% CI]	p	cut-off	Sensitivity	Specificity
White matter tracts						
UF	R	0.83 [0.62-1.00]	**0.047**	-0.51	100%	62.50%
	L	0.81 [0.61-1.00]	0.059	-	-	-
SLF	R	0.72 [0.50-0.93]	0.186	-	-	-
	L	0.64 [0.31-0.97]	0.395	-	-	-
gCC	n/a	0.91 [0.86-1.00]	**0.014**	-0.85	100%	81.30%
bCC	n/a	0.59 [0.26-0.93]	0.571	-	-	-
sCC	n/a	0.72 [0.46-0.97]	0.186	-	-	-
fornix	n/a	0.80 [0.54-1.00]	0.073	-	-	-
forceps minor	n/a	0.73 [0.47-0.99]	0.156	-	-	-
cingulum bundle	n/a	0.72 [0.36-1.00]	0.186	-	-	-
IFOF	R	0.77 [0.54-0.99]	0.108	-	-	-
	L	0.67 [0.41-0.94]	0.299	-	-	-
ILF	R	0.64 [0.37-0.91]	0.395	-	-	-
	L	0.63 [0.28-0.97]	0.450	-	-	-
	L/R	**AUC [95% CI]**	**P**	**cut-off**	**Sensitivity**	**Specificity**
Grey matter areas						
frontal lobe	R	0.53 [0.22-0.84]	0.832	-	-	-
	L	0.66 [0.30-1.00]	0.235	-	-	-
prefrontal cortex	R	0.52 [0.20-0.83]	0.899	-	-	-
	L	0.66 [0.31-1.00]	0.218	-	-	-
temporal lobe	R	0.69 [0.35-1.00]	0.137	-	-	-
	L	0.61 [0.33-0.89]	0.396	-	-	-
ATL	R	0.51 [0.25-0.78]	0.932	-	-	-
	L	0.76 [0.47-1.00]	0.051	-	-	-
insula	R	0.66 [0.38-0.94]	0.218	-	-	-
	L	0.60 [0.34-0.86]	0.445	-	-	-
cingulate cortex	R	0.61 [0.31-0.91]	0.396	-	-	-
	L	0.78 [0.50-1.00]	0.034	-0.29	83.30%	86.70%
ACC	R	0.74 [0.37-0.92]	0.270	-	-	-
	L	0.65 [0.36-0.94]	0.252	-	-	-

Abbreviations: L, left; R, right; AUC, area under the curve; UF, uncinate fasciculus; SLF, superior longitudinal fasciculus; gCC, genu corpus callosum; bCC, body corpus callosum; sCC, splenium corpus callosum; IFOF, inferior fronto-occipital fasciculus; ILF, inferior longitudinal fasciculus; ATL, anterior temporal lobe; ACC, anterior cingulate cortex. White matter tract values represent FA (fractional anisotropy), ranging between 0 and 1. Grey matter area values are expressed in milliliters, corrected for total intracranial volume (TIV). The optimal cut-off level was determined by the highest Youden's index (i.e. sensitivity + specificity-1) (Youden *et al*. 1950). Significant p-values are given in bold.

Table 3b. Diagnostic performance of white matter integrity and grey matter volume loss between converters and non-carriers.

	L/R	AUC [95% CI]	p	cut-off	Sensitivity	Specificity
White matter tracts						
UF	R	0.86 [0.69-1.00]	**0.024**	-0.39	100%	69.60%
	L	0.70 [0.44-0.95]	0.219	-	-	-
SLF	R	0.71 [0.47-0.94]	0.195	-	-	-
	L	0.66 [0.30-1.00]	0.306	-	-	-
gCC	n/a	0.96 [0.88-1.00]	**0.004**	-0.87	100%	91.30%
bCC	n/a	0.59 [0.36-0.82]	0.585	-	-	-
sCC	n/a	0.62 [0.36-0.88]	0.453	-	-	-
fornix	n/a	0.70 [0.43-0.96]	0.219	-	-	-
forceps minor	n/a	0.85 [0.64-1.00]	**0.029**	-0.06	100%	65.20%
cingulum bundle	n/a	0.72 [0.37-1.00]	0.172	-	-	-
IFOF	R	0.81 [0.65-0.98]	**0.048**	-0.35	100%	73.90%
	L	0.72 [0.52-0.92]	0.172	-	-	-
ILF	R	0.66 [0.37-0.95]	0.306	-	-	-
	L	0.58 [0.23-0.93]	0.633	-	-	-
	L/R	**AUC [95% CI]**	**p**	**cut-off**	**Sensitivity**	**Specificity**
Grey matter areas						
frontal lobe	R	0.57 [0.27-0.86]	0.621	-	-	-
	L	0.62 [0.27-0.97]	0.365	-	-	-
prefrontal cortex	R	0.51 [0.20-0.81]	0.967	-	-	-
	L	0.64 [0.31-0.97]	0.284	-	-	-
temporal lobe	R	0.71 [0.43-0.99]	0.108	-	-	-
	L	0.58 [0.29-0.87]	0.537	-	-	-
ATL	R	0.60 [0.32-0.88]	0.434	-	-	-
	L	0.80 [0.50-1.00]	**0.023**	-0.24	83.30%	90.30%
insula	R	0.76 [0.54-0.98]	**0.048**	-0.30	66.70%	77.40%
	L	0.63 [0.39-0.88]	0.303	-	-	-
cingulate cortex	R	0.57 [0.25-0.89]	0.592	-	-	-
	L	0.72 [0.45-0.99]	0.091	-	-	-
ACC	R	0.52 [0.24-0.81]	0.869	-	-	-
	L	0.61 [0.29-0.93]	0.410	-	-	-

Abbreviations: L, left; R, right; AUC, area under the curve; UF, uncinate fasciculus; SLF, superior longitudinal fasciculus; gCC, genu corpus callosum; bCC, body corpus callosum; sCC, splenium corpus callosum; IFOF, inferior fronto-occipital fasciculus; ILF, inferior longitudinal fasciculus; ATL, anterior temporal lobe; ACC, anterior cingulate cortex. White matter tract values represent FA (fractional anisotropy), ranging between 0 and 1. Grey matter area values are expressed in milliliters, corrected for total intracranial volume (TIV). The optimal cut-off level was determined by the highest Youden's index (i.e. sensitivity + specificity-1) (Youden et al. 1950). Significant p-values are given in bold

The present findings of a relatively rapid/abrupt trajectory of white and grey matter changes seems to be in contrast with that seen in familial Alzheimer's disease [12, 13]. However, studies in familial Alzheimer's disease also show accelerated decline in the proximity of symptom onset [14, 50], with disease rates being at least 3.6 times higher after the change-point [14]. FTD, having shorter survival and faster rates of decline than Alzheimer's disease [30], could have an even faster rate of disease progression after the change-point.

The spatial distribution of grey matter and white matter changes 2 years before onset corresponds with significant loss of both white matter integrity and grey matter volume over time in symptomatic FTD [3, 9, 10, 51]. The lower white matter integrity of the uncinated fasciculus in converters 2 years before symptom onset confirmed this tract as the molecularly most vulnerable hub, as also found in previous studies [17, 18, 22]. The involvement of several other tracts after symptom onset in our study supports the hypothesis of a network-led framework, in which neurodegeneration propagates along largescale distributed white matter networks with disease progression [5]. The spatial patterns of white matter integrity and grey matter volume loss revealed a strong co-localization, confirming some previous studies [52, 53], but contrasting with others [1, 10, 54-57]. Although cross-sectional in nature, the cascade of presymptomatic grey matter changes found in the GENFI cohort [19] was similar to the longitudinal patterns found in this study, with the atrophy spreading from the insula, temporal and frontal cortices to the cingulate, parietal and occipital cortices with approaching estimated symptom onset.

Prior studies have suggested that white matter abnormalities occur earlier and tend to exceed the grey matter atrophy [1-3, 9]. We found relatively simultaneous onset of changes in white matter integrity and grey matter volume loss. The small number of converters did not allow us to detect a robust sequential order of grey and white matter involvement or between specific cortical regions, while more extensive progression of white matter pathology than grey matter abnormalities were found in longitudinal studies in the symptomatic stage [3, 9]. In our study, the progression of grey matter atrophy seems visually larger than the white matter integrity loss. Potentially, this does not occur initially in the presymptomatic stage, but later on in the disease process [9]. Our findings are in contrast with the more temporal order found in familial Alzheimer's disease, reflected in elevated amyloid [Pittsburgh compound B (PiB)] PET 15 years before estimated onset, followed by reduced glucose metabolism [fluorodeoxyglucose (FDG)-PET] 10 years before estimated onset, and cortical thinning 5 years before estimated onset [13]. As FDG-PET scanning has only been carried out in a small series of presymptomatic mutation carriers [58], the use of FDG-PET in a larger cohort will definitively give more insights into the temporal sequence of pathophysiological changes. Analogous to PiB-PET scanning in Alzheimer's disease, the future availability of an optimal tau PET tracer in presymptomatic carriers with *MAPT* mutations will also give more

information about the topographical and spatial spreading of tau pathology and its trajectory relative to grey matter atrophy and white matter integrity loss [59, 60].

Regarding genotype-specific patterns of neuroimaging biomarkers, the uncinate fasciculus in *MAPT* converters tended to show the most decline in white matter integrity, and *GRN* converters showed the most decline in the genu corpus callosum, although the numbers in both groups were too low to perform statistical analyses in order to draw firmer conclusions. These findings are in line with reported white matter atrophy of the uncinate fasciculus in *MAPT*-associated FTD, and white matter atrophy of the corpus callosum in *GRN*-associated FTD [40]. Most of the *MAPT* converters in our study presented with bvFTD, which could explain the prominent involvement of the uncinate fasciculus, as reported earlier by Rohrer et al. [40]. Its role in both the language processing pathway [61] and its anatomical connections to the limbic system in the temporal lobe [62] explains the strong connection between early damage to the uncinate fasciculus and the clinical phenotypes of *MAPT* and bvFTD, characterized by severe semantic and behavioural disturbances. With respect to grey matter atrophy, visual inspection showed more temporal volume loss in *MAPT* converters and frontal volume loss in *GRN* converters, in line with previous studies into both presymptomatic [19] and symptomatic familial FTD [38, 39, 41]. Most of the *GRN* converters in our study presented with nfvPPA, in which the speech production impairments have been associated with prominent atrophy of the premotor cortex and the inferior frontal lobes [2]. With respect to disease progression, most converters with *MAPT* mutations had a slower progressive onset in clinical features, cognition, and grey matter atrophy and white matter integrity loss, indicating a more gradual disease progression. In contrast, all converters with *GRN* mutations had more rapid changes in these biomarkers around symptom onset, in line with a faster disease progression [7] and atrophy occurring nearer to symptom onset [41]. Our results suggest variable disease trajectories between genetic mutation groups as well as within different genetic mutations, yet it remains to be elucidated whether the structural changes are solely phenotype-specific (bvFTD versus nfvPPA) changes, or whether they will follow genotypic patterns as well. A larger cohort with more converters will provide us with more information on this matter, as—in contrast to amyloid-b in CSF and PIB-PET scans in Alzheimer's disease—there is a lack of pathophysiological-specific biomarkers for FTD.

The predictive value of changes in the uncinate fasciculus, genu corpus callosum and left cingulate cortex for conversion in the following 2 years is an important and novel finding, as multimodal studies into FTD are scarce [63]. The finding of the genu corpus callosum as a significant discriminator between converters and non-converters is in line with the hypothesis of FTD as a network disease, in which loss of specific white matter tracts connecting grey matter areas results in large network failure. Studies into frontotemporal and Alzheimer's disease have demonstrated both unimodal white matter and grey matter volume loss as being

significant discriminators between both conditions (albeit weaker for grey matter than white matter), but the optimal classification (87% sensitivity, 83% specificity) was achieved using a combination of techniques [64]. Furthermore, Möller et al. [65] showed that white matter integrity measures added complementary information to grey matter atrophy measures in FTD. It would be valuable for future studies to replicate the present classification findings, preferably with different and/or more neuroimaging techniques (e.g. resting state functional MRI, arterial spin labelling) or other statistical algorithms (e.g. support vector machines, machine learning techniques) to determine which combination of approaches could achieve the highest classification accuracy for conversion to the symptomatic disease stage.

With upcoming clinical trials, ongoing studies are investigating the potential of longitudinal MRI as sensitive disease biomarkers. These interventions should ideally be applied in the presymptomatic stage [66]. For both white matter integrity and grey matter volume loss present at 2 years prior to symptom onset, and increasing pathology when moving into the symptomatic stage, multimodal neuroimaging has proven its value as a disease staging and tracking biomarker. Longitudinal DTI changes in the genu corpus callosum as the strongest predictor for conversion makes it a potential neuroimaging biomarker for tracking disease progression in clinical trials, particularly since this is the white matter tract most consistently found across all clinical FTD syndromes [51]. Interestingly, the white matter integrity loss between 4 and 2 years before symptom onset seems to parallel the steep increase in neurofilament light chain levels found in converters in our previous study [23]. Future research should focus on the association between DTI parameters and neurofilament light chain levels in a larger sample, as they could serve as potential biomarkers for disease staging, the prediction of underlying pathology, and monitoring of treatment response in future therapeutic trials. Moreover, investigating the white matter tract abnormalities underlying neuropsychiatric features in conversion to the symptomatic stage would be an informative next step, as recent research demonstrated distinct spatial distributions of white matter pathology to be associated with specific behavioural symptoms across the major clinical FTD syndromes [67].

The key strength of our study is our longitudinal design, spanning a 4-year follow-up period of tracking at-risk participants from both *MAPT* and *GRN* families. The non-carriers from the same families were an ideal control group, as they had the same genetic and social background. Second, we used the true onset instead of estimated symptom onset. Third, all subjects underwent DTI imaging on the same scanner with the same sequencing parameters in a 4-year follow-up period. A drawback is the relatively small sample size and the clinical and pathological heterogeneity with respect to statistical power; this warrants replication in larger longitudinal cohorts with more converters, including *C9orf72* repeat expansion carriers. Although our cohort also involves participants from *C9orf72* families,

study inclusion started in 2014; therefore no 5-year follow-up data are available yet. In the current study, we only described changes in fractional anisotropy, being the most sensitive parameter in the presymptomatic phase and the most pronounced measure with disease progression [9, 18, 5]. However, to interpret the exact neuropathological processes underlying the DTI changes, future studies should also include other diffusivity measures. Further, DTI scan-rescan reliability in neurodegeneration has scarcely been studied, and can be potentially hampered by its unequal distribution throughout different brain regions (i.e. highly anisotropic white matter tracts have lower within-subject variability) and higher susceptibility to partial volume effects in smaller tracts [68]. Finally, the DTI field-of-view in the present study was too small to include the lower white matter tracts in our analyses, although this would have been interesting considering recent findings of corticospinal tract degeneration in both bvFTD and nfvPPA [69].

CONCLUSION

Our longitudinal study demonstrates the presence of presymptomatic structural neuroimaging changes in FTD mutation carriers, starting 2 years before onset, with predominant frontotemporal pathology spreading towards and into symptom onset. Presymptomatic decline of white matter integrity of the uncinate fasciculus and genu corpus callosum, and grey matter volume loss of the left cingulate cortex, are consistent predictors of symptom onset in converters. Our results confirm the presence of a presymptomatic neuroimaging stage of familial FTD, and highlight the potential value of longitudinal multimodal structural MRI as a sensitive prognostic and diagnostic biomarker for presymptomatic to early symptomatic familial FTD.

REFERENCES

1. Agosta F, Scola E, Canu E, et al. White matter damage in frontotemporal lobar degeneration spectrum. Cerebral Cortex 2012; 22: 2705-14.
2. Rohrer JD & Rosen HJ. Neuroimaging in frontotemporal dementia. International Review of Psychiatry 2013; 25: 221-29.
3. Frings L, Yew, B, Flanagan E, et al. Longitudinal grey and white matter changes in frontotemporal dementia and Alzheimer's Disease. PLOS one 2014; 9(3): e90814.
4. Warren JD, Rohrer JD and Rossor MN. Clinical review. Frontotemporal dementia. BMJ 2013; 347: f4827.
5. Seeley WW, Crawford R, Rascovsky K, et al. Frontal paralimbic network atrophy in very mild behavioral variant frontotemporal dementia. Arch Neurol 2008; 65: 249-55.
6. Whitwell JL, Przybelski SA, Weigand SD, et al. Distinct anatomical subtypes of the behavioural variant of frontotemporal dementia: a cluster analysis study. Brain 2009; 132: 2932-46.
7. Whitwell JL, Boeve BF, Weigand SD, et al. Brain atrophy over time in genetic and sporadic frontotemporal dementia: a study of 198 serial magnetic resonance images. Eur J Neurol 2015; 22(5):745-52.
8. Piguet O, Hornberger M, Mioshi E, et al. Behavioural variant frontotemporal dementia: diagnosis, clinical staging, and management. Lancet Neurol 2011; 10: 162-72.
9. Lam BYK, Halliday GM, Irish M, et al. Longitudinal white matter changes in frontotemporal dementia subtypes. Human Brain Mapping 2014; 35(7): 3547-57.
10. Mahoney CJ, Ridgway GR, Malone IB, et al. Profiles of white matter tract pathology in frontotemporal dementia. Human Brain Mapping 2014; 35: 4163-79.
11. Oishi K, Faria A, Hsu J, et al. The critical role of the right uncinate fasciculus in emotional empathy. Ann Neurol 2015; 77(1): 68-74.
12. Bateman RJ, Xiong C, Benzinger TLS, et al. Clinical and biomarker changes in dominantly inherited Alzheimer's Disease. N Engl J Med 2012; 367(9): 795-804.
13. Benzinger TLS, Blazey T, Jack Jr. CR, et al. Regional variability of imaging biomarkers in autosomal dominant Alzheimer's disease. Proc Natl Acad Sci 2013; 110: E4502-9.
14. Kinnunen KM, Cash DM, Poole T, et al. Presymptomatic atrophy in autosomal dominant Alzheimer's Disease: a serial magnetic resonance imaging study. Alzheimer's & Dementia 2018; 14: 43-53.
15. Tabrizi SJ, Scahill RI, Owen G, et al. Predictors of phenotypic progression and disease onset in premanifest and early-stage Huntington's disease in the TRACK-HD study: analysis of 36-month observational data. Lancet Neurol 2013; 12: 637-49.
16. Harrington DL, Long JD, Durgerian S, et al. Cross-sectional and longitudinal multimodal structural imaging in prodromal Huntington's Disease. Movement Disorders 2016; 31: 1664-75.
17. Borroni B, Alberici A, Premi E, et al. Brain magnetic resonance imaging structural changes in a pedigree of asymptomatic progranulin mutation carriers. Rejuvenation Res 2008; 11: 585–95.
18. Dopper EG, Rombouts SA, Jiskoot LC, et al. Structural and functional brain connectivity in presymptomatic familial frontotemporal dementia. Neurology 2014; 83(2): e19-26.
19. Rohrer JD, Nicholas JM, Cash DM, et al. Presymptomatic cognitive and neuroanatomical changes in genetic frontotemporal dementia in the Genetic Frontotemporal dementia Initiative (GENFI) study: a cross-sectional analysis. Lancet Neurology 2015; 14(3): 253-62.
20. Jiskoot LC, Dopper EG, Heijer T, et al. Presymptomatic cognitive decline in familial frontotemporal dementia: A longitudinal study. Neurology 2016; 87: 384-91.
21. Jiskoot LC, Panman JL, van Asseldonk L, et al. Longitudinal cognitive biomarkers predicting symptom onset in presymptomatic frontotemporal dementia. Journal of Neurology 2018a; doi: 10.1007/s00415-018-8850-7.
22. Jiskoot LC, Bocchetta M, Nicolas JM, et al. Presymptomatic white matter integrity loss in familial frontotemporal dementia in the GENFI cohort: a cross-sectional diffusion tensor imaging study. Annals of Clinical and Translational Neurology 2018b; in press.
23. Meeter, LH, Dopper EGP, Jiskoot LC, et al. Neurofilament light chain: a biomarker for genetic frontotemporal dementia. Ann Clin Transl Neurol 2016; 3(8): 623-636.
24. Janssen JC, Schott JM, Cipolotti L, et al. Mapping the onset and progression of atrophy in familial frontotemporal lobar degeneration. J Neurol Neurosurg Psychiatr 2005; 76: 162–68.
25. Cruchaga C, Fernández-Seara MA, Seijo-Martinez M, et al. Cortical atrophy and language network reorganization associated with a novel progranulin mutation. Cereb Cortex 2009; 19: 1751–60.

26. Schuster C, Elamin M, Hardiman O, et al. Presymptomatic and longitudinal neuroimaging in neurodegeneration – from snapshots to motion picture: a systematic review. J Neurol Neurosurg Psychiatry 2015; 86: 1089-96.
27. Ryman DC, Acosta-Baena N, Aisen PS, et al. Symptom onset in autosomal dominant Alzheimer disease: a systematic review and meta-analysis. Neurology 2014; 83: 253-260.
28. Swieten JC & Heutink P. Mutations in progranulin (GRN) within the spectrum of clinical and pathological phenotypes of frontotemporal dementia. The Lancet Neurology 2008; 7(10): 965-974.
29. Dopper EG, Chalos V, Ghariq E, et al. Cerebral blood flow in presymptomatic MAPT and GRN mutation carriers: A longitudinal arterial spin labeling study. Neuroimage Clin 2016; 12: 460-65.
30. Rascovsky K, Hodges JR, Knopman D, et al. Sensitivity of revised diagnostic criteria for the behavioural variant of frontotemporal dementia. Brain 2011; 134: 2456–77.
31. Gorno-Tempini ML, Hillis AE, Weintraub S, et al. Classification of primary progressive aphasia and its variants. Neurology 2011; 76(11): 1006-14.
32. Knopman DS, Kramer JH, Boeve BF, et al. Development of methodology for conducting clinical trials in frontotemporal lobar degeneration. Brain 2008; 131(11): 2957-68.
33. Kaufer DI, Cummings JL, Ketchel P, et al. Validation of the NPI-Q, a brief clinical form of the Neuropsychatric Inventory. J Neuropsychiatry Clin Neurosci 2000; 12(2): 233-39.
34. Beck AT, Ward CH, Mendelson M, et al. An inventory for measuring depression. Arch Gen Psychiatry 1961; 4: 561-71.
35. Folstein MF, Folstein SE and McHugh PR. "Mini-mental state". A practical method for grading the cognitive state of patients for the clinician. J Psychiatr Res 1975; 12(3): 189-98.
36. Dubois B, Litvan I. The FAB: A frontal assessment battery at bedside. Neurology 2000; 55(11): 1621-26.
37. Mori S, Wakana S, Nagae-Poetscher LM, et al. MRI atlas of human white matter. Amsterdam: Elsevier; 2005.
38. Whitwell JL, Jack CR, Boeve BF, et al. Voxel-based morphometry patterns of atrophy in FTLD with mutations in MAPT or PGRN. Neurology 2009; 72: 813–820.
39. Whitwell JL, Weigand SD, Boeve BF, et al. Neuroimaging signatures of frontotemporal dementia genetics: C9ORF72, tau, progranulin and sporadics. Brain 2012; 135: 794–806.
40. Rohrer, JD, Ridgway, GR, Modat M, et al. Distinct profiles of brain atrophy in frontotemporal lobar degeneration caused y progranulin and tau mutations. NeuroImage 2010; 53; 1070-6
41. Cash DM, Bocchetta M, Thomas DL, et al. Patterns of gray matter atrophy in genetic frontotemporal dementia: results from the GENFI study. Neurobiol Aging 2018; 62: 191-196.
42. Khan BK, Yokoyama JS, Takada LT et al. Atypical, slowly progressive behavioural variant frontotemporal dementia associated with C9ORF72 hexanucleotide expansion. Journal of Neurology, Neurosurgery & Psychiatry 2012; 83: 358–364.
43. Devenney E, Foxe D, Dobson-Stone C, et al. Clinical heterogeneity of the C9orf72 genetic mutation in frontotemporal dementia. Neurocase 2015; 21(4): 535-41.
44. Devenney E, Hornberger M, Irish M, et al. Frontotemporal dementia associated with the C9ORF72 mutation: a unique clinical profile. JAMA Neurol 2014; 71(3): 331-9.
45. Borroni B, Cosseddu M, Pilotto A, et al. Early stage of behavioural variant frontotemporal dementia: clinical and neuroimaging correlates. Neurobiology of aging 2015; 36: 3108-3115.
46. Hallam BJ, Silverberg ND, Lamarre AK, et al. Clinical presentation of prodromal frontotemporal dementia. Am J Alzheimers Dis Other Demen 2007; 22(6): 456-67.
47. De Mendonça A, Ribeiro F, Guerreiro M, et al. Frontotemporal mild cognitive impairment. J Alzheimerheimers Dis 2004; 6(1): 1-9.
48. Taragano FE, Allegri RF, Krupitzki H, et al. Mild behavioural impairment and risk of dementia: a prospective cohort study of 358 patients. J Clin Psychiatry 2009; 70(4): 584-92.
49. Cheran G, Silverman H, Manoochehri M, et al. Psychiatric symptoms in preclinical behavioural-variant frontotemporal dementia in MAPT mutation carriers. J Neurol Neurosurg Psychiatry 2018; 89(5): 449-455.
50. Hassenstab J, Aschenbrenner AJ, Balota DA, et al. Cognitive trajectories in DIAN: relationships with symptom onset, mutation types and clinical status. Alzheimers Dement 2016; 12(7): 368.
51. Elahi FM, Marx G, Cobigo Y, et al. Longitudinal white matter change in frontotemporal dementia subtypes and sporadic late onset Alzheimer's disease. NeuroImage: Clinical 2017; 16: 595-603.
52. Acosta-Cabronero J, Patterson K, Fryer TD, et al. Atrophy, hypometabolism and white matter abnormalities in semantic dementia tell a coherent story. Brain, 2011; 134(Pt 7): 2025-35.

53. Hornberger M, Geng J, Hodges JR. Convergent grey matter and white matter evidence of orbitofrontal cortex changes related to disinhibition in behavioural variant frontotemporal dementia. Brain 2011; 134: 2502-12.
54. Agosta F, Henry RG, Migliaccio R, et al. Language networks in semantic dementia. Brain 2010; 133:286–99.
55. Mahoney CJ, Malone IB, Ridgway GR, et al. White matter tract signatures of the progressive aphasias. Neurobiol Aging 2013; 34: 1687–99.
56. Schwindt GC, Graham NL, Rochon E, et al. Whole-brain white matter disruption in semantic and nonfluent variants of primary progressive aphasia. Hum Brain Mapp 2013; 34: 973–84.
57. Zhang Y, Tartaglia MC, Schuff N, et al. MRI signatures of brain macrostructural atrophy and microstructural degradation in frontotemporal lobar degeneration subtypes. J Alzheimer's Dis 2013; 33: 431–44.
58. Caroppo P, Habert MO, Durrleman S, et al. Lateral temporal lobe: an early imaging marker of the presymptomatic GRN disease. J Alzheimers Dis 2015; 47(3): 751-9.
59. Smith R, Puschmann A, Schöll M, et al. 18F-AV-1451 tau PET imaging correlates strongly with tau neuropathology in MAPT mutation carriers. Brain 2016; 139: 2372-2379.
60. Ono M, Sahara N, Kumata K, et al. Distinct binding of PET ligands PBB3 and AV-1451 to tau fibril strains in neurodegenerative tauopathies. Brain 2017; 140: 764-780.
61. Grossman M, McMillan C, Moore P, et al. What's in a name: voxel-based morphometric analyses of MRI and naming difficulty in Alzheimer's disease, frontotemporal dementia and corticobasal degeneration. Brain 2004; 127: 628–49.
62. Olson IR, von der Heide RJ, Alm KH, et al. Development of the uncinate fasciculus: implications for theory and developmental disorders. Developmental Cognitive Neuroscience 2015; 14: 50-61.
63. Zhang Y, Schuff N, Ching C, et al. Joint assessment of structural, perfusion, and diffusion MRI in Alzheimer's disease and frontotemporal dementia. Int J Alzheimers Dis 2011; 2011: 546-71.
64. McMillan CT, Brun C, Siddiqui S, et al. White matter imaging contributes to the multimodal diagnosis of frontotemporal lobar degeneration. Neurology 2012; 78(22): 1761-68.
65. Möller C, Hafkemeijer A, Pijnenburg YA, et al. Joint assessment of white matter integrity, cortical and subcortical atrophy to distinguish AD from behavioral variant FTD: a two-center study. Neuroimage Clin 2015; 9: 418-29.
66. Meeter LH, Donker Kaat L, Rohrer JD, et al. Imaging and fluid biomarkers in frontotemporal dementia. Nature Reviews Neurology 2017; 13: 406-419.
67. Lansdall CJ, Coyle-Gilchrist ITS, Simon Jones P, et al. White matter change with apathy and impulsivity in frontotemporal degeneration syndromes. Neurology 2018; 90(12): e1066-e1076.
68. Cole JH, Farmer RE, Rees EM, et al. Test-retest reliability of diffusion tensor imaging in Huntington's disease. PLOS Currents Huntington Disease 2014 Mar 21; 6.
69. Omer T, Finegan E, Hutchinson S, et al. Neuroimaging patterns along the ALS-FTD spectrum: a multiparametric imaging study. Amyotroph Lateral Scler Frontotemporal degener 2017: 1-13.

SUPPLEMENT 1. DEMOGRAPHIC, CLINICAL AND NEUROPSYCHOLOGICAL DATA OF THE CONVERTERS

Demographics	**Converter**							
	1	**2**	**3**	**4**	**5**	**6**	**7**	**8**
Clinical diagnosis	bvFTD	bvFTD	bvFTD	bvFTD	bvFTD	nfvPPA	nfvPPA	bvFTD
Age at onset	57	42	45	43	56	51	57	67
Mean onset age family	53.2	44.5	44.5	44.5	53.2	59.7	59.7	59.7
Gene	MAPT	MAPT	MAPT	MAPT	MAPT	GRN	GRN	GRN
Mutation	P301L	G272V	G272V	G272V	P301L	S82VfsX174	S82VfsX174	S82VfsX174
Gender	Male	Male	Male	Male	Female	Female	Female	Female
Global cognition and questionnaire scores (at symptom onset)								
FTD-CDR-SB	6	11	12	10	3	5	1	9
MMSE	27	26	26	27	30	29	26	28
FAB	13	15	16	17	16	18	15	16
NPI-Q	23	15	1	39	0	2	1	29
CBI-R	32	42	25	55	0	4	0	46
BDI	3	3	22	29	1	12	5	2
Neuropsychological test scores (at symptom onset)								
Social cognition								
Happé Cartoon Test	-2.2	-2.6	-1.2	0.2	-1.5	1.2	-1.4	-1.8
Ekman Faces Test	-2.0	-3.0	-1.6	-0.4	-3.3	0.6	-3.0	-0.7
Language								
Boston Naming Test-60-item	-0.6	>-3.0	>-3.0	0.1	0.4	0.7	0.2	-0.1
ScreeLing – phonology (/24)	24/24	24/24	24/24	24/24	24/24	23/24	23/24	23.5/24
Semantic Association Test (/30)	26/30	21/30	28/30	28/30	29/30	28/30	29/30	29/30
Similarities WAIS-III	-1.0	-1.4	1.4	-1.0	-1.0	0	-1.7	-0.7
Executive function								
Categorical fluency (animals)	-2.3	-2.3	-1.3	-1.5	-1.1	0.2	-1.5	-1.3
Phonological fluency	-1.7	-1.0	-0.1	-0.4	-2.1	-0.4	-1.1	-2.0
TMT part B | A	-1.1	-2.1	1.0	-0.5	-2.0	-1.6	>-3.0	-2.8
Stroop card 3 | 2	-0.2	1.3	1.1	-0.1	0	-0.9	-0.6	-0.7
WCST - concepts	-2.0	0.2	0.3	0.2	-2.2	-1.4	-1.0	-2.2
Attention & mental processing speed								
TMT part A	-1.5	1.7	1.3	-0.2	-0.7	1.1	-1.1	-0.9
TMT part B	-1.6	-0.1	1.6	-0.4	-2.1	-0.9	>-3.0	-2.9
Stroop card 1	-1.9	-1.4	-0.6	-2.3	0	-1.4	-1.4	-2.0
Stroop card 2	-3.1	-1.5	-1.1	-1.9	-1.2	-1.6	-1.4	-1.3
Stroop card 3	-2.1	0	0.1	-1.3	-0.9	-1.8	-1.5	-1.5
Letter Digit Substitution Test	-1.1	0.42	0.8	>-2.3	0	0.42	-0.4	-0.4
Memory								

RAVLT immediate recall	-2.3	-2.2	0	-2.0	0.7	2.6	-1.8	0.7
RAVLT delayed free recall	-2.1	-4.2	-0.2	-1.8	0.2	1.9	-0.2	0.4
RAVLT delayed cued recall (/30)	29/30	19/30	29/30	27/30	29/30	30/30	29/30	30/30
Visual Association Test	<-0.8	>-3.0	<-0.8	<-0.6	<-0.6	<-0.6	<-0.6	<-0.6
Digit Span WAIS-III	-0.4	1.0	-2.0	-0.4	-0.4	-1.0	-2.0	-0.4
Visuoconstruction								
Clock Drawing (/14)	13/14	11/14	12/14	13/14	13/14	13/14	12/14	13/14
Block Design WAIS-III	-0.4	-0.4	2.0	-0.4	-0.7	0.4	-1.0	-1.4

Abbreviations: bvFTD, behavioural variant FTD; PNFA, progressive non-fluent aphasia; *GRN*, progranulin; *MAPT*, microtubule-associated protein tau; MMSE, Mini-Mental State Examination; FAB, Frontal Assessment Battery; NPI-Q, Neuropsychiatric Inventory-Questionnaire; CBI-R, Cambridge Behavioural Inventory-Revised; WAIS, Wechsler Adult Intelligence Scale; TMT, Trailmaking Test; WCST, Wisconsin Card Sorting Test; RAVLT, Rey Auditory Verbal Learning Test. Test scores are at the visit after symptom onset. Cognitive deficits (>-2 SD below mean) are highlighted in red; minor deficits (between -1 and -2 SD below mean) are highlighted with orange. Scores have been transformed to z-scores (if applicable) or are expressed as their score/total score.

SUPPLEMENT 2. BRIEF DESCRIPTION OF THE CLINICAL DISEASE TRAJECTORIES OF CONVERTERS AND SLOPES SHOWING THE DEVELOPMENT OF COGNITIVE, NEUROPSYCHIATRIC AND NEUROIMAGING CHANGES

Converter 1 – *MAPT*, P301L, male

Four years prior to the diagnosis of bvFTD, the mutation carrier showed no signs of cognitive or behavioural changes (FTD-CDR-SB=0). Two years before the diagnosis, the mutation carrier demonstrated increased emotional reactions to significant events, accompanied by the presence of minor depressive symptoms (FTD-CDR-SB=0, NPI-Q=1, BDI=2). In the following two years, the mutation carrier developed word-finding difficulties. According to his spouse, he lost his capability to adequately communicate, cooperate and sympathize with colleagues at work – and as a result, the mutation carrier lost his job. Furthermore, delusions, agitation, depression, apathy, disinhibition, irritability and a change in appetite were reported on neuropsychiatric questionnaires (NPI-Q=23, CBI-R=32). The clinical diagnosis of bvFTD was supported by deficits on neuropsychological testing in word fluency, episodic memory and social cognition (theory of mind and emotion recognition), and asymmetrical (right > left) temporal and frontal atrophy on structural MRI (FTD-CDR-SB=6). Two years after the diagnosis, formal testing was no longer possible, and the mutation carrier was admitted to a nursing home. Four years post-diagnosis, the mutation carrier refuses to eat or drink and is bedridden.

Converter 2 – *MAPT*, G272V, male

Four years prior to the diagnosis of bvFTD, nor the mutation carrier or the spouse reported cognitive or behavioural problems (FTD-CDR-SB=0). Two years before the diagnosis, he had name and word-finding difficulties. The mutation carrier was jovial during the study visit, accompanied by neuropsychiatric questionnaires indicating inappropriate laughing (FTD-CDR-SB=1.5, NPI-Q=0, CBI-R=5), while neuropsychological testing and structural MRI were normal. At the diagnosis visit, the spouse reported memory problems, difficulties with keeping overview and structure, diminished patience, compulsive time keeping, childish behaviour and a changed sense of humour (FTD-CDR-SB=11), as well as restlessness, an agitated mood, odd or bizarre ideas, changes in eating habits, preoccupation with time, and disinhibition (CBI-R=42, NPI-Q=15). The study team observed stereotypical phrases, distractibility, and obsessive thinking. The clinical diagnosis bvFTD was further supported by neuropsychological testing, demonstrating deficits in language (e.g. naming, fluency, semantics), memory, social cognition, and executive function, as well as structural MRI

showing asymmetrical (right > left) atrophy of the frontal, temporal and parietal lobes. The mutation carrier was admitted to a nursing home one year post-diagnosis.

Converter 3 – *MAPT*, G272V, male

Neither four nor two years prior to the diagnosis of bvFTD, were there any cognitive or behavioural complaints (FTD-CDR-SB=0). The mutation carrier did have a slightly lower mood (BDI=11). One year before diagnosis, the mutation carrier was frequently disoriented in his work as a private chauffeur. At the diagnosis visit, he displayed disinhibited and highly associative thinking and speech. Questionnaires showed memory problems, disinhibition, restlessness, agitation, and rigidity regarding food preferences (FTD-CDR-SB=12, NPI=Q=1, CBI-R=25). The clinical diagnosis of bvFTD was supported by a lack of disease insight, and neuropsychological testing objectifying deficits in naming and social cognition. Structural MRI showed asymmetrical (right > left) atrophy of the frontal and temporal lobes. Two years after the diagnosis, the mutation carrier was admitted to a nursing home.

Converter 4 – *MAPT*, G272V, male

Four years prior to the diagnosis of bvFTD, the mutation carrier had a panic attack and noted occasional word-findings problems, although neuropsychological testing and structural MRI were normal (FTD-CDR-SB=0.5). Two years before the diagnosis, the mutation carrier had mild memory problems, and semantic paraphrases – while neuropsychological testing was normal (FTD-CDR-SB=1.5, NPI-Q=0, CBI-R=0). One year before the diagnosis, he complained about tiredness and depression, and was unable to work due to difficulties with keeping structure, planning, and remembering appointments. Six months before the diagnosis, mutation carrier was shortly hospitalized for a manic episode. At the diagnosis visit, neuropsychiatric questionnaires indicated mood problems, daytime sleeping, euphoria, apathy, disinhibition, agitation and aberrant motor behaviour (FTD-CDR-SB=10, NPI=Q=39, CBI-R=17). The clinical diagnosis of bvFTD was supported by observations of the study team, i.e. word-finding difficulties and phonological errors, neuropsychological assessment showing deficits in episodic memory, mental speed, attention and fluency, and structural MRI showing right-sided temporal atrophy. One year post-diagnosis, the mutation carrier could not perform the activities of daily living, and he attended daycare four times a week.

Converter 5 – *MAPT*, P301L, female

Two years before the diagnosis of bvFTD, the mutation carrier reported no cognitive or behavioural changes (FTD-CDR-SB=0, no CBI-R or NPI-Q available). Two years later, the

mutation carrier demonstrated agitated and disinhibited behaviour during the study visit, and her daughter reported behavioural disturbances in the form of less empathy and drive (FTD-CDR-SB=3, NPI=Q=0, CBI-R=0). The clinical diagnosis bvFTD was supported by deficits in fluency, attention, executive function and social cognition on neuropsychological testing. Structural MRI demonstrated asymmetrical (right > left) frontal atrophy. Two years after the diagnosis, the mutation carrier was unable to attend study visits due to the severity of her cognitive and behavioural problems. She passed away five years post-diagnosis.

Converter 6 – *GRN*, S82VfsX174, female

Four years before the diagnosis of nfvPPA, the mutation carrier did not mention cognitive or behavioural changes (FTD-CDR-SB=0, NPI-Q=0, CBI-R=0). Two years before the diagnosis, the mutation carriers reported some minor problems in maintaining an overview at work (FTD-CDR-SB=0.5). At the diagnosis visit, the mutation carrier complained about stuttering, mixing up words, word finding difficulties, and a depressed mood, from which she was suffering for a year (FTD-CDR-SB=5, NPI-Q=1, BDI=12, CBI-R=0). The clinical diagnosis of nfvPPA was supported by her halting, effortful speech with word-finding deficits and pauses, perseverations, semantic errors and phonological substitutions. Neuropsychological assessment demonstrated deficits regarding conceptshifting, episodic and working memory, fluency, syntax, and emotion recognition. Structural MRI furthermore showed asymmetrical (left > right) temporal and insular atrophy. Two years later, the mutation carrier was nearly mute, with prominent signs of parkinsonism. She passed away three years post-diagnosis.

Converter 7 – *GRN*, S82VfsX174, female

In the four years before the diagnosis of nfvPPA, there were no cognitive or behavioural changes (FTD-CDR-SB=0, NPI-Q=0, CBI-R=0). The study visit the diagnosis was set, the mutation carrier complained about stuttering and a depressed mood (FTD-CDR-SB=1). Questionnaires indicated forgetting the names of objects, disturbed sleeping, and crying (NPI=Q=2, CBI-R=4). The clinical diagnosis of nfvPPA was confirmed by the presence of phonological errors in spontaneous speech, and by minor deficits with respect to fluency and executive function on neuropsychological assessment. Furthermore, structural MRI demonstrated widened parietal ventricular spaces, and an FDG-PET scan showed decreased glucose metabolism in the left frontal and temporal lobes. Two years after diagnosis, formal cognitive testing was no longer possible due to the severity of the language problems. Three years post-diagnosis, the mutation carrier was nearly mute, and daily activities and personal care were severely impaired.

Converter 8 – *GRN,* S82VfsX174*,* female

Two years prior to the diagnosis of bvFTD, the mutation carrier had occasional word-finding difficulties, trouble with dividing attention, and was somewhat more talkative (FTD-CDR-SB=1.5, no CBI-R or NPI-Q available). Neuropsychological testing and structural MRI were normal. At the visit two years later, significant changes were reported by family members regarding cognition – i.e. trouble organizing finances, forgetting appointments, problems handling the TV remote – and behaviour – i.e. hoarding newspapers, being less thoughtful, apathy, a decline in personal hygiene and a preference for sweet foods (FTD-CDR-SB=9, NPI=Q=29, CBI-R=46). The clinical diagnosis of bvFTD was supported by a lack of disease insight, word-finding difficulties, and neuropsychological assessment showing deficits in fluency, attention, executive function, perceptual organization and theory of mind. Structural MRI showed asymmetrical (right > left) frontal and temporal atrophy. One year post-diagnosis, cognitive and behavioural problems had significantly progressed, with bad personal hygiene, repetitive behaviours (e.g. plucking clothes), and stereotypic phrases. Two years post-diagnosis, the mutation carrier was admitted to a nursing home.

SUPPLEMENT 3. IMAGE ACQUISITION PARAMETERS & PRE-PROCESSING PIPELINE

Image acquisition parameters

For grey matter volumetric comparisons and anatomical reference, T1-weighted images were acquired using the following scanning parameters: repetition time (TR) = 9.8 ms, echo time (TE) = 4.6 ms, flip angle = 8°, 140 slices, voxel size = 0.88 x 0.88 x 1.20 mm, total scan time = 4.50 min. Diffusion tensor images were acquired by means of single-shot echo planar images (EPI) with gradients applied along 61 diffusion-weighted directions (maximum b-value s/mm² 1000), using the following acquisition parameters: TR = 8250 ms, TE = 80 ms, flip angle = 90°, 70 contiguous axial slices, voxel size = 2 x 2 x 2 mm, field of view = 256 x 208 x 140 mm, total scan time = 8.48 minutes.

Pre-processing pipeline

We corrected raw diffusion data for motion artefacts and Eddy currents, we extracted binary brain masks using BET, and we fitted the diffusion tensor model at each voxel using DTIFIT – resulting in fractional anisotropy (FA) maps for each participant. We aligned the images to an FA standard template through nonlinear registration. A mean FA image was created and thinned to obtain a skeleton with tracts common to the entire group. Individual FA data was projected onto this skeleton (threshold 0.2). We performed pre-processing of the T1-weighted images through brain extraction followed by tissue segmentation and alignment to MNI-152 standard space (Montreal Neurological Institute, Montreal, QC, Canada) using non-linear registration. A study-specific template was created and native grey matter images were non-linearly re-registered to this template. The registered partial volume images were modulated to correct for local expansion or contraction by dividing by the Jacobian of the warp field. These modulated grey matter images were smoothed with an isotropic 4 mm Gaussian kernel (FWHM ~9 mm).

SUPPLEMENT 4 – OVERVIEW OF LITERATURE SEARCH FOR ROI SELECTION

Paper selection

Papers were selected on the basis of the following Pubmed searches: "(Diffusion* OR DTI) AND (frontotemporal* OR FTD)"; "(White matter OR WM) AND (frontotemporal* OR FTD)"; "(Diffusion tensor imaging OR DTI) AND (primary progressive aphasia* OR PPA)"; "(White matter OR WM) AND (primary progressive aphasia* OR PPA)"; "(grey matter OR gray matter OR GM) AND (frontotemporal* OR FTD)"; "(grey matter OR gray matter OR GM) AND (primary progressive aphasia* OR PPA)"; "(atrophy) AND (frontotemporal* OR FTD)"; "(atrophy) AND (primary progressive aphasia* OR PPA)". Reference lists of the identified papers were examined for further leads. The search was limited to full-text papers published in English over the past ten years. Case studies were excluded. The final selection was based on relevance, as judged by the authors. Due to the scarcity of presymptomatic papers, and regions corroborated with those of the symptomatic stage, ROI selection was primarily based on papers describing symptomatic FTD. We selected white matter tracts and grey matter regions if they were described to be affected in >75% of the selected papers.

SUPPLEMENT 5. SUMMARY LITERATURE ROI WM AND GM SELECTION

White matter tracts

Author	Technique	Patient groups	Regions
Presymptomatic studies			
Borroni et al. 2008	VBM	*GRN* carriers	UF, IFOF
Dopper et al. 2014	TBSS	*GRN* and *MAPT* carriers	UF
Lee et al. 2017	TBSS	*C9orf72* carriers	CC, cingulum, internal and external capsule
Symptomatic studies			
Agosta et al. 2010	VBM	svPPA	ILF, arcuate fasciculus, UF, SLF, gCC
Agosta et al. 2012	TBSS	bvFTD, PPA	CC (anterior-posterior gradient), cingulum bundles, corona radiata, external and internal capsule, fornix, cerebral and cerebellar peduncles, subcortical WM subjacent to frontal and parietal cortex, temporal and occipital WM, orbital and dorsolateral frontal WM
Acosta-Cabronero et al. 2011	TBSS, tractography	svPPA	UF, arcuate fasciculus
Borroni et al. 2007	Voxel-wise	fvFTD, tvFTD	SLF, ILF
D'Anna et al. 2016	ROI	PPA	UF, IFOF, ILF
Daianu et al. 2016	tractography	bvFTD, EOAD	UF, CC, ATR, cingulum, SLF
Hornberger et al. 2011	TBSS	bvFTD, AD	Frontal and anterior temporal regions
Lam et al. 2014	TBSS	bvFTD, PPA (nfPPA, svPPA)	ATR, anterior cingulum, SLF, ILF, IFOF, UF, CC
Lillo et al. 2012	TBSS	ALS, ALS-FTD, bvFTD	Forceps minor, anterior CC, ILF, CST
Lu et al. 2014	ROI	bvFTD, EOAD	Frontal lobes, genu CC
Mahoney et al. 2013	TBSS	PPA, AD	UF, ILF, SLF, subcortical projections
Mahoney et al. 2014	Voxel-wise	Familial/sporadic bvFTD, AD	UF, cingulum, CC, SLF, ILF, ATR, fornix
Mahoney et al. 2015	ROI	Sporadic bvFTD, *MAPT* carriers, *C9orf72* carriers	UF, cingulum
Matsuo et al. 2008	tractography	fvFTD, tvFTD	UF, ILF, arcuate fasciculus, CC (anterior-posterior gradient)
McMillan et al. 2012	ROI	bvFTD, PPA, CBS, AD	CST, IFOF, ILF, SLF, UF, CC (anterior-posterior gradient)
Meijboom et al. 2017	TBSS, tractography	bvFTD, svFTD	Forceps minor and major, CC, IFOF, ATR, cingulum, UF, ILF, SLF
Möller et al. 2015	TBSS, ROI	bvFTD, AD	Fornix, CC, forceps minor, thalamus, ATR, SLF, ILF, IFOF, UF, CST
Rohrer et al. 2010	VBM	Familial FTD (*GRN*, *MAPT*)	ILF, SLF, IFOF, cingulum, CC, brainstem, fornix, UF
Steketee et al. 2016	TBSS, tractography	bvFTD, AD	ATR, cingulum (cingulate gyrus, hippocampus), forceps major and minor, IFOF, ILF, SLF, UF

Schwindt et al. 2013	TBSS	svPPA, nfPPA	UF, IFOF, ILF, forceps minor, gCC, SLF, corona radiata, ATR, internal capsule
Whitwell et al. 2010	ROI	bvFTD, nfPPA, svPPA	ILF, UF, SLF, genu CC, anterior and posterior cingulate, corticospinal tract
Yoshiura et al. 2006	ROI	bvFTD	Frontal gyri, orbitofrontal gyri, anterior temporal lobes
Zhang et al. 2009	ROI, voxel-wise	fvFTD, AD	Anterior CC, ACC, cingulum, UF, thalamic radiation in ALIC, SLF, posterior CC
Zhang et al. 2011	Voxel-wise	FTD, AD	Frontal and temporal lobes, anterior CC, anterior cingulum
Zhang et al. 2013	VBM, ROI	bvFTD, svPPA, nfPPA	Arcuate fasciculus, UF, ILF, parahippocampus, anterior CC, fornix

Grey matter regions

Author	Technique	Patient groups	**Regions**
Presymptomatic studies			
Lee et al. 2017	VBM	*C9orf72* carriers	Midcingulate, thalamus, dorsolateral PFC
Rohrer et al. 2015	ROI	*MAPT*, *GRN* and *C9orf72* carriers	Insula, temporal, frontal, parietal, cingulate
Symptomatic studies			
D'Anna et al. 2016	Cortical thickness, ROI	PPA	Orbitofrontal cortex, anterior temporal lobe
Lillo et al. 2012	VBM	ALS, ALS-FTD, bvFTD	Frontal pole, OFC, ACC, superior frontal gyrus, (pre)motor cortices, anterior insula, temporal poles, thalamus, striatem
Mahoney et al. 2014	VBM	Familial/sporadic bvFTD, AD	Orbitofrontal, super/inferior frontal gyri, insula, cingulate, amygdala, middle/ inferior temporal gyri
McMillan et al. 2012	Voxel-wise	bvFTD, PPA, CBS, AD	Frontal cortex, anterior temporal cortex
Möller et al. 2015	VBM, ROI	bvFTD, AD	Superior, middle and inferior frontal gyrus, orbitofrontal gyrus, insula, temporal gyrus
Rohrer et al. 2010	VBM	Familial FTD (*GRN*, *MAPT*)	Frontal, temporal, parietal lobes, cingulate cortex, thalamus
Rohrer et al. 2015	ROI	*MAPT*, *GRN* and *C9orf72* carriers	Insula, temporal, frontal, parietal, cingulate
Steketee et al. 2016	ROI	bvFTD, AD	Frontal, temporal and parietal cortices, basal ganglia
Schwindt et al. 2013	VBM	svPPA, nfPPA	Insula, inferior frontal, medial frontal, temporal regions, precuneus, medial temporal lobe, putamen, nucleus accumbens
Whitwell et al. 2009	VBM	Familial FTD with *MAPT* and *GRN*	Frontal, temporal and parietal lobes (all mutation carriers); *GRN* vs. controls in posterior temporal and parietal; *MAPT* vs. controls in anteriomedial temporal lobes; *MAPT* vs. *GRN*: medial temporal, insula, putamen

Whitwell et al. 2010	VBM	bvFTD, nfPPA, svPPA	Frontal and temporal lobes, insula, supplemental motor area, medial and lateral parietal lobes and occipital lobes
Zhang et al. 2011	VBM	FTD, AD	Frontal (frontoinsula) and temporal lobes, ACC, uncus, parietal lobes, caudate, thalamus
Zhang et al. 2013	VBM, ROI	bvFTD, svPPA, nfPPA	ACC, striatem, (fronto)insula, frontopolar regions, temporal pole, inferior frontal gyrus, superior frontal gyrus, caudate nucleus

Abbreviations: VBM, voxel-based morphometry; TBSS, tract-based spatial statistics; ROI, region of interest; *GRN*, progranulin; *MAPT*, microtubule-associated protein tau; *C9orf72*, chromosome 9 open reading frame 72; bvFTD, behavioural variant FTD; PPA, primary progressive aphasia; svPPA, semantic variant PPA; fvFTD, frontal variant FTD; tvFTD, temporal variant FTD; EOAD, early-onset Alzheimer's disease; AD, Alzheimer's Disease; nfPPA, non-fluent PPA; ALS, Amyotrophic Lateral Sclerosis; CBS, corticobasal syndrome; UF, uncinate fasciculus; IFOF, inferior fronto-occipital fasciculus; CC, corpus callosum; gCC, genu corpus callosum; WM, white matter; SLF, superior longitudinal fasciculus; ILF, inferior longitudinal fasciculus; ATR, anterior thalamic radiation; CST, corticospinal tract; ALIC, anterior limb internal capsule; PFC, prefrontal cortex; OFC, orbitofrontal cortex; ACC, anterior cingulate cortex.

REFERENCES

1. Agosta F, Henry RG, Migliaccio R, et al. Language networks in semantic dementia. Brain 2010; 133:286–99.
2. Agosta F, Scola E, Canu E, et al. White matter damage in frontotemporal lobar degeneration spectrum. Cereb Cortex, 2012; 22(12): 2705-14.
3. Acosta-Cabronero J, Patterson K, Fryer TD, et al. Atrophy, hypometabolism and white matter abnormalities in semantic dementia tell a coherent story. Brain, 2011; 134(Pt 7): 2025-35.
4. Borroni B, Brambati SM, Agosti C, et al. Evidence of white matter changes on diffusion tensor imaging in frontotemporal dementia. Arch Neurol, 2007; 64: 246-251.
5. Borroni B, Alberici A, Premi E, et al. Brain magnetic resonance imaging structuralchanges in a pedigree of asymptomatic progranulin mutation carriers. Rejuvenation Res, 2008; 11(3): 585-95.
6. D'Anna L, Mesulam MM, Thiebaut de Schotten M. Frontotemporal networks and behavioral symptoms in primary progressive aphasia. Neurology, 2016; 86(15): 1393-1399.
7. Daianu M, Mendez MF, Baboyan VG. An advanced white matter tract analysis in frontotemporal dementia and early-onset Alzheimer's disease. Brain Imaging Behav, 2016; 10(4): 1038-1053.
8. Dopper EGP, Rombouts SA, Jiskoot LC, et al. Structural and functional brain connectivity in presymptomatic familial frontotemporal dementia. Neurology, 2014; 83(2): e19-26.
9. Hornberger M, Geng, J, Hodges JR. Convergent grey and white matter evidence of orbitofrontal cortex changes related to disinhibition in behavioural variant frontotemporal dementia. Brain, 2011; 134: 2502-2512.
10. Lam BYK, Halliday GM, Irish M, et al. Longitudinal white matter changes in frontotemporal dementia subtypes. Human Brain Mapping, 2011; 35(7): 3547-3557.
11. Lee S, Sias A, Mandelli ML, et al. Network degeneration and dysfunction in presymptomatic C9orf expansion carriers. NeuroImage: Clinical, 2017; 14: 286-297.
12. Lillo P, Mioshi E, Burrell JR, et al. Grey and white matter changes across the Amyotrophic lateral sclerosis-Frontotemporal dementia continuum. PLOS one, 2012; 7(8): e43993.
13. Lu PH, Lee GJ, Shapira J, et al. Regional differences in white matter breakdown between frontotemporal dementia and early-onset Alzheimer's disease. J Alzheimers Dis. 2014: 39(2); 261-269.
14. Mahoney CJ, Malone IB, Ridgway GR, et al. White matter tract signatures of the progressive aphasias. Neurobiol Aging 2013; 34: 1687–99.
15. Mahoney CJ, Ridgway GR, Malone IB, et al. Profiles of white matter tract pathology in Frontotemporal Dementia. Human Brain Mapping, 2014; 35: 4163-4179.
16. Mahoney CJ, Simpson IJ, Nicholas JM, et al. Longitudinal diffusion tensor imaging in frontotemporal dementia. Ann Neurol 2015; 77, 33–46.
17. Matsuo K, Mizuno T, Yamada K, et al. Cerebral white matter damage in frontotemporal dementia assessed by diffusion tensor tractography. Neuroradiology, 2008; 50(7): 605-11.
18. McMillan CT, Brun C, Siddiqui S, et al. White matter imaging contributes to the multimodal diagnosis of frontotemporal lobar degeneration. Neurology, 2012; 78(22): 1761-1768.
19. Meijboom R, Steketee RM, Ham LS, et al. Differential hemispheric predilection of microstructural white matter and functional connectivity abnormalities between respectively semantic and behavioral variant frontotemporal dementia. J Alzheimers Dis, 2017; 56(2): 789-804.
20. Möller C, Hafkemeijer A, Pijnenburg Y, et al. Joint assessment of white matter integrity, cortical and subcortical atrophy to distinguish AD from behavioral variant FTD: a two-center study. NeuroImage Cli, 2015; 9: 418-429.
21. Rohrer JD, Ridgway GR, Modat M, et al. Distinct profiles of brain atrophy in frontotemporal lobar degeneration caused by progranulin and tau mutations. Neuroimage, 2010; 53: 1070–1076.
22. Rohrer JD, Nicholas JM, Cash DM, et al. Presymptomatic cognitive and neuroanatomical changes in genetic frontotemporal dementia in the Genetic Frontotemporal dementia Initiative (GENFI) study: a cross-sectional analysis. Lancet Neurology, 2015; 14(3): 253-262.
23. Steketee RM, Meijboom R, de Groot M, et al. Concurrent white and gray matter degeneration of disease-specific networks in early-stage Alzheimer's disease and behavioral variant frontotemporal dementia. Neurobiol Aging, 2016; 43: 119-128.
24. Schwindt GC, Graham NL, Rochon E, et al. Whole-brain white matter disruption in semantic and nonfluent variants of primary progressive aphasia. Hum Brain Mapp 2013; 34: 973–84.

25. Whitwell JL, Jack Jr CR, Boeve BF, et al. Voxel-based morphometry patterns of atrophy in FTLD with mutations in MAPT or PGRN. Neurology, 2009; 72(9): 13-820.
26. Whitwell JL, Avula R, Senjem ML, et al. Gray and white matter water diffusion in the syndromic variants of frontotemporal dementia. Neurology, 2010; 74(16): 1279-87.
27. Yoshiura T, Mihara F, Koga H, et al. Cerebral white matter degeneration in frontotemporal dementia detected by diffusion-weighted magnetic resonance imaging. Acad Radiol, 2006; 13(11): 1373-8.
28. Zhang Y, Schuff N, Du AT, et al. White matter damage in frontotemporal dementia and Alzheimer's disease measures by diffusion MRI. Brain, 2009; 132(Pt9): 2579-92.
29. Zhang Y, Schuff N, Ching C, et al. Joint assessment of structural, perfusion, and diffusion MRI in Alzheimer's Disease and Frontotemporal Dementia. International Journal of Alzheimer's Disease, 2011; 2011: 546871.
30. Zhang Y, Tartaglia MC, Schuff N, et al. MRI signatures of brain macrostructural atrophy and microstructural degradation in frontotemporal lobar degeneration subtypes. J Alzheimer's Dis 2013; 33: 431–44.

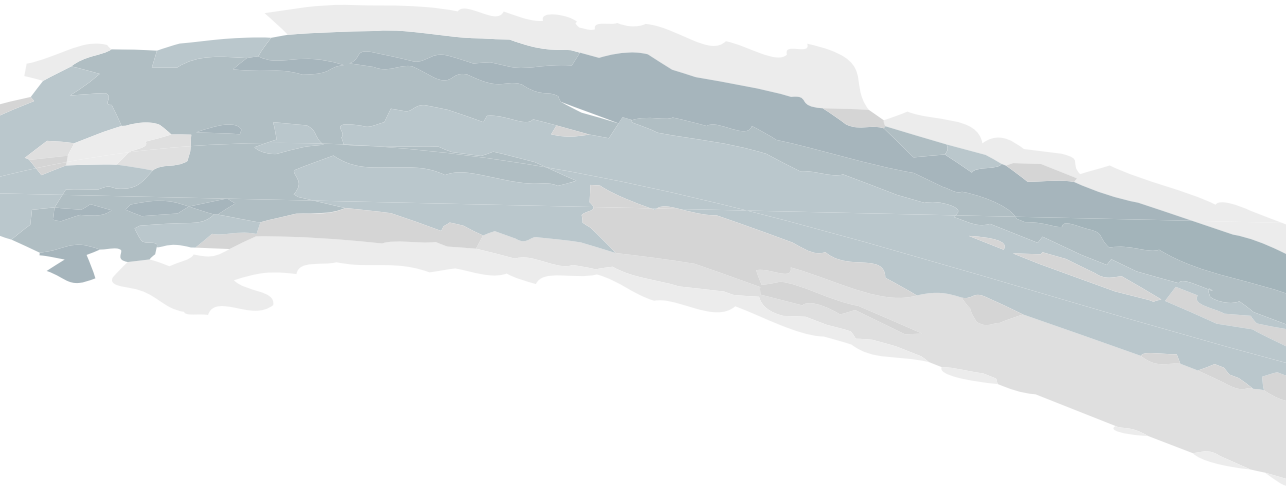

Chapter 3.3

Regional cerebral blood flow in genetic frontotemporal dementia – a pilot study

Panman, J.L.*
Steketee, R.M.E.*
Versteeg, A.
Bron, E.E.
Venkatraghavan, V.
Jiskoot, L.C.
Poos, J.M.
van der Ende, E.L.
Meeter, L.H.H.
Dopper, E.G.P.
Donker Kaat, L.
Rombouts, S.A.R.B.
Niessen, W.J.
van Osch, M.J.P.
Papma, J.M.
van Swieten, J.C.

* these authors contributed equally to this work

In preparation

ABSTRACT

Functional neuroimaging techniques such as arterial spin labeling (ASL) can aid the identification of the first disease related changes in the major genotypes of familial frontotemporal dementia (FTD). In this study, we aimed to investigate presymptomatic genotypic trajectories of regional cerebral blood flow (CBF) changes in familial FTD, and also examined regional CBF change in FTD mutation carriers that converted from the presymptomatic to the symptomatic stage during follow-up.

Ten years of follow-up ASL data of the FTD risk cohort (FTD-RisC) was considered in this project. After exclusion of acquisition and processing failures, 378 datasets were included, from 163 subjects. Our sample consisted of 92 carriers of genetic FTD mutations, divided according to genotype (i.e. *GRN*, *MAPT* or *C9orf72*) and disease stage (i.e. presymptomatic, converter, symptomatic). Healthy family members without an FTD gene mutation were included as control group (i.e. non-carriers, n=71). This pilot study describes our processing strategies, defines the effects of methodological choices, and visualizes FTD genotypic longitudinal trajectories of regional CBF.

During this study, we describe several issues related to acquisition, processing, and analyses, indicating the complexity of longitudinal ASL imaging. We demonstrated that quantitative CBF measurements are not stable over time, although most variation could be omitted by normalizing regional CBF relative to the global CBF within subjects. We observed a trend of CBF decline in *C9orf72* repeat expansion carriers with increasing age in several regions. *MAPT* converters showed a decline of CBF in the left insula, and *GRN* converters showed a decline of CBF in the right insula and frontal lobe.

Although the trends in this study indicate genotypic temporal and spatial trajectories of CBF decline, the methodological challenges of ASL acquisition, processing, and analyses limit the potential of ASL as a longitudinal neuroimaging biomarker for diagnostic or research purposes in genetic FTD.

INTRODUCTION

Frontotemporal dementia (FTD) is a highly heritable neurodegenerative disorder. Three main genotypes with autosomal dominant inheritance patterns that cause FTD are mutations in the progranulin (*GRN*) or micro-tubule associated protein tau (*MAPT*) genes, or a repeat expansion in chromosome 9 open reading frame 72 (*C9orf72*). By longitudinal follow-up of cognitively healthy first-degree relatives of FTD patients with a known gene mutation (i.e. presymptomatic FTD), who are 50% at-risk for carrying the same mutation, we can study the emerging pathological process of FTD [4, 5]. Previous research suggested that the temporal sequence of pathophysiological brain change in FTD might be network-based, in which functional changes precede loss of brain tissue [6, 7]. Functional neuroimaging with arterial spin labeling (ASL) MRI is a promising technique for investigating pathophysiological processes *in vivo* [8, 9]. With ASL, the flow of oxygenated blood can be measured, which is an important proxy of brain metabolism [10, 11]. Decreased regional cerebral blood flow (CBF) indicates decreased function of the tissue of interest [9]. For example, previous research using ASL demonstrated decreased functioning of the anterior cingulate cortex in FTD patients compared to healthy controls [12, 13]. Furthermore, regional changes in CBF may be a sensitive marker for the first disease related changes in FTD, as these were shown to precede cortical thinning in FTD patients [7]. These findings though were contradicted by the fact that other studies indicated that ASL may not be a very useful neuroimaging biomarker for FTD, as diffusion tensor imaging provided more insightful and sensitive markers in the same cohort [14].

To our knowledge, two studies investigated ASL as a potential neuroimaging biomarker for disease onset in presymptomatic FTD. A large cross-sectional study with a combined sample of *MAPT* and *GRN* mutation carriers, and *C9orf72* repeat expansion carriers, performed by the Genetic Frontotemporal Dementia Initiative (GENFI), showed an early decline in frontal, temporal and insular CBF in comparison to non-carriers. This effect was predominantly driven by the *C9orf72* repeat expansion carriers and was estimated to evolve 12.5 years before expected age of onset [15]. A previous single-center study in our Dutch FTD Risk cohort (FTD-RisC) in a combined sample of presymptomatic *GRN* and *MAPT* mutation carriers also showed a decrease of CBF between baseline and two-year follow up in specifically left sided frontal, temporal and parietal regions. Furthermore, a strong decline of CBF was demonstrated in two mutation carriers (1 *GRN*, 1 *MAPT*) that converted to clinical FTD [16]. Large-scale longitudinal studies that differentiate between genotypes are needed to examine genotypic trajectories of regional CBF changes. Furthermore, the inclusion of more converters, presymptomatic carriers that start to develop clinical symptoms, is crucial to investigate the potential value of CBF measurements as a marker for disease onset in genetic FTD. As genetic FTD is a rare disease, large datasets are usually obtained by pooling

data from multiple centers [5, 14, 17, 18]. However, both multi-center and longitudinal ASL studies are hampered by various methodological challenges. Multi-center ASL data are difficult to harmonize, due to differences in MRI vendors, scanner hardware, acquisition parameters, and read-out strategies [19-21]. Longitudinal studies suffer from extensive variability in absolute CBF measurements within-subjects introduced by physiological variability, positioning of participants, slice positioning, and time of scanning [22-24], making within-subjects trajectories difficult to interpret.

In our single center genetic FTD cohort (FTD-RisC), presymptomatic FTD mutation carriers and patients have been followed since 2010 with longitudinal MRI scanning, including ASL. As this is a single-center study, most methodological variability will be between time-points. In this project, we describe the difficulties we have encountered in our longitudinal study, we aimed to investigate genotypic trajectories of regional CBF, and to model the rate of decline in CBF from presymptomatic towards symptomatic stages. We quantified longitudinal regional CBF in 1) presymptomatic *GRN* and *MAPT* mutation carriers, and *C9orf72* repeat expansion carriers; 2) mutation carriers that converted to symptomatic FTD; in comparison to healthy non-carriers. This pilot study presents preliminary results from currently available data.

METHODS

Sample and procedures

We included 173 participants from the longitudinal prospective Frontotemporal Dementia Risk Cohort (FTD-RisC). The FTD-RisC study follows genetic FTD patients with a known gene mutation (*GRN, MAPT, C9orf72*) and their healthy first-degree relatives, who are 50% at-risk for carrying the same gene mutation. The study started in 2010, and currently includes over 200 participants. We perform cognitive testing, clinical questionnaires, neurological examination, blood sampling, and brain MRI, every year or every other year depending on the participants' choice. Participants are assigned to a specific mutation group, or to the healthy control group as non-carriers, based on DNA genotyping, as described before [4, 25]. Investigators and participants are blinded to the DNA status, unless participants have undergone predictive testing. Participants are labeled as 'symptomatic' or 'presymptomatic' based on clinical criteria for FTD [26], primary progressive aphasia (PPA) [27] and/or amyotrophic lateral sclerosis (ALS) [28], as described previously [29]. The Mini Mental State Examination [30] was administered as global indicator of cognitive functioning. The study was carried out in accordance to the declaration of Helsinki, and approved by the local ethics committee of the Erasmus University Medical Center, Rotterdam. All participants provided written informed consent.

MRI acquisition

MRI scans were acquired at 3.0 Tesla (Philips Achieva Medical Systems, Best, The Netherlands). 3D T1-weighted (T1w) images were used for gray matter segmentation and registration purposes, and were acquired using the following parameters: repetition time = 9.8 ms, echo time = 4.6 ms, flip angle = 8, 140 slices, voxel size = 0.88x0.88x1.20. A pseudo-continuous ASL sequence using single-shot echo-planar imaging (EPI) with a background suppression scheme was obtained with similar acquisition parameters as previously described [16]; saturation pulse applied directly before labeling, inversion pulses at 1680 and 2830 ms after the saturation pulse; repetition time 4020 ms, echo time 14 ms; label duration 1650 ms; post labeling delay 1525 ms; voxel size 3x3x7mm; 40 pairs of label and control images. The images were angulated perpendicular to the carotid arteries. Participants were instructed to lie still, stay awake and keep their eyes closed during scanning. Corresponding M0 images were acquired with the following parameters: echo time = 12.5 ms, flip angle = 90, slice thickness = 3mm, slice gap = 0.5mm, in plane resolution = 1x1mm. In the first months of scanning in 2010, we started with a repetition time for the M0 of 4000 ms. However, due to new insights in ASL acquisition [31], from January 2011 onwards, the TR was increased to 10.000 ms.

We switched from an 8-channel head coil (used in 58% of the current dataset) to a 32-channel head coil (used in 42% of the current dataset) in 2017. ASL images acquired with the 8-channel coil covered 17 slices and for the 32-channel coil we increased this to 20 slices, to include both the occipital cortex and cerebellum in the field of view. During the length of the study, we switched the data format for analysis and archiving from PAR/REC images from Philips to the unified DICOM images to preserve more acquisition related details. Finally, all our imaging was obtained on the same scanner, but a mandatory software update was installed in September 2015. The head coil switch, variations in data type (i.e. PAR/REC versus DICOM), and the software update resulted in six slightly different datasets, which we correct for in analyses.

MRI processing

We visualized the timeline of our processing strategies in Figure 1. The final image processing pipeline was constructed as follows: The pipeline was implemented in to FASTR, running in Python [32]. First, ASL, M0, and T1w images were converted to NIfTI (https://nifti.nimh.nih.gov). We performed a quality check on the converted NIfTI's to localize scan and motion artifacts. Second, the T1w image was brain extracted, bias field corrected with n4 correction, and matched to the brain mask of the Hammers atlas [33, 34] which comprises 30 labeled T1w images, each containing 83 ROIs. The brain mask and the Hammers ROI labels were registered to the T1w images in native space, using Elastix [35]. The 30 ROI labeled images

Figure 1. Image processing pipeline

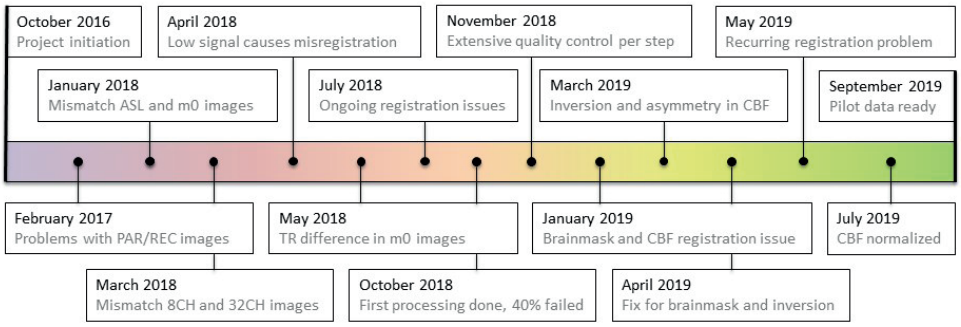

Abbreviations: ASL = arterial spin labeling, 8CH = 8 channel head coil, 32CH = 32 channel head coil, TR = repetition time, CBF = cerebral blood flow. Timeline of the processing issues from start of the project to the pilot data used in this paper.

were combined to a single segmentation using majority voting. These T1w images with brain mask and ROI registration were visually assessed to assure correct registration. Subcortical volumes were directly calculated from the T1w ROI images. Third, native T1w images were segmented into gray matter, white matter and cerebrospinal fluid using SPM [36]. The segmentations were binarized into non-overlapping gray matter, white matter, and CSF masks in native space. Again, all output was visually checked for correct segmentation. The gray matter segmentations were used for volume calculation of cortical ROI's. Fourth, ASL images were corrected for motion artifacts, including the M0 image, and masked into a non-zero ASL image. The gray matter segmentations were then registered to the ASL image. We checked accurate registration of the gray matter segmentations to the ASL images. The gray matter ASL images were corrected for partial volume error [37], smoothed using a 3D kernel of 3*3*3 voxels to correct for local noise, and CBF in gray matter tissue (ml/100g GM/min) was calculated. Fifth, the unscaled CBF maps and M0 images were transformed back to native T1w space, and regional unscaled CBF was calculated using the ROI labels. Last, regional unscaled CBF values were divided by the global M0 value.

Statistical analyses

Statistical analyses were performed in IBM SPSS Statistics v25. Absolute regional CBF values were normalized relative to the gray matter of the global supratentorial CBF. To visualize the effect of normalization, we plotted the absolute and normalized CBF of the posterior cingulate, without correction for confounding factors. We display the bilateral posterior cingulate as a control region, which is a preserved region in (genetic) FTD [12, 15, 16, 38]. Before continuing the analyses, we corrected the CBF values for the confounding factors of sex and scan protocol using multiple linear regression, based on the non-carriers. Next, we

Figure 2. Flowchart of inclusion and exclusion

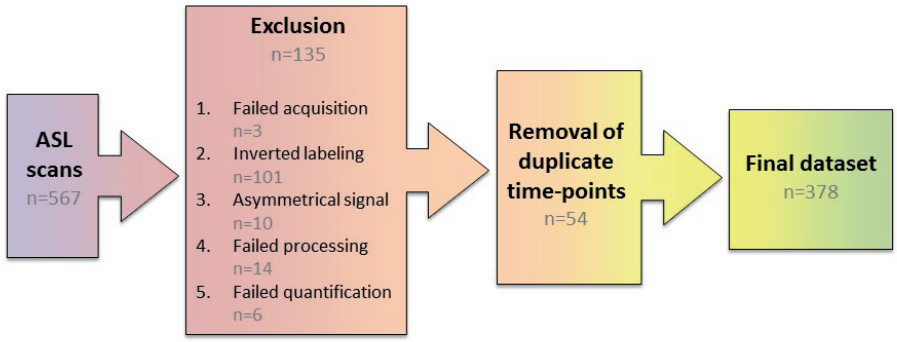

Abbreviations: ASL = arterial spin labeling. Flowchart of in- and exclusion of ASL images from start of processing to the pilot data used in this paper.

present the CBF trajectories as a function of age for each mutation group separately, and converters, in regions that have been indicated in previous ASL studies in FTD [12, 15, 16, 38], i.e. the frontal, temporal, parietal lobes, the insular regions and the anterior cingulate.

RESULTS

MRI availability

Initially, 567 ASL scans from the FTD-RisC cohort were collected for processing. 135 scans were excluded, due to multiple acquisition and processing issues (Figure 2). For example, labeled images seemed to be subtracted from control images in 101 datasets throughout the sample, including all baseline scans with the short TR of 4000 ms in the M0 image. As this can probably be solved, we expect that the major part of these datasets will be included in the final sample. However, this fix was not yet available for the current pilot study, and therefore we excluded all inverted CBF images from the pilot sample. Images with unexplainable asymmetry in CBF signal were excluded (n=37).

Figure 2 indicates that there were only 10 images with this artifact, but 27 of the inverted images excluded earlier also showed this asymmetry in CBF signal. Processing succeeded in 76.2% of the images (n=432). We removed duplicate time-points where both PAR/REC and DICOM data were available after processing by discarding duplicate PAR/REC data. In some cases, processing in one of both failed and then the other dataset could be included. The final sample consisted of 378 unique datasets from 163 subjects.

Table 1. Sample characterization

	Non-carriers	*GRN*			*MAPT*			*C9orf72*		
		Presympt	**Converter**	**Sympt**	**Presympt**	**Converter**	**Sympt**	**Presympt**	**Converter**	**Sympt**
N	71	37	3	3	11	5	2	21	2	8
Sex, m/f	31/40	14/23	0/3	1/2	6/5	1/4	0/2	13/8	0/2	3/5
Age, y	50.09 ± 12.52	53.48 ± 8.67	56.62 ± 8.97	61.04 ± 5.90	42.46 ± 8.40	44.08 ± 7.87	57.66 ± 1.38	43.50 ± 12.47	56.23 ± 10.36	61.06 ± 9.91
MMSE	29.19 ± 1.13	28.92 ± 1.52	28.67 ± 1.53	22.33 ± 3.51	28.36 ± 2.11	29.40 ± 0.89	27.00 ± 4.24	29.29 ± 1.06	29.00 ± 1.41	25.75 ± 6.14
Subjects with FU	48	29	3	N/A	8	5	N/A	16	2	1
FU, y	4.88 ± 1.88	5.18 ± 1.72	3.42 ± 1.40	N/A	3.72 ± 1.78	2.80 ± 1.90	N/A	2.81 ± 1.57	3.95 ± 0.19	4.08 ± N/A

Abbreviations: m/f = male/female, y = years, MMSE = Mini Mental State Examination, FU = follow up, N/A = not applicable. Age, MMSE, and average FU are presented as mean ± standard deviation.

Sample

In this study, 163 subjects were included across ten groups. The three mutation groups were separated per disease stage, i.e. presymptomatic, converter, and symptomatic. The tenth group consists of all non-carriers. The exact number of each group within our sample is presented in Table 1, together with a demographic and clinical characterization.

Absolute versus normalized CBF

In Figure 3, we show the absolute and normalized longitudinal CBF of the left and right posterior cingulate in non-carriers. It can be observed from the plots that absolute CBF declines with age (Figure 3A), while the normalized CBF does not decrease with age. A visual pattern of higher normalized CBF in the right posterior cingulate compared with the left posterior cingulate is visible (Figure 3B). The longitudinal plots indicate large physiological variability in absolute CBF values between time-points and subjects, while the normalized CBF is generally much more consistent.

Regional longitudinal CBF trends

We show longitudinal CBF trajectories for bilateral insular regions (Figure 4 and 5) and the right frontal lobes (Figure 6). In the plots with the entire longitudinal sample (Fig. 4A, 5A, 6A), it is hard to deduct if, and when, normalized CBF changes as a function of age. However, the entire *C9orf72* repeat expansion group shows a gradual decline in CBF with increasing age in the bilateral insula and right frontal lobe (Figure 4D-6D). We could not deduct any trends for the *MAPT* and *GRN* mutation groups related to age, but we observed some trends for the converters, as discussed below. CBF in other regions (i.e. right frontal, bilateral temporal, parietal lobes, and bilateral anterior cingulate) is shown in Supplementary Figure 1-7. We did not observe any trends or patterns over time in these regions.

CBF change in converters

When we focus on subjects that converted from the presymptomatic to the symptomatic stage during follow up, we see that for *MAPT* mutation carriers, converters (in red) show a decline in CBF in the left insula from the presymptomatic to the symptomatic stage (Figure 7A). For *GRN* mutation carriers, converters (in blue) show a slight decrease in CBF of the right insula and right frontal lobe from the presymptomatic to the symptomatic stage (Figure 7B,C). In contrast, *C9orf72* repeat expansion converters do not show a specific trend from the presymptomatic to the symptomatic stage (Figure 7A-C).

DISCUSSION

In this study, we aimed to investigate regional cerebral blood flow trajectories in different

Figure 3. Absolute versus normalized CBF of the posterior cingulate in non-carriers

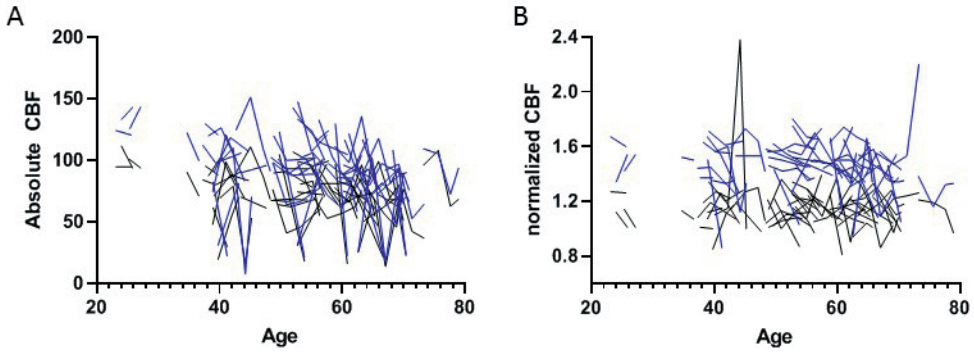

Abbreviations: CBF = cerebral blood flow. A: Longitudinal trajectories of absolute CBF in the posterior cingulate in non-carriers as a function of age. B: Longitudinal trajectories of CBF in the posterior cingulate relative to the global CBF in non-carriers as a function of age. Black = left posterior cingulate, blue = right posterior cingulate.

genotypes and disease stages of genetic FTD across 10 years of follow up. We have, at this stage, visualized the timeline of processing since the start of the project, visualized the differences between longitudinal absolute CBF and normalized CBF, and observed trends over time in the mutation groups and converters from pilot data.

We demonstrated that quantitative regional CBF measurements are not stable over time, in contrast to previous studies [39-41]. In our study, within-subject absolute CBF values heavily fluctuated compared to relative (i.e. normalized) CBF. In an attempt to correct for within-subject variation resulting from physiological variability, we normalized the regional CBF values to the global mean CBF of the entire gray matter, similar to other studies [42, 43]. While the relative CBF measurements showed considerably less variation within-subjects than the absolute CBF, the longitudinal trajectories were still characterized by longitudinal variation in CBF, that does not seem to be the result of pathophysiological processes. Possibly, everyday physiological variation in longitudinal ASL acquisition, such as participant positioning, time of scanning, caffeine consumption, and slice positioning [22-24], affects regional CBF, which may therefore not completely be omitted by using relative CBF. The longitudinal variation observed in both absolute and relative CBF, implies that ASL acquisition and processing needs further development in terms of intra-subject reliability and reproducibility in order to optimize longitudinal analyses.

Although we only discuss visually observed trends, without any statistical analyses, we found a general pattern in the absolute CBF measurements, where CBF declined with increasing age. This observation aligns well with previous studies in normal brain ageing [44, 45]. However, this effect disappeared using normalized CBF. Interestingly, in the entire group of

Figure 4. Regional CBF – left insula

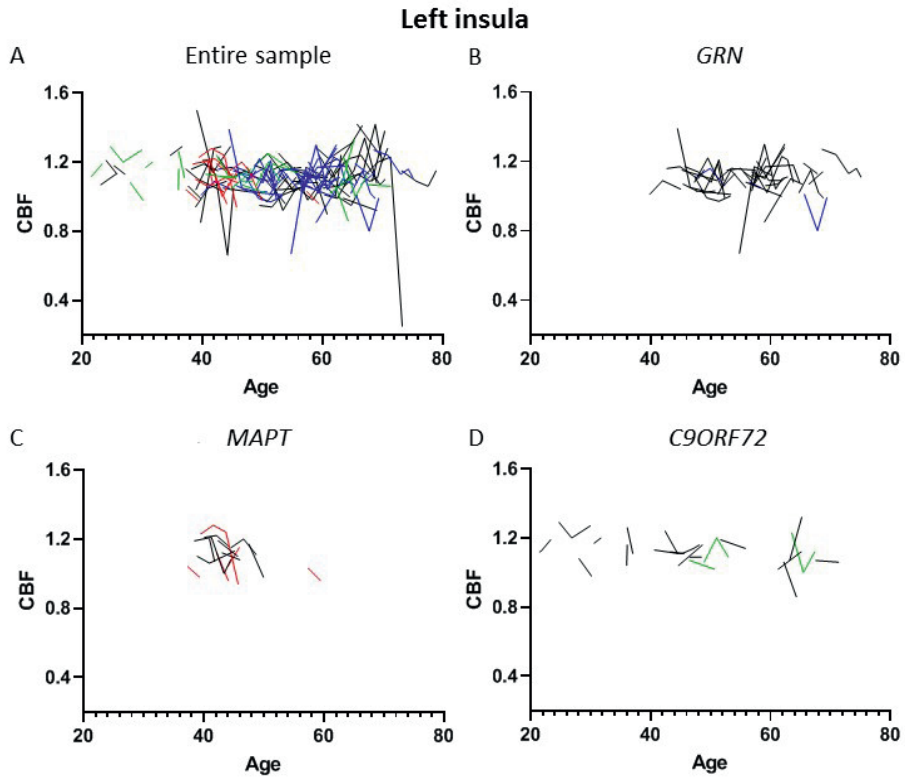

Abbreviations: CBF = cerebral blood flow, *GRN* = progranulin, *MAPT* = microtubule associated protein tau, *C9orf72* = chromosome 9 open reading frame 72. Longitudinal trajectories of normalized CBF in the left insula in A: the entire sample. Black = non-carriers, blue = *GRN* mutation carriers, red = *MAPT* mutation carriers, green = *C9orf72* repeat expansion carriers. B: *GRN* mutation carriers. Black = presymptomatic, blue = converter. C: *MAPT* mutation carriers. Black = presymptomatic, red = converter. D: *C9orf72* repeat expansion carriers. Black = presymptomatic, green = converter.

presymptomatic *C9orf72* repeat expansion carriers, normalized regional CBF appeared to be lower with increasing age. Within the larger GENFI cohort, the first CBF changes were detected around 12.5 years before expected symptom onset, and were most pronounced in *C9orf72* repeat expansion carriers [15]. However, in the same *C9orf72* repeat expansion cohort, gray matter and white matter decline were estimated to occur at 25 and 30 years respectively before expected symptom onset [46, 47]. The timeline of the imaging changes found in the GENFI cohort have to be interpreted with caution. Emerging evidence reveals that expected age at symptom onset is not a reliable method for genetic FTD mutation carriers [1, 18, Moore et al., 2019 *in press*]. In our study, a trend in *C9orf72* repeat expansion carriers, but not *MAPT* and *GRN* mutation carriers, shows CBF decline with increasing age. It

Figure 5. Regional CBF – right insula

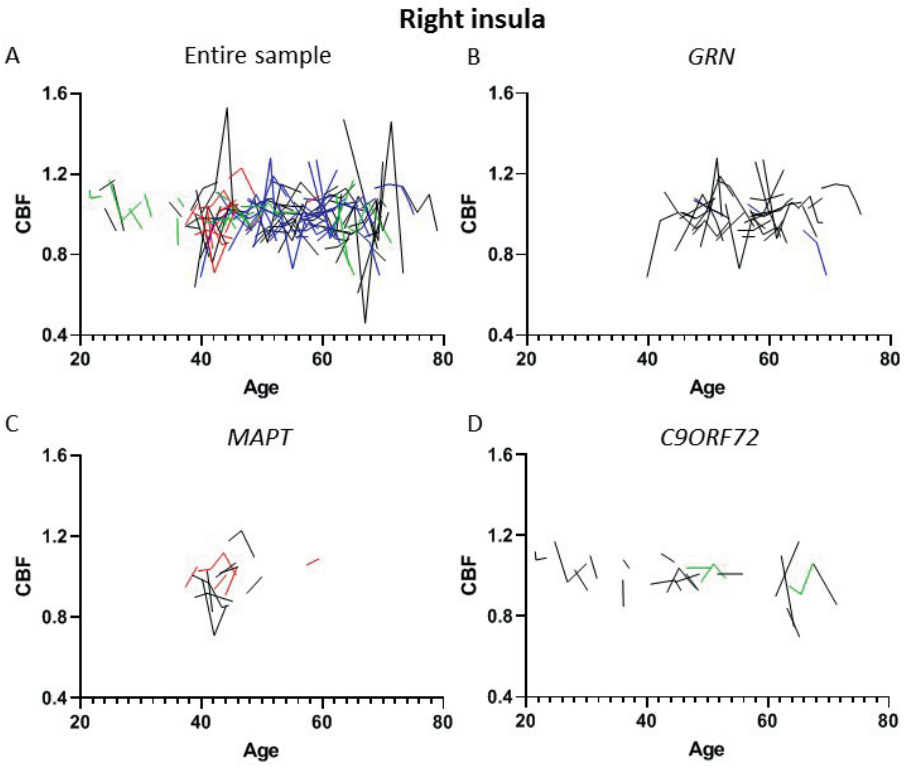

Abbreviations: CBF = cerebral blood flow, *GRN* = progranulin, *MAPT* = microtubule associated protein tau, *C9orf72* = chromosome 9 open reading frame 72. Longitudinal trajectories of normalized CBF in the right insula in A: the entire sample. Black = non-carriers, blue = *GRN* mutation carriers, red = *MAPT* mutation carriers, green = *C9orf72* repeat expansion carriers. B: *GRN* mutation carriers. Black = presymptomatic, blue = converter. C: *MAPT* mutation carriers. Black = presymptomatic, red = converter. D: *C9orf72* repeat expansion carriers. Black = presymptomatic, green = converter.

is therefore conceivable that the difference in CBF between presymptomatic *C9orf72* repeat expansion carriers and non-carriers becomes statistically significant before symptom onset. Our preliminary results support previous research, indicating that regional CBF changes may serve as a biomarker for the first disease related changes in *C9orf72* repeat expansion carriers.

We found a pattern of CBF decline in *MAPT* converters from the presymptomatic to the symptomatic stage in the left insula, and a similar pattern for *GRN* converters in the right insula and frontal lobe. Neither presymptomatic *MAPT* nor presymptomatic *GRN* mutation carriers showed any other observable decline in regional CBF trajectories. Functional brain

Figure 6. Regional CBF – right frontal lobe

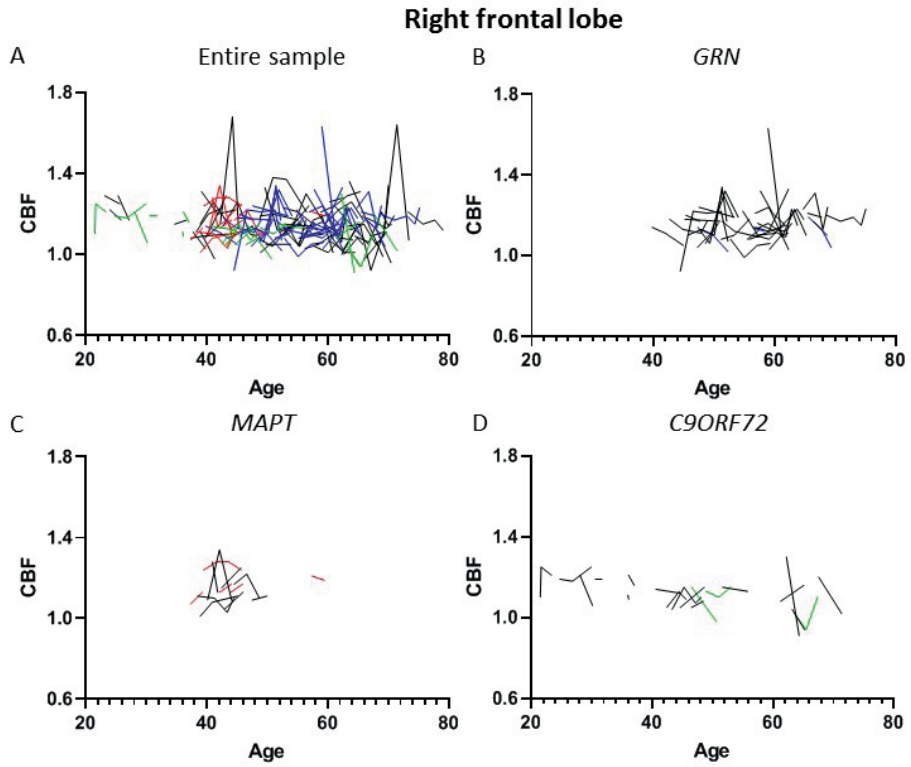

Abbreviations: CBF = cerebral blood flow, *GRN* = progranulin, *MAPT* = microtubule associated protein tau, *C9orf72* = chromosome 9 open reading frame 72. Longitudinal trajectories of normalized CBF in the right frontal lobe in A: the entire sample. Black = non-carriers, blue = *GRN* mutation carriers, red = *MAPT* mutation carriers, green = *C9orf72* repeat expansion carriers. B: *GRN* mutation carriers. Black = presymptomatic, blue = converter. C: *MAPT* mutation carriers. Black = presymptomatic, red = converter. D: *C9orf72* repeat expansion carriers. Black = presymptomatic, green = converter.

changes such as decreased CBF have been hypothesized to be sensitive biomarkers for the first disease related changes of genetic FTD, and may be present before structural changes emerge [6, 7]. However, previous presymptomatic FTD studies with ASL have not supported this assumption. The study of Dopper et al., [16], examining groups comprised of approximately the same *MAPT* and *GRN* mutation carriers as our current cohort, proposed that CBF changes occurred a few years before symptom onset. In that study, two mutation carriers (one *MAPT* and one *GRN*) that converted to symptomatic FTD at the first follow-up, already showed lower global CBF at baseline [16]. In the years after that, more *MAPT* and *GRN* mutation carriers converted to FTD. Jiskoot et al., investigated structural brain changes in the years before symptom onset in these converters and demonstrated that gray matter

Figure 7. Regional CBF - converters

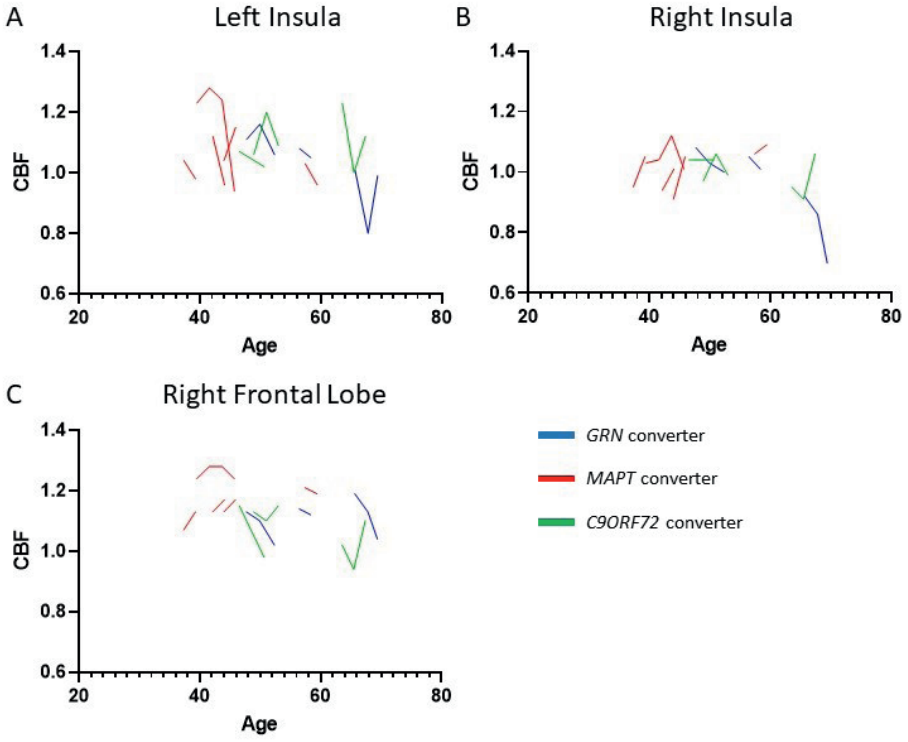

Abbreviations: CBF = cerebral blood flow, *GRN* = progranulin, *MAPT* = microtubule associated protein tau, *C9orf72* = chromosome 9 open reading frame 72. Longitudinal trajectories of normalized CBF in the converters (blue = *GRN*, red = *MAPT*, green = *C9orf72*), in A: the left insula. B: the right insula. C: right frontal lobe

volume (T1-weighted imaging) and white matter integrity (derived from diffusion tensor imaging) also declines approximately two years before symptom onset [48]. Together with the regional CBF trends in this pilot study, our data suggest that structural and functional changes emerge around the same time point, i.e. around two years before symptom onset, instead of the network-based temporal sequence, as suggested before [6, 7].

In future analyses, it would be interesting to investigate whether the CBF decline in FTD mutation carriers is linear, or whether there are periods of acceleration or deceleration. Previous work in Alzheimer's disease suggested that the trajectory of CBF change might evolve from an early increase in CBF to a decrease in CBF in carriers of the *APOE* genotype [49], following an inverted U pattern, indicating that change in CBF might not follow a pattern of linear decline. Similarly, other functional neuroimaging studies in genetic FTD proposed gradual, non-linear decline of connectivity [50]. Secondly, it may be worthwhile to

relate these trajectories to the clinical phenotype. For example, previous research indicated that a decline in CBF might especially be pronounced in semantic variant primary progressive aphasia [7, 14]. In terms of genetic FTD, Floeter et al [51] previously correlated white matter integrity decline with phenotypes of the *C9orf72* repeat expansion as well as sporadic ALS and FTD, and showed phenotypic patterns within the *C9orf72* genotype. Addressing phenotypic CBF trajectories within genotypes might be an interesting new perspective for future work.

Although the trends in our data may be promising for quantitative ASL in presymptomatic genetic FTD studies, caution is warranted when performing longitudinal ASL studies, as the results of this study were not easily obtained, and rely on several inference steps. Several years of solving issues in the processing of the images and CBF quantification preceded the final pilot dataset. This trajectory was similar to the GENFI study [15, 19]. Moreover, a few issues still need solutions before the intended statistical analyses can be performed and the potential richness of the dataset can be exploited. Ten years of ASL acquisition in our FTD-RisC study has inevitably led to updates in the scan protocol and hardware, as not only our understanding of genetic FTD has expanded, our knowledge on (experimental) functional neuroimaging techniques has broadened as well. Over the years, we made slight adaptations to our scanning protocol due to new insights in ASL-MRI [31], and necessary updates on scanner hardware [29, 52]. These variations have led to an increase in problems encountered during processing, as well as processing time. We demonstrated that even in a single center study, the CBF measures derived from ASL imaging within and between subjects are heavily susceptible to multiple factors, such as physiological variability, and variations in scanning hardware or parameters. Despite its potential benefits for clinical application compared to, for example, FDG-PET imaging [10, 13, 53, 54], this everyday variability could make ASL-MRI less suitable for longitudinal diagnostic or research purposes.

In this pilot study of regional CBF in genetic FTD, we observed trends related to disease stages in different mutation groups. *MAPT* and *GRN* converters in particular showed regional decline in CBF from the presymptomatic to the symptomatic stage, while the entire *C9orf72* repeat expansion group (i.e. including presymptomatic and symptomatic carriers as well as converters), showed gradual decline in CBF with advancing age in the bilateral insula and right frontal lobe. However, the current study only reported visual observations, and not statistically proven results, because of the difficulties encountered with ASL acquisition, processing, and analysis, which complicate large-scale evaluation of CBF trajectories in genetic FTD. Despite its potential as biomarker for disease onset, the methodological challenges that still exist with ASL currently limits its role as neuroimaging biomarker for genetic FTD.

REFERENCES

1. Olszewska, D.A., et al., Genetics of Frontotemporal Dementia. Curr Neurol Neurosci Rep, 2016. 16(12): p. 107.
2. Seelaar, H., et al., Clinical, genetic and pathological heterogeneity of frontotemporal dementia: a review. J Neurol Neurosurg Psychiatry, 2011. 82(5): p. 476-86.
3. Lashley, T., et al., Review: an update on clinical, genetic and pathological aspects of frontotemporal lobar degenerations. Neuropathol Appl Neurobiol, 2015. 41(7): p. 858-81.
4. Dopper, E.G., et al., Structural and functional brain connectivity in presymptomatic familial frontotemporal dementia. Neurology, 2014. 83(2): p. e19-26.
5. Rohrer, J.D., et al., Presymptomatic studies in genetic frontotemporal dementia. Rev Neurol (Paris), 2013. 169(10): p. 820-4.
6. Seeley, W.W., et al., Neurodegenerative diseases target large-scale human brain networks. Neuron, 2009. 62(1): p. 42-52.
7. Olm, C.A., et al., Arterial spin labeling perfusion predicts longitudinal decline in semantic variant primary progressive aphasia. J Neurol, 2016. 263(10): p. 1927-38.
8. Haller, S., et al., Arterial Spin Labeling Perfusion of the Brain: Emerging Clinical Applications. Radiology, 2016. 281(2): p. 337-356.
9. Grade, M., et al., A neuroradiologist's guide to arterial spin labeling MRI in clinical practice. Neuroradiology, 2015. 57(12): p. 1181-202.
10. Tosun, D., et al., Discriminative Power of Arterial Spin Labeling Magnetic Resonance Imaging and 18F-Fluorodeoxyglucose Positron Emission Tomography Changes for Amyloid-beta-Positive Subjects in the Alzheimer's Disease Continuum. Neurodegener Dis, 2016. 16(1-2): p. 87-94.
11. Anazodo, U.C., et al., Using simultaneous PET/MRI to compare the accuracy of diagnosing frontotemporal dementia by arterial spin labelling MRI and FDG-PET. Neuroimage Clin, 2018. 17: p. 405-414.
12. Steketee, R.M., et al., Early-stage differentiation between presenile Alzheimer's disease and frontotemporal dementia using arterial spin labeling MRI. Eur Radiol, 2016. 26(1): p. 244-53.
13. Verfaillie, S.C., et al., Cerebral perfusion and glucose metabolism in Alzheimer's disease and frontotemporal dementia: two sides of the same coin? Eur Radiol, 2015. 25(10): p. 3050-9.
14. Staffaroni, A.M., et al., Longitudinal multimodal imaging and clinical endpoints for frontotemporal dementia clinical trials. Brain, 2019. 142(2): p. 443-459.
15. Mutsaerts, H., et al., Cerebral perfusion changes in presymptomatic genetic frontotemporal dementia: a GENFI study. Brain, 2019. 142(4): p. 1108-1120.
16. Dopper, E.G., et al., Cerebral blood flow in presymptomatic MAPT and GRN mutation carriers: A longitudinal arterial spin labeling study. Neuroimage Clin, 2016. 12: p. 460-5.
17. Boeve, B., et al., The longitudinal evaluation of familial frontotemporal dementia subjects protocol: Framework and methodology. Alzheimers Dement, 2019.
18. Boeve, B.F. and H.J. Rosen, Multimodal imaging in familial FTLD: phenoconversion and planning for the future. Brain, 2019. 142(1): p. 8-11.
19. Mutsaerts, H., et al., Comparison of arterial spin labeling registration strategies in the multi-center GENetic frontotemporal dementia initiative (GENFI). J Magn Reson Imaging, 2018. 47(1): p. 131-140.
20. Mutsaerts, H.J., et al., Inter-vendor reproducibility of pseudo-continuous arterial spin labeling at 3 Tesla. PLoS One, 2014. 9(8): p. e104108.
21. Mutsaerts, H.J., et al., Multi-vendor reliability of arterial spin labeling perfusion MRI using a near-identical sequence: implications for multi-center studies. Neuroimage, 2015. 113: p. 143-52.
22. Steketee, R.M., et al., Quantitative Functional Arterial Spin Labeling (fASL) MRI--Sensitivity and Reproducibility of Regional CBF Changes Using Pseudo-Continuous ASL Product Sequences. PLoS One, 2015. 10(7): p. e0132929.
23. Chen, Y., D.J. Wang, and J.A. Detre, Test-retest reliability of arterial spin labeling with common labeling strategies. J Magn Reson Imaging, 2011. 33(4): p. 940-9.
24. Jiang, L., et al., Reliability and reproducibility of perfusion MRI in cognitively normal subjects. Magn Reson Imaging, 2010. 28(9): p. 1283-9.
25. Papma, J.M., et al., Cognition and gray and white matter characteristics of presymptomatic C9orf72 repeat expansion. Neurology, 2017. 89(12): p. 1256-1264.
26. Rascovsky, K., et al., Sensitivity of revised diagnostic criteria for the behavioural variant of

frontotemporal dementia. Brain, 2011. 134(Pt 9): p. 2456-77.
27. Gorno-Tempini, M.L., et al., Classification of primary progressive aphasia and its variants. Neurology, 2011. 76(11): p. 1006-14.
28. Ludolph, A., et al., A revision of the El Escorial criteria - 2015. Amyotroph Lateral Scler Frontotemporal Degener, 2015. 16(5-6): p. 291-2.
29. Panman, J.L., et al., Gray and white matter changes in presymptomatic genetic frontotemporal dementia: a longitudinal MRI study. Neurobiol Aging, 2019. 76: p. 115-124.
30. Folstein, M.F., S.E. Folstein, and P.R. McHugh, "Mini-mental state". A practical method for grading the cognitive state of patients for the clinician. J Psychiatr Res, 1975. 12(3): p. 189-98.
31. Alsop, D.C., et al., Recommended implementation of arterial spin-labeled perfusion MRI for clinical applications: A consensus of the ISMRM perfusion study group and the European consortium for ASL in dementia. Magn Reson Med, 2015. 73(1): p. 102-16.
32. Achterberg, H.C., M. Koek, and W.J. Niessen, Fastr: A Workflow Engine for Advanced Data Flows in Medical Image Analysis. Frontiers in ICT, 2016. 3(15).
33. Gousias, I.S., et al., Automatic segmentation of brain MRIs of 2-year-olds into 83 regions of interest. Neuroimage, 2008. 40(2): p. 672-684.
34. Hammers, A., et al., Three-dimensional maximum probability atlas of the human brain, with particular reference to the temporal lobe. Hum Brain Mapp, 2003. 19(4): p. 224-47.
35. Klein, S., et al., elastix: a toolbox for intensity-based medical image registration. IEEE Trans Med Imaging, 2010. 29(1): p. 196-205.
36. Ashburner, J. and K.J. Friston, Voxel-based morphometry--the methods. Neuroimage, 2000. 11(6 Pt 1): p. 805-21.
37. Asllani, I., A. Borogovac, and T.R. Brown, Regression algorithm correcting for partial volume effects in arterial spin labeling MRI. Magn Reson Med, 2008. 60(6): p. 1362-71.
38. Du, A.T., et al., Hypoperfusion in frontotemporal dementia and Alzheimer disease by arterial spin labeling MRI. Neurology, 2006. 67(7): p. 1215-20.
39. Yang, F.N., et al., Test-retest reliability of cerebral blood flow for assessing brain function at rest and during a vigilance task. Neuroimage, 2019. 193: p. 157-166.
40. Ssali, T., et al., Mapping Long-Term Functional Changes in Cerebral Blood Flow by Arterial Spin Labeling. PLoS One, 2016. 11(10): p. e0164112.
41. Holiga, S., et al., Test-retest reliability of task-based and resting-state blood oxygen level dependence and cerebral blood flow measures. PLoS One, 2018. 13(11): p. e0206583.
42. Aslan, S. and H. Lu, On the sensitivity of ASL MRI in detecting regional differences in cerebral blood flow. Magn Reson Imaging, 2010. 28(7): p. 928-35.
43. Dukart, J., et al., Differential effects of global and cerebellar normalization on detection and differentiation of dementia in FDG-PET studies. Neuroimage, 2010. 49(2): p. 1490-5.
44. Chen, J.J., H.D. Rosas, and D.H. Salat, Age-associated reductions in cerebral blood flow are independent from regional atrophy. Neuroimage, 2011. 55(2): p. 468-78.
45. Zhang, N., M.L. Gordon, and T.E. Goldberg, Cerebral blood flow measured by arterial spin labeling MRI at resting state in normal aging and Alzheimer's disease. Neurosci Biobehav Rev, 2017. 72: p. 168-175.
46. Jiskoot, L.C., et al., Presymptomatic white matter integrity loss in familial frontotemporal dementia in the GENFI cohort: A cross-sectional diffusion tensor imaging study. Ann Clin Transl Neurol, 2018. 5(9): p. 1025-1036.
47. Rohrer, J.D., et al., Presymptomatic cognitive and neuroanatomical changes in genetic frontotemporal dementia in the Genetic Frontotemporal dementia Initiative (GENFI) study: a cross-sectional analysis. Lancet Neurol, 2015. 14(3): p. 253-62.
48. Jiskoot, L.C., et al., Longitudinal multimodal MRI as prognostic and diagnostic biomarker in presymptomatic familial frontotemporal dementia. Brain, 2019. 142(1): p. 193-208.
49. Hays, C.C., Z.Z. Zlatar, and C.E. Wierenga, The Utility of Cerebral Blood Flow as a Biomarker of Preclinical Alzheimer's Disease. Cell Mol Neurobiol, 2016. 36(2): p. 167-79.
50. Benussi, A., et al., Clinical and biomarker changes in presymptomatic genetic frontotemporal dementia. Neurobiol Aging, 2019. 76: p. 133-140.
51. Floeter, M.K., et al., Longitudinal imaging in C9orf72 mutation carriers: Relationship to phenotype. Neuroimage Clin, 2016. 12: p. 1035-1043.
52. Panman, J.L., et al., Bias Introduced by Multiple Head Coils in MRI Research: An 8 Channel and 32 Channel Coil Comparison. Front Neurosci, 2019. 13: p. 729.

53. McMahon, P.M., et al., Cost-effectiveness of PET in the diagnosis of Alzheimer disease. Radiology, 2003. 228(2): p. 515-22.
54. Wolk, D.A. and J.A. Detre, Arterial spin labeling MRI: an emerging biomarker for Alzheimer's disease and other neurodegenerative conditions. Curr Opin Neurol, 2012. 25(4): p. 421-8.

SUPPLEMENTARY DATA

Supplementary Figure 1. Regional CBF – left frontal lobe

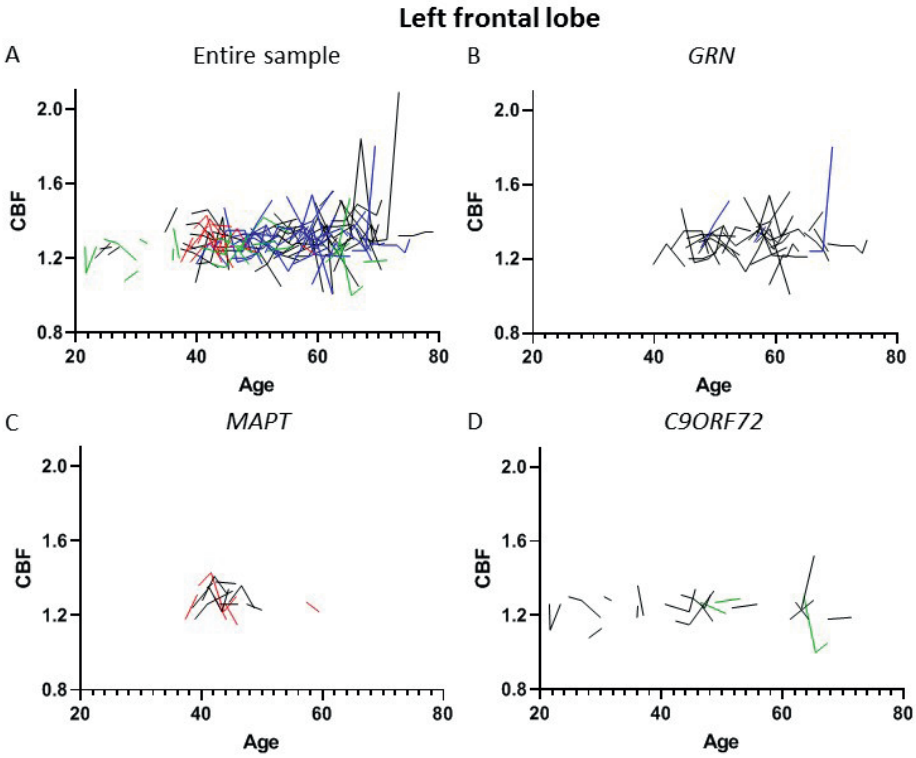

Abbreviations: CBF = cerebral blood flow, *GRN* = progranulin, *MAPT* = microtubule associated protein tau, *C9orf72* = chromosome 9 open reading frame 72. Longitudinal trajectories of normalized CBF in the left frontal lobe in A: the entire sample. Black = non-carriers, blue = *GRN* mutation carriers, red = *MAPT* mutation carriers, green = *C9orf72* repeat expansion carriers. B: *GRN* mutation carriers. Black = presymptomatic, blue = converter. C: *MAPT* mutation carriers. Black = presymptomatic, red = converter. D: *C9orf72* repeat expansion carriers. Black = presymptomatic, green = converter.

Supplementary Figure 2. Regional CBF – left anterior cingulate

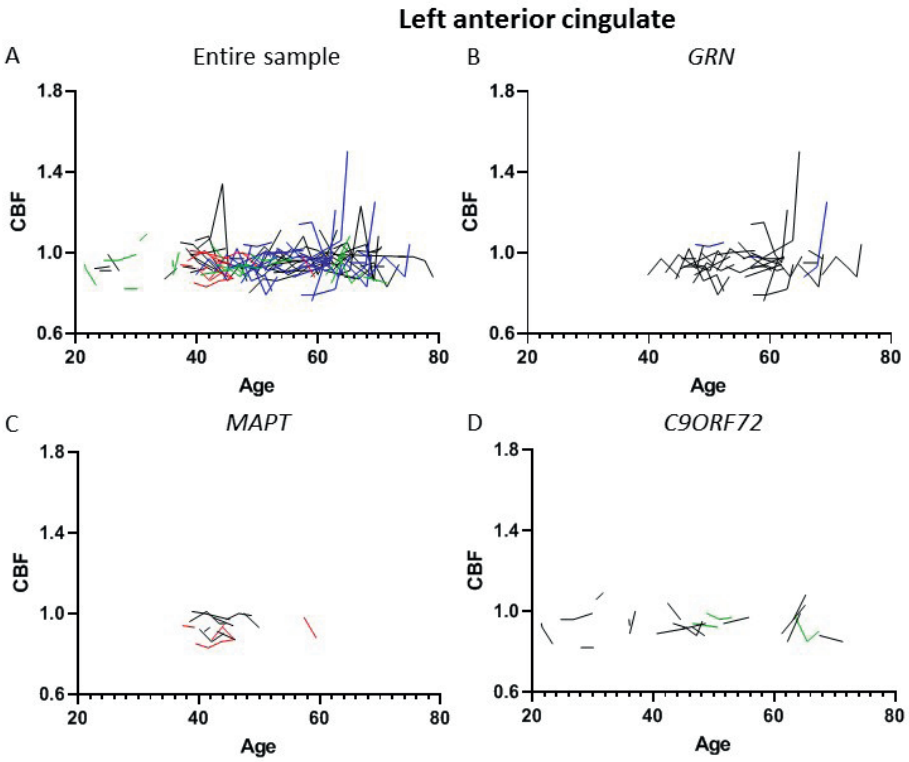

Abbreviations: CBF = cerebral blood flow, *GRN* = progranulin, *MAPT* = microtubule associated protein tau, *C9orf72* = chromosome 9 open reading frame 72. Longitudinal trajectories of normalized CBF in the left anterior cingulate in A: the entire sample. Black = non-carriers, blue = *GRN* mutation carriers, red = *MAPT* mutation carriers, green = *C9orf72* repeat expansion carriers. B: *GRN* mutation carriers. Black = presymptomatic, blue = converter. C: *MAPT* mutation carriers. Black = presymptomatic, red = converter. D: *C9orf72* repeat expansion carriers. Black = presymptomatic, green = converter.

Supplementary Figure 3. Regional CBF – right anterior cingulate

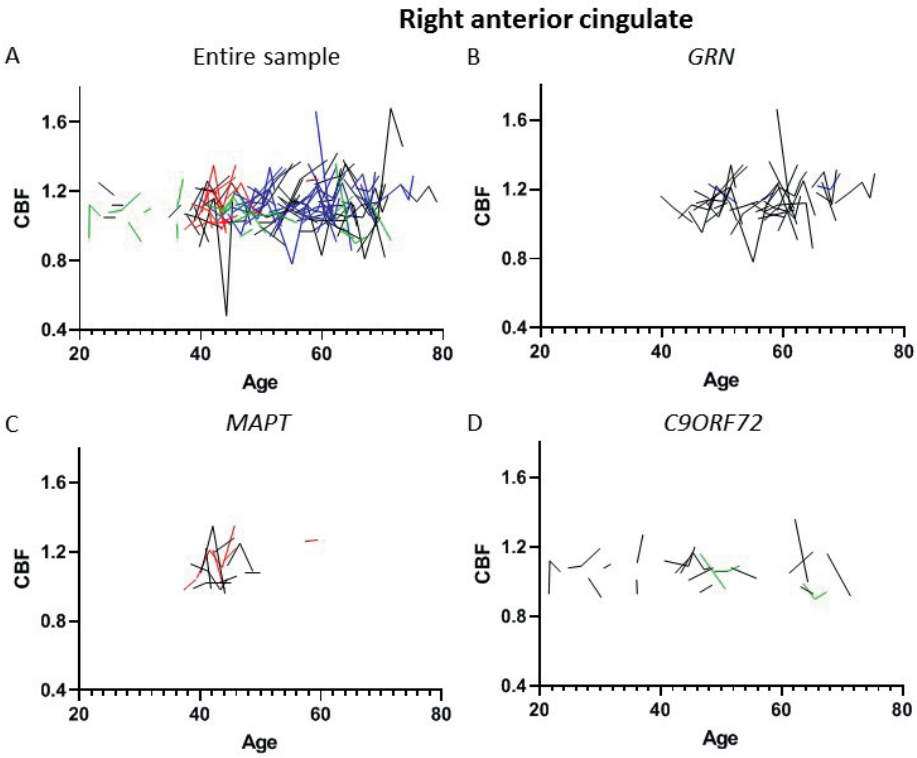

Abbreviations: CBF = cerebral blood flow, *GRN* = progranulin, *MAPT* = microtubule associated protein tau, *C9orf72* = chromosome 9 open reading frame 72. Longitudinal trajectories of normalized CBF in the right anterior cingulate in A: the entire sample. Black = non-carriers, blue = *GRN* mutation carriers, red = *MAPT* mutation carriers, green = *C9orf72* repeat expansion carriers. B: *GRN* mutation carriers. Black = presymptomatic, blue = converter. C: *MAPT* mutation carriers. Black = presymptomatic, red = converter. D: *C9orf72* repeat expansion carriers. Black = presymptomatic, green = converter.

Supplementary Figure 4. Regional CBF – left temporal lobe

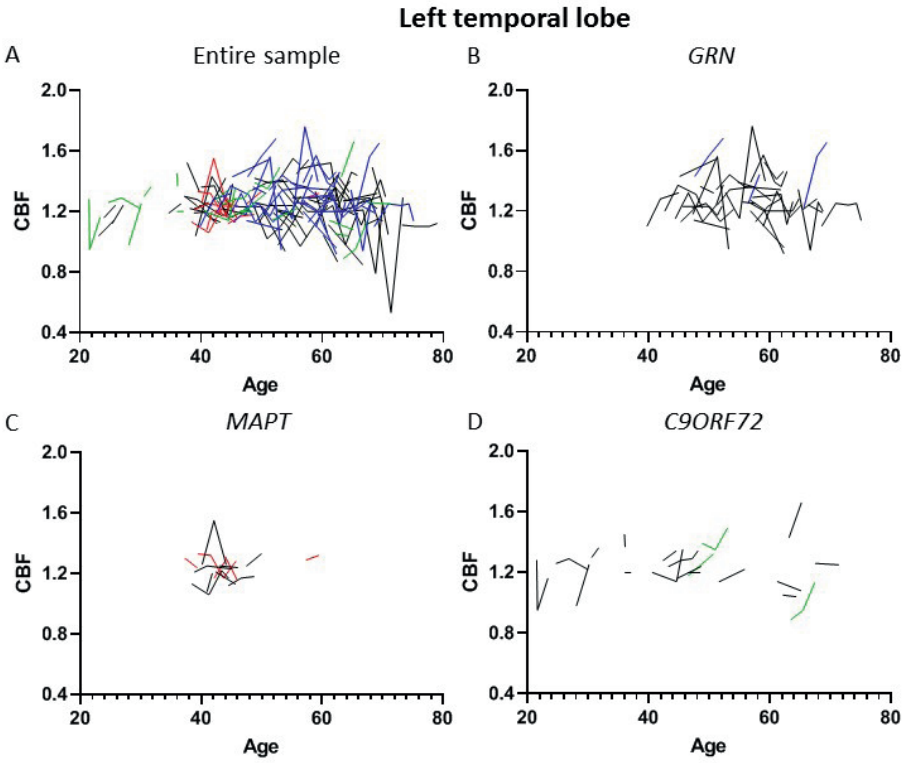

Abbreviations: CBF = cerebral blood flow, *GRN* = progranulin, *MAPT* = microtubule associated protein tau, *C9orf72* = chromosome 9 open reading frame 72. Longitudinal trajectories of normalized CBF in the left temporal lobe in A: the entire sample. Black = non-carriers, blue = *GRN* mutation carriers, red = *MAPT* mutation carriers, green = *C9orf72* repeat expansion carriers. B: *GRN* mutation carriers. Black = presymptomatic, blue = converter. C: *MAPT* mutation carriers. Black = presymptomatic, red = converter. D: *C9orf72* repeat expansion carriers. Black = presymptomatic, green = converter.

Supplementary Figure 5. Regional CBF – right temporal lobe

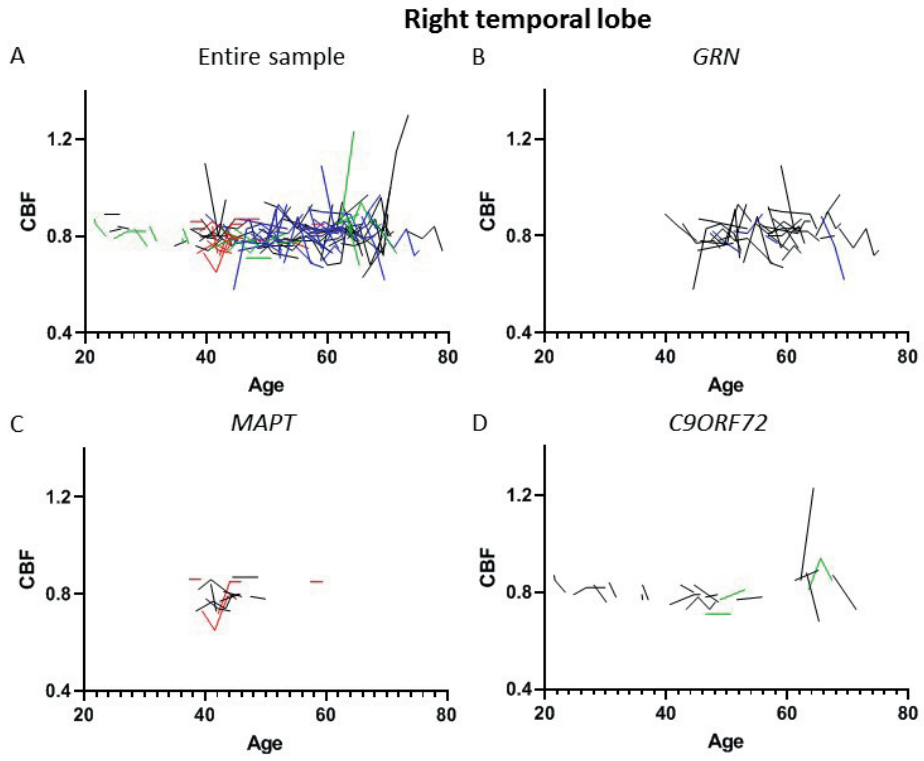

Abbreviations: CBF = cerebral blood flow, *GRN* = progranulin, *MAPT* = microtubule associated protein tau, *C9orf72* = chromosome 9 open reading frame 72. Longitudinal trajectories of normalized CBF in the right temporal lobe in A: the entire sample. Black = non-carriers, blue = *GRN* mutation carriers, red = *MAPT* mutation carriers, green = *C9orf72* repeat expansion carriers. B: *GRN* mutation carriers. Black = presymptomatic, blue = converter. C: *MAPT* mutation carriers. Black = presymptomatic, red = converter. D: *C9orf72* repeat expansion carriers. Black = presymptomatic, green = converter.

Supplementary Figure 6 Regional CBF – left parietal lobe

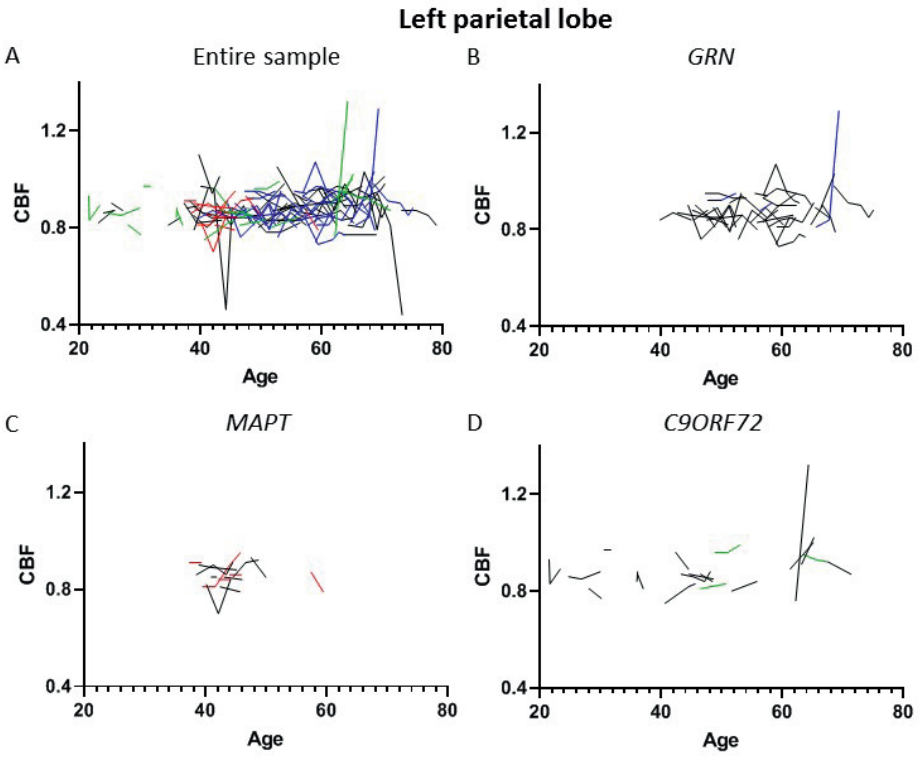

Abbreviations: CBF = cerebral blood flow, *GRN* = progranulin, *MAPT* = microtubule associated protein tau, *C9orf72* = chromosome 9 open reading frame 72. Longitudinal trajectories of normalized CBF in the left parietal lobe in A: the entire sample. Black = non-carriers, blue = *GRN* mutation carriers, red = *MAPT* mutation carriers, green = *C9orf72* repeat expansion carriers. B: *GRN* mutation carriers. Black = presymptomatic, blue = converter. C: *MAPT* mutation carriers. Black = presymptomatic, red = converter. D: *C9orf72* repeat expansion carriers. Black = presymptomatic, green = converter.

Supplementary Figure 7. Regional CBF – right parietal lobe

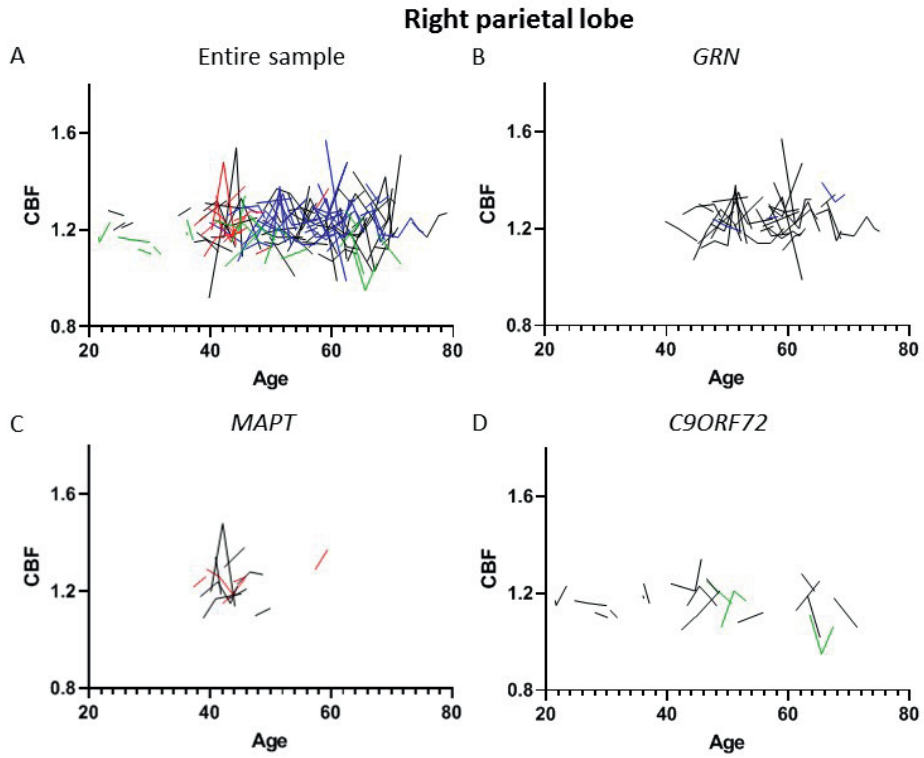

Abbreviations: CBF = cerebral blood flow, *GRN* = progranulin, *MAPT* = microtubule associated protein tau, *C9orf72* = chromosome 9 open reading frame 72. Longitudinal trajectories of normalized CBF in the right parietal lobe in A: the entire sample. Black = non-carriers, blue = *GRN* mutation carriers, red = *MAPT* mutation carriers, green = *C9orf72* repeat expansion carriers. B: *GRN* mutation carriers. Black = presymptomatic, blue = converter. C: *MAPT* mutation carriers. Black = presymptomatic, red = converter. D: *C9orf72* repeat expansion carriers. Black = presymptomatic, green = converter.

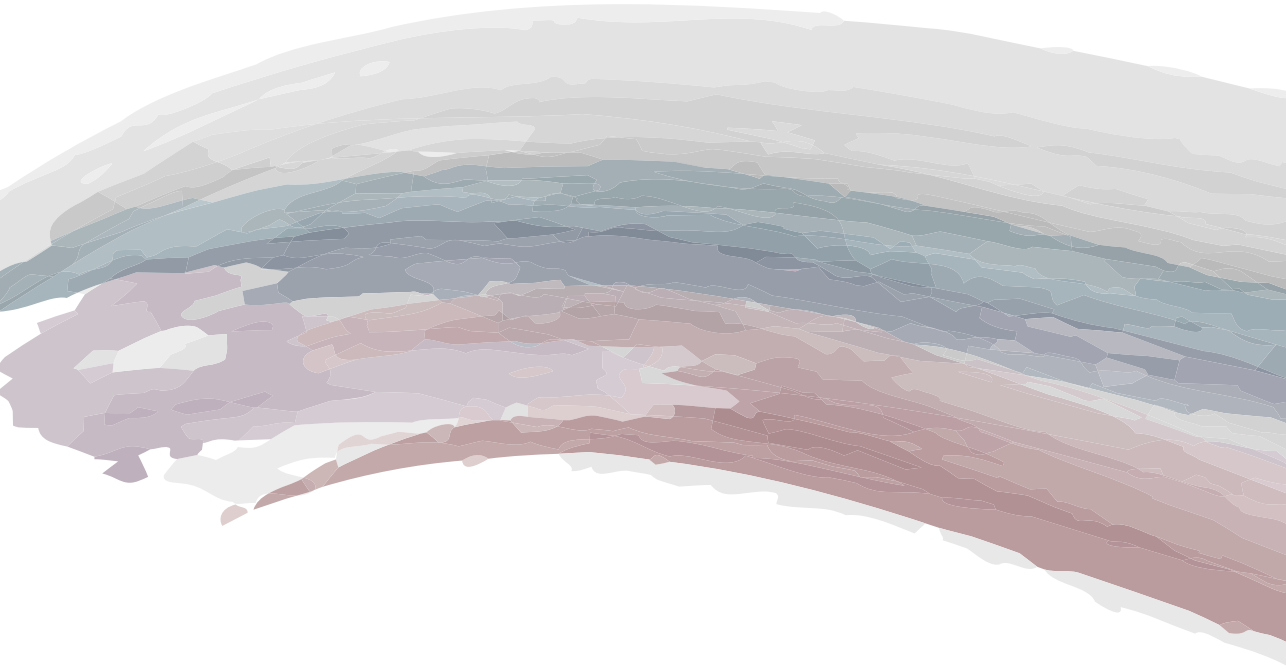

CHAPTER 4

RECOMMENDATIONS FOR NEUROIMAGING ANALYSES IN FRONTOTEMPORAL DEMENTIA RESEARCH

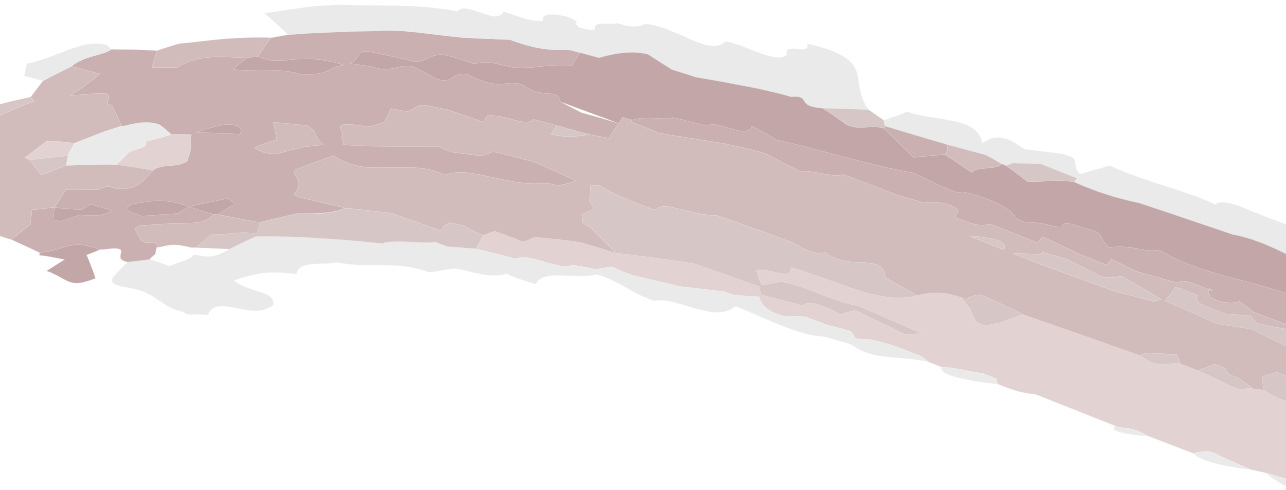

Chapter 4.1

Review and comparison of software packages for grey matter biomarkers in presymptomatic frontotemporal dementia

Panman, J.L.
Steketee, R.M.E.
de Witte, A.C.
To, Y.Y.
Jiskoot, L.C.
van der Ende, E.L.
Poos, J.M.
Meeter, L.H.H.
Dopper, E.G.P.
Donker Kaat, L.
van den Berg, E.
van Swieten, J.C.
Rombouts, S.A.R.B.
Papma, J.M.

Submitted (Neuroimage Clinical)

ABSTRACT

Neuroimaging studies have reported inconclusive results of grey matter atrophy in presymptomatic frontotemporal dementia (FTD) mutation carriers. The use of different software packages may be an important contributor to these inconsistencies. Clinical trials in FTD are currently upcoming, and consensus on methods to analyse grey matter outcome measurements is important for optimal study design. We compared different software packages and estimated sensitivity of cortical grey matter analyses in presymptomatic *MAPT* and *GRN* mutation carriers and *C9orf72* repeat expansion carriers. First, we reviewed the literature on whole brain grey matter analysis in presymptomatic FTD mutation carriers, and defined ROI's per mutation group based on the most commonly affected regions in literature. Second, we performed voxel-wise grey matter analyses to compare software packages (SPM, FSL, FreeSurfer and CAT12) within the same sample of *MAPT* mutation (n=16), *GRN* mutation (n=36), *C9orf72* repeat expansion (n=14) carriers and related non-carriers (n=59), using default pipelines. Third, in the aforementioned ROIs, we evaluated the capability of these software packages to detect grey matter differences in presymptomatic mutation carriers. We estimated the required sample sizes to detect grey matter differences between a specific mutation group and non-carriers within the predefined ROI's. We found that cortical thickness analysis with FreeSurfer outperformed other software packages in *MAPT* mutation carriers. The detection rate for grey matter atrophy in *GRN* mutation carriers was low, and SPM was most likely to detect differences. *C9orf72* repeat expansion carriers commonly showed grey matter differences in all software packages, along with manageable estimated sample sizes, with the lowest sample size required with SPM. With this study, we provide a framework for grey matter analyses in the specific presymptomatic mutation groups of genetic FTD, which may be valuable for upcoming pharmaceutical trials.

INTRODUCTION

In the past decade, numerous studies have focused on grey matter atrophy biomarkers using structural MRI in the presymptomatic stage of genetic frontotemporal dementia (FTD) [1-22]. Although these studies show both gene-specific [6, 16, 23] and phenotype-specific patterns [11, 23] of grey matter atrophy for *C9orf72* repeat expansion, *MAPT* and *GRN* mutation carriers, results between studies have been inconsistent. Several factors can underlie these inconsistencies, but the role of different software packages has been of particular interest in literature [24-30]. Each software method relies on its own settings for non-linear registration, tissue probabilities thresholds for segmentation and statistical analysis, which can reasonably cause variations in results. Similar to other preclinical study populations [31, 32], grey matter atrophy is subtle in presymptomatic FTD, and choosing the appropriate method could substantially increase sensitivity and statistical power. As clinical trials and therapeutic treatments become increasingly relevant for the presymptomatic genetic FTD population [33-35], consensus on affected grey matter regions in each mutation group has become critical. Recommendations on the sensitivity of standard software packages are urgent for the use of reliable structural imaging biomarkers, as well as sample stratification in clinical trial design. In this study, we aimed to address these issues with the following three objectives.

Objective 1: A priori define evidence-based regions of interest (ROI) per mutation group. We reviewed the existing literature on voxel-wise grey matter damage in presymptomatic genetic FTD mutation carriers, including all software packages. Based on that, we defined commonly affected ROIs per mutation group.

Objective 2: Compare software packages by analysing voxel-wise grey matter differences in one presymptomatic FTD cohort (*MAPT* mutation, *GRN* mutation and *C9orf72* repeat expansion carriers and non-carriers). We used commonly available software packages (Statistical Parametric Mapping (SPM12), FMRIB Software Library (FSL), FreeSurfer, Computational Anatomy Toolbox (CAT12)) with default processing parameters and restricted the results to the predefined ROIs from objective 1.

Objective 3: Determine the most sensitive software package for grey matter differences between mutation carriers and non-carriers. We extracted volumetric and cortical thickness measurements from the predefined ROIs and estimated sensitivity and minimal sample size of the ROIs in each software package.

METHODS

Objective 1: Literature review

We based the ROI selection on previous MRI grey matter findings in presymptomatic FTD. In a systematic review of existing, we searched Embase, Medline, Web of Science, Cochrane CENTRAL and Google Scholar without any restrictions on year of publication, according to the PRISMA guidelines for reviews and meta-analyses [36]. We used the following key search terms in full or truncated versions: *"frontotemporal" or "FTD" or "FTLD" or "progressive aphasia" or "PPA" or "bvFTD" and "genetic" or "familial" or "hereditary" or "mutation" or "preclinical" and "grey matter" or "gray matter" or "brain" or "atrophy"* which resulted in 1264 unique hits (full search terms are listed in the Appendix). We included original research articles that investigated (i) voxel-wise grey matter atrophy in (ii) presymptomatic FTD mutation carriers compared to non-carriers. Title and abstract selection narrowed our results down to 29 original studies, covering a period from January 2008 to April 2019. Based on full text selection, we included seventeen studies with voxel-wise grey matter analyses in a specific presymptomatic mutation group compared to non-carriers. We excluded papers without primary grey matter analysis (n=1) [37], papers that used ROI-based analyses or feature selection (n=8) [1, 2, 20, 38-42], papers combining multiple disease stages or mutation groups (n=2) [11, 43]. Furthermore, we excluded papers that included overlapping patient samples, and used the same software package (n = 1) [4].

From the included papers, we listed which software packages were commonly used for voxel-wise presymptomatic grey matter analysis in genetic FTD. Subsequently, these software packages were applied to our presymptomatic FTD cohort in order to compare voxel-wise grey matter analyses. Furthermore, we scored the reported voxel-wise grey matter differences between a specific mutation group and non-carriers, separated for results with and without multiple comparison correction. We scored the grey matter differences per study in the structures of the MNI-atlas per hemisphere, i.e. caudate, cerebellum, frontal lobe, insula, occipital lobe, parietal lobe, putamen, thalamus, and temporal lobe [44]. Per mutation group, the two most often reported regions were used for our ROI-based analyses.

Objective 2 and 3 – Compare software packages in one presymptomatic FTD cohort

Sample and study procedures. In our frontotemporal dementia risk cohort (FTD-RisC) [8, 17], we investigate first-degree relatives of FTD patients carrying one of the three major autosomal dominant pathogenic mutations (*C9orf72, MAPT, GRN*). We considered participants as presymptomatic based on (i) not fulfilling the recommended clinical criteria for possible FTD, primary progressive aphasia, or amyotrophic lateral sclerosis [45-47], (ii) the absence of cognitive impairment on neuropsychological assessment, (iii) the absence of signs of motor neuron disease on neurological examination, (iv) normal cognitive and behavioural functioning as reported by the participant and knowledgeable informant, as previously described [16]. The Mini-Mental State Examination (MMSE) and Neuropsychiatric Inventory Questionnaire (NPI-Q) are reported as proxy screening measures for cognitive

and behavioural symptoms.

For the current study, we selected all presymptomatic participants included in FTD-RisC before September 2015 (n=125), to avoid methodological variations from a scanner update [16]. Participants were divided into four groups: non-carriers (n=59), *GRN* mutation carriers (n=36), *MAPT* mutation carriers (n=16) and *C9orf72* repeat expansion carriers (n=14) based on the results of double-blinded genetic analysis, as described in our previous baseline studies [8, 17]. Sample characteristics were compared between groups in SPSS Statistics 24.0 for Windows (SPSS Inc., Chicago, IL, USA), using ANOVAs with post-hoc Bonferroni tests to analyse age and total intracranial volume (TIV). We used Kruskal-Wallis non-parametric tests for MMSE and NPI-Q scores because of skewed distributions, and a Chi-square test for the male/female ratio across groups. The Medical Ethics Committee of the Erasmus University Medical Centre Rotterdam approved the study, and written informed consent was obtained from all participants.

MRI acquisition. We acquired T1-weighted MRI scans on a 3T Philips Achieva MRI system (Philips Medical Systems, Best, the Netherlands) using an 8-channel SENSE head coil and the following parameters: TR = 9.7ms, TE = 4.6ms, FOV = 224 x 177 x 168 mm^3, flip angle = 8º, slices = 140, voxel size = 0.88 x 0.88 x 1.2 mm^3, SENSE = no, acquisition time = 4 minutes and 56 seconds [8, 16]. Images were carefully inspected for motion artefacts and gross pathology, and excluded from analyses when quality proved insufficient (n=1) or absence of neurological disease could not be assumed (n=1).

Objective 2: MRI pre-processing and voxel-wise analyses

In each software package, we compared grey matter differences in the same cohort of *MAPT* mutation, *GRN* mutation and *C9orf72* repeat expansion carriers and non-carriers, using default settings for processing and analyses. Further details on processing and analyses for each software package can be found in the Appendix.

For VBM analyses, we used SPM12 and FSL. Analyses were corrected for age, sex and TIV. TIV was calculated as the sum of grey matter, white matter and cerebrospinal fluid volumes in SPM12. For cortical thickness analyses, we used CAT12 and FreeSurfer. Analyses were restricted to cortical cerebral regions and, as recommended, TIV was not used as covariate for the cortical thickness analyses [16, 29].

We report the results only for the predefined ROIs (Table 5), separated for voxel-wise multiple comparisons correction at $p^{FWE}<0.05$ or at an uncorrected threshold of $p<0.001$. The effective T-distribution without threshold for all voxel-wise comparisons is also computed, in order to visualize differences between software packages (Appendix).

Objective 3: ROI extraction and analyses

We extracted mean volumetric and thickness measurements from the predefined ROIs. For extraction of volumetric data, we used the MNI-atlas directly. In SPM, we masked the grey matter segmentations in standard space, and extracted volumetric data within the ROIs using Marsbar. The mean grey matter density values were multiplied with the total ROI volume, resulting in the grey matter volume of the ROI. In FSL, we masked the grey matter segmentations in standard space and extracted volumetric data within the ROIs. The mean grey matter density was multiplied to the total volume of the ROI, resulting in the grey matter volume per ROI.

For the cortical thickness packages, parcellation was based on the Desikan-Killiany atlas [48]. We combined regions from the Desikan-Killiany atlas to match the shape and size of the structures of the MNI atlas, to allow for comparisons with the VBM analyses. Part of the automated CAT12 cortical thickness pipeline is calculation of thickness within predefined atlases. Therefore, mean cortical thickness values per region can easily be extracted from the data. In FreeSurfer, mean cortical thickness values of the ROIs were extracted using the cortical parcellation and annotation pipeline [48, 49].

After extraction of volumetric and thickness data from predefined ROI's per software package, ROI analyses were carried out in three steps using SPSS and G-power [50]. First, grey matter volume and thickness for the chosen ROI's per software package in the mutation groups versus non-carriers were compared with ANCOVA's. We corrected for age and sex, and for TIV in volumetric comparisons. The statistical threshold was set at $p<0.05$ two-tailed and effect sizes (η^2) were reported. Second, we calculated the required sample size per software package to obtain significant differences compared to non-carriers for each mutation. We set the statistical threshold at a p-value of <0.05 and power $\beta>0.8$ for each ROI, corrected for age and sex, and TIV for volumetric data. Third, we determined the area under the curve (AUC) in each ROI per software package to accurately classify carriers from non-carriers in each mutation group with ROC curves.

RESULTS

Objective 1: Literature review

Seventeen original research papers were included in our review (Table 1-3), using VBM (n=9; SPM in 7, FSL in 2) or cortical thickness (n=9; FreeSurfer in 7, CAT12 in 1, Advanced Normalization Tools (ANTs) in 1). One study examined both VBM and cortical thickness in the same sample. Four studies included more than one mutation group (*MAPT* and *GRN*: n=1; *GRN* and *C9orf72*: n=1; all three mutation groups: n=2). Three studies examined both cross-sectional and longitudinal voxel-wise grey matter differences and the remaining

fourteen studies focused only on cross-sectional analyses. A full review of methods can be found in Table 1 to 3.

MAPT mutation carriers. Two out of four studies found no significant differences between *MAPT* mutation carriers and non-carriers. The other two papers found grey matter differences in the temporal lobes, both using SPM (Table 1). The temporal lobes were thus the two most frequently affected regions in this mutation group, which were selected as ROIs for the *MAPT* mutation group.

GRN mutation carriers. Seven out of twelve papers found voxel-wise grey matter differences in presymptomatic *GRN* mutation carriers compared to non-carriers (SPM in 3, FreeSurfer in 3, ANTS in 1; Table 2). Only one study, using FreeSurfer, found differences after multiple comparison correction. The right frontal lobe was the most frequently affected region in *GRN* mutation carriers, reported in four studies, followed by the left temporal lobe, reported in three studies (Table 2). These two regions were selected as ROI's for the current study in the *GRN* mutation group.

C9orf72 repeat expansion carriers. All studies but one found grey matter differences in presymptomatic *C9orf72* repeat expansion carriers compared with non-carriers, in the left frontal lobe and left parietal lobe (Table 3). VBM analysis was performed in four studies (SPM in 3, FSL in 1) and four studies applied cortical thickness analysis (FreeSurfer in 3, CAT12 in 1). The study that did not find presymptomatic grey matter differences used FreeSurfer. The left frontal lobe and left parietal regions were selected as ROIs for *C9orf72* repeat expansion carriers.

Objective 2 and 3: Characteristics of the presymptomatic cohort

A global characterisation of our sample can be found in Table 4. The *MAPT* mutation carriers were significantly younger than the non-carriers and *GRN* mutation carriers. *C9orf72* repeat expansion carriers had smaller TIV compared to non-carriers. Other characteristics were similar across groups, including MMSE and NPI-Q scores.

Objective 2: Voxel-wise comparisons across software platforms

We displayed the effective T-distribution of the voxel-wise whole brain comparisons for all contrasts and all software packages in colour scaled whole brain maps with a range of T -5 to 5 in the Appendix, as well as the results from the whole brain analyses with $p^{FWE}<0.05$ and $p<0.001$.

MAPT mutation carriers. Using cortical thickness analysis, both temporal lobes showed thinning in *MAPT* mutation carriers compared with non-carriers at the uncorrected threshold of $p<0.001$, for both CAT12 and FreeSurfer (Table 5).

Table 1. Literature review - *MAPT*

Methods																			
First Author	**Year**	**Carriers (mean age)**	**NC(mean age)**	**Field strength**	**Software**	**Study design**	**Method**	**Confounding variables**											
Whitwell	2011	8 (39)	8 (49)	3T	SPM5	Cross-sectional	VBM	Age, gender, TIV											
Dopper	2014	11 (43.7)	8 (50.3)a	3T	FSL	Cross-sectional	VBM	Age, gender											
Cash	2017	23 (38.6)	144 (48.7)	3Tb	SPM12	Cross-sectional	VBM	Age, gender, family, TIV, site											
Panman	2019	15 (41.8)	53 (50.7)	3T	SPM12	Cross-sectional BL	VBM	Age, gender, TIV											
					SPM12	Cross-sectional FU	VBM	Age, gender, TIV, software											
					SPM12	Longitudinal	VBM	Age, gender, TIV, software											
Panman	2019	15 (41.8)	53 (50.7)	3T	CAT12	Cross-sectional BL	CT	Age, gender											
					CAT12	Cross-sectional FU	CT	Age, gender, software											
					CAT12	Longitudinal	CT	Age, gender, software											
Results																			
First Author	**Year**	**Caudatus**		**Cerebellum**		**Frontal**		**Insula**		**Occipital**		**Parietal**		**Putamen**		**Temporal**		**Thalamus**	
		L	R	L	R	L	R	L	R	L	R	L	R	L	R	L	R	L	R
Whitwell	2011	-	-	-	-	-	-	-	-	-	-	-	-	-	-	-	-	-	-
Dopper	2014	-	-	-	-	-	-	-	-	-	-	-	-	-	-	-	-	-	-
Cash	2017	-	-	-	-	1	1	1	1	-	-	-	-	-	-	1	1	-	-
Panman	2019	-	-	-	-	-	-	-	-	-	-	-	-	-	-	2	2	-	-

Abbreviations: VBM = voxel based morphometry, CT = cortical thickness, TIV = total intracranial volume, BL = baseline, FU = follow up, L = left hemisphere, R = right hemisphere. a mean age based on full sample, b study with multiple centres and scanners, c results were trending towards significance at pcorr < 0.072. Scoring: - = no results, 1 = results uncorrected for multiple comparisons, 2 = results corrected for multiple comparisons.

Table 2. Literature review – *GRN*

					Methods			
First Author	**Year**	**Carriers (mean age)**	**Non-carriers (mean age)**	**Field strength**	**Software**	**Study design**	**Method**	**Confounding variables**
Cruchaga	2009	3 (61.3)	11 (59.0)	1.5T	SPM5	Cross-sectional	VBM	TIV
Borroni	2012	9 (40.1)	13 (40.5)	1.5T	SPM8	Cross-sectional	VBM	Age, gender, TIV, education
Dopper	2014	27 (53.9)	28 (50.3)[a]	3T	FSL	Cross-sectional	VBM	Age, gender
Cash	2017	65 (48.9)	144 (48.7)	3T[b]	SPM12	Cross-sectional	VBM	Age, gender, family, TIV, site
Panman	2019	33 (52.1)	53 (50.7)	3T	SPM12	Cross-sectional BL	VBM	Age, gender, TIV
					SPM12	Cross-sectional FU	VBM	Age, gender, TIV, software
					SPM12	Longitudinal	VBM	Age, gender, TIV, software
Lee	2019	17 (53.6)	30 (53.3)	3T	SPM12	Cross-sectional	VBM	Age, sex, TIV, handedness
Moreno	2013	13 (53.8)	13 (52.8)	1.5T	FreeSurfer	Cross-sectional	CT	Age, gender
Pievani	2014	5 (45)	5 (46)	1.5T	FreeSurfer	Cross-sectional	CT	Not reported
Caroppo	2015	16 (41.9)	17 (40)	1.5 & 3T[b]	FreeSurfer	Cross-sectional BL	CT	Not reported
		14 (43)	14 (42.1)	1.5 & 3T[b]	FreeSurfer	Longitudinal	CT	Not reported
Popuri	2018	9 (50.1)	37 (51.5)	1.5T	FreeSurfer	Cross-sectional	CT	Age, gender, EYO
Olm	2018	11 (41.4)	11 (53.6)	3T	ANTS	Cross-sectional BL	CT	Age
						Longitudinal	CT	Age
Gazzina	2018	17 (44.1)	19 (46.0)	3T	FreeSurfer	Cross-sectional	CT	Not reported
							SA	Not reported
Panman	2019	33 (52.1)	53 (50.7)	3T	CAT12	Cross-sectional BL	CT	Age, gender
					CAT12	Cross-sectional FU	CT	Age, gender, software
					CAT12	Longitudinal	CT	Age, gender, software

Results																			
First Author	Year	Caudate		Cerebellum		Frontal		Insula		Occipital		Parietal		Putamen		Temporal		**Thalamus**	
		L	*R*	*L*	*R*	*L*	*R*	*L*	*R*	*L*	*R*	*L*	*R*	*L*	*R*	*L*	*R*	*L*	*R*
Cruchaga	2009	-	-	-	-	1	1	-	-	-	-	1	-	-	-	1	-	-	-
Borroni	2012	-	-	-	-	-	-	-	-	-	-	-	-	-	-	-	-	-	-
Moreno	2013	N/A	N/A	N/A	N/A	-	-	-	-	-	-	-	-	N/A	N/A	-	-	N/A	N/A
Dopper	2014	-	-	-	-	-	-	-	-	-	-	-	-	-	-	-	-	-	-
Pievani	2014	N/A	N/A	N/A	N/A	1	1	-	-	-	-	-	-	N/A	N/A	-	-	N/A	N/A
Caroppo	2015	N/A	N/A	N/A	N/A	-	-	-	-	-	-	-	-	N/A	N/A	2	-	N/A	N/A
Cash	2017	-	-	-	-	-	1	-	1	-	-	-	1	-	1	-	1	-	-
Gazzina	2018	N/A	N/A	N/A	N/A	-	-	-	-	-	-	1	1	N/A	N/A	-	-	N/A	N/A
Olm	2018	-	-	-	-	-	1	-	1	1	1	-	-	-	-	1	-	-	-
Popuri	2018	-	-	-	-	-	-	-	-	-	-	-	-	-	-	-	-	-	-
Panman	2019	-	-	-	-	-	-	-	-	-	-	-	-	-	-	-	-	-	-

Abbreviations: VBM = voxel based morphometry, CT = cortical thickness, SA = surface areas, TIV = total intracranial volume, EYO = estimated years to symptom onset, BL = baseline, FU = follow up, L = left hemisphere, R = right hemisphere, N/A = not applicable. [a] mean age based on full sample, [b] study with multiple centres and scanners. Scoring: - = no results, 1 = results uncorrected for multiple comparisons, 2 = results corrected for multiple comparisons.

Table 3. Literature review – *C9orf72*

Methods																			
First Author	Year	Carriers (mean age)		Non-carriers (mean age)		Field strength		Software		Study design		**Method**		**Confounding variables**					
Cash	2017	40 (43.5)		144 (48.7)		3T[a]		SPM12		Cross-sectional		VBM		Age, gender, family, TIV, site					
Lee	2017	15 (43.7)		46 (47.8)		3T		SPM12		Cross-sectional		VBM		Age, gender, TIV, handedness					
Papma	2017	18 (45.8)		15 (47.8)		3T		FSL		Cross-sectional		VBM		Age, gender, head coil					
Panman	2019	11 (49.7)		53 (50.7)		3T		SPM12		Cross-sectional BL		VBM		Age, gender, TIV					
								SPM12		Cross-sectional FU		VBM		Age, gender, TIV, software					
								SPM12		Longitudinal		VBM		Age, gender, TIV, software					
Walhout	2015	16 (45.5)		23 (41.8)		3T		FreeSurfer		Cross-sectional		CT		Age, gender, *VAPB*, kinship					
Floeter	2016	7 (41.2)		28 (52.8)		3T		FreeSurfer		Cross-sectional		CT		Gender					
Popuri	2018	15 (42.6)		37 (51.5)		1.5T		FreeSurfer		Cross-sectional		CT		Age, gender, EYO					
Panman	2019	11 (49.7)		53 (50.7)		3T		CAT12		Cross-sectional BL		CT		Age, gender					
								CAT12		Cross-sectional FU		CT		Age, gender, software					
								CAT12		Longitudinal		CT		Age, gender, software					
Results																			
First Author	Year	Caudatus		Cerebellum		Frontal		Insula		Occipital		Parietal		Putamen		Temporal		Thalamus	
		L	R	L	R	L	R	L	R	L	R	L	R	L	R	L	R	L	R
Walhout	2015	2	-	-	-	2	-	-	-	2	-	2	-	2	-	2	2	-	-
Floeter	2016	-	-	N/A	N/A	-	-	-	-	-	-	-	-	-	-	-	-	-	-
Cash	2017	-	-	2	2	2	2	1	1	-	-	1	1	-	-	2	2	2	2
Lee	2017	1	1	-	-	2	2	1	1	1	1	2	2	1	1	1	1	2	2
Papma[b]	2017	-	-	-	2	2	-	-	-	-	-	2	-	-	-	2	2	2	2
Popuri	2018	2	-	-	-	2	-	-	-	2	-	2	2	-	-	-	2	2	2
Panman	2019	-	-	2	2	2	2	2	2	-	-	2	2	-	-	2	-	-	-

Abbreviations: VBM = voxel based morphometry, CT = cortical thickness, TIV = total intracranial volume, EYO = estimated years to symptom onset, BL = baseline, FU = follow up, L = left hemisphere, R = right hemisphere, N/A = not applicable. a study with multiple centres and scanners, b results were detected when restricted to carriers > 40 years of age. Scoring: - = no results, 1 = results uncorrected for multiple comparisons, 2 = results corrected for multiple comparisons.

Table 4. Sample characterization

	Non-carrier	*MAPT*	*GRN*	*C9orf72*	p-value
N (female)	59 (39)	16 (9)	36 (24)	14 (11)	0.643
Age	50.29 (11.45)	42.38 (9.81)	52.95 (7.88)	49.77 (12.27)	0.012[a]
TIV in litres	1.69 (0.13)	1.66 (0.11)	1.66 (0.11)	1.56 (0.12)	0.007[b]
MMSE	29.15 (1.17)	29.31 (0.87)	28.97 (1.50)	29.57 (0.65)	0.67
NPI-Q	0.18 (0.53)	1.27 (3.61)	0.70 (1.42)	0.46 (1.13)	0.264

Abbreviations: TIV=total intracranial volume, MMSE=Mini Mental State Examination, NPI-Q=Neuropsychiatric Inventory Revised. [a]: *MAPT* mutation carriers were younger than non-carriers and *GRN* mutation carriers [b]: *C9orf72* repeat expansion carriers had smaller TIV than non-carriers.

GRN mutation carriers. We found voxel-wise grey matter differences in the right frontal lobe only with SPM, at $p<0.001$. For the left temporal lobe, both SPM and FSL showed grey matter volume differences at $p<0.001$ (Table 5).

C9orf72 repeat expansion carriers. Voxel-wise volumetric analyses with SPM detected differences between *C9orf72* repeat expansion carriers and non-carriers at $p^{FWE}<0.05$ in the left parietal lobe, and at $p<0.001$ for the left frontal lobe. Using FSL, we found lower grey matter volume of both ROIs at $p<0.001$. We found thinning of both ROIs with FreeSurfer at $p^{FWE}<0.05$. With CAT12, the left parietal lobe showed thinning compared with non-carriers at $p^{FWE}<0.05$, and the left frontal lobe at $p<0.001$ (Table 5).

Objective 3: ROI sensitivity and sample size estimation

MAPT mutation carriers. In *MAPT* mutation carriers, the mean cortical thickness of both temporal lobes estimated by FreeSurfer significantly differed from non-carriers with the largest effect size (left: $\eta^2 = 0.166$, right $\eta^2 = 0.148$), and required the smallest sample size for correct classification and sufficient power (left: n=42, right: n=48). FreeSurfer classified *MAPT* mutation carriers from non-carriers within these ROI's with an AUC of 0.673 and 0.649, respectively (Table 6).

GRN mutation carriers. In *GRN* mutation carriers, the grey matter volume of the left temporal lobe measured with SPM significantly differed from non-carriers, and resulted in the largest effect size ($\eta^2 = 0.05$), and smallest estimated sample size (n=152). Using SPM for volumetric measurement of the left temporal lobe also resulted in the largest AUC to discriminate *GRN* mutation carriers from non-carriers (AUC=0.665) (Table 6).

C9orf72 repeat expansion carriers. In *C9orf72* repeat expansion carriers, grey matter volume and mean cortical thickness of the left parietal lobe significantly differed from non-carriers in all software packages. We found the largest effect size for the left parietal lobe measured

Table 5. Voxel-wise results restricted to predefined ROI's

***MAPT* mutation carriers**		
Software	Left temporal	Right temporal
FSL	-	-
SPM	-	-
FreeSurfer	1	1
CAT12	1	1
***GRN* mutation carriers**		
	Right frontal	Left temporal
FSL	-	1
SPM	1	1
FreeSurfer	-	-
CAT12	-	-
***C9orf72* repeat expansion carriers**		
	Left frontal	Left parietal
FSL	1	1
SPM	1	2
FreeSurfer	2	2
CAT12	1	2

Voxel-wise results in the same cohort using commonly available software packages, restricted to the predefined ROI's. Scoring: - = no results, 1 = results uncorrected for multiple comparisons, 2 = results corrected for multiple comparison. Abbreviations: L = left, R = right.

with SPM (η^2=0.118), the smallest sample size (n=61) and highest AUC (0.730) (Table 6).

DISCUSSION

We reviewed and compared the sensitivity of different software packages for cortical grey matter analysis in presymptomatic FTD. We demonstrated that FreeSurfer outperformed other software packages and required the smallest sample size to distinguish *MAPT* mutation carriers from non-carriers, and that SPM classified both *GRN* mutation carriers and *C9orf72* repeat expansion carriers from non-carriers with a higher AUC, larger effect size, and smaller estimated sample size than other software packages.

Previous papers have focused on detecting voxel-wise grey matter differences in the presymptomatic stage of *MAPT,* of which two studies demonstrated grey matter atrophy

Table 6. ROI sensitivity and sample size estimation

***MAPT* mutation carriers**							
Software	Region	F	p-value	η^2	Sample (adj)	AUC	p-value
FSL	Temporal L	1.781	0.186	0.025	309	0.512	0.887
	Temporal R	0.327	0.569	0.005	1564	0.507	0.928
SPM	Temporal L	0.460	0.500	0.007	1116	0.557	0.485
	Temporal R	0.048	0.826	0.001	7843	0.546	0.578
FreeSurfer	Temporal L	14.090	<0.001	0.166	42	0.673	0.034
	Temporal R	12.373	0.001	0.148	48	0.649	0.068
CAT12	Temporal L	5.833	0.018	0.076	98	0.564	0.438
	Temporal R	5.631	0.020	0.073	102	0.640	0.088
***GRN* mutation carriers**							
Software	Region	F	p-value	η^2	Sample (adj)	AUC	p-value
FSL	Frontal R	0.268	0.606	0.003	2611	0.467	0.591
	Temporal L	2.091	0.152	0.023	336	0.577	0.208
SPM	Frontal R	0.123	0.727	0.001	7843	0.550	0.412
	Temporal L	4.696	0.033	0.050	152	0.665	0.007
FreeSurfer	Frontal R	0.477	0.491	0.005	1564	0.546	0.450
	Temporal L	0.448	0.505	0.005	1564	0.573	0.237
CAT12	Frontal R	0.281	0.597	0.003	2611	0.564	0.297
	Temporal L	0.002	0.968	0	N/A	0.532	0.602
***C9orf72* repeat expansion carriers**							
Software	Region	F	p-value	η^2	Sample (adj)	AUC	p-value
FSL	Frontal L	0.823	0.368	0.012	649	0.485	0.866
	Parietal L	5.063	0.028	0.069	108	0.535	0.684
SPM	Frontal L	2.386	0.127	0.034	225	0.706	0.017
	Parietal L	9.075	0.004	0.118	61	0.730	0.008
FreeSurfer	Frontal L	2.967	0.089	0.041	186	0.597	0.259
	Parietal L	5.646	0.020	0.076	98	0.674	0.044
CAT12	Frontal L	3.627	0.061	0.050	152	0.592	0.287
	Parietal L	5.774	0.019	0.077	97	0.598	0.256

Sensitivity and minimal sample size estimation in extracted measurements of predefined ROIs compared with non-carriers. Abbreviations: L = left hemisphere, R = right hemisphere, GM = grey matter, AUC = area under the curve, adj = adjusted for age, sex and TIV (when appropriate).

in both temporal lobes [6, 16]. Furthermore, the majority of the studies performed volumetric analysis [6, 8, 22], while recently, we demonstrated that cortical thinning occurs in presymptomatic *MAPT* mutation carriers [16]. Our current results suggest that cortical thickness methods in general could be more sensitive than VBM to detect early grey matter atrophy in presymptomatic *MAPT* mutation carriers. A study comparing types of grey matter differences in both bvFTD and Alzheimer's disease demonstrated that cortical thinning was commonly present in bvFTD, while the cortical surface area was most affected in Alzheimer's disease [51]. VBM analyses are based on a combination of cortical surface, folding and thickness measures [24, 29, 52], holding more complex information than solely cortical thickness analysis, but also potentially leading to less sensitivity. The latter may explain the absence of VBM findings in presymptomatic *MAPT* mutation carriers. Our current review and analyses were limited by the low number of previous studies and small sample size in the current studies. Keeping in mind these limitations, we found that FreeSurfer outperformed other software packages, and might therefore be considered as standard software package for *MAPT* mutation carriers in pharmaceutical trial design.

Interestingly, one single study focusing on presymptomatic *GRN* mutation carriers (n=14) found grey matter differences compared with non-carriers after multiple comparisons correction [5]. However, this study combined T1-weighted MRI scans from 1.5T and 3T systems of four different centres, without reporting correction for confounding factors in their analysis. In the studies that reported grey matter differences in presymptomatic *GRN* mutation carriers without correction for multiple comparisons [6, 7, 10, 12, 15, 18], SPM was the most commonly used software package [6, 7, 12]. Our evidence-based ROI selection in *GRN* led to the inclusion of the right frontal lobe and left temporal lobe. From a clinical perspective, other regions such as the left frontal lobe, right temporal lobe and both parietal lobes, known to be affected in symptomatic FTD may be of interest as well [53, 54]. Based on our a priori selection method in presymptomatic FTD-*GRN* though, these regions were not included. In current literature it now seems that white matter lesions may be an early marker for (presymptomatic) FTD-*GRN*, while grey matter atrophy arises near symptom onset [55-57]. Other imaging biomarkers, such as diffusion tensor imaging or arterial spin labelling [11, 58, 59], but also fluid [60], or clinical markers [61, 62] may be more sensitive for brain degeneration in the presymptomatic stage of this specific group. We expect that mixed effects modelling of multimodal biomarkers will be used in clinical trials for *GRN* mutation carriers, to detect the start of the disease process before symptom onset and to monitor longitudinal disease progression. Based on our current review and empirical analyses, SPM seems to be preferential as software package in *GRN* mutation carriers. This could result from the segmentation algorithm of SPM [25, 26, 30], which was thought to be quite thorough, and therefore may have caught the small differences in the grey matter / white matter boundaries compared to other the other segmentation protocols. In *GRN*

mutation carriers, SPM seems to be the most sensitive software package for quantitative extraction of grey matter measures.

In *C9orf72* repeat expansion carriers, both previous studies and our current analyses showed that VBM and cortical thickness consistently detect grey matter differences between carriers and non-carriers, especially in the left frontal and parietal lobe [6, 13, 16, 17, 19, 21]. Furthermore, previous studies using linear mixed modelling suggested that the onset of grey matter atrophy in *C9orf72* repeat expansion carriers may occur before the age of 40 [2, 20]. Our previous longitudinal study with two year follow up in *C9orf72* repeat expansion carriers showed no apparent grey matter change over time [16]. If the trajectory of brain changes in *C9orf72* repeat expansion carriers indeed starts several decades before symptom onset, other biomarkers are needed to detect accelerated neurodegeneration that announces symptom onset, such as neurofilament light chain levels [60, 63] or cognitive functioning [20]. Furthermore, from a clinical point of view, grey matter atrophy may occur in a symmetric pattern rather than only left-sided [53, 63]. With our evidence-based ROI analyses, we demonstrated that sample size estimation to detect a grey matter difference between non-carriers and *C9orf72* repeat expansion carriers was the smallest for the left parietal lobe using SPM, but the other software packages yielded relatively manageable sample sizes with the left parietal lobe as well. Similar to *GRN* mutation carriers, this difference between packages in *C9orf72* repeat expansion carriers may be due to an optimization of segmentation of grey and white matter within SPM. However, this is speculative and should be investigated further.

In the current study, we showed that software packages differ in their sensitivity of grey matter deficits for all mutation groups, despite using an identical sample and default parameters for the analyses. In literature, SPM has performed best in brain segmentation [25, 26, 30] and non-linear registration [27], as FSL was found to be more heavily influenced by noise and image intensity [25, 30] and FreeSurfer consistently underestimated grey matter volume [26]. On the other hand, FreeSurfer may be more robust to poor image quality and is more stable over repeated measurements than SPM and FSL for grey matter computation [26]. Furthermore, results from FSL's VBM and FreeSurfer cortical thickness analyses possibly resemble true pathology in neurodegenerative disease more than SPM, through the use of cluster-wise statistical enhancement [28], as cluster-wise techniques use spatial neighbouring information to increase sensitivity for finding true signal. Regarding cortical thickness software, CAT12 systematically estimates higher thickness compared with FreeSurfer, but the correlation between both methods was very high [65]. Clinical studies, including but not limited to FTD studies [32, 66], often rely on these widely available software packages, but the complexity in processing and statistical choices may cause more false positive or negative results than expected [26, 30]. The choice of software packages

to measure grey matter in pharmaceutical trials appears to be crucial for an optimal study design and outcome, and could for example lead to lower required sample sizes, which is extremely important in a rare and heterogeneous population as genetic FTD.

A major strength of our study is the comparison of standard software methods and packages with default parameters in the same sample, to detect inconsistencies between software packages. Our current sample consisted of highly homogeneous data and we avoided noise from hardware or software updates on the scanner, which made comparison of methodologies possible. However, as most pharmaceutical trials are designed as multicentre studies, our results cannot completely be inferred, but could best be appreciated as recommendations. Including our previous studies did not lead to a circularity or overestimation of our current results and analyses, as first, we excluded studies that used overlapping patient samples and software packages, and second, the aim of our empirical analyses was not to identify the first affected brain regions in genetic FTD, as was the aim in the previous studies used for our selection of ROIs, but to investigate and compare multiple software packages. Although the majority of clinical studies will use the default parameters, most software methods are designed with various expert options and adjustable settings to optimize processing, depending on the data fed into the pipelines. Furthermore, similar to most of the previous grey matter studies, we focused on cross-sectional data. Longitudinal within-subject registrations are part of longitudinal processing streams of all standard software packages [67], and could result in other considerations for intra-individual grey matter changes over time, compared with the results of the current cross-sectional study. Future efforts should be directed at providing the optimal framework for analysis of longitudinal data, as well as other types of neuroimaging data such as diffusion tensor imaging and arterial spin labelling, as the field of presymptomatic FTD research is shifting towards the potential use of multimodal biomarker modelling in both clinical diagnostic trajectories [1, 11], and clinical trial design [34, 68].

We reviewed and examined software methods and packages for cortical grey matter analyses on their sensitivity in presymptomatic FTD, in order to provide an all-encompassing recommendation for upcoming pharmaceutical trial design. We demonstrated inconsistencies in results from different software methods and packages, and estimated sensitivity, effect sizes and sample size for grey matter differences in predefined ROIs per mutation group. Derived from this systematic literature review and from empirical data analyses, we propose that for *MAPT* mutation carriers, cortical thickness analysis of the bilateral temporal lobes in FreeSurfer may obtain optimal sensitivity. The detection rate of presymptomatic grey matter abnormalities in *GRN* mutation carriers compared with non-carriers is extremely low, and SPM is most likely to detect differences. Lastly, we showed that in *C9orf72* repeat expansion carriers, all cortical grey matter software packages and methods replicated differences in

the left parietal lobe, with relatively manageable sample sizes. In conclusion, the choice of software packages in pharmaceutical trials may be crucial for optimisation of study design and sensitivity of grey matter biomarkers in presymptomatic genetic FTD.

REFERENCES

1. Benussi, A., Gazzina, S., Premi, E., et al. 2019. Clinical and biomarker changes in presymptomatic genetic frontotemporal dementia. Neurobiol Aging 76, 133-140.
2. Bertrand, A., Wen, J., Rinaldi, D., et al. 2017. Early Cognitive, Structural, and Microstructural Changes in Presymptomatic C9orf72 Carriers Younger Than 40 Years. JAMA Neurol.
3. Borroni, B., Alberici, A., Cercignani, M., et al. 2012. Granulin mutation drives brain damage and reorganization from preclinical to symptomatic FTLD. Neurobiol Aging 33, 2506-2520.
4. Borroni, B., Alberici, A., Premi, E., et al. 2008. Brain magnetic resonance imaging structural changes in a pedigree of asymptomatic progranulin mutation carriers. Rejuvenation Res 11, 585-595.
5. Caroppo, P., Habert, M.O., Durrleman, S., et al. 2015. Lateral Temporal Lobe: An Early Imaging Marker of the Presymptomatic GRN Disease? J Alzheimers Dis 47, 751-759.
6. Cash, D.M., Bocchetta, M., Thomas, D.L., et al. 2017. Patterns of gray matter atrophy in genetic frontotemporal dementia: results from the GENFI study. Neurobiol Aging 62, 191-196.
7. Cruchaga, C., Fernández-Seara, M.A., Seijo-Martínez, M., et al. 2009. Cortical atrophy and language network reorganization associated with a novel progranulin mutation. Cereb Cortex 19, 1751-1760.
8. Dopper, E.G., Rombouts, S.A., Jiskoot, L.C., et al. 2014. Structural and functional brain connectivity in presymptomatic familial frontotemporal dementia. Neurology 83, e19-26.
9. Floeter, M.K., Bageac, D., Danielian, L.E., et al. 2016. Longitudinal imaging in C9orf72 mutation carriers: Relationship to phenotype. Neuroimage Clin 12, 1035-1043.
10. Gazzina, S., Benussi, A., Premi, E., et al. 2018. Neuroanatomical Correlates of Transcranial Magnetic Stimulation in Presymptomatic Granulin Mutation Carriers. Brain Topogr 31, 488-497.
11. Jiskoot, L.C., Panman, J.L., Meeter, L.H., et al. 2019. Longitudinal multimodal MRI as prognostic and diagnostic biomarker in presymptomatic familial frontotemporal dementia. Brain 142, 193-208.
12. Lee, S.E., Sias, A.C., Kosik, E.L., et al. 2019. Thalamo-cortical network hyperconnectivity in preclinical progranulin mutation carriers. NeuroImage Clin 22.
13. Lee, S.E., Sias, A.C., Mandelli, M.L., et al. 2017. Network degeneration and dysfunction in presymptomatic C9ORF72 expansion carriers. Neuroimage Clin 14, 286-297.
14. Moreno, F., Sala-Llonch, R., Barandiaran, M., et al. 2013. Distinctive age-related temporal cortical thinning in asymptomatic granulin gene mutation carriers. Neurobiol Aging 34, 1462-1468.
15. Olm, C.A., McMillan, C.T., Irwin, D.J., et al. 2018. Longitudinal structural gray matter and white matter MRI changes in presymptomatic progranulin mutation carriers. Neuroimage Clin 19, 497-506.
16. Panman, J.L., Jiskoot, L.C., Bouts, M., et al. 2019. Gray and white matter changes in presymptomatic genetic frontotemporal dementia: a longitudinal MRI study. Neurobiol Aging 76, 115-124.
17. Papma, J.M., Jiskoot, L.C., Panman, J.L., et al. 2017. Cognition and gray and white matter characteristics of presymptomatic C9orf72 repeat expansion. Neurology 89, 1256-1264.
18. Pievani, M., Paternico, D., Benussi, L., et al. 2014a. Pattern of structural and functional brain abnormalities in asymptomatic granulin mutation carriers. Alzheimers. Dement. 10, S354-+.
19. Popuri, K., Dowds, E., Beg, M.F., et al. 2018. Gray matter changes in asymptomatic C9orf72 and GRN mutation carriers. Neuroimage Clin 18, 591-598.
20. Rohrer, J.D., Nicholas, J.M., Cash, D.M., et al. 2015c. Presymptomatic cognitive and neuroanatomical changes in genetic frontotemporal dementia in the Genetic Frontotemporal dementia Initiative (GENFI) study: a cross-sectional analysis. Lancet Neurol. 14, 253-262.
21. Walhout, R., Schmidt, R., Westeneng, H.J., et al. 2015. Brain morphologic changes in asymptomatic C9orf72 repeat expansion carriers. Neurology 85, 1780-1788.
22. Whitwell, J.L., Josephs, K.A., Avula, R., et al. 2011. Altered functional connectivity in asymptomatic MAPT subjects A comparison to bvFTD. Neurology 77, 866-874.
23. Young, A.L., Marinescu, R.V., Oxtoby, N.P., et al. 2018. Uncovering the heterogeneity and temporal complexity of neurodegenerative diseases with Subtype and Stage Inference. Nat Commun 9, 4273.
24. Hutton, C., Draganski, B., Ashburner, J., et al. 2009. A comparison between voxel-based cortical thickness and voxel-based morphometry in normal aging. Neuroimage 48, 371-380.

25. Kazemi, K., Noorizadeh, N., 2014. Quantitative Comparison of SPM, FSL, and Brainsuite for Brain MR Image Segmentation. J Biomed Phys Eng 4, 13-26.
26. Klauschen, F., Goldman, A., Barra, V., et al. 2009. Evaluation of automated brain MR image segmentation and volumetry methods. Hum Brain Mapp 30, 1310-1327.
27. Klein, A., Andersson, J., Ardekani, B.A., et al. 2009. Evaluation of 14 nonlinear deformation algorithms applied to human brain MRI registration. Neuroimage 46, 786-802.
28. Rajagopalan, V., Pioro, E.P., 2015. Disparate voxel based morphometry (VBM) results between SPM and FSL softwares in ALS patients with frontotemporal dementia: which VBM results to consider? BMC Neurol 15, 32.
29. Schwarz, C.G., Gunter, J.L., Wiste, H.J., et al. 2016. A large-scale comparison of cortical thickness and volume methods for measuring Alzheimer's disease severity. NeuroImage Clin 11, 802-812.
30. Tudorascu, D.L., Karim, H.T., Maronge, J.M., et al. 2016. Reproducibility and Bias in Healthy Brain Segmentation: Comparison of Two Popular Neuroimaging Platforms. Front Neurosci 10, 503.
31. Lambrecq, V., Langbour, N., Guehl, D., et al. 2013. Evolution of brain gray matter loss in Huntington's disease: a meta-analysis. Eur J Neurol 20, 315-321.
32. Mak, E., Gabel, S., Mirette, H., et al. 2017. Structural neuroimaging in preclinical dementia: From microstructural deficits and grey matter atrophy to macroscale connectomic changes. Ageing Res Rev 35, 250-264.
33. Desmarais, P., Rohrer, J.D., Nguyen, Q.D., et al. 2018. Therapeutic trial design for frontotemporal dementia and related disorders. J Neurol Neurosurg Psychiatry.
34. Staffaroni, A.M., Ljubenkov, P.A., Kornak, J., et al. 2019. Longitudinal multimodal imaging and clinical endpoints for frontotemporal dementia clinical trials. Brain 142, 443-459.
35. Tsai, R.M., Boxer, A.L., 2016. Therapy and clinical trials in frontotemporal dementia: past, present, and future. J Neurochem 138 Suppl 1, 211-221.
36. Liberati, A., Altman, D.G., Tetzlaff, J., et al. 2009. The PRISMA statement for reporting systematic reviews and meta-analyses of studies that evaluate health care interventions: explanation and elaboration. J Clin Epidemiol 62, e1-34.
37. Milanesi, E., Bonvicini, C., Alberici, A., et al. 2013. Molecular signature of disease onset in Granulin mutation carriers: A gene expression analysis study. Neurobiol Aging 34, 1837-1845.
38. Feis, R.A., Bouts, M.J.R.J., Panman, J.L., et al. 2018. Single-subject classification of presymptomatic frontotemporal dementia mutation carriers using multimodal MRI. NeuroImage Clin 20, 188-196.
39. Premi, E., Cauda, F., Costa, T., et al. 2016. Looking for Neuroimaging Markers in Frontotemporal Lobar Degeneration Clinical Trials: A Multi-Voxel Pattern Analysis Study in Granulin Disease. J Alzheimer's Dis 51, 249-262.
40. Premi, E., Cauda, F., Gasparotti, R., et al. 2014. Multimodal fMRI resting-state functional connectivity in Granulin mutations: The case of fronto-parietal dementia. PLoS ONE 9.
41. Premi, E., Grassi, M., Van Swieten, J., et al. 2017. Cognitive reserve and TMEM106B genotype modulate brain damage in presymptomatic frontotemporal dementia: A GENFI study. BRAIN 140, 1784-1791.
42. Wen, J., Zhang, H., Alexander, D.C., et al. 2018. Neurite density is reduced in the presymptomatic phase of C9orf72 disease. J Neurol Neurosurg Psychiatry.
43. Deters, K.D., Risacher, S.L., Farlow, M.R., et al. 2014. Cerebral hypometabolism and grey matter density in MAPT intron 10 +3 mutation carriers. Am J Neurodegenerative Dis 3, 103-114.
44. Collins, D.L., Holmes, C.J., Peters, T.M., et al. 1995. Automatic 3-D model-based neuroanatomical segmentation. Hum. Brain Mapp. 3, 190-208.
45. Rascovsky, K., Hodges, J.R., Knopman, D., et al. 2011. Sensitivity of revised diagnostic criteria for the behavioural variant of frontotemporal dementia. Brain 134, 2456-2477.
46. Gorno-Tempini, M.L., Hillis, A.E., Weintraub, S., et al. 2011. Classification of primary progressive aphasia and its variants. Neurology 76, 1006-1014.
47. Ludolph, A., Drory, V., Hardiman, O., et al. 2015. A revision of the El Escorial criteria - 2015. Amyotroph Lateral Scler Frontotemporal Degener 16, 291-292.
48. Desikan, R.S., Segonne, F., Fischl, B., et al. 2006. An automated labeling system for subdividing the human cerebral cortex on MRI scans into gyral based regions of interest. NeuroImage 31, 968-980.
49. Fischl, B., van der Kouwe, A., Destrieux, C., et al. 2004. Automatically parcellating the human cerebral cortex. Cereb Cortex 14, 11-22.

50. Faul, F., Erdfelder, E., Lang, A.G., et al. 2007. G*Power 3: a flexible statistical power analysis program for the social, behavioral, and biomedical sciences. Behav Res Methods 39, 175-191.
51. Vuksanovic, V., Staff, R.T., Ahearn, T., et al. 2018. Cortical Thickness and Surface Area Networks in Healthy Aging, Alzheimer's Disease and Behavioral Variant Fronto-Temporal Dementia. Int J Neural Syst, 1850055.
52. Kong, L., Herold, C.J., Zollner, F., et al. 2015. Comparison of grey matter volume and thickness for analysing cortical changes in chronic schizophrenia: a matter of surface area, grey/white matter intensity contrast, and curvature. Psychiatry Res 231, 176-183.
53. Gordon, E., Rohrer, J.D., Fox, N.C., 2016. Advances in neuroimaging in frontotemporal dementia. J Neurochem, 193-210.
54. Whitwell, J.L., Weigand, S.D., Boeve, B.F., et al. 2012. Neuroimaging signatures of frontotemporal dementia genetics: C9ORF72, tau, progranulin and sporadics. BRAIN 135, 794-806.
55. Ameur, F., Colliot, O., Caroppo, P., et al. 2016. White matter lesions in FTLD: distinct phenotypes characterize GRN and C9ORF72 mutations. Neurol Genet 2, e47.
56. Paternico, D., Premi, E., Gazzina, S., et al. 2016. White matter hyperintensities characterize monogenic frontotemporal dementia with granulin mutations. Neurobiol Aging 38, 176-180.
57. Sudre, C.H., Bocchetta, M., Cash, D., et al. 2017. White matter hyperintensities are seen only in GRN mutation carriers in the GENFI cohort. NeuroImage Clin 15, 171-180.
58. Alexander, C., Pisner, D., Jacova, C., 2019. Predementia Brain Changes in Progranulin Mutation: A Systematic Review of Neuroimaging Evidence. Dement Geriatr Cogn Disord 47, 1-18.
59. Dopper, E.G.P., Chalos, V., Ghariq, E., et al. 2016. Cerebral blood flow in presymptomatic MAPT and GRN mutation carriers: A longitudinal arterial spin labeling study. NeuroImage Clin 12, 460-465.
60. Meeter, L.H., Dopper, E.G., Jiskoot, L.C., et al. 2016. Neurofilament light chain: a biomarker for genetic frontotemporal dementia. Ann Clin Transl Neurol 3, 623-636.
61. Barandiaran, M., Moreno, F., de Arriba, M., et al. 2019. Longitudinal Neuropsychological Study of Presymptomatic c.709-1G>A Progranulin Mutation Carriers. J Int Neuropsychol Soc 25, 39-47.
62. Jiskoot, L.C., Panman, J.L., van Asseldonk, L., et al. 2018. Longitudinal cognitive biomarkers predicting symptom onset in presymptomatic frontotemporal dementia. J. Neurol. 265, 1381-1392.
63. Meeter, L.H.H., Gendron, T.F., Sias, A.C., et al. 2018. Poly(GP), neurofilament and grey matter deficits in C9orf72 expansion carriers. Ann Clin Transl Neurol 5, 583-597.
64. Mahoney, C.J., Beck, J., Rohrer, J.D., et al. 2012. Frontotemporal dementia with the C9ORF72 hexanucleotide repeat expansion: Clinical, neuroanatomical and neuropathological features. BRAIN 135, 736-750.
65. Seiger, R., Ganger, S., Kranz, G.S., et al. 2018. Cortical Thickness Estimations of FreeSurfer and the CAT12 Toolbox in Patients with Alzheimer's Disease and Healthy Controls. J Neuroimaging 28, 515-523.
66. Chapleau, M., Aldebert, J., Montembeault, M., et al. 2016. Atrophy in Alzheimer's Disease and Semantic Dementia: An ALE Meta-Analysis of Voxel-Based Morphometry Studies. J Alzheimers Dis 54, 941-955.
67. Reuter, M., Schmansky, N.J., Rosas, H.D., et al. 2012. Within-subject template estimation for unbiased longitudinal image analysis. NeuroImage 61, 1402-1418.
68. Boeve, B.F., Rosen, H.J., 2019. Multimodal imaging in familial FTLD: phenoconversion and planning for the future. BRAIN 142, 8-11.

APPENDIX

Review search strategies

embase.com

('frontotemporal dementia'/exp OR 'Pick presenile dementia'/de OR (((frontotemporal OR fronto-temporal) NEAR/3 (dementia OR degenerat*)) OR ftd OR bvftd OR fvftd OR tvftd OR ftld OR ppa OR (progressive NEAR/6 aphasi*) OR (Pick* NOT niemann*)):ab,ti) AND ('gray matter'/de OR 'central gray matter'/de OR 'atrophy'/de OR 'brain atrophy'/exp OR 'cerebellum atrophy'/exp OR 'brain cortex atrophy'/de OR (((gray OR grey) NEXT/3 matter) OR 'substantia grisea' OR atroph*):ab,ti) AND ('asymptomatic disease'/de OR 'heredity'/de OR genotype/exp OR heritability/de OR inheritance/exp OR mutation/exp OR 'genetic disorder'/de OR 'preclinical study'/de OR 'familial disease'/de OR gene/de OR (heredit* OR genetic* OR presymptom* OR pre-symptom* OR preclinical* OR asymptom* OR a-symptomatic* OR mutat* OR familial* OR chromosom* OR gene OR genes OR dna OR deletion*):ab,ti) NOT ([Conference Abstract]/lim) AND [English]/lim NOT ([animals]/lim NOT [humans]/lim) NOT ('case report'/de OR 'case report':ti)

Medline Ovid

(exp Frontotemporal Lobar Degeneration/ OR (((frontotemporal OR fronto-temporal) ADJ3 (dementia OR degenerat*)) OR ftd OR bvftd OR fvftd OR tvftd OR ftld OR ppa OR (progressive ADJ6 aphasi*) OR (Pick* NOT niemann*)).ab,ti.) AND (Gray Matter/ OR atrophy/ OR Atrophy/ OR (((gray OR grey) ADJ3 matter) OR substantia grisea OR atroph*).ab,ti.) AND (Asymptomatic Diseases/ OR Genotype/ OR Heredity/ OR Genetics/ OR Mutation/ OR Genetic Diseases, Inborn/ OR Genes/ OR (heredit* OR genetic* OR presymptom* OR pre-symptom* OR preclinical* OR asymptom* OR a-symptomatic* OR mutat* OR familial* OR chromosom* OR gene OR genes OR dna OR deletion*).ab,ti.) AND english.la. NOT (exp animals/ NOT humans/) NOT (case reports/ OR case report.ti.)

Web of science

TS=(((((frontotemporal OR fronto-temporal) NEAR/2 ("dementia" OR degenerat*)) OR (progressive NEAR/5 aphasi*))) AND ((((("gray" OR "grey") NEAR/2 "matter") OR "substantia grisea" OR atroph*)) AND ((heredit* OR genetic* OR presymptom* OR pre-symptom* OR preclinical* OR asymptom* OR a-symptomatic* OR mutat* OR familial* OR chromosom* OR "gene" OR "genes" OR deletion*))) NOT TI=("case report") AND DT=(article) AND LA=(english)

Cochrane CENTRAL

((((frontotemporal OR fronto-temporal) NEAR/3 (dementia OR degenerat*)) OR ftd

OR bvftd OR fvftd OR tvftd OR ftld OR ppa OR (progressive NEAR/6 aphasi*) OR (Pick* NOT niemann*)):ab,ti) AND ((((gray OR grey) NEXT/3 matter) OR 'substantia grisea' OR atroph*):ab,ti) AND ((heredit* OR genetic* OR presymptom* OR pre-symptom* OR preclinical* OR asymptom* OR a-symptomatic* OR mutat* OR familial* OR chromosom* OR gene OR genes OR dna OR deletion*):ab,ti)

Google scholar

"frontotemporal|temporal dementia|degeneration"|"progressive aphasia"
"gray|grey matter"|atrophy heredit|genetic|presymptomatic|"pre|a symptomatic"|preclinical|asymptomatic|mutation|familial

MRI processing methods

Default settings and processing steps were used per software package. Processing pipelines are described briefly below.

SPM. VBM analysis was performed using SPM12 [1] running in Matlab 2013b (Mathworks, Natick, MA, USA), using default settings. Realignment consisted of manually centering the T1-weighted images to the anterior commissure and automatic spatial alignment of the images to each other after that. Subsequently, images were segmented with two Gaussian curves for classification, resulting in bias-corrected grey and white matter and cerebrospinal fluid (CSF) segmentations rigidly aligned to MNI-space. Using DARTEL, we created a study-specific template that consisted of randomly chosen subjects, balanced over all groups. Next, grey matter segmentations were warped and normalized to the template, and then registered to the MNI152 template. After registrations, grey matter images were smoothed using a full width at half maximum (FWHM) kernel of 8 mm to correct for individual brain differences. Total intracranial volume (TIV) was calculated by the sum of grey matter, white matter and CSF volumes. We applied a voxel-wise analysis of variance to compare grey matter differences between *MAPT* mutation, *GRN* mutation, or *C9orf72* repeat expansion carriers and non-carriers, corrected for age, sex and TIV.

FSL. Our second VBM analysis was performed using the automated VBM-pipeline from FSL [2]. Preprocessing of the T1-weighted images included brain extraction, tissue segmentation of grey matter, white matter and CSF, and non-linear registration into MNI space. A study-specific template in MNI space was created, consisting of a balanced set of images across groups, which were the same subjects as were randomly chosen for the template of the SPM analysis. Native grey matter segmentations were registered to this template and divided by the Jacobian of the warp field to normalize for local expansions or contractions. Lastly, grey matter images were smoothed with an isotropic Gaussian kernel with a sigma of 3mm, which roughly corresponds to a FWHM kernel of 7 mm. We applied a voxel-wise analysis

of variance to compare grey matter differences between *MAPT* mutation, *GRN* mutation, or *C9orf72* repeat expansion carriers and non-carriers with correction for age, sex and TIV. We used the TIV calculation from SPM, in order to maintain similar statistical models for both SPM and FSL

CAT12. For cortical thickness analysis, we used CAT12 [3] as implemented in SPM12. T1-weighted images were skull-stripped and normalized to template space for European brains. After that, images were registered to a high-dimensional standard DARTEL template and transposed to MNI-space. We executed the standard brain segmentation protocol with surface based cortical thickness estimation using projection-based thickness. Using the tissue segmentations, the distance from CSF/grey matter border to the white matter boundary is estimated. The local maximum distance to the white matter boundary is equal to the cortical thickness, and is subsequently projected to other grey matter voxels using neighboring relationships. At last, a smoothing kernel of 15mm FWHM was used to resample and smooth the surfaces of both hemispheres. We used a voxel-wise analysis of variance to compare cortical thickness differences between *MAPT* mutation, *GRN* mutation, or *C9orf72* repeat expansion carriers and non-carriers, with correction for age and sex. As recommended, TIV correction was not applied in the cortical thickness analysis [4, 5]. Analyses were restricted to cerebral cortical regions.

FreeSurfer. The automated processing stream from FreeSurfer [6, 7] was used for the second cortical thickness analysis. First, affine registration was applied to normalize images into MNI-space and bias field corrections were based on white matter intensity. Then, skull was removed and white matter tissue was segmented from the images. Grey and white matter, CSF and subcortical structures were classified based on localization, intensity and neighboring voxels. A first surface was then calculated and refined following the outside border of the white matter segmentation for each hemisphere. Based on this initial surface and intensity variations, the pial border between grey matter and CSF was estimated and the distance between the white matter and pial border yielded the grey matter thickness for the cortex. Data from each subject was then resampled onto the average subject for each hemisphere, and smoothed with a kernel of FWHM 15mm. We fitted a general linear model to compare cortical thickness differences between *MAPT* mutation, *GRN* mutation, or *C9orf72* repeat expansion carriers and non-carriers with correction for age and sex, using Monte Carlo simulation. No TIV correction was used in order to maintain similar models for the cortical thickness analyses in FreeSurfer and CAT12. Analyses were restricted to cerebral cortical regions.

Voxel-wise results

Figure A.1. Effective T-distribution for all software packages in color scaled whole brain maps.

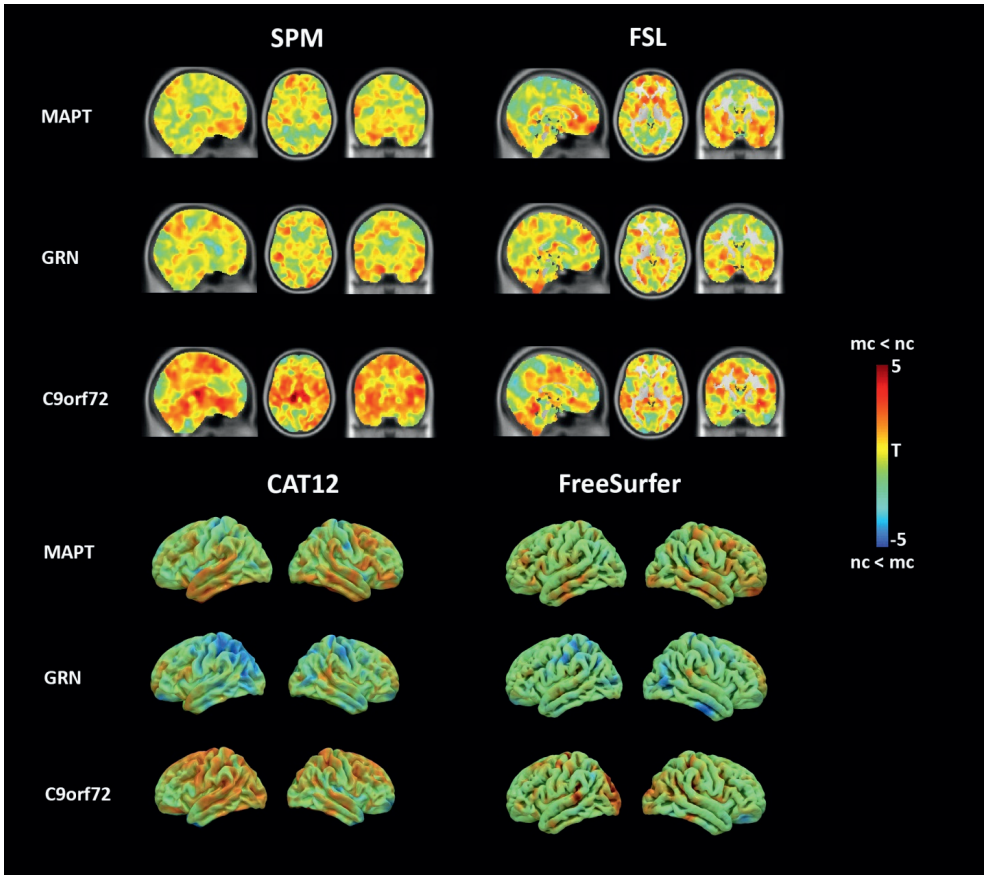

Effective T-distribution from voxel-wise analyses in SPM and FSL and surface-based analyses in CAT12 and FreeSurfer between *MAPT* mutation, *GRN* mutation and *C9orf72* repeat expansion carriers and non-carriers. Color bar, range and scheme is the same for every comparison, and represents a scale of T-values, ranging from -5 to 5.. Abbreviations: MC = mutation carrier, NC = non-carrier.

Table A.1. Voxel-wise results clusters - SPM

$p^{FWE} < 0.05$ cluster level	p-value	cluster	X	Y	Z	peak voxel location
Non-carrier > *GRN*	x					
GRN > Non-carrier	x					
Non-carrier > *MAPT*	0.019	533	23	36	-11	right frontal pole
MAPT > Non-carrier	x					
Non-carrier > *C9orf72*	0.000	3645	-14	-24	2	left thalamus
	0.000	2337	39	-63	-21	right cerebellum
	0.000	2179	-45	-35	6	left planum temporale
	0.000	1964	-27	-38	44	left postcentral gyrus
	0.000	1795	-39	-44	-29	left cerebellum
	0.016	559	44	-14	9	right Heschl's gyrus
	0.022	501	8	-41	-9	right cerebellum
	0.024	486	54	-5	39	right precentral gyrus
	0.030	438	6	23	-5	right subcallosal cortex
	0.031	436	30	-29	54	right cerebellum
C9orf72 > Non-carrier	x					
***p < 0.001* k20 peak level**	**p-value**	**cluster**	**X**	**Y**	**Z**	**peak voxel location**
Non-carrier > *GRN*	0.000	206	-15	-12	-23	left parahippocampal gyrus
	0.000	74	-62	-12	-12	left middle temporal gyrus
	0.000	63	-48	-23	32	left postcentral gyrus
	0.000	52	-47	-26	-2	left superior temporal gyrus
	0.000	44	17	-71	65	right parietal lobe
	0.001	39	48	6	-27	right temporal pole
	0.000	37	-47	-50	-24	left inferior temporal gyrus
	0.000	35	47	12	12	right inferior frontal gyrus
GRN > Non-carrier	0.000	112	2	17	11	right lateral ventricle
	0.001	47	-8	3	24	left lateral ventricle
Non-carrier > *MAPT*	0.000	533	23	36	-11	right frontal pole
	0.000	46	-27	-51	74	left parietal lobe
MAPT > Non-carrier	0.000	114	36	-57	9	right lateral occipital cortex
	0.000	90	25	-45	-12	right temporal occipital fusiform gyrus
Non-carrier > *C9orf72*	0.000	3645	-14	24	2	left caudatus
	0.000	2337	39	-63	-21	right cerebellum
	0.000	2179	-45	-35	6	left planum temporale
	0.000	1964	-27	-38	44	right postcentral gyrus

	0.000	1795	-39	-44	-29	left cerebellum
	0.000	559	44	-14	9	right heschl's gyrus
	0.000	501	8	-41	-9	right cerebellum
	0.000	486	54	-5	39	left precentral gyrus
	0.000	438	6	23	-5	right subcallosal cortex
	0.000	436	30	-29	54	left postcentral gyrus
	0.000	265	27	-72	18	right lateral occipital cortex
	0.000	218	-51	-17	36	left postcentral gyrus
	0.000	203	-24	-63	-44	left cerebellum
	0.000	72	2	18	51	right paracingulate gyrus
	0.000	50	-32	-45	-42	left cerebellum
	0.000	45	-23	-51	69	left superior parietal lobule
	0.000	23	-60	14	23	left inferior frontal gyrus
	0.000	20	-27	-17	50	left precentral gyrus
	0.001	20	-23	12	-14	left orbitofrontal cortex
C9orf72 > Non-carrier	0.000	62	-41	60	-6	right frontal pole

Table A.2. Voxel-wise results clusters - FSL

$p^{FWE} < 0.05$ cluster level	p-value	cluster	X	Y	Z	peak voxel location
Non-carrier > *GRN*	x					
GRN > Non-carrier	x					
Non-carrier > *MAPT*	x					
MAPT > Non-carrier	x					
Non-carrier > *C9orf72*	0.000	10953	-28	-68	-32	left cerebellum
	0.032	22	26	-74	20	right lateral occipital cortex
C9orf72 > Non-carrier	x					
***p < 0.001* k20 peak level**	**p-value**	**cluster**	**X**	**Y**	**Z**	**peak voxel location**
Non-carrier > *GRN*	0.000	138	-16	-10	-28	Left parahippocampal gyrus
	0.000	72	-16	50	32	left frontal pole
	0.000	41	-46	-54	-22	Left inferior temporal gyrus
	0.000	37	-52	-24	38	Left postcentral gyrus
GRN > Non-carrier	0.000	30	-40	-82	20	Left occipital lobe
Non-carrier > *MAPT*	0.000	250	32	-62	34	Right parietal lobe
	0.000	37	0	58	-18	Right frontal pole
	0.000	27	12	-62	58	Right parietal lobe
	0.000	23	10	54	-14	right frontal pole
	0.000	22	-24	66	12	left frontal pole
	0.000	22	10	20	-8	right caudatus
MAPT > Non-carrier	0.000	122	26	-56	-18	Right cerebellum
	0.000	32	50	-6	26	right precentral gyrus
	0.000	24	12	-22	60	Right precentral gyrus
Non-carrier > *C9orf72*	0.000	1004	-4	-86	-40	left cerebellum
	0.000	823	28	-42	-36	right cerebellum
	0.000	115	28	-74	16	right lateral occipital cortex
	0.000	109	24	-68	-62	right cerebellum
	0.000	103	36	-10	6	right insula
	0.000	53	-24	-74	-58	left cerebellum
	0.000	50	-20	-28	54	left precentral gyrus
	0.000	48	-32	-36	42	left postcentral gyrus
	0.000	37	-52	-36	26	left parietal operculum
	0.000	32	-52	-44	18	left supramarginal gyrus

	0.000	29	-8	-20	2	left thalamus
	0.000	21	36	0	-10	right insula
C9orf72 > Non-carrier	0.000	112	8	-36	58	right postcentral gyrus
	0.000	47	-6	-88	22	left cuneal cortex
	0.000	44	20	-22	-38	right cerebellum
	0.000	29	-8	-78	2	left intracalcarine

Table A.3. Voxel-wise result clusters - CAT12

$p^{FWE} < 0.05$ cluster level	pvalue	cluster	X	Y	Z	peak voxel location
Non-carrier > *GRN*	x					
GRN > Non-carrier	x					
Non-carrier > *MAPT*	x					
MAPT > Non-carrier	x					
Non-carrier > *C9orf72*	0.015	189	-12	-54	33	left precuneus
C9orf72 > Non-carrier	x					
***p < 0.001* k20 peak level**	**pvalue**	**cluster**	**X**	**Y**	**Z**	**peak voxel location**
Non-carrier > *GRN*	x					
GRN > Non-carrier	0.000	39	-27	-55	47	left superior parietal lobule
Non-carrier > *MAPT*	0.000	48	4	-46	23	right posterior cingulate
	0.000	46	45	30	-7	right orbitofrontal cortex
	0.000	42	63	-41	-10	right middle temporal gyrus
	0.000	39	-40	-28	-23	left temporal fusiform
	0.000	29	60	-37	24	right supramarginal
	0.000	27	35	-9	-37	right temporal fusiform
	0.000	26	38	-24	-27	right temporal fusiform
MAPT > Non-carrier	x					
Non-carrier > *C9orf72*	0.000	189	-12	-54	33	left precuneus
	0.000	129	27	-38	53	right postcentral gyrus
	0.000	100	-20	-18	70	left precentral gyrus
	0.000	98	-53	1	35	left precentral gyrus
	0.000	84	-45	-37	24	left parietal operculum
	0.000	67	-36	-47	46	left superior parietal lobule
	0.000	40	7	-5	59	right precentral gyrus
	0.001	35	11	-38	54	right postcentral gyrus
	0.000	20	-27	-73	35	left lateral occipital cortex
C9orf72 > Non-carrier	x					

Table A.4. Voxel-wise results clusters - FreeSurfer

***p*^{FWE} < *0.05* cluster level**	**p-value**	**cluster**	**X**	**Y**	**Z**	**peak voxel location**
Non-carrier > *GRN*	x					
GRN > Non-carrier	x					
Non-carrier > *MAPT*	0.044	227	26	17	41	right middle frontal gyrus
MAPT > Non-carrier	x					
Non-carrier > *C9orf72*	0.005	591	13	-48	30	right posterior cingulate
	0.000	566	-17	-92	17	left occipital pole
	0.007	512	-22	-18	69	left precentral gyrus
	0.024	290	-18	-65	27	left precuneus
	0.043	254	-63	-38	7	left superior temporal gyrus
C9orf72 > Non-carrier	0.039	334	6	-5	33	right anterior cingulate
***p < 0.001* k20 peak level**	**p-value**	**cluster**	**X**	**Y**	**Z**	**peak voxel location**
Non-carrier > *GRN*	x					
GRN > Non-carrier	p<0.000	110	59	-17	-35	right inferior temporal
Non-carrier > *MAPT*	p<0.000	462	25	18	37	right middle frontal gyrus
	p<0.001	179	54	-14	17	right parietal lobe
	p<0.000	169	-60	-16	-19	left middle temporal gyrus
	p<0.000	168	-61	-37	-11	left middle temporal gyrus
	p<0.000	166	14	55	-19	right frontal pole
	p<0.000	164	47	1	38	right precentral gyrus
	p<0.001	97	-11	-38	58	left postcentral gyrus
	p<0.001	86	58	-24	-22	right middle temporal gyrus
MAPT > Non-carrier	x					
Non-carrier > *C9orf72*	p<0.000	1620	-17	-93	19	left occipital pole
	p<0.000	1301	13	-48	31	right posterior cingulate
	p<0.000	1019	-31	-65	44	left lateral occipital
	p<0.000	868	-19	-65	29	left precuneus
	p<0.000	819	-22	-20	71	left precentral gyrus
	p<0.000	536	39	-33	20	right parietal operculum
	p<0.000	515	-42	-38	17	left planum temporale
	p<0.000	483	-66	-37	4	left superior temporal gyrus
	p<0.000	387	24	-38	55	right postcentral gyrus
	p<0.000	304	17	-95	16	right occipital pole

	p<0.000	175	37	6	11	right insula
	p<0.000	168	28	-67	24	right lateral occipital
	p<0.000	166	-40	-8	58	left precentral gyrus
	p<0.000	129	40	2	33	right precentral gyrus
	p<0.001	113	16	-24	39	right posterior cingulate
	p<0.001	54	-17	-42	54	left postcentral gyrus
C9orf72 > Non-carrier	p<0.000	528	6	-5	33	right anterior cingulate

REFERENCES

1. Ashburner, J., Friston, K.J., 2000. Voxel-based morphometry--the methods. Neuroimage 11, 805-821.
2. Smith, S.M., Jenkinson, M., Woolrich, M.W., et al. 2004. Advances in functional and structural MR image analysis and implementation as FSL. Neuroimage 23 Suppl 1, S208-219.
3. Dahnke, R., Yotter, R.A., Gaser, C., 2013. Cortical thickness and central surface estimation. Neuroimage 65, 336-348.
4. Panman, J.L., Jiskoot, L.C., Bouts, M., et al. 2019. Gray and white matter changes in presymptomatic genetic frontotemporal dementia: a longitudinal MRI study. Neurobiol Aging 76, 115-124.
5. Schwarz, C.G., Gunter, J.L., Wiste, H.J., et al. 2016. A large-scale comparison of cortical thickness and volume methods for measuring Alzheimer's disease severity. NeuroImage Clin 11, 802-812.
6. Dale, A.M., Fischl, B., Sereno, M.I., 1999. Cortical surface-based analysis. I. Segmentation and surface reconstruction. Neuroimage 9, 179-194.
7. Fischl, B., Sereno, M.I., Dale, A.M., 1999. Cortical surface-based analysis. II: Inflation, flattening, and a surface-based coordinate system. Neuroimage 9, 195-207.

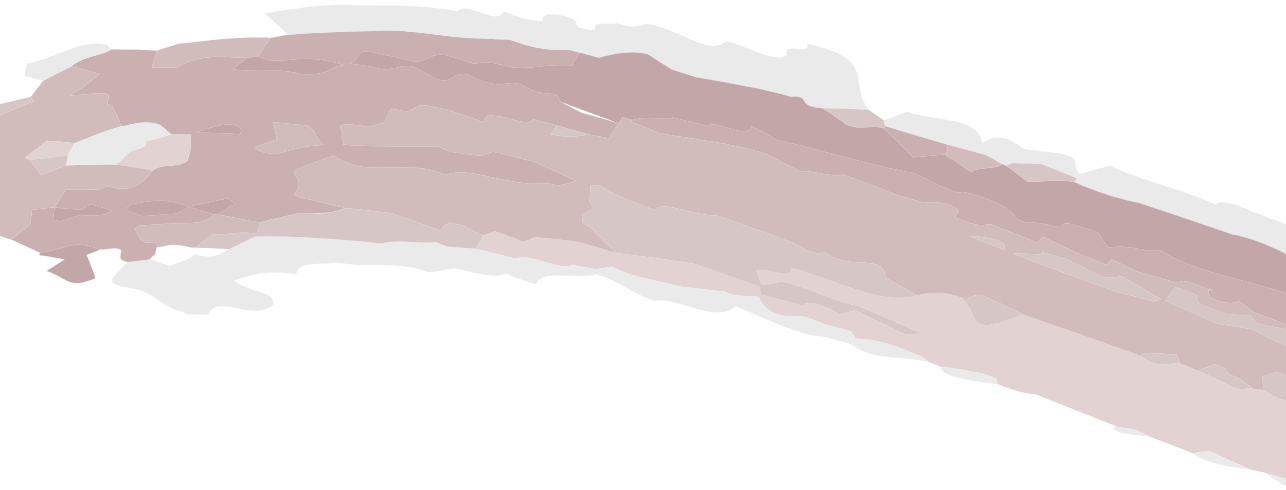

Chapter 4.2

Bias introduced by multiple head coils in MRI research: an 8 channel and 32 channel coil comparison

Panman, J.L.
To, Y.Y.
van der Ende, E.L.
Poos, J.M.
Jiskoot, L.C.
Meeter, L.H.H.
Dopper, E.G.P.
Bouts, M.J.R.J.
van Osch, M.J.P.
Rombouts, S.A.R.B.
van Swieten, J.C.
van der Grond, J.
Papma, J.M.
Hafkemeijer, A.

Frontiers in Neuroscience, 2019

ABSTRACT

Neuroimaging MRI data in scientific research is increasingly pooled, but the reliability of such studies may be hampered by the use of different hardware elements. This might introduce bias, for example when cross-sectional studies pool data acquired with different head coils, or when longitudinal clinical studies change head coils halfway. In the present study, we aimed to estimate this possible bias introduced by using different head coils to create awareness and to avoid misinterpretation of results. We acquired, with both an 8 channel and 32 channel head coil, T1-weighted, diffusion tensor imaging and resting state fMRI images at 3T MRI (Philips Achieva) with stable acquisition parameters in a large group of cognitively healthy participants (n=77). Standard analysis methods, i.e. voxel-based morphometry, tract-based spatial statistics and resting state functional network analyses, were used in a within-subject design to compare 8 and 32 channel head coil data. Signal-to-noise ratios (SNR) for both head coils showed similar ranges, although the 32 channel SNR profile was more homogeneous. Our data demonstrates specific patterns of grey and white matter volume differences between head coils (relative volume change of 6 to 9%), related to altered image contrast and therefore, altered tissue segmentation. White matter connectivity (fractional anisotropy and diffusivity measures) showed hemispherical dependent differences between head coils (relative connectivity change of 4 to 6%), and functional connectivity in resting state networks was higher using the 32 channel head coil in posterior cortical areas (relative change up to 27.5%). This study shows that, even when acquisition protocols are harmonized, the results of standardized analysis models can be severely affected by the use of different head coils. Researchers should be aware of this when combining multiple neuroimaging MRI datasets, to prevent coil-related bias and avoid misinterpretation of their findings.

INTRODUCTION

Large multicenter data samples are increasingly used to establish and reproduce MRI neuroimaging findings. Although pooling MR imaging data contributes to increased study power, the reliability and results from such studies may be compromised by the use of different hardware elements [1, 2]. For example, changing head coils during a longitudinal study, or combining cross-sectional data acquired with different head coils may introduce a coil-related bias [3, 4]. Studies that depict the effect of using multiple head coils are currently limited to analysis of T1 weighted imaging data [3, 4], demonstrating a difference in grey matter volume [3], and cortical thickness [4]. Still, the effects on other quantitative MRI variables, for instance obtained with diffusion tensor imaging or resting state functional MRI, are unknown, but highly important for multicenter or longitudinal studies using different types of hardware. Identification of the brain regions affected by coil-related bias is essential, not only to increase awareness, but more importantly to avoid misinterpretation of results from studies using multiple MRI hardware elements [5]. In the present study, we aimed to estimate and depict the impact of using different receive-only phased array head coils (8 channel head coil and 32 channel head coil) on T1 weighted, DTI and resting state functional MRI data using a within-subject design in a large cohort of cognitively healthy subjects.

METHODS

Study procedure and participants**.** For the present study, we included 77 cognitively healthy participants who underwent MRI of the brain on a 3Tesla Philips Achieva scanner (Philips Medical Systems, Best, The Netherlands) at the Leiden University Medical Center, Leiden, The Netherlands. The MRI protocol contained T1 weighted, DTI and resting state functional MR images, acquired with both an 8 channel SENSE head coil (8CH) and an 32 channel SENSE head coil (32CH) within one MRI session (coil geometry is displayed in Supplementary Figure 1). During acquisition, optimal image quality was obtained by using the incorporated 'constant level appearance' (CLEAR) inhomogeneity correction algorithm on the scanner. We display one raw dataset for all sequences from both coils from a representative healthy participant in Supplementary Figure 1.

Cognitively healthy participants were included in the context of the prospective longitudinal frontotemporal dementia risk cohort (FTD-RisC) in which families with autosomal dominant inherited FTD gene mutations are followed using standardized assessment protocols including an MRI of the brain every year, as described previously [6, 7]. To confirm cognitively healthy status of all participants, Mini Mental State Examination (MMSE [8]) and the Frontal Assessment Battery (FAB [9]) are reported as cognitive screening measures and

the Neuropsychiatric Inventory (NPI-Q [10]) and Frontotemporal Dementia Rating Scale (FRS [11]) are reported as behavioral screening questionnaires. The study has been carried out in accordance with the Declaration of Helsinki and has been approved by the Medical and Ethical Review Committees of the Erasmus MC University Medical Center, Rotterdam, The Netherlands and the Leiden University Medical Center, Leiden, the Netherlands. Written informed consent has been obtained from all participants.

MRI acquisition

Signal to noise assessment. For signal to noise ratio's (SNR) assessment, we acquired proton density weighted single-slice images with one noise-only image, i.e. without radiofrequency pulses, in one healthy volunteer, following the procedures described by Wiggins et al. [12]. For both coils, we acquired the images in the axial, coronal and sagittal direction, with the following parameters: Repetition time (TR) = 200ms, echo time (TE) = 3.1ms, field of view (FOV) = 220 x 220 x 3 mm, flip angle = 20º (for noise scan 0º), slice thickness = 3 mm, voxel size 0.85 x 0.85 x 3.0 mm, number of averages = 10, acquisition time = 9 minutes and 24 seconds.

T1 weighted imaging. For the 3DT1 weighted acquisition, scanning parameters were as follows: MPRAGE, TR = 9.7ms, TE = 4.6ms, FOV = 224 x 177 x 168 mm, flip angle = 8º, slices = 140, voxel size = 0.88 x 0.88 x 1.2 mm, SENSE = none, acquisition time = 4 minutes and 56 seconds. Identical parameters were used for both the 8CH and the 32CH coils.

Diffusion imaging. Diffusion imaging was performed in 60 non-collinear gradient directions using single shot echo planar imaging. The phase encoding direction was anterior to posterior for both coils. The following parameters were used for the 8CH coil: 60 b = 1000 s/mm^2, TR = 8250ms, TE = 80ms, FOV = 256 x 208 x 140 mm, flip angle = 90º, slices = 70, voxel size = 2 x 2 x 2 mm, SENSE = 2.0, one b = 0 s/mm2 acquisition, scan time = 8 minutes and 48 seconds, 2 signal averages. For the 32CH coil, we increased the number of slices to 80, to have sufficient coverage to include the cerebellum in the imaging volume for our longitudinal FTD-RisC study [6]. As a result, the TR for the 32CH coil was 9245 ms, FOV was 256 x 232 x 160 mm, and acquisition time increased to 9 minutes and 52 seconds with a SENSE factor of 2.3. Other parameters were identical between both head coils.

Resting state functional MRI**.** For resting state fMRI, T2*-weighted images were acquired using whole brain multislice gradient echo planar imaging. For both coils, the following parameters were used: TR = 2200ms, TE = 30ms, FOV = 220 x 220 x 113 mm, flip angle = 80º, slices = 38, voxel size = 2.75 x 2.75 x 2.99 mm, including 10% interslice gap, SENSE = 3.0, volumes = 200, acquisition time = 7 minutes and 28 seconds. Participants were instructed to lie still with their eyes closed and stay awake during the resting state fMRI

scans.

MRI processing

Before image preprocessing and analysis, we checked the scans thoroughly for image quality and the presence of artifacts. Data processing and statistical analyses were carried out using Functional Magnetic Resonance Imaging of the Brain Software Library (FSL) version 5.0.8. [13].

Signal to noise ratio. For both the 8CH coil and 32CH coil, we isolated an average signal image and one noise-only image for each orientation plane. We subdivided the signal and noise images into non-overlapping regions of interest (ROI) of 16 by 16 voxels. Next, we calculated the mean signal of the ROI using the averaged signal image, and the standard deviation of the noise of the ROI using the noise-only image. Since the noise images were amplitude-reconstructed, the measured standard deviation was corrected for the Rician noise distribution [14]. Ultimately, for each ROI, SNR was calculated according to:

$$SNR = \frac{Mean\ Signal}{\sqrt{\frac{2}{4-\pi}} * \ Std.Noise}$$

Third, we translated the SNR ROI matrices into color-coded maps, in order to visualize the SNR distribution throughout the brain for both coils.

Structural imaging. To assess the influence of the head coil on grey and white matter volume measurements, we applied the standard voxel-based morphometry (VBM) pipeline as implemented in FSL. Preprocessing of the T1 weighted images included brain extraction followed by radiofrequency (RF) inhomogeneity correction, tissue segmentation and realignment to Montreal Neurological Institute (MNI) standard space using non-linear registration. We performed quality control to ensure good brain extraction, that was not different between both head coils. Next, FMRIB's Automated Segmentation Tool (FAST) was used for correction for spatial intensity variations, also known as bias field or RF inhomogeneity, and segmentation of the T1 weighted images [15]. The corrected, segmented grey matter images were re-registered non-linearly to a study-specific template with a balanced set of 8CH and 32CH coil images. The registered partial volume images were divided by the Jacobian of the warp field to correct for any local expansion or contraction. An isotropic Gaussian kernel with a sigma of 3 mm, which corresponds to a full width at half maximum kernel (FWHM) of approximately 7 mm, was used to smooth the grey matter segmentations. We also applied the VBM processing pipeline to the white matter segmentations, resulting in registered, corrected and smoothed white matter images for

voxel-wise analyses.

Diffusion imaging. Diffusion scans were corrected for motion artifacts and eddy currents by alignment to the b=0 image using the FMRBIB Diffusion Toolbox. The tensor was fitted each voxel to create fractional anisotropy (FA) and mean diffusivity (MD) images. Subsequently, we applied standard tract-based spatial statistics (TBSS) as implemented in FSL [16]. FA images were aligned to standard space using non-linear registration and averaged into a mean FA image. To create a study-specific FA mask, we thresholded the mean FA image with a minimum value of FA ≥ 0.2. This binarised FA mask was applied to voxel-wise comparisons of FA and MD between coils.

Resting state functional MRI. For preprocessing of the resting state fMRI scans, we applied the FMRI Expert Analysis Tool (FEAT) as implemented in FSL, consisting of motion correction with MCFLIRT and spatial smoothing with a kernel of 6 mm FWHM. The data-driven Independent Component Analysis (ICA) based Automatic Removal of Motion Artifacts (ICA-AROMA) approach was used to identify and remove noise components from the resting state fMRI data [17]. After denoising, high pass temporal filtering was performed with a cut-off frequency of 0.01 Hz. The functional resting state images were registered to the corresponding T1 weighted images using Boundary-Based Registration and were subsequently registered to the 2 mm isotropic MNI standard space using non-linear registration with a warp resolution of 10 mm. Voxel-based functional connectivity was studied in a standardized manner using the eight standard Beckmann resting-state functional networks of interest [18], i.e. the medial and lateral visual system network, the primary auditory network – also known as the salience network –, the sensory motor network, the default mode network, the executive control network and the left and right dorsal visual processing stream networks. To further account for noise, white matter and CSF templates were included in the analyses as regressors. Functional connectivity of each network of interest was calculated using dual regression, as previously described [19]. In short, the eight standard resting state networks [18] were used as a reference. Voxel-based resting state functional connectivity was determined in terms of similarity of the BOLD fluctuations in the brain in relation to characteristic fluctuations in the standard resting state networks. With dual regression, individual time series were first extracted for each template, using the resting state networks, and the two additional white matter and cerebrospinal fluid maps, in a spatial regression against the individual fMRI data set (regression 1). The resulting matrices described temporal dynamics for each template and individual. Next, the temporal regressors were used to fit a linear model to the individual fMRI data set (regression 2), to estimate the spatial maps for each individual. This results in 3D images for each individual, with voxel-wise z-scores representing the functional connectivity to each of the predefined standard networks.

Statistical analysis. For all analyses, we designed within-subject paired sample t-tests with each subject's mean effect to analyze head coil differences in grey and white matter volume, FA, MD and resting state functional connectivity. We performed voxel-based non-parametric permutation testing [20] with 5000 permutations using FSL-randomise. The statistical threshold was set at $p<0.05$, using threshold-free cluster enhancement (TFCE) technique and family-wise error (FWE) correction to correct for multiple comparisons across voxels. We quantified the severity of head coil differences by calculating effect sizes and percentage of change.

Voxel-specific scaling factors. For our own longitudinal clinical study [6, 7], we aimed to create voxel-based scaling factors to correct for the use of different head coils. For the T1-weighted, DTI and resting state fMRI images, we calculated and validated voxel-specific scaling images. Procedures are described in detail in the Supplements. In short, we separated our sample into a template dataset (n=39) and validation dataset (n=38), matched for age and sex. For the template dataset, we merged and averaged the images into a mean 8CH coil image and 32CH coil image. The averaged 32CH coil image was divided by the averaged 8CH coil image, resulting in a voxel-based scaling factor. We reduced noise by applying a median filter with a kernel of 5 mm. Next, the 8CH coil images from the validation set were multiplied with the voxel-based scaling factor, equalizing the 8CH coil images to the signal intensity of the 32CH coil images. We repeated previous described statistical analysis on the validation set to complete verification of the scaling factor.

RESULTS

Participants. In total 77 participants were included in this study (Table 1). Cognitive and behavioral screening tests confirmed a cognitively healthy status of all participants.

Signal to noise ratio. Visualization of the SNR ROI matrices revealed a quite homogeneous distribution of SNR throughout the brain using the 32CH coil, with the highest SNR in posterior cortical areas of the brain. SNR of the 8CH coil was highest in the frontal lobe, but dropped in central and medial areas (Figure 1).

Structural imaging**.** Quality control showed no differences in brain extraction of the T1 weighted images between the 8CH and 32CH coil. Grey matter volumes obtained with the 32CH coil were larger than obtained with the 8CH coil ($p^{FWE}<0.05$, effect size = 2.096, increase = 6.2%), particularly in the middle and inferior frontal lobe, the superior and middle temporal lobe, the anterior insular cortex, the temporo-parietal junction, the paracingulate and the cuneus (yellow areas in Figure 2A). Grey matter volumes appeared smaller using the 32CH coil ($p^{FWE}<0.05$, effect size = 2.571, decrease = 8.9%) in frontal and deeper cerebral areas,

Table 1. Sample characterization

Age, years	54.2 (28-76)
Sex, female/male	54/23
Education[a]	5.29 (1-7)
MMSE[b]	29.3 (25-30)
FAB[b]	16.8 (11-18)
NPI[b]	1.6 (0-18)
FRS[b]	96.4 (73-100)

Values are means (range) for continuous variables and ratio for dichotomous variables. Abbreviations: MMSE = Mini-Mental State Examination; FAB = Frontal Assessment Battery; NPI = Neuropsychiatric Inventory; FRS = Frontotemporal Dementia Rating Scale. [a] Education is presented on a 7-point scale ranging from 1 (less than elementary school) to 7 (university or technical college) according to Verhage [21] [b] Missing data: MMSE 1/77, FAB 1/77, NPI 17/77, FRS 16/77.

such as the medial temporal lobe, medial frontal lobe, basal ganglia, posterior insular cortex, anterior cingulate, superior frontal cortex, occipital lobe and the cerebellum (blue areas in Figure 2A). In the white matter, we found larger white matter volumes in subcortical and posterior cortical regions using the 32CH coil compared with the 8CH coil ($p^{FWE}<0.05$, effect size = 1.951, increase = 8.5%; see yellow areas in Figure 2B). White matter volumes were smaller using the 32CH coil in frontotemporal regions ($p^{FWE}<0.05$, effect size = 1.637, decrease = 6.1%; see blue areas in Figure 2B).

Diffusion tensor imaging. We found higher FA values ($p^{FWE}<0.05$, effect size = 2.197, increase = 5.7%) with the 32CH coil compared with the 8CH coil in all tracts of the right hemisphere and frontal tracts of the left hemisphere, such as the forceps minor, anterior parts of the uncinate fasciculus, anterior thalamic radiation, inferior fronto-occipital fasciculus and superior longitudinal fasciculus (yellow areas in Figure 3A). On the contrary, we found lower FA values using the 32CH coil ($p^{FWE}<0.05$, effect size = 2.038, decrease = 5.0%) in part of the left-sided posterior tracts, such as the forceps major, the corticospinal tract, the inferior longitudinal fasciculus, and the central and posterior parts of the anterior thalamic radiation (blue areas in Figure 3A). MD was lower using the 32CH coil compared to 8CH coil ($p^{FWE}<0.05$, effect size = 1.871, decrease = 4.6%) in the entire right hemisphere, and some tracts of the left hemisphere located in the prefrontal and the occipital lobe (red-yellow areas in Figure 3B). Using the 32CH coil, MD was higher ($p^{FWE}<0.05$, effect size = 1.952, increase = 4.7%) in all tracts of the left hemisphere, except for the prefrontal and occipital lobe (blue areas in Figure 3B).

Resting state functional MRI. Resting state functional connectivity was predominantly higher when using the 32CH coil compared with the 8CH coil (yellow areas in Figure 4), between

Figure 1. Signal to noise ratio's

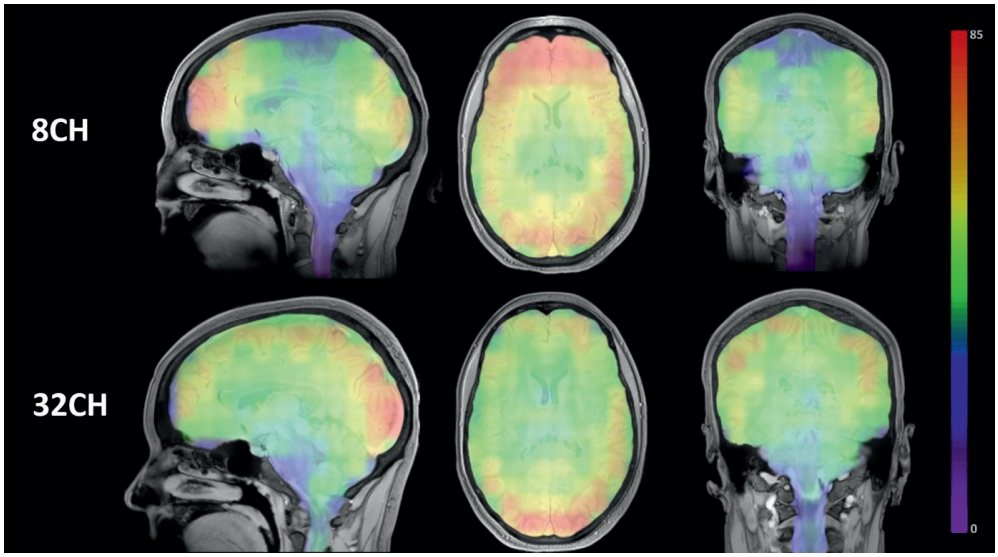

Color-coded SNR brain maps in the sagittal, axial and coronal direction for 8-channel head coil (8CH) and 32-channel head coil (32CH). Colorbar represents SNR values, ranging from 0 to 85.

Figure 2. Voxel-based coil differences in grey and white matter volume

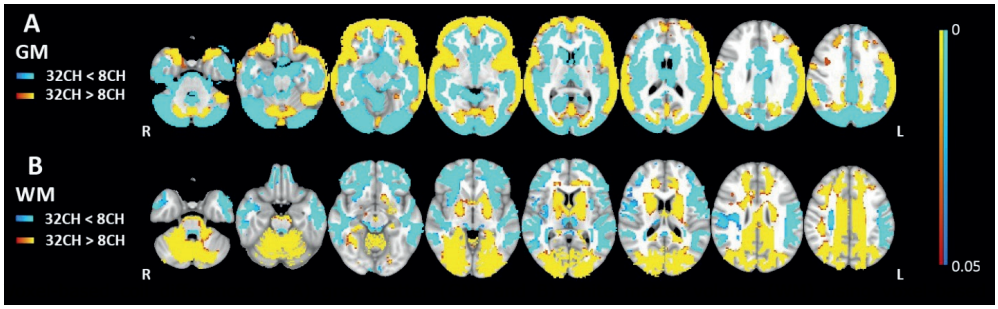

morphometry paired sample t-tests on T1 weighted images. 8CH = 8 channel head coil, 32CH = 32 channel head coil. P values are color coded from 0.05 to < 0.0001 FWE corrected.

the medial visual network and the lateral occipital cortex, calcarine cortex and lingual gyrus ($p^{FWE}<0.05$, effect size = 0.392, increase = 13.5%; Figure 4A), between the lateral visual network, the lateral occipital cortex and the occipital pole ($p^{FWE}<0.05$, effect size = 0.637, increase = 27.5%; Figure 4B), between the default mode network and the lateral occipital cortex ($p^{FWE}<0.05$, effect size = 0.505, increase = 9.4%; Figure 4E), and between the dorsal visual stream networks and regions of the lateral occipital cortex (right: $p^{FWE}<0.05$, effect size = 0.368, increase = 13.6%; Figure 4G and left: $p^{FWE}<0.05$, effect size = 0.391, increase =12.04%; Figure 4H). Functional connectivity was lower with the 32CH coil in the

Figure 3. Voxel-based coil differences in fractional anisotropy and mean diffusivity

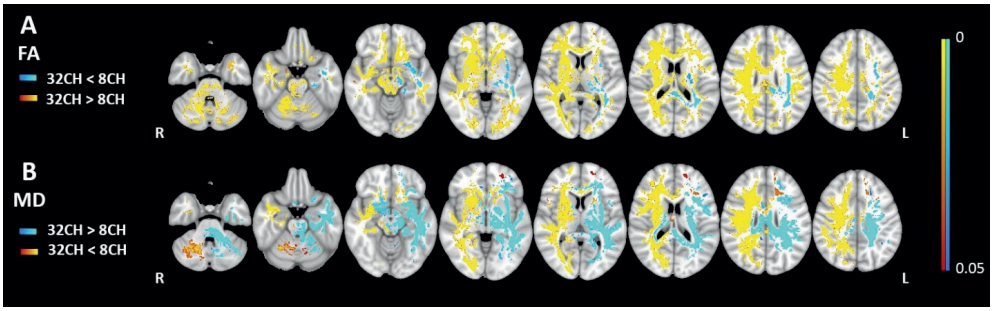

Voxel-based coil differences in A) fractional anisotropy (FA) and B) mean diffusivity (MD) using tract-based spatial statistics paired sample t-test on diffusion weighted images. 8CH = 8 channel head coil, 32CH = 32 channel head coil. P values are color coded from 0.05 to < 0.0001 FWE corrected.

executive control network and a small area in the frontal pole ($p^{FWE}<0.05$, effect size = 0.608, decrease = 23.1%; blue area in Figure 4F). No differences in functional connectivity between both coils were found neither in the auditory, or salience network (Figure 4C), nor the sensory-motor network (Figure 4D).

Voxel-specific scaling factors**.** Results are described in detail in the Supplements. For T1-weighted imaging, after applying the scaling factor, VBM analyses showed almost complete removal of the head coil differences throughout the brain for both GM and WM (Supplementary Figure 2). Validation of the DTI scaling factors showed a successful harmonization of the FA images, removing all significant coil differences. For MD, head coil differences were reduced, except for some small areas at the forceps major and right thalamus (Supplementary Figure 3). For resting state analyses, validation of the scaling factors showed extensive reduction of coil differences in the medial and lateral visual networks, and complete removal of all significant differences in the default mode network, executive control network (salience network), and the left and right dorsal visual stream networks (Supplementary Figure 4).

DISCUSSION

In this study, we demonstrated that quantitative results of standard processing pipelines for T1-weighted MRI, diffusion tensor imaging and resting state fMRI will be severely affected by the use of different head coils. Paired-wise group analyses between coils revealed different patterns of grey and white matter volume, white matter connectivity and functional connectivity.

Voxel-based morphometric analysis of T1-weighted imaging data, revealed smaller apparent grey matter volume for the 32CH coil in the outer frontal, temporal and parietal cortex, the inner cerebellum, the precuneus, and posterior cingulate cortex compared to the 8CH

Figure 4. Voxel-based coil differences in network-based functional connectivity

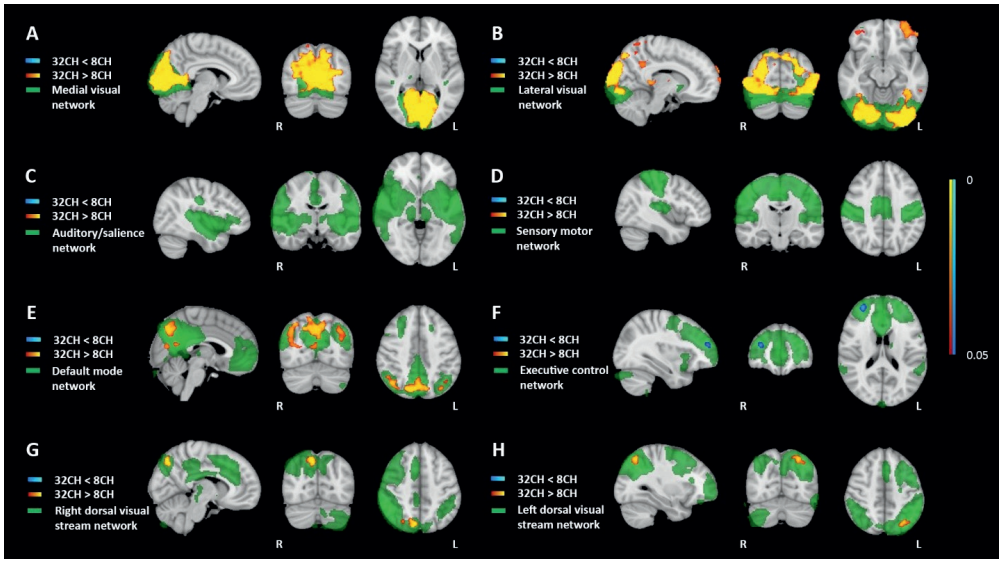

Voxel-based coil differences in network-based functional connectivity using dual regression paired sample t-tests on resting state fMRI images. 8CH = 8 channel head coil, 32CH = 32 channel head coil. Resting state networks of interest are illustrated in green. P values are color coded from 0.05 to <0.0001 FWE corrected.

coil. Grey matter volume was larger using the 32CH coil in the occipital lobe, the central layer of the frontal, temporal, parietal cortex, the peripheral layer of the cerebellum, and subcortical areas. A less extensive but similar pattern of grey matter volume differences was previously found using two identical scanners with respectively an 8-channel and a 12-channel head coil [3]. Compared to grey matter VBM, we found an opposite pattern of head coil differences for the white matter VBM, meaning that in areas where grey matter volume was larger, white matter volume was smaller and vice versa. The visual overlap of grey and white matter differences may be a result of the spatial smoothing (7mm). When the contrast between grey and white matter is unclear, a higher level of smoothing is necessary to account for the uncertainties in partial volume estimation. Our results indicate that differences in grey/white matter contrast of the images leads to differences in tissue classification during segmentation [15, 22]. Three factors could have led to altered image contrast: (1) Despite using inhomogeneity correction prior to segmentation, the SNR of the 8CH and 32CH coil has affected the probabilities of grey and white matter [12, 23]. For example, in our case, higher SNR in posterior cortical areas for the 32CH coil increased the probability of a voxel being white matter, and the same principle may explain the results in the frontal areas of the 8CH coil. (2) Both coils have differences in signal distribution due to the coil geometry [24] and the CLEAR algorithm does not fully correct for these [25], or (3) there has been a difference in the effective b1 distribution [26]. As we demonstrate here, differences in image contrast in structural images could pose serious problems for studies

combining MRI hardware elements and need to be equalized before tissue segmentation and partial volume estimation to prevent methodological errors.

We demonstrated that for DTI, measured FA was higher for nearly the entire white matter when comparing the 32CH coil with the 8CH coil, except for parts of the left temporal and parietal lobe. For MD, the results were hemispherical dependent, i.e. the 32CH coil showed higher MD compared to the 8CH coil in the white matter of the left hemisphere but lower MDs in the right hemisphere. The asymmetry in especially MD metrics was unexpected and inexplicable. Previous research demonstrated that MD may have more variance and be less reproducible than FA, even within sites [27-29]. Interestingly, the unexpected pattern in diffusion metrics was different from the SNR profiles of both coils and volumetric results. Therefore, we emphasize that SNR profiles and pattern of changes that occur in T1-weighted data cannot be translated to DTI data. Our results underline previous studies that already demonstrated the possible pitfalls of pooling diffusion data [30-33]. Harmonization methods have been investigated in a number of studies, in attempt to overcome the problems with pooled DTI data, but sufficient harmonization has proven to be difficult [32, 34-36]. Note that we slightly increased our FOV to allow coverage of the cerebellum for the 32CH coil data, which also increased TR, and could have influenced our results. This is, however, expected to be a very minor effect, since both TRs are significantly longer than five times the T1 of the white matter.

Resting state fMRI analyses showed increased functional connectivity between multiple posterior located networks and brains areas using the 32CH coil, corresponding to the SNR profile. Decreased functional connectivity using the 32CH coil was found between a small frontal area and the executive control network. Previous studies demonstrated around 10 percent variability between scanner hardware [37-39], but others could not detect significant differences in resting state networks between the 8CH and 32CH Philips head coils [40]. As our current sample size (n=77) is larger than previous studies (n=26), we assume that the increased power in our study allowed for detection of coil differences in resting state functional connectivity. Concordant with the results from our study, past research demonstrated that the 32CH coil has particularly increased SNR in posterior cortical areas compared to coils with less channels, caused by a difference in coil geometry [12, 23]. Resting state functional MRI studies may benefit from increased SNR in the 32CH coil, especially when posterior cortical areas are of interest.

Since changing head coils during longitudinal clinical research might introduce bias, we aimed to create voxel-based scaling images (Supplements) for our own longitudinal clinical study [6, 7]. The unique within-subject design in a large cohort (n=77) with stable acquisition parameters allowed for the use of voxel-specific information for VBM, DTI and resting state fMRI scaling. We validated the use of the scaling factors on independent data

and demonstrated that coil differences can be substantially reduced when using voxel-based scaling in all modalities (see supplements). Our voxel-specific scaling factors may be an interesting harmonization method for within-subject variation. In previous literature, many harmonization methods have aimed to equalize neuroimaging data, all with their own advantages and shortcomings [4, 5, 32, 34-36, 41-47]. For example, additional complexity in statistical models may cause decreased sensitivity for the actual outcome of interest [5]. Neuroimaging studies combining multiple MRI head coils and other hardware elements should be aware of confounding factors and be committed to use robust, sensitive and validated methods to deal with these factors [1, 48, 49]. We aim to deepen our research into neuroimaging harmonization methods and our scaling factors in the near future.

Major strengths of this study are the large sample size and the within-subject study design of two protocols within one scanning session using similar acquisition parameters. Despite our best efforts, some confounding factors are essentially inevitable, such as scanner drift, re-positioning of the participants heads inside the different coils and use of head cushions [50]. Other factors that could have influenced the results in our study may be habituation of the subject and scanner warm-up, especially for the resting state fMRI, and the anisotropic voxel size of the T1 weighted sequence. We are aware that extrapolating the results from our study to other head coils or other vendors may be difficult. Instead, we emphasize that our study may be appreciated as increasing awareness for the variability and possible bias in quantitative MRI metrics in data originating from different hardware elements. This is especially important for clinical research, where data acquired with different hardware elements is increasingly pooled.

In conclusion, this study provides evidence that the results of standard analysis models are severely compromised when data from different head coils is combined, or when head coils are changed during longitudinal clinical studies, even though acquisition protocols are completely harmonized. Studies combining neuroimaging MRI data with multiple head coils or other MRI hardware elements should be aware that measurements of grey and white matter volume, white matter connectivity and functional connectivity will differ between head coils and should handle these confounding factors with caution.

REFERENCES

1. Smith, S.M. and T.E. Nichols, Statistical Challenges in "Big Data" Human Neuroimaging. Neuron, 2018. 97(2): p. 263-268.
2. Cannon, T.D., et al., Reliability of neuroanatomical measurements in a multisite longitudinal study of youth at risk for psychosis. Hum Brain Mapp, 2014. 35(5): p. 2424-34.
3. Focke, N.K., et al., Multi-site voxel-based morphometry--not quite there yet. Neuroimage, 2011. 56(3): p. 1164-70.
4. Pardoe, H.R., et al., Pooling Morphometric Estimates: A Statistical Equivalence Approach. J Neuroimaging, 2016. 26(1): p. 109-15.
5. Li, H., et al., Combining Multi-Site/Multi-Study MRI DATA: Linked-ICA Denoising for Removing Scanner and Site Variability from Multimodal MRI data 2018.
6. Papma, J.M., et al., Cognition and gray and white matter characteristics of presymptomatic C9orf72 repeat expansion. Neurology, 2017. 89(12): p. 1256-1264.
7. Dopper, E.G., et al., Structural and functional brain connectivity in presymptomatic familial frontotemporal dementia. Neurology, 2014. 83(2): p. e19-26.
8. Folstein, M.F., S.E. Folstein, and P.R. McHugh, "Mini-mental state". A practical method for grading the cognitive state of patients for the clinician. J Psychiatr Res, 1975. 12(3): p. 189-98.
9. Dubois, B., et al., The FAB: a Frontal Assessment Battery at bedside. Neurology, 2000. 55(11): p. 1621-6.
10. Cummings, J.L., et al., The Neuropsychiatric Inventory: comprehensive assessment of psychopathology in dementia. Neurology, 1994. 44(12): p. 2308-14.
11. Mioshi, E., et al., Clinical staging and disease progression in frontotemporal dementia. Neurology, 2010. 74(20): p. 1591-7.
12. Wiggins, G.C., et al., 32-channel 3 Tesla receive-only phased-array head coil with soccer-ball element geometry. Magn Reson Med, 2006. 56(1): p. 216-23.
13. Jenkinson, M., et al., Fsl. Neuroimage, 2012. 62(2): p. 782-90.
14. Haacke, C., Magnetic resonance imaging : physical principles and sequence design. 1999, New York: Wiley-Liss.
15. Zhang, Y., M. Brady, and S. Smith, Segmentation of brain MR images through a hidden Markov random field model and the expectation-maximization algorithm. IEEE Trans Med Imaging, 2001. 20(1): p. 45-57.
16. Smith, S.M., et al., Tract-based spatial statistics: voxelwise analysis of multi-subject diffusion data. Neuroimage, 2006. 31(4): p. 1487-505.
17. Pruim, R.H.R., et al., Evaluation of ICA-AROMA and alternative strategies for motion artifact removal in resting state fMRI. Neuroimage, 2015. 112: p. 278-287.
18. Beckmann, C.F., et al., Investigations into resting-state connectivity using independent component analysis. Philos Trans R Soc Lond B Biol Sci, 2005. 360(1457): p. 1001-13.
19. Hafkemeijer, A., et al., A Longitudinal Study on Resting State Functional Connectivity in Behavioral Variant Frontotemporal Dementia and Alzheimer's Disease. J Alzheimers Dis, 2017. 55(2): p. 521-537.
20. Nichols, T.E. and A.P. Holmes, Nonparametric permutation tests for functional neuroimaging: a primer with examples. Hum Brain Mapp, 2002. 15(1): p. 1-25.
21. Verhage, F., Intelligence and Age: Study with Dutch people Aged 12-77 1964, Assen: van Gorcum.
22. Tohka, J., Partial volume effect modeling for segmentation and tissue classification of brain magnetic resonance images: A review. World J Radiol, 2014. 6(11): p. 855-64.
23. Reiss-Zimmermann, M., et al., Improvement of SNR and acquisition acceleration using a 32-channel head coil compared to a 12-channel head coil at 3T. Acta Radiol, 2013. 54(6): p. 702-8.
24. Blamire, A.M., The technology of MRI--the next 10 years? Br J Radiol, 2008. 81(968): p. 601-17.
25. Yun, S., et al., Projection-based estimation and nonuniformity correction of sensitivity profiles in phased-array surface coils. J Magn Reson Imaging, 2007. 25(3): p. 588-97.
26. Marques, J.P., et al., MP2RAGE, a self bias-field corrected sequence for improved segmentation and T1-mapping at high field. Neuroimage, 2010. 49(2): p. 1271-81.
27. Helmer, K.G., et al., Multi-site Study of Diffusion Metric Variability: Characterizing the Effects of Site, Vendor, Field Strength, and Echo Time using the Histogram Distance. Proc SPIE Int Soc Opt Eng, 2016. 9788.

28. Jovicich, J., et al., Multisite longitudinal reliability of tract-based spatial statistics in diffusion tensor imaging of healthy elderly subjects. Neuroimage, 2014. 101: p. 390-403.
29. Fox, R.J., et al., A validation study of multicenter diffusion tensor imaging: reliability of fractional anisotropy and diffusivity values. AJNR Am J Neuroradiol, 2012. 33(4): p. 695-700.
30. Takao, H., et al., Effect of scanner in longitudinal diffusion tensor imaging studies. Hum Brain Mapp, 2012. 33(2): p. 466-77.
31. Pagani, E., et al., Intercenter differences in diffusion tensor MRI acquisition. J Magn Reson Imaging, 2010. 31(6): p. 1458-68.
32. Venkatraman, V.K., et al., Region of interest correction factors improve reliability of diffusion imaging measures within and across scanners and field strengths. Neuroimage, 2015. 119: p. 406-16.
33. Vollmar, C., et al., Identical, but not the same: intra-site and inter-site reproducibility of fractional anisotropy measures on two 3.0T scanners. Neuroimage, 2010. 51(4): p. 1384-94.
34. Fortin, J.P., et al., Harmonization of multi-site diffusion tensor imaging data. Neuroimage, 2017. 161: p. 149-170.
35. Pohl, K.M., et al., Harmonizing DTI measurements across scanners to examine the development of white matter microstructure in 803 adolescents of the NCANDA study. Neuroimage, 2016. 130: p. 194-213.
36. Mirzaalian, H., et al., Harmonizing Diffusion MRI Data Across Multiple Sites and Scanners. Med Image Comput Comput Assist Interv, 2015. 9349: p. 12-19.
37. Costafreda, S.G., et al., Multisite fMRI reproducibility of a motor task using identical MR systems. J Magn Reson Imaging, 2007. 26(4): p. 1122-6.
38. Friedman, L., et al., Test-retest and between-site reliability in a multicenter fMRI study. Hum Brain Mapp, 2008. 29(8): p. 958-72.
39. Kaza, E., U. Klose, and M. Lotze, Comparison of a 32-channel with a 12-channel head coil: are there relevant improvements for functional imaging? J Magn Reson Imaging, 2011. 34(1): p. 173-83.
40. Paolini, M., et al., Resting-state networks in healthy adult subjects: a comparison between a 32-element and an 8-element phased array head coil at 3.0 Tesla. Acta Radiol, 2015. 56(5): p. 605-13.
41. Feis, R.A., et al., ICA-based artifact removal diminishes scan site differences in multi-center resting-state fMRI. Front Neurosci, 2015. 9: p. 395.
42. Griffanti, L., et al., ICA-based artefact removal and accelerated fMRI acquisition for improved resting state network imaging. Neuroimage, 2014. 95: p. 232-47.
43. Salimi-Khorshidi, G., et al., Automatic denoising of functional MRI data: combining independent component analysis and hierarchical fusion of classifiers. Neuroimage, 2014. 90: p. 449-68.
44. Fennema-Notestine, C., et al., Feasibility of multi-site clinical structural neuroimaging studies of aging using legacy data. Neuroinformatics, 2007. 5(4): p. 235-45.
45. Chen, J., et al., Exploration of scanning effects in multi-site structural MRI studies. J Neurosci Methods, 2014. 230: p. 37-50.
46. Takao, H., N. Hayashi, and K. Ohtomo, Effect of scanner in longitudinal studies of brain volume changes. J Magn Reson Imaging, 2011. 34(2): p. 438-44.
47. Keihaninejad, S., et al., A robust method to estimate the intracranial volume across MRI field strengths (1.5T and 3T). Neuroimage, 2010. 50(4): p. 1427-37.
48. Jack, C.R., Jr., et al., The Alzheimer's Disease Neuroimaging Initiative (ADNI): MRI methods. J Magn Reson Imaging, 2008. 27(4): p. 685-91.
49. Boeve, B.F. and H.J. Rosen, Multimodal imaging in familial FTLD: phenoconversion and planning for the future. Brain, 2019. 142(1): p. 8-11.
50. Littmann, A., et al., Acquisition-related morphological variability in structural MRI. Acad Radiol, 2006. 13(9): p. 1055-61.

SUPPLEMENTARY MATERIAL

Supplementary Figure 1. Coil geometry

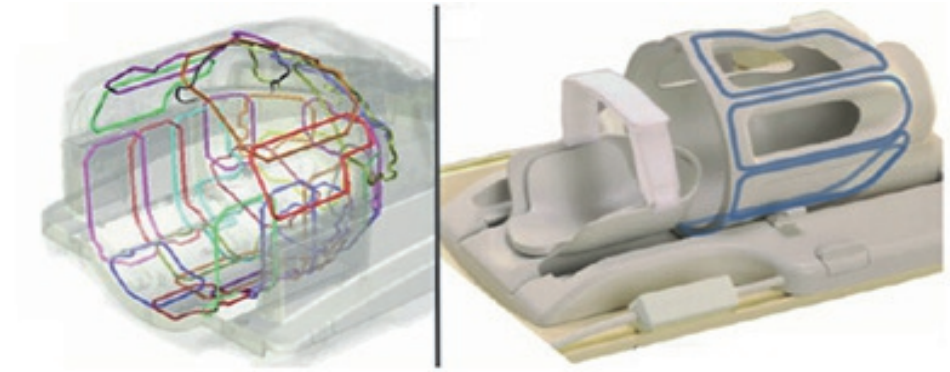

Coil geometry for the 32 channel head coil (left) and the 8 channel head coil (right). Inside diameter at the opening is 26 cm for the 32 channel and 25.5 cm for the 8 channel head coil. Reprinted with permission from Philips, Best, The Netherlands.

Supplementary Figure 2. Raw image types examples

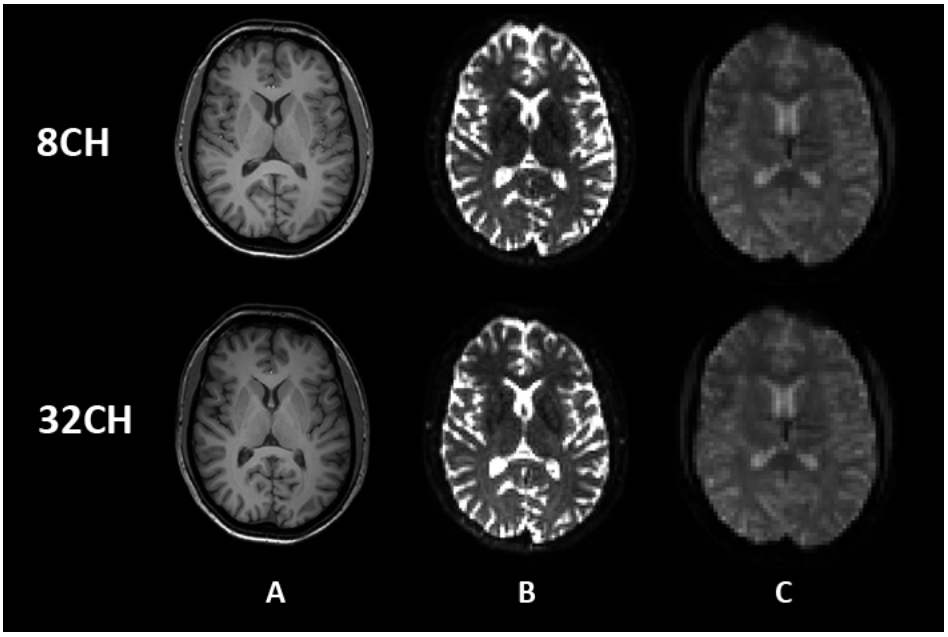

Raw image types from 8 channel head coil and 32 channel head coil for one representative healthy participant. A: 3DT1-weighted, B: b0 image from DTI, C: BOLD EPI image from resting state fMRI.

SCALING FACTOR

Methods

To correct for the use of different head coils (8CH versus 32CH), we defined voxel-based scaling factors for T1-weighted grey matter and white matter segmentations, for FA and MD images derived from DTI and for time-course data from the resting state fMRI images. First, we separated the sample into two datasets, matched for age and sex, into a 'template' dataset (n=39) and a 'validation' dataset (n=38). The template dataset was used to create the scaling factor, and in order to validate it, we applied the scaling factor to the validation dataset.

For the template dataset, each subject's images from the 8CH coil and their corresponding 32CH coil images were merged and averaged into a separate mean 8CH coil image and a mean 32CH coil image. Subsequently, the mean 32CH coil was divided by the mean 8CH coil image, resulting in a voxel-based scaling factor. The scaling factor was reduced from noise using median filtering with a kernel of 5 mm.

For validation purposes, we multiplied images from the 8CH coil in the validation dataset with the scaling factor, equalizing the 8CH coil images to the signal intensity of the 32CH coil images in the validation dataset. In order to confirm successful usage of the scaling factor, voxel-based statistical testing with the corrected 8CH coil images and the original 32CH coil images of the validation dataset was repeated using the previous described analysis steps for the T1, DTI and resting state fMRI images.

Finally, we created the voxel-based scaling factors using the full dataset (n=77), to correct for head coil differences in our current longitudinal FTD-RisC study. These scaling factors are available for other researchers upon request.

Results

T1-weighted. Before applying the scaling factor, VBM analysis in the validation dataset (n=38) showed the same differences in grey and white matter between head coils as when using the full dataset (n=77) (Supplementary Figure 3, uncorrected). After applying the scaling factor, the VBM analyses showed extensive reduction of the head coil differences throughout the brain for both GM and WM (Supplementary Figure 3, corrected). For GM, head coil differences remained present in only a small superior part of the cerebellum (Supplementary Figure 3, GM corrected). For WM, the head coil differences were reduced after applying the scaling factor, except some small areas on the grey-white matter border in the brain (Supplementary Figure 3, WM corrected).

Diffusion tensor imaging. Coil differences in FA and MD, before applying the scaling factors, were similar in the validation dataset (n=38) compared with the coil differences found using

the full dataset (n=77) (Supplementary Figure 4, uncorrected). Validation of the DTI scaling factors showed a successful harmonization of the FA images, removing all significant coil differences (Supplementary Figure 4, FA corrected). For MD, head coil differences were reduced, except for some small areas at the forceps major and right thalamus (Supplementary Figure 4, MD corrected).

Resting state functional MRI. Before applying the scaling factors, coil differences in functional connectivity were similar in the validation dataset (n=38) compared with the differences found using the full dataset (n=77) (Supplementary Figure 5, A-H, uncorrected). After applying the scaling factor, the resting state analyses showed extensive reduction in functional connectivity coil differences in the medial and lateral visual system networks (Supplementary Figure 5, networks A and B, corrected). The validation of the resting state scaling factors showed successful harmonization and removed all significant coil differences for the default mode network (Supplementary Figure 5, E, corrected), executive control network (also referred to as the salience network) (Supplementary Figure 5, F, corrected), and the left and right dorsal visual stream networks (Supplementary Figure 5, networks G and H, corrected).

Supplementary Figure 3. Corrected coil differences in grey and white matter volume

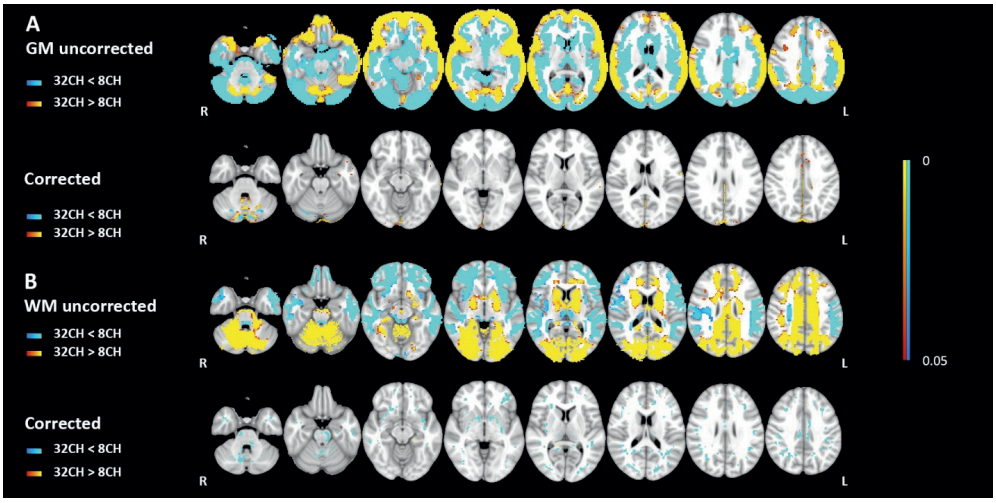

A) Voxel-based coil differences in grey matter volume (GM) before (uncorrected) and after applying the scaling factor to the validation dataset (corrected). B) Voxel-based coil differences in white matter volume (WM uncorrected) and remaining coil differences after applying the scaling factor to the validation dataset (corrected). P values are color coded from 0.05 to < 0.0001 FWE corrected

Supplementary figure 4. Corrected coil differences in fractional anisotropy and mean diffusivity

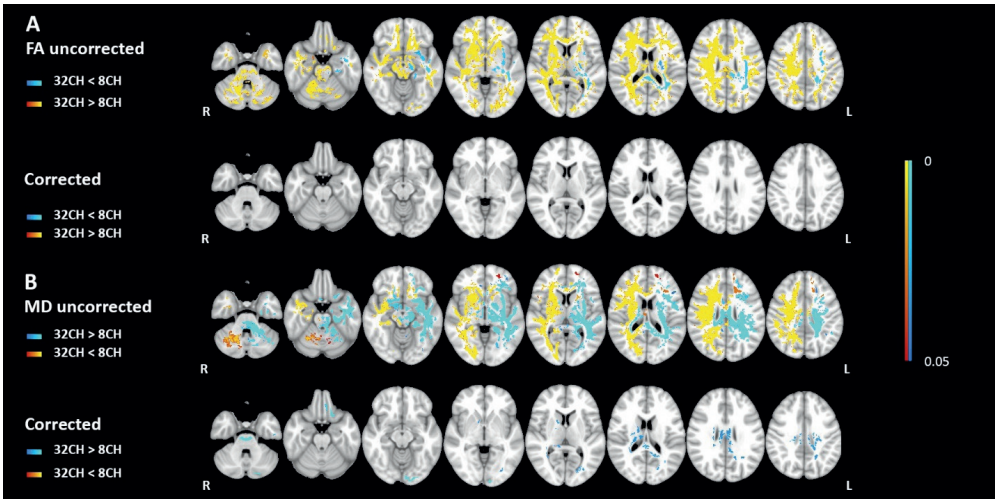

A) Voxel-based coil differences in fractional anisotropy (FA) before (uncorrected) and after applying the scaling factor to the validation dataset (corrected). B) Voxel-based coil differences in mean diffusivity (MD) before (uncorrected) and after applying the scaling factor to the validation dataset (corrected). P values are color coded from *0.05 to < 0.0001* FWE corrected.

Supplementary Figure 5. Corrected coil differences in network-based functional connectivity

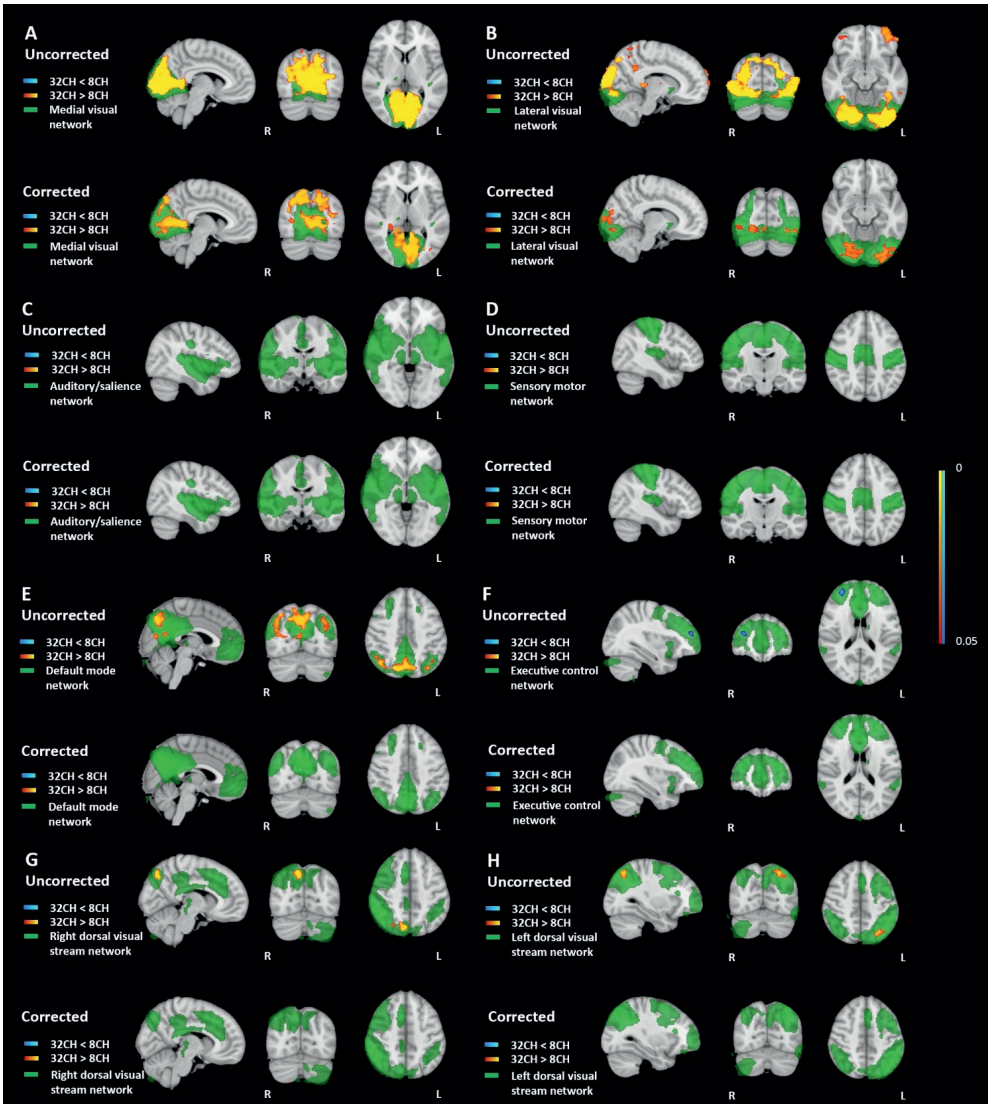

Voxel-based coil differences in network-based functional connectivity. Resting state networks of interest are indicated in green (A-H). Coil differences in functional connectivity before (uncorrected) and after applying the scaling factor to the validation dataset (corrected). P values are color coded from *0.05 to < 0.0001* FWE corrected.

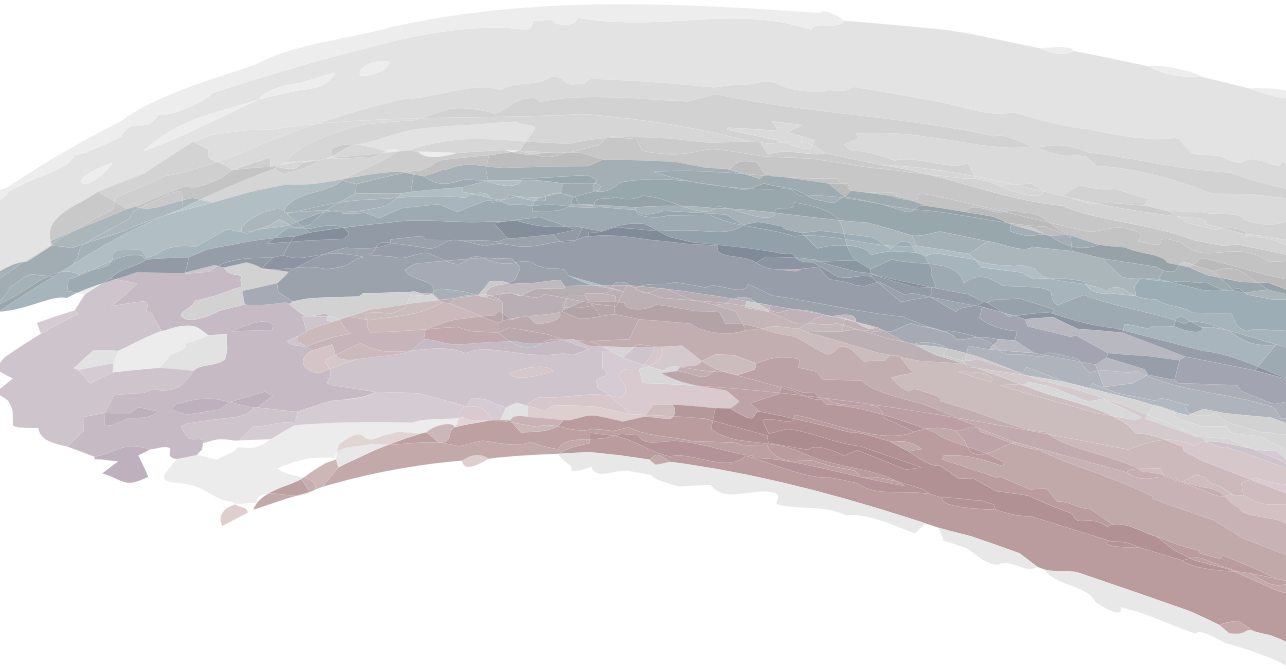

CHAPTER 5

GENERAL DISCUSSION

Frontotemporal dementia (FTD) is a form of early onset dementia, characterized by heterogeneous clinical presentations and underlying disease mechanisms. FTD is highly heritable, with three major autosomal dominant genetic causes, consisting of mutations in the microtubule associated protein tau (*MAPT*) or progranulin (*GRN*) gene, and a repeat expansion in the chromosome 9 open reading frame 72 (*C9orf72*) gene [1, 2]. In the Dutch FTD Risk Cohort (FTD-RisC), we follow cognitively healthy first degree relatives of FTD patients with a known genetic mutation, who are therefore 50% at risk for inheriting the same mutation. Longitudinal research with presymptomatic at-risk subjects allows investigation of the cascade of pathophysiological changes in the presymptomatic and eventually symptomatic stage, as well as development of biomarkers for onset prediction, diagnosis, prognosis, disease monitoring, and disease progression. Neuroimaging techniques such as structural and functional MRI are ideal non-invasive methods to study the changing brain, enabling research into different brain structures and regions. In this thesis, I have focused on three main topics for neuroimaging research in presymptomatic FTD mutation carriers. I aimed to determine genotypic imaging signatures, investigate temporal trajectories of brain change, and address and overcome methodological challenges in neuroimaging research.

GENOTYPIC IMAGING SIGNATURES IN PRESYMPTOMATIC GENETIC FTD

At the start of this thesis in 2015, a few studies already started neuroimaging research in genetic FTD. It was shown that grey matter changes appeared in *GRN* mutation carriers before symptom onset [3], cortical thinning emerged in presymptomatic *C9orf72* repeat expansion carriers [4], and white matter changes had been found in our baseline study with presymptomatic *GRN* and *MAPT* mutation carriers [5]. However, large-scale longitudinal neuroimaging cohorts examining genotypic imaging signatures were still lacking, which I aimed to investigate in this thesis.

GRN

My research showed that little grey and white matter changes occur in the presymptomatic stage of *GRN* mutation carriers (Chapter 3.1), until a few years before symptom onset (Chapter 3.2). In a review of current literature, it appears that very few studies have been able to detect grey matter changes in group-wise comparisons with non-carriers (Chapter 4.1), and also longitudinally, grey matter is not significantly changing in presymptomatic *GRN* mutation carriers compared with non-carriers (Chapter 3.1). Whenever grey matter changes were found in *GRN* mutation carriers, these were mostly located in the frontal, temporal, and parietal lobe (Chapter 4.1). Yet, from two years before symptom onset, grey matter atrophy emerged and progressed quickly, accompanied by a decrease in white matter integrity (Chapter 3.2). This might indicate that the disease progresses rapidly and therefore, the conversion stage from presymptomatic to symptomatic is short.

In Chapter 2.1 we demonstrated that the first pathophysiological changes in FTD-*GRN* are captured by an increase in neurofilament light chain (NfL) levels and regional degeneration of white matter integrity, derived from diffusion tensor imaging (DTI), before grey matter atrophy (Chapter 2.1). Our results demonstrate the importance of white matter biomarkers for *GRN*. For example, increasing evidence suggests white matter damage in *GRN* mutation carriers [6-9], even in the presymptomatic stage [6]. However, white matter hyperintensities are not present in all *GRN* patients [9], leaving the exact pathophysiological mechanism and mediating factors unknown.

Behavioral variant FTD (bvFTD) and non-fluent variant primary progressive aphasia (nfvPPA) are the two major clinical phenotypes of FTD-*GRN* [10]. We examined phenotypic disease progression models within FTD-*GRN* (Chapter 2.1). For nfvPPA patients, the model estimated that NfL levels and cognitive domains became abnormal in early disease stages, and a decrease in white matter integrity and volumetric grey matter loss followed at a more advanced stage. Interestingly, only left-sided tracts and regions were affected, compatible with the strong involvement of the left hemisphere in language disorders [11, 12]. For bvFTD subjects, the estimated biomarker cascade and disease severity correlation were uncertain, complicated by the large pathophysiological heterogeneity (i.e. dominant side of atrophy) and small sample of MRI scans. This heterogeneity is concordant with a study from Young and colleagues [13], who indicated two typical atrophy progression patterns in FTD-*GRN*: asymmetrical (left) or symmetrical with involvement of frontal, temporal and parietal regions.

MAPT

In presymptomatic *MAPT* mutation carriers, we consistently found cortical thinning of the temporal lobes (Chapter 3.1, 4.1), and white matter degeneration occurs in tracts connecting the temporal lobes with the frontal lobe (Chapter 3.1), and in the uncinate fasciculus, a tract connecting the frontal lobe with the insula (Chapter 3.2). Our findings align well with other studies in presymptomatic *MAPT* mutation carriers. In the Genetic Frontotemporal dementia Initiative (GENFI) cohort, early involvement of the hippocampus, amygdala, and temporal lobe was demonstrated in *MAPT* mutation carriers [14]. DTI studies have found an increase in diffusivity in presymptomatic *MAPT* mutation carriers in proximity to symptom onset in the anterior temporal cortex [15] and uncinate fasciculus [16] compared with healthy non-carriers.

Accordingly, we highlighted the potential of white matter integrity decline in the uncinate fasciculus and genu of the corpus callosum as biomarkers for FTD disease onset, as well as grey matter volume loss of the left cingulate cortex, in Chapter 3.2. In eight mutation carriers (*MAPT* and *GRN*) that converted to clinical FTD, changes within the white matter integrity

and grey matter volume of these regions were significant predictors of symptom onset with high sensitivity and specificity, while the diagnostic performance of grey matter biomarkers was considerably lower. In fact, recent machine learning classification studies confirmed the importance of white matter measures in combination with grey matter volumetric data for both sporadic and genetic FTD [17-19].

The anatomical pattern of brain degeneration correlates strongly with common clinical features of FTD-*MAPT*. Disinhibited behaviors may be more profound in *MAPT* patients than in *GRN* and *C9orf72* repeat expansion patients [20], and have been correlated with thinning of the right parahippocampal gyrus and orbitofrontal cortex and decreased white matter integrity of the right uncinate fasciculus, indicating a distinct disinhibition network [21]. Furthermore, anterior temporal lobe atrophy has been associated with semantic memory problems [22], which is another profound clinical symptom in *MAPT* [20].

C9orf72

Very early structural brain changes are found in different *C9orf72* presymptomatic cohorts (Chapter 4.1), indicating a genuine presymptomatic pathophysiological difference between *GRN* and *C9orf72* genotypes, despite their shared association with trans-activation response element (TAR) DNA-binding protein 43 (TDP-43) pathology [1]. In our cohort, we demonstrated smaller grey matter volume of the thalamus, cerebellum and cortical regions in presymptomatic *C9orf72* repeat expansion carriers compared to non-carriers (Chapter 2.2), which remained stable over two years of follow up (Chapter 3.1). This aligns well with studies suggesting that the trajectory of brain change in presymptomatic *C9orf72* repeat expansion carriers is slowly progressive, and may take decades [14, 16, 23]. Moreover, it has been proposed that early brain differences in presymptomatic *C9orf72* repeat expansion carriers might result from a neurodevelopmental deficit [4, 24]. Thalamic volume loss could potentially be indicative of FTD in *C9orf72* repeat expansion carriers, as previous research separating *C9orf72* phenotypes discovered that thalamic atrophy was present in bvFTD and FTD – amyotrophic lateral sclerosis (ALS) patients, but not in patients with only ALS [25].

In the white matter, changes in diffusion metrics were found widespread throughout the brain, when compared to non-carriers. These changes were also stable over a two year period (Chapter 3.1). Previous diffusion studies in *C9orf72* repeat expansion carriers suggested longitudinal change in the cingulum, uncinate fasciculus in patients with an bvFTD phenotype [26], and in the corticospinal tracts in patients with ALS [27]. Although the spatial pattern of diffusion changes in our presymptomatic cohort is difficult to interpret with respect to future phenotypes, the extent of the diffusion changes compared with the subtle grey matter atrophy suggests that diffusion biomarkers derived from DTI may be more sensitive to early disease related change than grey matter atrophy.

Modelling pathophysiological change in *C9orf72* repeat expansion carriers is very complicated, due to the heterogeneity in age at symptom onset, clinical phenotype, and rate of progression. For example, the two major clinical phenotypes are ALS and bvFTD [28, 29], but patients can also present with psychiatric disorders or symptoms resembling Alzheimer's disease [30]. We investigated the pathophysiological relation between neuroimaging biomarkers and cognitive biomarkers in presymptomatic *C9orf72* repeat expansion carriers in Chapter 2.2. In this baseline characterization of our *C9orf72* cohort, differences in white matter integrity, grey matter volume, and executive functioning were found. However, there was no neuroanatomical correlation between the decline in executive functions and grey matter regions or white matter tracts. In contrast, letter fluency – a cognitive task associated with language and executive functioning domains [31] – was previously associated with degeneration within parts of the orbitofrontal and motor cortex in *C9orf72* repeat expansion patients [25]. Future elucidation of the neuroanatomical substrates of clinical symptoms in the spectrum of the *C9orf72* repeat expansion may be aided by modelling the major phenotypes separately. As *C9orf72*-ALS patients progress faster when cognitive deficits emerge [29], understanding the clinico-spatial relationship of symptoms could also aid individual prediction of disease progression.

In this thesis, I demonstrated, in concordance with previous studies [32], that the neuroimaging signatures of the three main genotypes of FTD are significantly different. In clinical practice, recognition of the distinct genotypic atrophy patterns might aid differential diagnosis, especially when a possible FTD is suspected. In research, studies in the presymptomatic stage of FTD that pool genotypes into a single FTD mutation carrier population in order to increase sample size, are hampered by the genotypic pathophysiological heterogeneity, and are therefore less reliable and relevant for clinical practice. Although sample sizes for each genotype may be small, investigating all genotypes separately would lead to a more in depth understanding of underlying disease mechanisms [33].

TEMPORAL TRAJECTORIES OF BRAIN CHANGE

In multiple neurodegenerative conditions, longitudinal neuroimaging studies are increasingly used to analyze brain alterations in vivo [34]. Study designs and hypotheses for longitudinal neuroimaging studies in FTD have been inferred from previous successful cohorts such as the Alzheimer Disease Neuroimaging Initiative (ADNI) [35, 36], the Dominant Inherited Alzheimer Network (DIAN) [37-39], and track Huntington's Disease (TrackHD) [40, 41]. With longitudinal research, we investigate the disease process of genetic FTD and the conversion from presymptomatic to the symptomatic stage.

Presymptomatic to symptomatic stage

Results from longitudinal research in this thesis suggest that approximately two years before symptoms emerge, degeneration of frontotemporal grey and white matter tissue accelerates and may therefore announce symptom onset in *MAPT* and *GRN* mutation carriers (Chapter 3.2). Furthermore, a subtle decrease in cognitive functioning was demonstrated in the same cohort, also evolving around the same time-point [31]. In contrast, in *C9orf72* repeat expansion carriers, changes in grey and white matter arise much earlier and slowly gradually progress over decades, as discussed above (Chapter 3.1).

The GENFI cohort and other cross-sectional studies proposed a different progression timeline of neuroanatomical change, where grey matter changes in *MAPT* mutation carriers started about fifteen years before estimated symptom onset [14], and white matter integrity decreases around three years before onset, although the timeframe of diffusion changes was difficult to interpret due to the small sample size [16]. Grey matter volume in *GRN* mutation carriers decreased ten years before expected symptom onset, especially in the insula [14, 42], with simultaneous change in white matter integrity [16]. For *C9orf72* repeat expansion carriers, grey matter volume declined much earlier, approximately 25 years before onset [14, 23], and changes in white matter integrity occurred from 30 years before onset [16].

However, the abovementioned studies modelled biomarkers with mixed effect models using cross-sectional data, and estimated age to symptom onset. For autosomal dominant AD, age at onset is highly correlated with familial age at onset, which justifies the individual prediction of age at symptom onset based on the average familial age at onset [43]. Although previous research in genetic FTD used estimated age at onset to model cross-sectional data [14, 16, 23, 42, 44], we know that age at onset is variable even within families, especially in the *GRN* and *C9orf72* genotypes [45]. Moreover, a world-wide study demonstrated the lack of correlation between familial age at onset and actual age at onset [Moore *et al.,* 2019 *in press*]. Therefore, modelling longitudinal biomarker change and defining the conversion stage of genetic FTD needs a different procedure.

In this thesis, we have used two different but effective approaches for modelling of neuroimaging biomarkers. In Chapter 3.2, we used the actual age at symptom onset in a group of eight subjects that converted to the symptomatic stage during follow up. Using the actual age of onset enables exact modelling of individual trajectories, which of course, is the optimal study design [33]. However, waiting for mutation carriers to convert is time consuming and susceptible to small sample sizes. In Chapter 2.1, we used discriminative event based modelling, a data-driven disease progression model that estimates the cascade of biomarker change, on the basis of cross-sectional data. In this way, using age as a predictor of expected or actual age at onset is no longer necessary [46].

Cascade of biomarker change

By using data-driven disease progression models, the timeline of disease progression for a certain genotype, phenotype, or underlying pathology can become more clear. The DIAN study demonstrated the cascade of biomarker change in presymptomatic carriers of AD mutations [37, 39, 47]. The trajectory of change in autosomal dominant AD from healthy to symptomatic stages may take up to 25 years, with slow gradual progression, starting with decrease of amyloid-beta levels in the cerebrospinal fluid [37, 39], followed by an increase of amyloid-beta deposition in the brain, grey matter atrophy, and tau protein levels in the CSF approximately 15 years before symptom onset. The pathophysiological change takes decades before the first subtle cognitive changes emerge.

In Chapter 2.1, we modelled multimodal biomarkers (fluid, imaging, and cognitive) for *GRN* mutation carriers, herewith considering all available information in a dynamic model, instead of using arbitrary cut-off scores for all biomarkers individually. With this multimodal approach, the temporal sequence of biomarker change for *GRN* could be estimated. We demonstrated that neurofilament light chain (NfL), white matter integrity measurements and impairments in attention and processing speed show early changes in FTD-*GRN*. The combination of increased NfL levels, white matter degeneration and cognitive dysfunction, i.e. slower processing speed, confirms early axonal degeneration in FTD-*GRN.* Next, grey matter regions connected by specific white matter tracts lose volume. This follows the hypothesis that the disease process spreads in a network-based pattern [42, 48, 49], where connectivity is lost (i.e. axonal degeneration) and afterwards, grey matter will be affected (Wallerian degeneration [50]).

The discriminative event based model was previously applied to sporadic AD [51], and demonstrated that MCI subjects converting to clinical AD had higher disease severity scores than MCI non-converters. With a similar model, we identified presymptomatic *GRN* subjects with biomarker profiles developing towards abnormality. These subjects showed high estimated disease severity scores, and may be vulnerable for approaching symptom onset. Through the use of disease progression models, the conversion from the presymptomatic into symptomatic FTD or 'MCI-stage' can potentially be based on the full biomarker profile instead of observed impairments in behavior or cognition. However, longitudinal data is needed to confirm whether the presymptomatic subjects with high estimated disease severity scores will develop symptoms.

Functional versus structural imaging

While structural FTD-related brain changes may remain undetected until the last few years before symptom onset, research in autosomal dominant AD demonstrated that functional neuroimaging changes precede structural neuroimaging changes [37, 39, 52]. For

example, fluorodeoxyglucose positron emission tomography scans (FDG-PET), can indicate hypometabolism in the brain before grey matter atrophy is present [52]. This leads to the hypothesis that functional changes may precede structural changes in genetic FTD as well [53]. Our previous arterial spin labeling (ASL) study with *MAPT* and *GRN* mutation carriers [54] demonstrated that cerebral blood flow (CBF) was lower two years prior to symptom onset in two mutation carriers (one *MAPT*, one *GRN*) that converted to bvFTD. This, however, would suggest that functional change in *MAPT* and *GRN* carriers may occur simultaneously with the grey and white matter degeneration observed in Chapter 3.2. We built upon that first ASL study in Chapter 3.3, with inclusion of *C9orf72* repeat expansion carriers, larger sample sizes, and more converters to the symptomatic FTD stage, to investigate the trajectory of functional change in the disease timeline of genetic FTD. Despite elaborate methodological hardships, we observed a trend of normalized CBF decline in the left insula in *MAPT* converters, the right frontal lobe and insula in *GRN* converters (Chapter 3.3). As regional CBF remained stable in presymptomatic *MAPT* and *GRN* mutation carriers, we hypothesize that perfusion changes show the same temporal trajectory as structural brain changes in these mutation groups (Chapter 3.2 and 3.3).

We found an association of higher age and lower normalized CBF in presymptomatic *C9orf72* repeat expansion carriers in the bilateral insular region and right frontal lobe (Chapter 3.3). Although these results are still preliminary, it seems that the lifelong decrease of CBF in presymptomatic *C9orf72* repeat expansion carriers fits with a recent cross-sectional ASL study within GENFI. Decreased perfusion was found in several brain regions before estimated symptom onset [44]. Though the use of estimated age at onset clouds the results, the GENFI study showed that decreased perfusion was most pronounced in the *C9orf72* repeat expansion carriers, and started around 12.5 years before expected age at onset. In the same cohort, volumetric insular changes in *C9orf72* repeat expansion carriers were observed at 25 years before expected age at onset [14], and white matter integrity changes occurred at least 30 years before onset [16]. This would suggest that functional changes do not precede structural changes, at least not in *C9orf72* repeat expansion carriers. The interrelation between changes in grey matter, white matter, and CBF in the various GENFI studies could also be misinterpreted, due to the use of estimated age at symptom onset.

The temporal and spatial trajectories of brain changes in genetic FTD remains somewhat inconclusive. In *C9orf72* repeat expansion carriers, structural and functional brain change may span over decades before symptom onset, but the exact timing of change and its interrelation is difficult to interpret due to the use of expected age at onset in various studies. For *GRN* and *MAPT* mutation carriers, this thesis demonstrates fast progressive grey and white matter degeneration in carriers converting from presymptomatic to symptomatic stages, possibly simultaneously accompanied by functional change. Future longitudinal

research may focus on temporal and spatial relations between multimodal neuroimaging markers, both in genotypic and phenotypic disease progression models.

METHODOLOGICAL CHALLENGES IN NEUROIMAGING RESEARCH

Large-scale research into presymptomatic FTD mutation carriers calls for longitudinal multi-center cohorts, in order to increase sample sizes and statistical power. However, the obvious challenge of longitudinal imaging and evolving multi-center cohorts, as well as in therapeutic trials, is handling the MRI acquisition and available data properly. For example, harmonization of hardware differences between sites and within sites is extremely important, as even small variations can overpower subtle pathophysiological effects. Next, also choices in analysis methods need to be made carefully [34, 55].

Hardware harmonization

Clearly, our single-center FTD-RisC cohort with one scanner and stable parameters, has bypassed a great deal of MRI analysis difficulties related to differences in scanners, vendors, and protocols, and therefore, we have created the circumstances for optimal reliability in our neuroimaging studies [33]. However, as we demonstrated in Chapter 4.2, a change in head coils during follow-up compromised the outcome of standard analysis models for several MRI sequences, including but not limited to T1-weighted, diffusion tensor imaging and resting state functional MRI. Although numerous studies have attempted to investigate methods to harmonize MRI sequences with different hardware [56-68], there is no clear, best-practice solution yet. Longitudinal imaging studies with hardware changes are therefore vulnerable for bias and reduced reliability of the study results. We showed a voxel-based method to eliminate the majority of a coil related bias for our study specifically, but also our methods cannot easily be extrapolated to other studies, as these studies would have other acquisition parameters or even other scanner vendors.

Multi-center cohorts such as GENFI, with 26 collaborating sites, are even more prone to MRI variability due to site differences. Previously, the ADNI cohort has accomplished to obtain volumetric imaging across all sites with comparable parameters and quality [69]. Adapting the guidelines from ADNI not only decreases between-site variation for new multi-center studies, as for example in the familial FTD cohort of the United States (LEFFTDS) [70], it also aids standardization and comparison between neurodegenerative cohorts. However, not only multi-center differences need harmonization, also within-center variability related to hardware (Chapter 4.2) and software changes (Chapter 3.1) are harmful and introduce bias. Especially for studies involving presymptomatic FTD, where brain changes can still be subtle and validation cohorts are scarce, researchers need to be aware of possible false results caused by methodological variation.

More problematic is the acquisition and harmonization of DTI, as we discussed in Chapter 4.2. The most striking differences between head coils were lateralized and asymmetrical, leaving us without a reasonable explanation for the observed effect. Other studies also showed that consecutive scanning on the same day, same scanner, and same parameters may not result in identical images [71-74]. Even more so, multi-center DTI is vulnerable for noise introduced by variations in parameters, and needs substantial technical development prior to clinical implementation for FTD [16, 33]. Currently, the application of ComBat [53] is one of the promising harmonization methods in multi-parameter diffusion studies. Although considerable efforts towards multi-site harmonization are being made, the reliability of longitudinal and multi-center DTI studies remains subject of debate.

Also for arterial spin labeling, many obstacles are still to overcome. 3-dimensional pseudo-continuous ASL series are increasingly common across vendors [75], but harmonization in longitudinal settings or multi-site studies is incredibly complicated. In Chapter 3.3, we presented ten year of ASL follow up data from the FTD-RisC study, and the methodological issues that came along with it. For example, we made slight adaptions to our protocol, by changing the data type, switching head coils, and a mandatory software update on the scanner. These variations have hampered processing of the data. Furthermore, harmonization of multi-site ASL is hampered by differences in read-out modules at acquisition level and choice of registration method at analysis level [76, 77]. Our and previous studies imply that ASL acquisition and processing needs further development in terms of intra-subject reliability and reproducibility in order to optimize longitudinal and multi-center analyses.

Longitudinal imaging analysis

Even the smallest changes in MRI parameters may be harmful for longitudinal research, as it introduces variability with huge consequences. A software change on the MRI scanner in Chapter 3.1 was controlled for by covariates, to decrease the bias in follow up images from subjects that were scanned after the software update [78].

In Chapter 3.3, we showed the many challenges of longitudinal ASL and the questionable reliability of absolute CBF values. We described our attempts to harmonize longitudinal CBF data from a single site. In contrast to previous studies, absolute CBF measurements were not stable over time [79-81]. We normalized CBF data to reduce everyday physiological variability in ASL acquisition and quantitative assessment, such as the positioning of subjects, slice positioning, time of scanning, and medicine use [82-84]. However, the longitudinal normalized CBF trajectories were still characterized by fluctuations between time-points. Previous ASL studies pointed out that CBF is severely influenced by multiple factors, such as moment of scanning, positioning of the subject in the MRI scanner, slice positioning, use of caffeine, use of medicines, and so forth [82-85]. Therefore, longitudinal analyses with

regional CBF cannot be performed without controlling for these common characteristics.

Furthermore, longitudinal analyses with neuroimaging data are complicated. Regarding whole brain analyses, common longitudinal statistical models are based on either the amount of change or the rate of change. For analysis of the amount of change in a certain mutation group compared with non-carriers, we extracted follow up images from baseline images in Chapter 3.1 and 3.2, and determined whether the mutation carriers showed more change in grey matter volume or white matter integrity than non-carriers. However, if the interest is to compare the rate of change between groups, we could compare the slopes rather than the absolute volume. Focusing on the rate of change would be interesting to unveil for example the temporal trajectory of a specific genotype or phenotype. Perhaps this might be more appropriate to model with mixed effects models, instead of voxel-wise t-statistics on a group level, as mixed effects models deliver more information than just the significant difference between slopes at a certain spatial location [34]. For example, with non-linear modelling, acceleration or deceleration of change at a specific moment in time can be demonstrated. I have not used non-linear modelling for the trajectories of brain change in genetic FTD, as I aimed to locate the regions of brain change without a priori assumptions first, but may do so in upcoming projects.

Variability related to software packages

Neuroimaging biomarkers are also important for clinical trials. As therapeutic trials become increasingly relevant for genetic FTD [86-88], optimal study design and consensus on (neuroimaging) biomarkers is crucial. For example the choice of software algorithm, which I addressed in Chapter 4.1. We exposed inconsistencies in results from different software packages for each of the three major genotypes, despite using an identical sample and default algorithm parameters. An important contributor to these inconsistencies may be the difference in segmentation protocol. The Statistical Parameter Mapping (SPM) software [89] has performed best in brain segmentation according to literature [90-92]. Especially in presymptomatic FTD mutation carriers, where grey matter atrophy is often still subtle, optimal segmentation is crucial to detect true anatomical change.

For *MAPT* mutation carriers, we discovered that cortical thickness analyses were more sensitive than voxel-based morphometry for temporal lobe degeneration (Chapter 3.1 and 4.1). Therefore, we suggested that cortical thickness methods could be more appropriate for *MAPT* mutation carriers (Chapter 4.1). The benefits of cortical thickness analyses for (behavioural variant) FTD has been discussed before [93], after comparing origins of grey matter differences in bvFTD and Alzheimer's disease. As VBM is based on a mixture of cortical surface, folding and thickness measures, it could be less sensitive than solely cortical thinning [94-96], and therefore potentially less sensitive to the earliest grey matter changes

in presymptomatic *MAPT* mutation carriers. It could be worthwhile to investigate whether cortical thickness analyses or VBM is the most sensitive method for capturing grey matter change caused by FTD pathology, in different genotypes and phenotypes.

In Chapter 4.1, I estimated the required sample sizes to detect grey matter differences between presymptomatic mutation carriers and non-carriers when using different neuroimaging software packages. For *MAPT* mutation carriers, the smallest sample size was estimated by using FreeSurfer software for measuring the thickness of the left temporal lobe (n=42). For *GRN* mutation carriers, the volume of the temporal lobe measured by SPM resulted in the smallest estimated sample size (n=152). For *C9orf72* repeat expansion carriers, using SPM for the volume of the left parietal lobe led to the smallest sample size (n=61). We demonstrated that each mutation group needs its own approach for neuroimaging biomarker and measurement selection to reach optimal design of the clinical trial.

My research in Chapter 4.1 regarding the sensitivity of grey matter analysis methods in the different mutation groups emphasizes the need for genotype dependent approaches when choosing analysis methods, instead of 'one size fits all'. As each software package also has its own algorithm for longitudinal analyses [97], the sensitivity of these longitudinal algorithms in presymptomatic and early symptomatic FTD mutation carriers is still unclear, and needs further investigation before recommendations can be made.

Choices in analysis

The list of factors in study design for neuroimaging analyses that possibly affect outcome and comparability with other studies is long. In my review of previous grey matter studies, I have shown that studies also differ in their use of confounding factors (Chapter 4.1). For example, analyses are commonly corrected for the effect of age and sex [5, 98, 99], and often also for head size (i.e. total intracranial volume) [24, 100, 101]. Some studies also chose to correct for kinship [4, 32]. However, using multiple confounding factors in small sample sizes decreases power [102]. Next, even though voxel-wise analyses are subject to high false positive rates [89, 103], some studies omit multiple comparisons correction [104, 105], which could lead to an overestimation of brain differences through multiple testing. Without insights into the effects of controlling for confounding factors in neuroimaging analysis versus the effects of not controlling, we cannot exactly know how these factors influence the outcome, and that reduces the comparability across cohorts.

The rapidly advancing quality of neuroimaging biomarkers has secured the utility of neuroimaging in clinical practice for FTD [19, 106, 107]. Depicting the brain with traditional sequences such as T1-weighted imaging and possibly also functional imaging like ASL provides insights in focal changes in the brain, while various quantitative measurements can aid diagnostic and prognostic accuracy for clinical practice and optimization of clinical

trial design. However, in this thesis, I demonstrated that differences in hardware, software, and analyses strategies complicate the generalizability of neuroimaging findings, which is disadvantageous for research in rare diseases such as genetic FTD. Especially longitudinal and multi-center studies investigating presymptomatic FTD mutation carriers are susceptible, as brain changes are still subtle and the reliability of results may be affected by methodological variation.

THE ROAD TO CLINICAL IMPLEMENTATION

In order to apply the findings of this thesis in daily clinical practice and upcoming clinical trial design, a number of issues are important to consider for the development of quantitative biomarkers for genetic FTD.

Sequence optimization

The T1-weighted scan is widely incorporated in both clinical practice and neurodegenerative research since numerous years [108, 109]. It allows assessment of structural changes and atrophy in the brain, currently using qualitative scales such as the medial temporal lobe atrophy scale [110, 111]. However, qualitative appreciation of atrophy is always dependent on the eye of the beholder, and is therefore not uniform. Especially for rare young onset diseases such as genetic FTD, distinguishing abnormal from normal brain ageing can be quite complex [112, 113]. Recently, the Rotterdam study developed an exciting application for quantitative volumetric imaging for individual patients from the memory clinic. Using reference data from almost 5000 healthy subjects, the volumes of several brain regions of an individual patient can be assessed for relative normality or abnormality [112]. When these relative quantitative assessment were combined with regular visual rating of atrophy, diagnostic accuracy improved for AD patients [112]. Also, normative values for subcortical structures were interchangeable across several reference cohorts [113]. However, reference data did not improve diagnostic accuracy for FTD yet [112]. One explanation could be that only volumetric measurements based on T1-weighted imaging are currently feasible with normative reference data. As we thoroughly discussed in this thesis, other measurements could be more sensitive for early stage FTD, such as white matter integrity derived from DTI.

Acquisition of DTI within neurodegenerative MRI protocols is rising, but the evaluation for individual patients is running behind. Assessment of white matter degeneration is often still based on FLAIR images, which may reveal gross pathology and white matter hyperintensities [114, 115]. However, early, subtle changes may then be overlooked. Several advanced DTI sequences are upcoming, such as multi-shell constrained spherical deconvolution [116]. With these relatively new techniques, white matter pathology can be studied with much more detail [116, 117]. Another advantage of constrained spherical deconvolution is the reduced

uncertainty of the diffusion direction in crossing-fibres [118], which is a well-known problem of DTI. While increasing evidence advocates the clinical value of DTI-derived biomarkers for diagnosis and prognosis of FTD, the methodological challenges for quantitative DTI biomarkers are complicated. As discussed above, a lot of variability within and between studies have been demonstrated, sometimes successfully harmonized [67, 73], but mostly without good solutions for routine application [63, 64, 66, 74, 119, 120]. Enhancing the quality of DTI acquisition and harmonization might be a first step towards the right direction.

Qualitative assessment of diffusion tensor imaging is already incorporated in the work-up for multiple neurological conditions. For example, DTI-based tractography can be used for surgical planning [121], demonstrating the clinical potential of DTI derived biomarkers for an individual patient. Also, the UK Biobank made averaged tractography images based on more than 4000 images publicly available [122], therefore paving the way to relative appreciation of white matter tracts from individual patients. When, if ever, DTI-related methodological challenges are history, and consensus on analysis methods is reached, implementing quantitative biomarkers relative to reference data could improve diagnostic trajectories for FTD tremendously.

Regarding ASL-MRI, we showed that even in a single center study, CBF measures within and between subjects are heavily susceptible to everyday variation in acquisition. Furthermore, a longitudinal multimodal study showed that ASL was less useful than for example DTI as longitudinal clinical trial endpoint in several FTD phenotypes [87]. Therefore, ASL-MRI might be less suitable as longitudinal neuroimaging biomarker for FTD, despite its potential benefits for clinical application compared to, for example FDG-PET imaging [123-126]. Instead, previous ASL studies showed that qualitative assessment of perfusion in the anterior cingulate could discriminate FTD from other neurodegenerative conditions and controls [124, 127]. Therefore, the clinical value of ASL for FTD may lie in qualitative assessment rather than quantitative measurements, at least until substantial improvements in ASL acquisition, harmonization, and processing are realized.

Recommendations for analyses

Next, standardization of analyses in genetic FTD cohorts and studies is imperative, especially when quantitative neuroimaging biomarkers are implemented in clinical practice. In this way, comparisons between individuals and the world-wide genetic FTD population is allowed for, and tracking of individual disease progression can then be evidence-based. In Chapter 4.1, we started drawing up recommendations for the choice of software analyses per mutation group for grey matter volumetric measurements. However, not only the choice of software method, but also the choice of region of interest for each mutation group should be reviewed. Again, we started in Chapter 4.1 with evidence-based regions of interest,

based on voxel-wise presymptomatic studies. This work may be continued, for example by conducting a voxel-wise meta-analysis, and by incorporating symptomatic cohorts as well. With consensus on the earliest affected brain regions, longitudinal modelling of brain degeneration becomes easier, as the risk of omitting unexpected brain atrophy decreases. Also, recommendations for standardization of longitudinal grey matter analyses as well as white matter integrity (using DTI) are not yet available, and may be reviewed in future studies. For example, the clinical value of DTI may be enhanced by using tractography, as consideration of the entire white matter tract could be more sensitive for subtle changes then a skeleton-based approach such as tract-based spatial statistics [128, 129]. However, the disadvantage of tractography is the manual predefinition of seed and target regions of interest for the white matter tract, and the choice of tracking method, which decreases its utility in clinical practice [130]. These differences between analysis methods for DTI in (genetic) FTD need to be reviewed to provide evidence-based recommendations.

The multimodal approach

Last, integrating information from multimodal neuroimaging biomarkers is needed to uncover the temporal and spatial progression of disease related brain changes. For example, extending the spatial progression model of Young et al [13] with incorporation of DTI next to grey matter volume, and possibly functional imaging could reveal genotypic and phenotypic progression patterns. Also, combining neuroimaging markers with fluid and cognitive biomarkers is needed to identify relationships between earliest disease related changes, and determining the temporal relation between biomarkers. For example, a dynamic disease progression model as used in Chapter 2.1 allows for appreciation of entire biomarker profiles. By implementing models like discriminative event based modelling [46, 51] in clinical practice, individual prognosis can be estimated for all genetic FTD mutation carriers.

CONCLUSION

In conclusion, in this thesis I have demonstrated that the three major genotypes of familial FTD have distinct neuroimaging signatures, that reflect distinct underlying disease mechanisms. Longitudinally, the trajectories of grey and white matter changes in *MAPT* and *GRN* may be short and fast progressive, with rapid change in a few years before symptom onset, while brain changes *C9orf72* repeat expansion carriers may gradually progress, spanning over decades. Last, I have focused on methodological hardships and provided recommendations for acquisition, harmonization, and analysis of MRI in longitudinal studies into genetic FTD. Implementation of quantitative neuroimaging biomarkers for genetic FTD should be focused on complementary, multimodal assessments, for example both grey and white matter measurements, but incorporation of cognitive and fluid biomarkers also

showed important benefits in my research. Neuroimaging biomarkers enable appraisal of both spatial and temporal brain alterations, and are therefore extremely valuable for clinical practice and research with genetic FTD.

REFERENCES

1. Lashley, T., et al., Review: an update on clinical, genetic and pathological aspects of frontotemporal lobar degenerations. Neuropathol Appl Neurobiol, 2015. 41(7): p. 858-81.
2. Blauwendraat, C., et al., The wide genetic landscape of clinical frontotemporal dementia: systematic combined sequencing of 121 consecutive subjects. Genet Med, 2018. 20(2): p. 240-249.
3. Caroppo, P., et al., Lateral Temporal Lobe: An Early Imaging Marker of the Presymptomatic GRN Disease? J Alzheimers Dis, 2015. 47(3): p. 751-9.
4. Walhout, R., et al., Brain morphologic changes in asymptomatic C9orf72 repeat expansion carriers. Neurology, 2015. 85(20): p. 1780-8.
5. Dopper, E.G., et al., Structural and functional brain connectivity in presymptomatic familial frontotemporal dementia. Neurology, 2014. 83(2): p. e19-26.
6. Sudre, C.H., et al., White matter hyperintensities are seen only in GRN mutation carriers in the GENFI cohort. Neuroimage Clin, 2017. 15: p. 171-180.
7. Ameur, F., et al., White matter lesions in FTLD: distinct phenotypes characterize GRN and C9ORF72 mutations. Neurol Genet, 2016. 2(1): p. e47.
8. Paternico, D., et al., White matter hyperintensities characterize monogenic frontotemporal dementia with granulin mutations. Neurobiol Aging, 2016. 38: p. 176-180.
9. Caroppo, P., et al., Extensive white matter involvement in patients with frontotemporal lobar degeneration: think progranulin. JAMA Neurol, 2014. 71(12): p. 1562-6.
10. Alexander, C., D. Pisner, and C. Jacova, Predementia Brain Changes in Progranulin Mutation: A Systematic Review of Neuroimaging Evidence. Dement Geriatr Cogn Disord, 2019. 47(1-2): p. 1-18.
11. Grossman, M., The non-fluent/agrammatic variant of primary progressive aphasia. Lancet Neurol, 2012. 11(6): p. 545-55.
12. Rohrer, J.D. and H.J. Rosen, Neuroimaging in frontotemporal dementia. Int Rev Psychiatry, 2013. 25(2): p. 221-9.
13. Young, A.L., et al., Uncovering the heterogeneity and temporal complexity of neurodegenerative diseases with Subtype and Stage Inference. Nat Commun, 2018. 9(1): p. 4273.
14. Rohrer, J.D., et al., Presymptomatic cognitive and neuroanatomical changes in genetic frontotemporal dementia in the Genetic Frontotemporal dementia Initiative (GENFI) study: a cross-sectional analysis. Lancet Neurol, 2015. 14(3): p. 253-62.
15. Chen, Q., et al., Tracking white matter degeneration in asymptomatic and symptomatic MAPT mutation carriers. Neurobiol Aging, 2019. 83: p. 54-62.
16. Jiskoot, L.C., et al., Presymptomatic white matter integrity loss in familial frontotemporal dementia in the GENFI cohort: A cross-sectional diffusion tensor imaging study. Ann Clin Transl Neurol, 2018. 5(9): p. 1025-1036.
17. Bouts, M., et al., Single Subject Classification of Alzheimer's Disease and Behavioral Variant Frontotemporal Dementia Using Anatomical, Diffusion Tensor, and Resting-State Functional Magnetic Resonance Imaging. J Alzheimers Dis, 2018. 62(4): p. 1827-1839.
18. Feis, R.A., et al., Single-subject classification of presymptomatic frontotemporal dementia mutation carriers using multimodal MRI. Neuroimage Clin, 2019. 22: p. 101718.
19. McMillan, C.T., et al., The power of neuroimaging biomarkers for screening frontotemporal dementia. Hum Brain Mapp, 2014. 35(9): p. 4827-40.
20. Snowden, J.S., et al., Distinct clinical and pathological phenotypes in frontotemporal dementia associated with MAPT, PGRN and C9orf72 mutations. Amyotroph Lateral Scler Frontotemporal Degener, 2015. 16(7-8): p. 497-505.
21. Santillo, A.F., et al., Grey and White Matter Clinico-Anatomical Correlates of Disinhibition in Neurodegenerative Disease. PLoS One, 2016. 11(10): p. e0164122.
22. Binder, J.R. and R.H. Desai, The neurobiology of semantic memory. Trends Cogn Sci, 2011. 15(11): p. 527-36.
23. Bertrand, A., et al., Early Cognitive, Structural, and Microstructural Changes in Presymptomatic C9orf72 Carriers Younger Than 40 Years. JAMA Neurol, 2017.
24. Lee, S.E., et al., Network degeneration and dysfunction in presymptomatic C9ORF72 expansion carriers. Neuroimage Clin, 2017. 14: p. 286-297.
25. Floeter, M.K., et al., Longitudinal imaging in C9orf72 mutation carriers: Relationship to phenotype.

Neuroimage Clin, 2016. 12: p. 1035-1043.
26. Mahoney, C.J., et al., Longitudinal diffusion tensor imaging in frontotemporal dementia. Ann Neurol, 2015. 77(1): p. 33-46.
27. Floeter, M.K., et al., Longitudinal diffusion imaging across the C9orf72 clinical spectrum. J Neurol Neurosurg Psychiatry, 2018. 89(1): p. 53-60.
28. Burrell, J.R., et al., The frontotemporal dementia-motor neuron disease continuum. Lancet, 2016. 388(10047): p. 919-31.
29. Patel, A.N. and J.B. Sampson, Cognitive Profile of C9orf72 in Frontotemporal Dementia and Amyotrophic Lateral Sclerosis. Curr Neurol Neurosci Rep, 2015. 15(9): p. 59.
30. Boeve, B.F., et al., Characterization of frontotemporal dementia and/or amyotrophic lateral sclerosis associated with the GGGGCC repeat expansion in C9ORF72. Brain, 2012. 135(Pt 3): p. 765-83.
31. Jiskoot, L.C., et al., Longitudinal cognitive biomarkers predicting symptom onset in presymptomatic frontotemporal dementia. J Neurol, 2018.
32. Cash, D.M., et al., Patterns of gray matter atrophy in genetic frontotemporal dementia: results from the GENFI study. Neurobiol Aging, 2017. 62: p. 191-196.
33. Boeve, B.F. and H.J. Rosen, Multimodal imaging in familial FTLD: phenoconversion and planning for the future. Brain, 2019. 142(1): p. 8-11.
34. Schuster, C., et al., Presymptomatic and longitudinal neuroimaging in neurodegeneration--from snapshots to motion picture: a systematic review. J Neurol Neurosurg Psychiatry, 2015. 86(10): p. 1089-96.
35. Risacher, S.L., et al., Longitudinal MRI atrophy biomarkers: relationship to conversion in the ADNI cohort. Neurobiol Aging, 2010. 31(8): p. 1401-18.
36. Misra, C., Y. Fan, and C. Davatzikos, Baseline and longitudinal patterns of brain atrophy in MCI patients, and their use in prediction of short-term conversion to AD: results from ADNI. Neuroimage, 2009. 44(4): p. 1415-22.
37. Bateman, R.J., et al., Clinical and biomarker changes in dominantly inherited Alzheimer's disease. N Engl J Med, 2012. 367(9): p. 795-804.
38. Moulder, K.L., et al., Dominantly Inherited Alzheimer Network: facilitating research and clinical trials. Alzheimers Res Ther, 2013. 5(5): p. 48.
39. McDade, E., et al., Longitudinal cognitive and biomarker changes in dominantly inherited Alzheimer disease. Neurology, 2018. 91(14): p. e1295-e1306.
40. Tabrizi, S.J., et al., Biological and clinical manifestations of Huntington's disease in the longitudinal TRACK-HD study: cross-sectional analysis of baseline data. Lancet Neurol, 2009. 8(9): p. 791-801.
41. Tabrizi, S.J., et al., Predictors of phenotypic progression and disease onset in premanifest and early-stage Huntington's disease in the TRACK-HD study: analysis of 36-month observational data. Lancet Neurol, 2013. 12(7): p. 637-49.
42. Benussi, A., et al., Clinical and biomarker changes in presymptomatic genetic frontotemporal dementia. Neurobiol Aging, 2019. 76: p. 133-140.
43. Ryman, D.C., et al., Symptom onset in autosomal dominant Alzheimer disease: a systematic review and meta-analysis. Neurology, 2014. 83(3): p. 253-60.
44. Mutsaerts, H., et al., Cerebral perfusion changes in presymptomatic genetic frontotemporal dementia: a GENFI study. Brain, 2019. 142(4): p. 1108-1120.
45. Olszewska, D.A., et al., Genetics of Frontotemporal Dementia. Curr Neurol Neurosci Rep, 2016. 16(12): p. 107.
46. Venkatraghavan, V., Bron, EE, Niessen, WJ, Klein, S, A discriminative event based model for Alzheimer's disease progression modelling. Information Processing in Medical Imaging, 2017: p. 121-133.
47. Kinnunen, K.M., et al., Presymptomatic atrophy in autosomal dominant Alzheimer's disease: A serial magnetic resonance imaging study. Alzheimers Dement, 2018. 14(1): p. 43-53.
48. Seeley, W.W., et al., Neurodegenerative diseases target large-scale human brain networks. Neuron, 2009. 62(1): p. 42-52.
49. Olm, C.A., et al., Longitudinal structural gray matter and white matter MRI changes in presymptomatic progranulin mutation carriers. Neuroimage Clin, 2018. 19: p. 497-506.
50. White, M.A., et al., Sarm1 deletion suppresses TDP-43-linked motor neuron degeneration and cortical spine loss. Acta Neuropathol Commun, 2019. 7(1): p. 166.
51. Venkatraghavan, V., et al., Disease progression timeline estimation for Alzheimer's disease using

discriminative event based modeling. Neuroimage, 2019. 186: p. 518-532.
52. Gordon, B.A., et al., Spatial patterns of neuroimaging biomarker change in individuals from families with autosomal dominant Alzheimer's disease: a longitudinal study. Lancet Neurol, 2018. 17(3): p. 241-250.
53. Rohrer, J.D., et al., Presymptomatic studies in genetic frontotemporal dementia. Rev Neurol (Paris), 2013. 169(10): p. 820-4.
54. Dopper, E.G., et al., Cerebral blood flow in presymptomatic MAPT and GRN mutation carriers: A longitudinal arterial spin labeling study. Neuroimage Clin, 2016. 12: p. 460-5.
55. Smith, S.M. and T.E. Nichols, Statistical Challenges in "Big Data" Human Neuroimaging. Neuron, 2018. 97(2): p. 263-268.
56. Fennema-Notestine, C., et al., Feasibility of multi-site clinical structural neuroimaging studies of aging using legacy data. Neuroinformatics, 2007. 5(4): p. 235-45.
57. Keihaninejad, S., et al., A robust method to estimate the intracranial volume across MRI field strengths (1.5T and 3T). Neuroimage, 2010. 50(4): p. 1427-37.
58. Takao, H., N. Hayashi, and K. Ohtomo, Effect of scanner in longitudinal studies of brain volume changes. J Magn Reson Imaging, 2011. 34(2): p. 438-44.
59. Chen, J., et al., Exploration of scanning effects in multi-site structural MRI studies. J Neurosci Methods, 2014. 230: p. 37-50.
60. Griffanti, L., et al., ICA-based artefact removal and accelerated fMRI acquisition for improved resting state network imaging. Neuroimage, 2014. 95: p. 232-47.
61. Salimi-Khorshidi, G., et al., Automatic denoising of functional MRI data: combining independent component analysis and hierarchical fusion of classifiers. Neuroimage, 2014. 90: p. 449-68.
62. Feis, R.A., et al., ICA-based artifact removal diminishes scan site differences in multi-center resting-state fMRI. Front Neurosci, 2015. 9: p. 395.
63. Mirzaalian, H., et al., Harmonizing Diffusion MRI Data Across Multiple Sites and Scanners. Med Image Comput Comput Assist Interv, 2015. 9349: p. 12-19.
64. Venkatraman, V.K., et al., Region of interest correction factors improve reliability of diffusion imaging measures within and across scanners and field strengths. Neuroimage, 2015. 119: p. 406-16.
65. Pardoe, H.R., et al., Pooling Morphometric Estimates: A Statistical Equivalence Approach. J Neuroimaging, 2016. 26(1): p. 109-15.
66. Pohl, K.M., et al., Harmonizing DTI measurements across scanners to examine the development of white matter microstructure in 803 adolescents of the NCANDA study. Neuroimage, 2016. 130: p. 194-213.
67. Fortin, J.P., et al., Harmonization of multi-site diffusion tensor imaging data. Neuroimage, 2017. 161: p. 149-170.
68. Li, H., Smith, S.M., Gruber, S., Lukas, S.E., Silveri, M.M., Hill, K.P., Killgore, W.D.S., Nickerson, L.D. , Combining Multi-Site/Multi-Study MRI DATA: Linked-ICA Denoising for Removing Scanner and Site Variability from Multimodal MRI data 2018.
69. Jack, C.R., Jr., et al., The Alzheimer's Disease Neuroimaging Initiative (ADNI): MRI methods. J Magn Reson Imaging, 2008. 27(4): p. 685-91.
70. Boeve, B., et al., The longitudinal evaluation of familial frontotemporal dementia subjects protocol: Framework and methodology. Alzheimers Dement, 2019.
71. Lawrenz, M., S. Brassen, and J. Finsterbusch, Microscopic diffusion anisotropy in the human brain: reproducibility, normal values, and comparison with the fractional anisotropy. Neuroimage, 2015. 109: p. 283-97.
72. Veenith, T.V., et al., Inter subject variability and reproducibility of diffusion tensor imaging within and between different imaging sessions. PLoS One, 2013. 8(6): p. e65941.
73. Palacios, E.M., et al., Toward Precision and Reproducibility of Diffusion Tensor Imaging: A Multicenter Diffusion Phantom and Traveling Volunteer Study. AJNR Am J Neuroradiol, 2017. 38(3): p. 537-545.
74. Takao, H., et al., Effect of scanner in longitudinal diffusion tensor imaging studies. Hum Brain Mapp, 2012. 33(2): p. 466-77.
75. Alsop, D.C., et al., Recommended implementation of arterial spin-labeled perfusion MRI for clinical applications: A consensus of the ISMRM perfusion study group and the European consortium for ASL in dementia. Magn Reson Med, 2015. 73(1): p. 102-16.
76. Mutsaerts, H., et al., Comparison of arterial spin labeling registration strategies in the multi-center

GENetic frontotemporal dementia initiative (GENFI). J Magn Reson Imaging, 2018. 47(1): p. 131-140
77. Mutsaerts, H.J., et al., Multi-vendor reliability of arterial spin labeling perfusion MRI using a near-identical sequence: implications for multi-center studies. Neuroimage, 2015. 113: p. 143-52.
78. Takao, H., N. Hayashi, and K. Ohtomo, Effects of the use of multiple scanners and of scanner upgrade in longitudinal voxel-based morphometry studies. J Magn Reson Imaging, 2013. 38(5): p. 1283-91.
79. Yang, F.N., et al., Test-retest reliability of cerebral blood flow for assessing brain function at rest and during a vigilance task. Neuroimage, 2019. 193: p. 157-166.
80. Ssali, T., et al., Mapping Long-Term Functional Changes in Cerebral Blood Flow by Arterial Spin Labeling. PLoS One, 2016. 11(10): p. e0164112.
81. Holiga, S., et al., Test-retest reliability of task-based and resting-state blood oxygen level dependence and cerebral blood flow measures. PLoS One, 2018. 13(11): p. e0206583.
82. Steketee, R.M., et al., Quantitative Functional Arterial Spin Labeling (fASL) MRI--Sensitivity and Reproducibility of Regional CBF Changes Using Pseudo-Continuous ASL Product Sequences. PLoS One, 2015. 10(7): p. e0132929.
83. Chen, Y., D.J. Wang, and J.A. Detre, Test-retest reliability of arterial spin labeling with common labeling strategies. J Magn Reson Imaging, 2011. 33(4): p. 940-9.
84. Jiang, L., et al., Reliability and reproducibility of perfusion MRI in cognitively normal subjects. Magn Reson Imaging, 2010. 28(9): p. 1283-9.
85. Mutsaerts, H.J., et al., Inter-vendor reproducibility of pseudo-continuous arterial spin labeling at 3 Tesla. PLoS One, 2014. 9(8): p. e104108.
86. Desmarais, P., et al., Therapeutic trial design for frontotemporal dementia and related disorders. J Neurol Neurosurg Psychiatry, 2018.
87. Staffaroni, A.M., et al., Longitudinal multimodal imaging and clinical endpoints for frontotemporal dementia clinical trials. Brain, 2019. 142(2): p. 443-459.
88. Tsai, R.M. and A.L. Boxer, Therapy and clinical trials in frontotemporal dementia: past, present, and future. J Neurochem, 2016. 138 Suppl 1: p. 211-21.
89. Ashburner, J. and K.J. Friston, Voxel-based morphometry--the methods. Neuroimage, 2000. 11(6 Pt 1): p. 805-21.
90. Kazemi, K. and N. Noorizadeh, Quantitative Comparison of SPM, FSL, and Brainsuite for Brain MR Image Segmentation. J Biomed Phys Eng, 2014. 4(1): p. 13-26.
91. Klauschen, F., et al., Evaluation of automated brain MR image segmentation and volumetry methods. Hum Brain Mapp, 2009. 30(4): p. 1310-27.
92. Tudorascu, D.L., et al., Reproducibility and Bias in Healthy Brain Segmentation: Comparison of Two Popular Neuroimaging Platforms. Front Neurosci, 2016. 10: p. 503.
93. Vuksanovic, V., et al., Cortical Thickness and Surface Area Networks in Healthy Aging, Alzheimer's Disease and Behavioral Variant Fronto-Temporal Dementia. Int J Neural Syst, 2019. 29(6): p. 1850055.
94. Hutton, C., et al., A comparison between voxel-based cortical thickness and voxel-based morphometry in normal aging. Neuroimage, 2009. 48(2): p. 371-80.
95. Kong, L., et al., Comparison of grey matter volume and thickness for analysing cortical changes in chronic schizophrenia: a matter of surface area, grey/white matter intensity contrast, and curvature. Psychiatry Res, 2015. 231(2): p. 176-83.
96. Schwarz, C.G., et al., A large-scale comparison of cortical thickness and volume methods for measuring Alzheimer's disease severity. Neuroimage Clin, 2016. 11: p. 802-812.
97. Reuter, M., et al., Within-subject template estimation for unbiased longitudinal image analysis. Neuroimage, 2012. 61(4): p. 1402-18.
98. Moreno, F., et al., Distinctive age-related temporal cortical thinning in asymptomatic granulin gene mutation carriers. Neurobiol Aging, 2013. 34(5): p. 1462-8.
99. Popuri, K., et al., Gray matter changes in asymptomatic C9orf72 and GRN mutation carriers. Neuroimage Clin, 2018. 18: p. 591-598.
100. Whitwell, J.L., et al., Altered functional connectivity in asymptomatic MAPT subjects: a comparison to bvFTD. Neurology, 2011. 77(9): p. 866-74.
101. Lee, S.E., et al., Thalamo-cortical network hyperconnectivity in preclinical progranulin mutation carriers. Neuroimage Clin, 2019. 22: p. 101751.
102. Wilson, S.R. and I. Gordon, Calculating Sample Sizes in the Presence of Confounding Variables.

Journal of the Royal Statistical Society Series C (Applied Statistics), 1986. 35(2): p. 207-213.
103. Bullmore, E.T., et al., Global, voxel, and cluster tests, by theory and permutation, for a difference between two groups of structural MR images of the brain. IEEE Trans Med Imaging, 1999. 18(1): p. 32-42.
104. Pievani, M., et al., Pattern of structural and functional brain abnormalities in asymptomatic granulin mutation carriers. Alzheimers Dement, 2014. 10(5 Suppl): p. S354-S363 e1.
105. Cruchaga, C., et al., Cortical atrophy and language network reorganization associated with a novel progranulin mutation. Cereb Cortex, 2009. 19(8): p. 1751-60.
106. Meeter, L.H., et al., Imaging and fluid biomarkers in frontotemporal dementia. Nat Rev Neurol, 2017. 13(7): p. 406-419.
107. Gordon, E., J.D. Rohrer, and N.C. Fox, Advances in neuroimaging in frontotemporal dementia. J Neurochem, 2016. 138 Suppl 1: p. 193-210.
108. Cummings, J.L., Neuroimaging in the dementia assessment: is it necessary? J Am Geriatr Soc, 2000. 48(10): p. 1345-6.
109. Hentschel, F., et al., The clinical utility of structural neuroimaging with MRI for diagnosis and differential diagnosis of dementia: a memory clinic study. Int J Geriatr Psychiatry, 2005. 20(7): p. 645-50.
110. Harper, L., et al., MRI visual rating scales in the diagnosis of dementia: evaluation in 184 post-mortem confirmed cases. Brain, 2016. 139(Pt 4): p. 1211-25.
111. Scheltens, P., et al., Visual assessment of medial temporal lobe atrophy on magnetic resonance imaging: interobserver reliability. J Neurol, 1995. 242(9): p. 557-60.
112. Vernooij, M.W., et al., Automatic normative quantification of brain tissue volume to support the diagnosis of dementia: A clinical evaluation of diagnostic accuracy. Neuroimage Clin, 2018. 20: p. 374-379.
113. Vinke, E.J., et al., Normative brain volumetry derived from different reference populations: impact on single-subject diagnostic assessment in dementia. Neurobiol Aging, 2019. 84: p. 9-16.
114. Woollacott, I.O.C., et al., Pathological correlates of white matter hyperintensities in a case of progranulin mutation associated frontotemporal dementia. Neurocase, 2018. 24(3): p. 166-174.
115. Riphagen, J.M., et al., Shades of white: diffusion properties of T1- and FLAIR-defined white matter signal abnormalities differ in stages from cognitively normal to dementia. Neurobiol Aging, 2018. 68: p. 48-58.
116. Dell'Acqua, F., et al., Can spherical deconvolution provide more information than fiber orientations? Hindrance modulated orientational anisotropy, a true-tract specific index to characterize white matter diffusion. Hum Brain Mapp, 2013. 34(10): p. 2464-83.
117. Kamagata, K., et al., Connectome analysis with diffusion MRI in idiopathic Parkinson's disease: Evaluation using multi-shell, multi-tissue, constrained spherical deconvolution. Neuroimage Clin, 2018. 17: p. 518-529
118. Wilkins, B., et al., Fiber estimation and tractography in diffusion MRI: development of simulated brain images and comparison of multi-fiber analysis methods at clinical b-values. Neuroimage, 2015. 109: p. 341-56.
119. Pagani, E., et al., Intercenter differences in diffusion tensor MRI acquisition. J Magn Reson Imaging, 2010. 31(6): p. 1458-68.
120. Vollmar, C., et al., Identical, but not the same: intra-site and inter-site reproducibility of fractional anisotropy measures on two 3.0T scanners. Neuroimage, 2010. 51(4): p. 1384-94.
121. Drake-Perez, M., et al., Clinical applications of diffusion weighted imaging in neuroradiology. Insights Imaging, 2018. 9(4): p. 535-547.
122. Miller, K.L., et al., Multimodal population brain imaging in the UK Biobank prospective epidemiological study. Nat Neurosci, 2016. 19(11): p. 1523-1536.
123. Tosun, D., et al., Discriminative Power of Arterial Spin Labeling Magnetic Resonance Imaging and 18F-Fluorodeoxyglucose Positron Emission Tomography Changes for Amyloid-beta-Positive Subjects in the Alzheimer's Disease Continuum. Neurodegener Dis, 2016. 16(1-2): p. 87-94.
124. Verfaillie, S.C., et al., Cerebral perfusion and glucose metabolism in Alzheimer's disease and frontotemporal dementia: two sides of the same coin? Eur Radiol, 2015. 25(10): p. 3050-9.
125. McMahon, P.M., et al., Cost-effectiveness of PET in the diagnosis of Alzheimer disease. Radiology, 2003. 228(2): p. 515-22.
126. Wolk, D.A. and J.A. Detre, Arterial spin labeling MRI: an emerging biomarker for Alzheimer's disease and other neurodegenerative conditions. Curr Opin Neurol, 2012. 25(4): p. 421-8.

127. Steketee, R.M., et al., Early-stage differentiation between presenile Alzheimer's disease and frontotemporal dementia using arterial spin labeling MRI. Eur Radiol, 2016. 26(1): p. 244-53.
128. Preti, M.G., et al., Assessing corpus callosum changes in Alzheimer's disease: comparison between tract-based spatial statistics and atlas-based tractography. PLoS One, 2012. 7(4): p. e35856.
129. Kamagata, K., et al., Relationship between cognitive impairment and white-matter alteration in Parkinson's disease with dementia: tract-based spatial statistics and tract-specific analysis. Eur Radiol, 2013. 23(7): p. 1946-55.
130. Kuchling, J., et al., Comparison of probabilistic tractography and tract-based spatial statistics for assessing optic radiation damage in patients with autoimmune inflammatory disorders of the central nervous system. Neuroimage Clin, 2018. 19: p. 538-550.

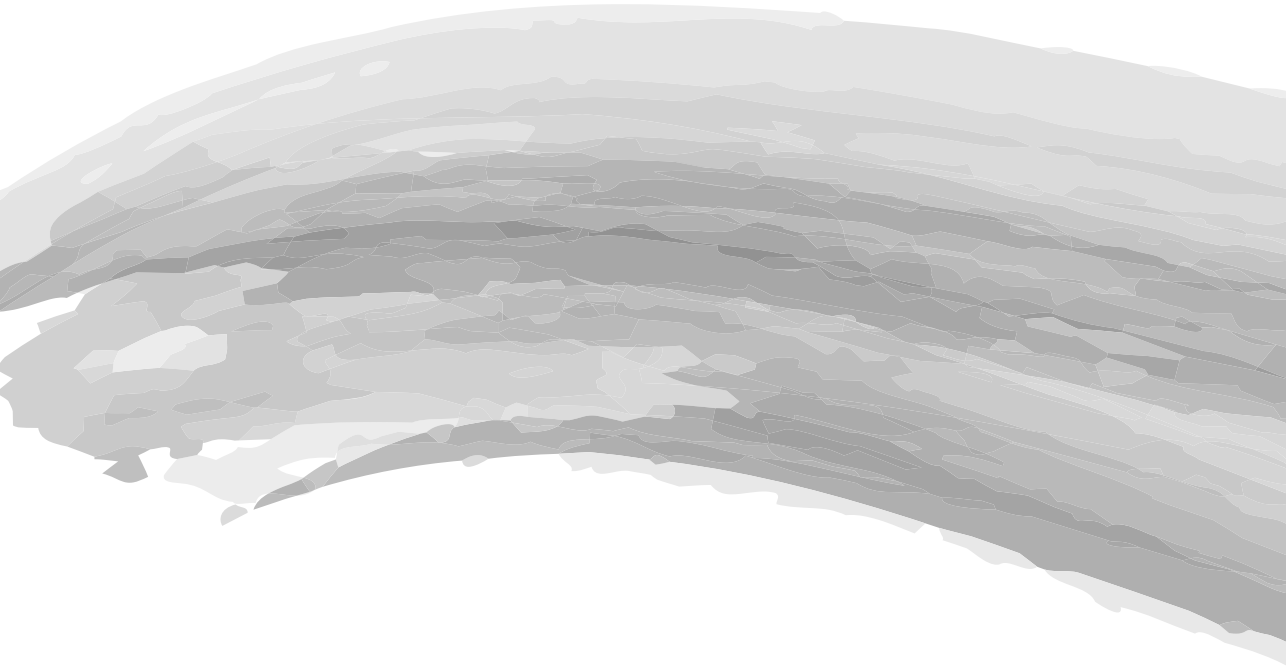

CHAPTER 6

SUMMARY

Chapter 6.1

English summary

Frontotemporal dementia (FTD) is the second most common form of early onset dementia, characterized by heterogeneous clinical presentations, genetic mutations, and underlying pathology. Phenotypic manifestions are usually either behavioral variant FTD (bvFTD), typified by behavioral deficits such as apathy and disinhibition, or primary progressive aphasia (PPA), presenting with language disorders. Some patients also develop concomitant motor neuron disorders. Up to 30% of all FTD cases is caused by autosomal dominant gene mutations. The three major genotypes causing FTD are mutations in the progranulin (*GRN*) or microtubule associated protein tau (*MAPT*) genes, and a repeat expansion in chromosome 9 open reading frame 72 (*C9orf72*). First-degree relatives of genetic FTD patients have fifty percent chance of inheriting the genetic mutation, and thereby developing FTD. By following these at-risk individuals while they are still cognitively healthy ('presymptomatic'), the emerging disease process of FTD can be examined. In my thesis, I have focused on patterns of brain change in presymptomatic FTD mutation carriers, using MRI.

In **Chapter 1**, the introduction of this thesis, I have described the genetic forms of FTD, the associated clinical phenotypes, and previously demonstrated genotypic atrophy patterns. I have also summarized the previous presymptomatic FTD studies that used various MRI sequences that are investigated in this thesis, i.e. such as T1-weighted imaging (investigating grey matter), diffusion tensor imaging (DTI, for white matter microstructure), and arterial spin labelling (ASL, investigating cerebral blood flow as proxy of brain metabolism).

Chapter 2 focusses on genotypic imaging signatures in presymptomatic genetic FTD. I have modelled multiple biomarkers, i.e. fluid, cognitive, and neuroimaging, in presymptomatic and symptomatic *GRN* mutation carriers in **Chapter 2.1**. Herewith, the temporal sequence of biomarker changes has been demonstrated for *GRN*-related FTD. We found that serum neurofilament light chain was the earliest abnormal biomarker for *GRN* mutation carriers, closely followed by degeneration of white matter microstructure in the left anterior thalamic radiation. Furthermore, attention and mental processing speed were also affected early in the disease process. These multimodal biomarkers all relate to axonal degeneration. Also, white matter biomarkers became abnormal before grey matter volumes, and the left hemisphere was affected before the right hemisphere. In the same study, we have identified phenotypic differences of non-fluent variant PPA (nfvPPA) patients and bvFTD patients within the GRN genotype. Interestingly, estimated disease severity scores based on individual biomarker profiles were strongly correlated with actual years since symptom

onset in nfvPPA patients, indicating a good proxy for disease progression. However, in bvFTD patients, the biomarker cascade and individual disease severity correlation were uncertain, possibly due to large heterogeneity in atrophy patterns between bvFTD patients. **Chapter 2.2** describes a cross-sectional characterization of grey and white matter differences and cognitive function in presymptomatic *C9orf72* repeat expansion carriers, compared with their non-carrying first degree family members. We demonstrated early grey matter loss of the bilateral thalamus and cerebellum, but only in repeat expansion carriers of 40 years and older. The white matter microstructure of the entire presymptomatic group, including those younger than 40, showed lower integrity than healthy non-carriers in multiple frontal white matter tracts, the anterior thalamic radiation and corticospinal tracts. Regarding cognition, repeat expansion carriers performed worse on tests for executive functioning.

I have addressed longitudinal trajectories of presymptomatic brain change in **Chapter 3**. In **Chapter 3.1**, I investigated longitudinal grey and white matter change in the presymptomatic stage in all three genotypes. Building upon results from Chapter 2.2, my research showed that *C9orf72* repeat expansion carriers have early grey and white matter differences, but those differences do not change over two years of follow up compared with healthy non-carriers. In presymptomatic *MAPT* mutation carriers, temporal lobe atrophy and degeneration of white matter microstructure emerged during the two year follow up. Interestingly, *GRN* mutation carriers did not show any presymptomatic brain changes compared with non-carriers. In this chapter, I also demonstrated that the three genotypes are significantly different from each other, indicating that trajectories of brain change are unique for each genotype. **Chapter 3.2** reports results from *MAPT* and *GRN* mutation carriers that converted from the presymptomatic to the symptomatic stage during follow-up. From two years before symptom onset, both grey and white matter degenerated in these converters. Although the changes in grey and white matter appeared simultaneously, classification based on white matter biomarkers between converters and non-converters resulted in the highest diagnostic accuracy, suggesting that white matter biomarkers could be more sensitive for disease onset in *MAPT* and *GRN* mutation carriers. In **Chapter 3.3**, I explored longitudinal functional change in the genetic FTD. By means of ASL-MRI, we measured longitudinal changes in regional cerebral blood flow (CBF). In this pilot study, I observed trends of regional CBF change in both *MAPT* and *GRN* converters, but not in the respective presymptomatic groups. In contrast, *C9orf72* repeat expansion carriers showed a decline of CBF with advancing age, but converters showed no specific regional decrease in CBF. However, this pilot study was severely hampered by multiple methodological challenges of ASL acquisition, processing, and analysis. Therefore, the potential of ASL-MRI as neuroimaging biomarker for diagnostic and research purposes within genetic FTD may be limited.

In **Chapter 4**, I addressed several methodological challenges related to neuroimaging

research. I have reviewed the current literature on voxel-wise grey matter differences in presymptomatic genetic FTD in **Chapter 4.1**, and demonstrated that choices in software and analysis methods lead to differences in results for each genotype. Furthermore, I studied the sensitivity of four default software packages for grey matter comparisons and showed that the voxel-based morphometry approach in SPM (Statistical Parameter Mapping, one of the software packages) needed the smallest sample size to reach statistical significance in presymptomatic *GRN* mutation carriers and *C9orf72* repeat expansion carriers. However, for *MAPT* mutation carriers, cortical thickness analysis with FreeSurfer led to the smallest sample size estimation. The results from this study emphasize the need for genotype dependent methodology, and calls for standardization of analysis methods across studies to allow for comparisons between genetic FTD cohorts. **Chapter 4.2** focusses on the bias introduced in our longitudinal cohort, by switching head coils during follow-up. In this study, we demonstrated that using an 8-channel head coil and an 32-channel head coil severely compromises the comparability of T1-weighted imaging, DTI, and resting state fMRI sequences within subjects. This means that using multiple head coils during a longitudinal study will affect the outcome, and therefore decreases the reliability of the results. We calculated and validated voxel-wise scaling factors for the abovementioned sequences, that eliminates the majority of differences between head coils for our longitudinal study.

In **Chapter 5**, I have discussed and reviewed the results of my thesis relative to the field of genetic FTD and neuroimaging research. In summary, my research demonstrates that the neuroimaging signatures in presymptomatic FTD are genotypic, reflecting distinct trajectories of brain change in each genotype. Although complicated by methodological challenges, neuroimaging allows investigation of temporal and spatial disease related brain alterations, and is therefore extremely important for clinical practice and future clinical trials in FTD.

Chapter 6.2

Nederlandse samenvatting

Frontotemporale dementie (FTD) is de tweede meest voorkomende dementie op jonge leeftijd, en wordt gekarakteriseerd door heterogene klinische presentaties en onderliggende pathologie. FTD resulteert in de meeste gevallen in de gedragsvariant FTD, getypeerd door gedragsproblemen zoals apathie en disinhibitie, of primair progressieve afasie, gekenmerkt door taalstoornissen. Sommige patiënten ontwikkelen ook bijkomende motorische problemen. Ongeveer 30% van alle FTD gevallen wordt veroorzaakt door autosomaal dominante gen mutaties. De drie meest voorkomende genotypes van FTD zijn mutaties in het progranuline (*GRN*) en microtubule associated protein tau (*MAPT*) gen, en een repeat expansie in chromosome 9 open reading frame 72 (*C9orf72*). Eerstegraads familieleden van FTD patiënten met een gen mutatie hebben 50% kans op het erven van die mutatie, en dus op het ontwikkelen van FTD. Door deze individuen te volgen terwijl zij nog cognitief gezond zijn ('presymptomatisch') kan het ontwikkelende ziekte proces van FTD worden bestudeerd. In dit proefschrift heb ik patronen van hersenveranderingen onderzocht in presymptomatische FTD mutatie dragers, door middel van MRI scans.

In **hoofdstuk 1,** de inleiding op dit proefschrift, heb ik de genetische vormen van FTD beschreven, evenals de geassocieerde klinische fenotypes. Daarnaast heb ik eerdere presymptomatische FTD studies samengevat die gebruik hebben gemaakt van verschillende MRI sequenties waarmee in dit proefschrift onderzoek wordt verricht, te weten T1-gewogen MRI (voor het bestuderen van de grijze stof), diffusie gewogen MRI (voor het bestuderen van de microstructuur van de witte stof) en ASL (om de bloedtoevoer als maat voor hersenmetabolisme te bestuderen).

Hoofdstuk 2 is gericht op het identificeren van gen-specifieke patronen op beeldvorming in de presymptomatische fase van genetische FTD. Ik heb verschillende biomarkers, te weten fluïde, cognitieve, en neuroimaging biomarkers, gemodelleerd in presymptomatische en symptomatische *GRN* mutatie dragers in **hoofdstuk 2.1**. Hiermee hebben we de temporele sequentie van veranderingen in biomarkers voor *progranuline* gerelateerde FTD aangetoond. Onze bevindingen lieten zien dat neurofilament light chain levels in serum de eerst afwijkingen toonden in presymptomatische *GRN* mutatie dragers, op de voet gevolgd door een afname van de witte stof microstructuur in een witte stofbaan gelegen in de linker thalamus. Daarnaast waren cognitieve functies als aandacht en mentale verwerkingssnelheid vroeg in het ziekteproces aangedaan. Deze verschillende biomarkers wijzen allen op axonale, witte stof, degeneratie. Verder vonden wij dat de witte stof microstructuur afneemt

voordat het grijze stof volume afneemt, en dat de linker hemisfeer eerder dan de rechter hemisfeer was aangedaan. In hetzelfde onderzoek hebben we verschillen gevonden in het ziektebeloop tussen *GRN* patiënten met een niet-vloeiende primaire progressieve afasie en gedragsvariant FTD. Opmerkelijk was dat geschatte ziekte progressie in m.n. niet-vloeiende afasie patiënten sterk correleerde met de daadwerkelijke jaren na het ontstaan van symptomen, wat suggereert dat zowel de biomarkers en deze schattingen een goede proxy kunnen zijn voor ziekteprogressie. Daarentegen waren de temporele sequentie van biomarker veranderingen en de geschatte ziekte progressie scores in gedragsvariant FTD patiënten onzeker, mogelijk veroorzaakt doordat er veel heterogeniteit in atrofie patronen tussen patiënten was. **Hoofdstuk 2.2** beschrijft een cross-sectionele karakterisatie van grijze stof en witte stof verschillen en cognitief functioneren in presymptomatische *C9orf72* repeat expansie dragers ten opzichte van gezonde familieleden zonder repeat expansie. Wij toonden vroege grijze stof veranderingen aan in de thalamus en het cerebellum, maar deze werden alleen gevonden in dragers van 40 jaar en ouder. De witte stof microstructuur van de gehele groep dragers, inclusief individuen jonger dan 40, liet verminderde integriteit zien in verschillende frontaal gelegen witte stofbanen, in de thalamus, en de cortico-spinale witte stofbanen. Wat betreft cognitie presteerden dragers van de repeat expansie slechter op taken voor het executieve functioneren dan hun niet-dragende familieleden.

Ik heb longitudinale presymptomatische hersenveranderingen onderzocht in **hoofdstuk 3.** In **hoofdstuk 3.1** heb ik de longitudinale grijze en witte stof veranderingen bestudeerd in de presymptomatische fase van de drie genotypes. Voortbordurend op de resultaten van hoofdstuk 2.2, liet mijn onderzoek zien dat *C9orf72* repeat expansie dragers vroege grijze en witte stof afwijkingen hebben, maar dat deze afwijkingen niet significant veranderen gedurende de follow-up van twee jaar vergeleken met gezonde niet-dragers. In presymptomatische *MAPT* mutatie dragers ontstond er temporale atrofie en afname van de witte stof microstructuur tijdens de follow-up van twee jaar. Er waren geen presymptomatische hersenveranderingen in *GRN* mutatie dragers vergeleken ten opzichte van niet-dragers. In dit onderzoek toonde ik ook aan dat de grijze stof en witte stof in de drie genotypes significant van elkaar verschilden, ook over tijd, wat indiceert dat het beloop van hersenveranderingen uniek is voor elk genotype. **Hoofdstuk 3.2** rapporteert de resultaten van een groep *MAPT* en *GRN* mutatie dragers die tijdens de studie converteerden van de presymptomatische fase naar de symptomatische fase. Vanaf twee jaar voor het ontstaan van klinische symptomen ontstonden er zowel grijze als witte stof veranderingen in deze converters. Hoewel de grijze en witte stof veranderingen tegelijk zichtbaar werden, resulteerde classificatie gebaseerd op witte stof biomarkers in de hoogste diagnostische accuratesse. Dit suggereert dat witte stof biomarkers gevoeliger zijn voor het aantonen van de start van klinische symptomen in *MAPT* en *GRN* mutatie dragers. In **hoofdstuk 3.3** heb ik longitudinale functionele hersenveranderingen in genetische FTD onderzocht. Door middel

van ASL hebben we longitudinale veranderingen in regionale hersendoorbloeding gemeten. In dit pilot project werden trends van regionale hersendoorbloeding veranderingen gevonden in zowel *MAPT* als *GRN* converters, maar niet in de respectievelijke presymptomatische mutatie drager groepen. Daarentegen lieten *C9orf72* repeat expansie dragers een afname van regionale doorbloeding zien met het toenemen van de leeftijd, maar er werd geen specifieke trend gevonden in regionale hersendoorbloeding in *C9orf72* converters. Dit pilot project werd ernstig belemmerd door meerdere methodologische problemen van ASL acquisitie, beeldverwerking, en analyses. Hierdoor is de potentie van ASL als beeldvormende biomarker voor diagnostische en onderzoek activiteiten in genetische FTD mogelijk gelimiteerd.

In **hoofdstuk 4** beschreef ik verschillende methodologische problemen die gerelateerd zijn aan longitudinaal neuroimaging onderzoek. Ik heb de bestaande literatuur met betrekking tot voxel-specifieke grijze stof verschillen in genetische FTD beoordeeld in **hoofdstuk 4.1**. Hierin toonde ik aan dat keuzes voor software en analyse methoden tot verschillen in uitkomst leiden in elk genotype. Vervolgens heb ik de sensitiviteit van vier verschillende standaard methoden voor grijze stof analyses vergeleken, en liet ik zien dat voxel-specifieke analyse in SPM (Statistical Parameter Mapping, een software programma) de kleinste groepsgrootte nodig had om een significant verschil te bereiken in zowel presymptomatische *GRN* mutatie dragers en *C9orf72* repeat expansie dragers. Daarentegen, voor *MAPT* mutatie dragers leidde analyse van de corticale schorsdikte in FreeSurfer tot de kleinst benodigde groepsgrootte. De resultaten van deze studie benadrukken dat elk genotype zijn eigen aanpak nodig heeft, en roepen op tot standaardisatie van analyse methodes tussen studies, zodat de vergelijking tussen verschillende genetische FTD populaties mogelijk wordt. **Hoofdstuk 4.2** focust op de geïntroduceerde systematische afwijking in ons longitudinale cohort, veroorzaakt door de wisseling van hoofdspoelen gedurende de studie. In dit hoofdstuk hebben we aangetoond dat het gebruik van de 8 kanaal hoofdspoel en de 32 kanaal hoofdspoel, de betrouwbaarheid tussen meetmomenten van T1 gewogen MRI, diffusie gewogen MRI, en functionele MRI in rust vermindert. Dit betekent dat het gebruik van meerdere hoofdspoelen tijdens een longitudinale studie de uitkomsten beïnvloeden, wat de betrouwbaarheid van de resultaten aantast. In deze studie hebben we voxel-specifieke factoren berekend en gevalideerd voor de genoemde sequenties, die het grootste deel van hoofdspoel verschillen in onze longitudinale studie kunnen elimineren.

In **hoofdstuk 5** heb ik de resultaten in mijn proefschrift bediscussieerd in het licht van genetische FTD en beeldvormend onderzoek. Samenvattend, zijn de patronen van hersenafwijkingen op beeldvorming in presymptomatisch FTD gen-specifiek, en bestaat er een uniek beloop van hersenveranderingen voor elk genotype. Alhoewel neuroimaging onderzoek wordt bemoeilijkt door methodologische problemen, faciliteert neuroimaging ook het onderzoek naar temporele en regionale hersenveranderingen gerelateerd aan FTD.

Daarmee is beeldvorming uitermate belangrijk voor zowel diagnostiek als toekomstige medicatie trials bij FTD.

Dankwoord

Dit proefschrift is niet alleen door mijn handen, maar door vele handen tot stand gekomen. Ten eerste wil ik de families en deelnemers uit de FTD-RisC studie bedanken. Jullie inzet op alle vlakken is niet onopgemerkt voorbij gegaan. In tegendeel, het is een inspiratie geweest om door te gaan. Ik hoop dat de resultaten uit dit onderzoek weer een klein stapje zullen zijn in jullie strijd tegen FTD.

Ten tweede, mijn promotoren prof.dr. John van Swieten en prof.dr. Serge Rombouts. Bedankt voor jullie begeleiding, inzichten, en scherpe blikken die mij hebben gevormd en tot een betere wetenschapper hebben gemaakt. Mijn co-promotor Janne Papma, jij had het vertrouwen om mij van stagiair tot promovendus te maken. Ik heb de afgelopen jaren zoveel van je geleerd en tegen je op gekeken. Ik waardeer alle tijd en moeite die je voor mij nam. Bedankt voor alles. Prof.dr. Meike Vernooij, dr. Jeroen van der Grond and prof.dr. Mario Masellis, thank you all for being a member of the reading committee, and moreover, for inspiring and motivating me in my research.

Mijn geweldige paranimfen. Marijke, we hebben elkaar er doorheen gesleept. Zoveel ups gevierd met taart en nog veel meer downs van ons afgepraat met drama-koffie. Bedankt dat ik op je kon terugvallen in het hele traject, en dat je naast me wil staan. Alhoewel niet meer in het Erasmus MC, drink ik nog heel graag koffie met jou. Je bent een topvriendin. Inge, al 12 jaar door dik en dun. You got my back. Bedankt dat je altijd en elke dag naar mij luistert en soms een spiegel voorhoudt. Nog een paar weken en dan wonen we eindelijk weer bij elkaar in de buurt, en kunnen we weer onbeperkt samen sporten, wandelen, thee drinken, etc. Ik hoop dat we nog vele jaren elkaars mooie en mindere momenten mogen delen.

Aan het fantastische FTD-RisC team, Lize, Jackie, Lieke, Emma, Elise, bedankt voor al het werk dat dit onderzoek mogelijk maakt. Van dagjes uit naar Urk tot zweten bij de MRI scanner: we are in this together. Mijn verzamelde neuroimaging collega's uit zowel Rotterdam als Leiden: Rebecca, Anne, Vikram, Rogier, Mark, samenwerken met jullie was altijd zo leerzaam en stimulerend. Bedankt voor jullie adviezen en perspectieven. Lieve andere (oud) collega's en kamergenoten van 2238: Leonie, Jeroen, Tsz, Janneke, Merel, Sanne, Willem, Judy, Harro, bedankt voor de – soms zo hard nodige – afleiding, koffie, praatjes, wandelingetjes naar de Appie, borrels, en taart! Alle overige collega's van het Alzheimercentrum Erasmus MC: bedankt voor jullie inzet, betrokkenheid en interesse in de afgelopen jaren. Ook de verschillende master studenten die ik over de afgelopen jaren heb mogen begeleiden, in het bijzonder Yang Yang, Lauren, en Anda, hartelijk dank voor jullie enthousiasme.

Dank aan mijn nieuwe collega's bij de sectie Klinische Psychologie van de Erasmus Universiteit Rotterdam, voor een warm bad en fijne nieuwe werkplek. Dit geldt ook voor de staf teamleden van @ease Rotterdam: wat een enthousiasme en teamspirit. Ik ben er trots op dat ik met jullie de handen uit de mouwen mag steken voor jongeren in Rotterdam.

Al mijn lieve vrienden die om mij heen hebben gestaan in de afgelopen jaren, bedankt dat jullie mij overeind hebben gehouden als ik het nodig had. Vriendinnen van NSL, medetienerleiders van de Reveilweken, vrienden uit Rotterdam en Maassluis: jullie gezelschap en positieve woorden zorgden ervoor dat ik met beide benen op de grond bleef staan en motiveerden mij in mijn werk. Speciaal wil ik graag Caroline, Eva, Mirte, en Iris benoemen. Bedankt voor alle wijntjes, diepe gesprekken, spelletjes, dinertjes, en liefde gedurende de afgelopen jaren. Ik kijk uit naar de komende jaren, helemaal met al die veranderende levensfases!

Lieve familie Panman, Bakker, en de Bruijn. Bedankt voor alle jaren van steun, interesse, en betrokkenheid. Robert en Yvonne, jullie hebben er voor gezorgd dat ik me thuis ben gaan voelen in de familie. We blijven nog even dankbaar gebruik maken van jullie heerlijke tuin om in te ontspannen. Pap, jij bent een echte rots in de branding. Ik weet dat jij er altijd zal zijn als ik dat nodig heb. Mama, jouw doorzettingsvermogen, vastberadenheid en rotsvaste geloof zijn iedere dag een bron van inspiratie voor mij. Je was zo trots op mij – dit proefschrift is voor jou.

Lieve Tiemen, mijn laatste woorden zijn natuurlijk voor jou. Ik kan niet in woorden uitdrukken hoe dankbaar ik ben om je in mijn leven te hebben. Je houdt me altijd scherp en moedigt me aan. Ik geniet van elke dag met jou.

Curriculum Vitae

Jessica Panman was born in Delfzijl in 1992 and raised in Appingedam, in the north-east part of Groningen, the Netherlands. After primary school, she attended the first four years of Atheneum at Fivel College, and finished high school at the Meander College in Zwolle after moving to Nieuwleusen at age fifteen. She studied Psychology at Leiden University and obtained her master's degree in Clinical Neuropsychology.

Jessica first came across neuroimaging research when writing her master thesis at the Neurology department of the Erasmus Medical Center. After finishing her masters, she started working as a project assistant for the Alzheimercenter Erasmus MC in 2015, but quickly also commenced her PhD project in neuroimaging in the FTD-RisC cohort. Her research has been a joint project of both the Neurology department in the Erasmus Medical Center and the Radiology department in the Leiden University Medical Center.

She has been teaching (Clinical) Psychology and supervising bachelor and master thesis projects at the Erasmus University Rotterdam since September 2019. Besides teaching, she enjoys doing voluntary work with teenagers. Jessica is happily married to Tiemen de Bruijn, and they currently live together in Rotterdam.

List of publications

Panman J.L. Steketee R.M.E., de Witte A.C., To Y.Y., Jiskoot L.C., van der Ende E.L., Poos J.M., Meeter L.H.H., Dopper E.G.P., Donker Kaat L., van den Berg E., van Swieten J.C., Rombouts S.A.R.B., Papma J.M. (2020). Review and comparison of software packages for grey matter biomarkers in presymptomatic frontotemporal dementia. *Submitted (Neuroimage Clinical)*

Panman J.L.*, Venkatraghavan V.*, van der Ende E.L., Steketee R.M.E., Jiskoot L.C., Poos J.M., Dopper E.G.P., Meeter L.H.H., Donker Kaat L., Rombouts S.A.R.B., Vernooij M.W., Kievit J.A., Premi E., Cosseddu M., Bonomi E., Olives J., Rohrer J.D., Sanchez-Valle R., Borroni B., Bron E.E., van Swieten J.C., Papma J.M., Klein S.; Genetic FTD initiative (GENFI). (2020). Modelling the cascade of biomarker changes in *GRN* related frontotemporal dementia. *Submitted (Journal of Neurology, Neursurgery, and Psychiatry)*

Panman J.L.*, Steketee R.M.E.*, Versteeg A., Bron E.E., Venkatraghavan V., Jiskoot L.C., Poos J.M., van der Ende E.L., Meeter L.H.H., Dopper E.G.P., Donker Kaat L., Rombouts S.A.R.B., Niessen W.J., van Osch M.J.P., Papma J.M., van Swieten J.C. (2020). Regional cerebral blood flow changes in genetic frontotemporal dementia – a pilot study. *In preparation*

Panman J.L., Jiskoot L.C., Bouts M.J.R.J., Meeter L.H.H., van der Ende E.L., Poos J.M., Feis R.A., Kievit A.J.A., van Minkelen R., Dopper E.G.P., Rombouts S.A.R.B., van Swieten J.C., Papma J.M. (2019). Gray and white matter changes in presymptomatic genetic frontotemporal dementia: a longitudinal MRI study. *Neurobiology of Aging,* (76), 115-124

Panman J.L., To Y.Y., van der Ende E.L., Poos J.M., Jiskoot L.C., Meeter L.H.H., Dopper E.G.P., Bouts M.J.R.J., van Osch M.J.P., Rombouts S.A.R.B., van Swieten J.C., van der Grond J., Papma J.M., Hafkemeijer A. (2019). Bias introduced by multiple head coils in MRI research: an 8 channel and 32 channel coil comparison. *Frontiers in Neuroscience*, (13), 729

Jiskoot L.C., **Panman J.L**., Meeter L.H., Dopper E.G.P., Donker Kaat L., Franzen S., van der Ende E.L., van Minkelen R., Rombouts S.A.R.B., Papma J.M., van Swieten J.C. (2019). Longitudinal multimodal MRI as prognostic and diagnostic biomarker in presymptomatic familial frontotemporal dementia. *Brain, 142*(1), 193-208

Jiskoot L.C., **Panman J.L**., van Asseldonk L., Franzen S., Meeter L.H.H., Donker Kaat L., van der Ende E.L., Dopper E.G.P., Timman R., van Minkelen R., van Swieten J.C., van den Berg E., Papma J.M. (2018). Longitudinal cognitive biomarkers predicting symptom onset in presymptomatic frontotemporal dementia. *Journal of Neurology, 265*(6), 1381-1392

Papma J.M.*, Jiskoot L.C.*, **Panman J.L**., Dopper E.G., den Heijer T., Donker Kaat L., Pijnenburg Y.A.L., Meeter L.H., van Minkelen R., Rombouts S.A.R.B., van Swieten J.C. (2017) Cognition and gray and white matter characteristics of presymptomatic *C9orf72* repeat

expansion. *Neurology, 89*(12), 1256-1264

Feis R.A., Bouts M.J.R.J., **Panman J.L**., Jiskoot L.C., Dopper E.G.P., Schouten T.M., de Vos F., van der Grond J., van Swieten J.C., Rombouts S.A.R.B. (2019). Single-subject classification of presymptomatic frontotemporal dementia mutation carriers using multimodal MRI. *Neuroimage Clinical*, (22), 101718

van der Ende E.L., Meeter L.H., Poos J.M., **Panman J.L.**, Jiskoot L.C., Dopper E.G.P., Papma J.M., de Jong F.J., Verberk I., Teunissen C.E., Rizopoulos D., Heller C., Convery R.S., Moore K.M., Bocchetta M., Neason M., Cash D.M., Borroni B., Galimberti D., Sanchez-Valle R., Laforce Jr R., Moreno F., Synofzik M., Graff C., Masellis M., Tartaglia M.C., Rowe J.B., Vandenberghe R., Finger E., Tagliavini F., de Mendonça A., Santana I., Butler C., Ducharme S., Gerhard A., Danek A., Levin J., Otto M., Frisoni G.B., Cappa S., Pijnenburg Y.A.L., on behalf of the Genetic Frontotemporal dementia Initiative (GENFI), Rohrer J.D., van Swieten J.C. (2019). Serum neurofilament light chain in genetic frontotemporal dementia: a longitudinal multicenter cohort study. *Lancet Neurology* (12), 1103-1111

Poos, J.M., Jiskoot, L.C., Leijdesdorff, S.M.J., Seelaar, H., **Panman, J.L**., van der Ende, E.L., Mol, M.O., Meeter, L.H.H., Pijnenburg, Y.A.L., Donker Kaat, L., de Jong, F.J., van Swieten, J.C., Papma, J.M., van den Berg, E. (2020) Cognitive profiles discriminate between genetic variants of behavioral frontotemporal dementia. *Journal of Neurology*, doi:10.1007/s00415-020-09738-y

van der Ende, E.L., Xiao, M., Xu, D., Poos, J.M., **Panman, J.L**., Jiskoot, L.C., Meeter, L.H., Dopper, E.G.P., Papma, J.M., Heller, C., Convery, R., Moore, K., Bocchetta, M., Neason, M., Peakman, G., Cash, D.M., Teunissen, C.E., Graff, C., Synofzik, M., Moreno, F., Finger, E., Sánchez-Valle, R., Vandenberghe, R., Laforce, R. jr., Masellis, M., Tartaglia, M.C., Rowe, J.B., Butler, C.R., Ducharme, S., Gerhard, A., Danek, A., Levin, J., Pijnenburg, Y.A., Otto, M., Borroni, B., Tagliavini, F., de Mendonca, A., Santana, I., Galimberti, D., Seelaar, H., Rohrer, J.D., Worley, P.F., van Swieten, J.C., on behalf of the Genetic Frontotemporal Dementia Initiative (GENFI). (2020) Neuronal pentraxin 2: a synapse-derived CSF biomarker in genetic frontotemporal dementia. *Journal of Neurology, Neurosurgery, and Psychiatry, 91*(6), 612-621

Feis R.A., Bouts M.J.R.J., de Vos F., Schouten T.M., **Panman J.L**., Jiskoot L.C., Dopper E.G.P., van der Grond J., van Swieten J.C., Rombouts S.A.R.B. (2019). A multimodal MRI-based classification signature emerges just prior to symptom onset in frontotemporal dementia mutation carriers. *Journal of Neurology, Neurosurgery, and Psychiatry, 90(*11), 1207-1214

Meeter L.H.H., Gendron T.F., Sias A.C., Jiskoot L.C., Russo S.P., Donker Kaat L., Papma J.M., **Panman J.L**., van der Ende E.L., Dopper E.G., Franzen S., Graff C., Boxer A.L., Rosen H.J., Sanchez-Valle R., Galimberti D., Pijnenburg Y.A.L., Benussi L., Ghidoni R., Borroni B., Laforce

R. jr., Del Campo M., Teunissen C.E., van Minkelen R., Rojas J.C., Coppola G., Geschwind D.H., Rademakers R., Karydas A.M., Oijerstedt L., Scarpini E., Binetti G., Padovani A., Cash D.M., Dick K.M., Bocchetta M., Miller B.L., Rohrer J.D., Petrucelli L., van Swieten J.C., Lee S.E. (2018). Poly(GP), neurofilament and grey matter deficits in *C9orf72* expansion carriers. *Annals of Clinical and Translational Neurology 5*(5), 583-597

Jiskoot L.C, Bocchetta M., Nicholas J.M., Cash D.M., Thomas D., Modat M., Ourselin S., Rombouts S.A.R.B., Dopper E.G.P., Meeter L.H., **Panman J.L**., van Minkelen R., van der Ende E.L., Donker Kaat L., Pijnenburg Y.A.L., Borroni B., Galimberti D., Masellis M., Tartaglia M.C., Rowe J., Graff C., Tagliavini F., Frisoni G.B., Laforce R. jr., Finger E., de Mendonça A., Sorbi S.; Genetic Frontotemporal dementia Initiative (GENFI), Papma J.M., van Swieten J.C., Rohrer J.D. (2018). Presymptomatic white matter integrity loss in familial frontotemporal dementia in the GENFI cohort: A cross-sectional diffusion tensor imaging study. *Annals of Clinical and Translational Neurology, 5*(9), 1025-1036

PUBLICATIONS AS GENFI CONSORTIUM AUTHOR

Moore K.M., Nicholas J., Grossman M., McMillan C.T., Irwin D.J., Massimo L., Van Deerlin V.M., Warren J.D., Fox N.C., Rossor M.N., Mead S., Bocchetta M., Boeve B.F., Knopman D.S., Graff-Radford N.R., Forsberg L.K., Rademakers R., Wszolek Z.K., van Swieten J.C., Jiskoot L.C., Meeter L.H., Dopper E.G., Papma J.M., Snowden J.S., Saxon J., Jones M., Pickering-Brown S., Le Ber I., Camuzat A., Brice A., Caroppo P., Ghidoni R., Pievani M., Benussi L., Binetti G., Dickerson B.C., Lucente D., Krivensky S., Graff C., Öijerstedt L., Fallström M., Thonberg H., Ghoshal N., Morris J.C., Borroni B., Benussi A., Padovani A., Galimberti D., Scarpini E., Fumagalli G.G., Mackenzie I.R., Hsiung G.R., Sengdy P., Boxer A.L., Rosen H., Taylor J.B., Synofzik M., Wilke C., Sulzer P., Hodges J.R., Halliday G., Kwok J., Sanchez-Valle R., Lladó A., Borrego-Ecija S., Santana I., Almeida M.R., Tábuas-Pereira M., Moreno F., Barandiaran M., Indakoetxea B., Levin J., Danek A., Rowe J.B., Cope T.E., Otto M., Anderl-Straub S., de Mendonça A., Maruta C., Masellis M., Black S.E., Couratier P., Lautrette G., Huey E.D., Sorbi S., Nacmias B., Laforce R. Jr., Tremblay M.L., Vandenberghe R., Damme P.V., Rogalski E.J., Weintraub S., Gerhard A., Onyike C.U., Ducharme S., Papageorgiou S.G., Ng A.S.L., Brodtmann A., Finger E., Guerreiro R., Bras J., Rohrer J.D.; **FTD Prevention Initiative**. (2020). Age at symptom onset and death and disease duration in genetic frontotemporal dementia: an international retrospective cohort study. *Lancet Neurology, 19*(2), 145-156

Mutsaerts H.J.M.M., Mirza S., Petr J., Thomas D.L., Cash D.M., Bocchetta M., De Vita E., Metcalfe A.W.S., Shirzadi Z., Robertson A.D., Tartaglia M.C., Mitchell S.B., Black S.E., Freedman M., Tang-Wai D., Keren R., Rogaeva E., van Swieten J., Laforce Jr. R., Tagliavini F., Borroni B., Galimberti D., Rowe J.B., Graff C., Frisoni G.B., Finger E., Sandro S., de Mendonça

A., Rohrer J.D., MacIntosh B.J., Masellis M., **on behalf of the GENetic Frontotemporal dementia Initiative**. (2019). Cerebral perfusion changes in presymptomatic genetic frontotemporal dementia: a GENFI study. *Brain, 142*(4), 1108-1120.

Premi E., Calhoun V.D., Diano M., Gazzina S., Cosseddu M., Alberici A., Archetti S., Paternicò D., Gasparotti R., van Swieten J., Galimberti D., Sanchez-Valle R., Laforce R. Jr., Moreno F., Synofzik M., Graff C., Masellis M., Tartaglia M.C., Rowe J., Vandenberghe R., Finger E., Tagliavini F., de Mendonça A., Santana I., Butler C., Ducharme S., Gerhard A., Danek A., Levin J., Otto M., Frisoni G., Cappa S., Sorbi S., Padovani A., Rohrer J.D., Borroni B.; **Genetic FTD Initiative, GENFI**. The inner fluctuations of the brain in presymptomatic Frontotemporal Dementia: The chronnectome fingerprint. *Neuroimage*, 189, 645-654.

Gazzina S., Grassi M., Premi E., Cosseddu M., Alberici A., Archetti S., Gasparotti R., Van Swieten J., Galimberti D., Sanchez-Valle R., Laforce R.J., Moreno F., Synofzik M., Graff C., Masellis M., Tartaglia M.C., Rowe J.B., Vandenberghe R., Finger E., Tagliavini F., de Mendonça A., Santana I., Butler C.R., Ducharme S., Gerhard A., Danek A., Levin J., Otto M., Frisoni G., Sorbi S., Padovani A., Rohrer J.D., Borroni B.; **Genetic FTD Initiative, GENFI**. (2019). Education modulates brain maintenance in presymptomatic frontotemporal dementia. *Journal of Neurology Neurosurgery and Psychiatry, 90*(10), 1124-1130.

Sudre C.H., Bocchetta M., Heller C., Convery R., Neason M., Moore K.M., Cash D.M., Thomas D.L., Woollacott I., Foiani M., Heslegrave A., Shafei R., Greaves C., van Swieten J., Moreno F., Sanchez-Valle R., Borroni B., Laforce R., Masellis M., Tartaglia M.C., Graff C., Galimberti D., Rowe J.B., Finger E., Synofzik M., Vandenberghe R., De Mendonca A., Tagliavini F., Santana I., Ducharme S., Butler C., Gerhard A., Levin J., Danek A., Frisoni G.B., Sorbi S., Otto M., Zetterberg H., Modat M., Ourselin S., Cardoso M.J., Rohrer J.D., **on behalf of GENFI**. (2019) White matter hyperintensities in progranulin-associated frontotemporal dementia - a longitudinal study. *Neuroimage Clinical* [in press]

Tavares T.P., Mitchell D.G.V., Coleman K., Shoesmith C., Bartha R., Cash D.M., Moore K.M., van Swieten J., Borroni B., Galimberti D., Tartaglia M.C., Rowe J., Graff C., Tagliavini F., Frisoni G., Cappa S., Laforce R. Jr., de Mendonça A., Sorbi S., Wallstrom G., Masellis M., Rohrer J.D., Finger EC; **Genetic FTD Initiative, GENFI.** (2019). Ventricular volume expansion in presymptomatic genetic frontotemporal dementia. *Neurology, 93*(18), e1699-e1706.

Rittman T., Borchert R., Jones S., van Swieten J., Borroni B., Galimberti D., Masellis M., Tartaglia M.C., Graff C., Tagliavini F., Frisoni G.B., Laforce Jr. R., Finger E., Mendonça A., Sorbi S., Rohrer J.D., Rowe J.B., **The Genetic Frontotemporal Dementia Initiative (GENFI).** (2019). Functional network resilience to pathology in presymptomatic genetic frontotemporal dementia. *Neurobiology of Aging,* 77, 169-177.

Young A., Marinescu R.V., Oxtoby N., Bocchetta M., Yong K., Firth N., Cash D., Thomas

D., Dick K., Cardoso J., van Swieten J., Borroni B., Galimberti D., Masellis M., Tartaglia M.C., Rowe J., Graff C., Tagliavini F., Frisoni G., Laforce Jr. R., Finger E., Medonca A., Sorbi S., Warren J., Crutch S., Fox N., Ourselin S., Schott J., Rohrer J., Alexander D. (2018) Uncovering the heterogeneity and temporal complexity of neurodegenerative diseases with Subtype and Stage Inference. *Nature Communications, 9(1),* 4273.

Cury C., Durrleman S., Cash D.M., Lorenzi M., Nicholas J., Bocchetta M., van Swieten J.C., Borroni B., Galimberti D., Masellis M., Tartaglia M.C., Rowe J.B., Graff C., Tagliavini F., Frisoni G.B., Laforce R., Finger E., de Mendonca A., Sorbi S., Ourselin S., Rohrer J.D., Modat M. (2018). Spatiotemporal analysis for detection of pre-symptomatic shape changes in neurodegenerative diseases: Initial application to the GENFI cohort. *Neuroimage*, (188), 282-290.

Fumagalli G.G, Basilico P., Arighi A., Bocchetta M., Dick K.M., Cash D.M., Harding S., Mercurio M., Fenoglio C., Pietroboni A.M., Ghezzi L., van Swieten J., Borroni B., de Mendonça A., Masellis M., Tartaglia M.C., Rowe J.B., Graff C., Tagliavini F., Frisoni G.B., Laforce R. Jr., Finger E., Sorbi S., Scarpini E., Rohrer J.D., Galimberti D.; **Genetic FTD Initiative (GENFI).** (2018). Distinct patterns of brain atrophy in Genetic Frontotemporal Dementia Initiative (GENFI) cohort revealed by visual rating scales. *Alzheimers Research Therapy, 10*(1), 46.

Sellami L.*, Bocchetta M.*, Masellis M., Cash D.M., Dick K.M., van Swieten J., Borroni B., Galimberti D., Tartaglia M.C., Rowe J.B., Graff C., Tagliavini F., Frisoni G., Finger E., Mendonça A., Sorbi S., Warren J.D., Rohrer J.D.^, Laforce Jr. R.^, **on behalf of the Genetic FTD Initiative**. (2018). Distinct Neuroanatomical Correlates of Neuropsychiatric Symptoms in the Three Main Forms of Genetic Frontotemporal Dementia in the GENFI Cohort. *Journal of Alzheimers Disease, 65*(1), 147-163.

Mutsaerts H.J.M.M., Petr J., Thomas D.L., De Vita E., Cash D.M., van Osch M.J.P., Golay X., Groot P.F.C., Ourselin S., van Swieten J., Laforce R. Jr., Tagliavini F., Borroni B., Galimberti D., Rowe J.B., Graff C., Pizzini F.B., Finger E., Sorbi S., Castelo Branco M., Rohrer J.D., Masellis M., MacIntosh B.J.; **GENFI investigators**. (2018). Comparison of arterial spin labeling registration strategies in the multi-center GENetic frontotemporal dementia initiative (GENFI). *Journal of Magnetic Resonance Imaging, 47*(1), 131-140.

Schneider R., McKeever P., Kim T., Graff C., van Swieten J.C., Karydas A., Boxer A., Rosen H., Miller B.L., Laforce R. Jr., Galimberti D., Masellis M., Borroni B., Zhang Z., Zinman L., Rohrer J.D., Tartaglia M.C., Robertson J.; **Genetic FTD Initiative (GENFI).** (2018). Downregulation of exosomal miR-204-5p and miR-632 as a biomarker for FTD: a GENFI study. *Journal of Neurology Neurosurgery and Psychiatry, 89*(8), 851-858.

Cash D.M., Bocchetta M., Thomas D.L., Dick K.M., van Swieten J.C., Borroni B., Galimberti D., Masellis M., Tartaglia M.C., Rowe J.B., Graff C., Tagliavini F., Frisoni G.B., Laforce R. Jr., Finger

E., de Mendonça A., Sorbi S., Rossor M.N., Ourselin S., Rohrer J.D.; **Genetic FTD Initiative, GENFI.** (2018) Patterns of gray matter atrophy in genetic frontotemporal dementia: results from the GENFI study. *Neurobiology of Aging*, (62), 191-196.

Galimberti D., Fumagalli G.G., Fenoglio C., Cioffi S.M.G., Arighi A., Serpente M., Borroni B., Padovani A., Tagliavini F., Masellis M., Tartaglia M.C., van Swieten J., Meeter L., Graff C., de Mendonça A., Bocchetta M., Rohrer J.D., Scarpini E.; **Genetic FTD Initiative (GENFI).** (2018). Progranulin plasma levels predict the presence of GRN mutations in asymptomatic subjects and do not correlate with brain atrophy: results from the GENFI study. *Neurobiology of Aging*, (62), 245.

Premi E., Grassi M., van Swieten J., Galimberti D., Graff C., Masellis M., Tartaglia C., Tagliavini F., Rowe J.B., Laforce R. Jr., Finger E., Frisoni G.B., de Mendonça A., Sorbi S., Gazzina S., Cosseddu M., Archetti S., Gasparotti R., Manes M., Alberici A., Cardoso M.J., Bocchetta M., Cash D.M., Ourselin S., Padovani A., Rohrer J.D., Borroni B.; **Genetic FTD Initiative (GENFI)**. (2017). Cognitive reserve and TMEM106B modulate brain damage in presymptomatic frontotemporal dementia: a GENFI study. *Brain, 140*(6), 1784-1791.

Sudre C.H., Bocchetta M., Cash D., Thomas D.L., Woollacott I., Dick K.M., van Swieten J., Borroni B., Galimberti D., Masellis M., Tartaglia M.C., Rowe J.B., Graff C., Tagliavini F., Frisoni G., Laforce R. Jr., Finger E., de Mendonça A., Sorbi S., Ourselin S., Cardoso M.J., Rohrer J.D.; **Genetic FTD Initiative, GENFI.** (2017). White matter hyperintensities are seen only in GRN mutation carriers in the GENFI cohort. Neuroimage Clinical, (15), 171-180.

PhD portfolio

PhD training	Year	ECTS
General Courses		
Good Clinical Practice (BROK)	2015	1.5
Biomedical English Writing and Communication	2016	3
Personal Efficacy training	2016	1
Research integrity	2017	0.3
Biostatistical Methods 1: Basic Principles Part A (NIHES)	2017	2
Adobe Photoshop and Illustrator CS6 workshop	2018	0.3
Specific courses		
FMRIB Software Library, Hawaii, USA	2015	1.5
Research management for PhD students and Post-docs (MolMed)	2018	0.6
Repeated measurements (NIHES)	2018	1.4
Scripting for Life Science researchers, Leiden University Medical Center	2018	0.6
Conferences and Seminars		
Alzheimer's Association International Conference	2016	2
AAIC, Toronto, Canada - oral presentation		
10th International Conference on Frontotemporal Dementias	2016	1
IC-FTD, Munich, Germany - poster presentation		
Lancet Neurology conference on preclinical neurodegenerative diseases	2016	1
London, United Kingdom - poster presentation		
Human Brain Mapping	2017	1
HBM, Vancouver, Canada - poster presentation		
11th International Conference on Frontotemporal Dementias	2018	2
IC-FTD, Sydney, Australia - oral presentation		
Mix and Match meetings, Alzheimer Nederland	2015-2018	1
GENFI investigators meetings	2016-2019	1
Other		
Alzheimercenter Erasmus MC project assistant	2015-2017	30
Research meeting Alzheimercenter Erasmus MC, weekly	2015-2019	4
Alzheimercenter Erasmus MC Journal club, monthly	2017	1
VICI neuroimaging meeting, Leiden University Medical Center, monthly	2017-2019	2
Imaging of Dementia in Epidemiology and the Alzheimer Center, Erasmus MC, monthly	2017-2019	2

Projectmeetings FTD-RisC study, weekly	2017-2019	2.5
Teaching		
Thesis supervision, four students	2016-2019	6
Organization informational meetings for FTD-RisC participants	2017-2019	2
Presentations Dutch FTD caregivers	2018-2019	0.3
Total		**71**

List of abbreviations

32CH	32 channel head coil
3T	3 Tesla
8CH	8 channel head coil
AD	Alzheimer’s disease
ADNI	Alzheimer’s Disease Neuroimaging Initiative
ALS	amyotrophic lateral sclerosis
ANOVA	analysis of variance
ASL	arterial spin labeling
AUC	area under the curve
AxD	axial diffusivity
BDI	Beck depression inventory
BET	brain extraction tool
bvFTD	behavioral variant frontotemporal dementia
C9orf72	chromosome 9 open reading frame 72
C9orf72RE	chromosome 9 open reading frame 72 repeat expansion
CAT12	Computation Anatomy Toolbox
CBF	cerebral blood flow
CBI-R	Cambridge Behavioural Inventory - Revised
CBS	cortico-basal syndrome
CLEAR	constant level appearance
CSF	cerebrospinal fluid
DARTEL	diffeomorpic image registration
DEBM	discriminative event based modelling
DIAN	Dominant Inherited Alzheimer Network
DTI	diffusion tensor imaging
EPI	echo planar image
FA	fractional anisotropy
FAB	frontal assessment battery
FAST	FMRIB automated sementation tool
FDG	fluorodeoxyglucose
FEAT	FMRI expert analysis tool
FOV	field of view
FRS	frontotemporal dementia rating scale
FSL	FMRIB Software Library
FTD	frontotemporal dementia

FTD-GRN	progranulin related frontotemporal dementia
FTD-RisC	Frontotemporal dementia Risk Cohort
FTLD	frontotemporal lobar degeneration
FTLD-CDR-SB	frontotemporal lobar degeneration - clinical dementia rating scale - sum of boxes
FWE	family wise error
FWHM	full width at half maximum
GENFI	Genetic Frontotemporal dementia Initiative
GM	grey matter
GMM	gaussian mixture modelling
GRN	progranulin
HC	healthy controls
ICA	independent component analysis
ICA-AROMA	ICA automatic removal of motion artifacts
LEFFTDS	Longitudinal Evaluation of Familial Frontotemporal Dementia
MAPT	microtubule associated protein tau
MCI	mild cognitive impairment
MD	mean diffusivity
MINI-SEA	Mini Social Cognition and Emotional Assessment
MMSE	Mini Mental State Examination
MND	motor neuron disease
MNI	Montreal Neurological Institute
MRI	magnetic resonance imaging
NfL	neurofilament light chain
nfvPPA	non-fluent variant primary progressive aphasia
NPI	Neuropsychiatric Inventory
NPI-Q	Neuropsychiatric Inventory - Questionnaire
PET	positron emission tomography
PIB	Pittsburgh compound B
PPA	primary progressive aphasia
PSP	progressive supranuclear palsy
RD	radial diffusivity
RF	radiofrequency
ROC	receiver operater characteristic
ROI	region of interest
rsfMRI	resting state functional MRI
SD	standard deviation
SNR	signal to noise ratio

SPM	Statistical Parametric Mapping
svPPA	semantic variant primary progressive aphasia
T1w	T1-weighted
TBSS	tract based spatial statistics
TE	echo time
TFCE	treshold-free cluster enhancement
TIV	total intracranial volume
TMT	Trail Making Test
TR	repetition time
TrackHD	Track Huntington’s disease
VBM	voxel-based morphometry
WAIS	Wechsler Adult Intelligence Scale
WM	white matter

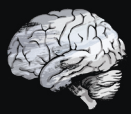

JESSICA PANMAN